UNIVERSITÄT
ZU KÖLN

"Activation and modulation of lipid- and polysaccharide-induced plant immunity during beneficial plant-microbe interactions"

Inaugural-Dissertation
zur Erlangung des Doktorgrades
der Mathematisch-Naturwissenschaftlichen Fakultät
der Universität zu Köln

vorgelegt von

Pia Saake

aus Stolberg (Rhld.)

Köln, 13. Januar 2025

Angenommen im Jahr 2025

Advisory committee	**Thesis committee**
First supervisor	**First Reviewer**
Prof. Dr. Alga Zuccaro	Prof. Dr. Alga Zuccaro
Second supervisor	**Second Reviewer**
Prof. Dr. Oliver Ebenhöh	Prof. Dr. Bart Thomma
Third supervisor	**Chair of thesis committee**
Prof. Dr. Gabriel Schaaf	Prof. Dr. Jan Riemer
	Minute taker
	Dr. Mathias Brands
Date of oral exam:	21.03.2025

The presented research was conducted under the auspices of the Graduate School of Biological Sciences (University of Cologne) and the CEPLAS Graduate School (Cluster of Excellence in Plant Sciences, Heinrich-Heine University Düsseldorf, University of Cologne)

List of Abbreviations

AEQ	Aequorin
AMF	Arbuscular mycorrhiza fungi
AMS	AMF symbiosis
ASG	Acyl sterol glycosides
At	*Arabidopsis thaliana*
ATP	Adenosine triphosphate
Bs	*Bipolaris sorokinana*
β-GD	β-1,3-glucan decasaccharide
CAZymes	Carbohydrate active enzymes
Ca^{2+}	Calcium
CDPK	Calcium dependent protein kinase
CO	Chitoligosaccharide
CW	Cell wall
CWA	Cell wall aposition
DAMP	Damage associated molecular pattern
dpi	Days post inoculation
DP	Degree of polymerization
Eb	*Eisenia bicyclis*
ECD	Extracellular domain
ETI	Effector triggered immunity
ETS	Effector triggered susceptibility
EPS	Extracellular polysaccharides
flg22	Peptide (22 amino acids) derived from flagellin
FS	Free sterols
GC-MS	Gas chromatography - mass spectrometry
Hv	*Hordeum vulgare*
ISR	Induced systemic resistance
JA	Jasmonic acid
Ld	*Laminaria digitata*
LD	Lipid droplet
LCO	Lipochitoligosaccharide
Lj	*Lotus japonicus*

LPS	Lipopolysaccharide
LRR	Leucine-rich repeat
LysM	Lysin motif
MALDI-TOF	Matrix-assisted laser desorption / ionization - time of flight
MAMP	Microbe-associated molecular pattern
MAPK	Mitogen associated protein kinase
NLR	Nucleotide-binding leucine-rich repeat receptor
NMR	Nuclear magnetic resonance
PGPB	Plant growth promoting bacteria
PGPF	Plant growth promoting fungi
Pi-Cer D	*Phytophtora infestans* ceramide D
PM	Plasma membrane
PR	Pathogenesis related
PRR	Pattern recognition receptor
PTI	Pattern triggered immunity
qRT-PCR	Quantitative real time polymerase chain reaction
RBOHD	Reactive burst oxidase homolog D
RLCK	Receptor-like cytoplasmic kinase
RLK	Receptor-like kinase
RLP	Receptor-like protein
RNS	Root nodule symbiosis
ROS	Reactive oxygen species
SA	Salicylic acid
SE	Sterol ester
SG	Sterol glucosides
Si	*Serendipita indica*
TF	Transcription factor
UBI	Ubiquitin
WT	Wild type

Publications

Publications included in this thesis:

Tiemblo-Martín, M., Pistorio, V., Saake, P., Mahdi, LK., Asunción Campanero-Rhodes, M., Di Girolamo, R., Di Carluccio, C., Marchetti, R., Molinaro, A., Solís, D., Zuccaro, A., Silipo, A. (2024). Structure and properties of the exopolysaccharide isolated from *Flavobacterium* sp. Root935. Carbohydrate Polymers. https://doi.org/10.1016/j.carbpol.2024.122433

Chandrasekar, B.*, Wanke, A.*, Wawra, S.*, Saake, P., Mahdi, L., Charura, N., Neidert, M., Poschmann, G., Malisic, M., Thiele, M., Stuhler, K., Dama, M., Pauly, M., Zuccaro, A. (2022). Fungi hijack a ubiquitous plant apoplastic endoglucanase to release a ROS scavenging β-glucan decasaccharide to subvert immune responses. The Plant Cell. https://doi.org/10.1093/plcell/koac114

van Boerdonk, S., Saake, P., Wanke, A., Neumann, U and Zuccaro, A. (2024). β-Glucan-binding proteins are key modulators of immunity and symbiosis in mutualistic plant–microbe interactions. Current Opinion in Plant Biology. https://doi.org/10.1016/ j.pbi.2024.102610

Saake, P., Brands, M., Endeshaw, A., Stolze, SC., Westhoff,P., Balcke, GU., Tissier, A., Hensel, G., Nakagami, H., Zuccaro, A. (2024). Plant Lipids Mediate Immune Responses to Fungal Lipids in Barley. Accepted in New Phytologist with minor revisions.

Further publications published in the framework of this thesis (not included):

Wanke, A., van Boerdonk, S., Mahdi, LK., Wawra, S., Neidert, M., Chandrasekar, B., Saake, P., Saur, IML., Derbyshire, P., Holton, N., Menke, FLH., Brands, M., Pauly, M., Acosta, IF., Zipfel, C., Zuccaro, A. (2023). A GH81-type β-glucan-binding protein enhances colonization by mutualistic fungi in barley. Current Biology. https://doi.org/10.1016/j.cub.2023.10.048

Kelly, S., Hansen, SB., Rübsam, H., Saake, P., Pedersen, EM., Gysel, K., Madland, E., Wu, S., Wawra, S., Reid, D., Sullivan, JT., Blahovska, Z., Vinther, M., Muszynski, A., Azadi, P., Thygesen, MB., Aachmann, FL., Ronson, CW., Zuccaro, A., Andersen, KR., Radutoiu, S., Stougaard, J. (2023). A glycan receptor kinase facilitates intracellular accommodation of arbuscular mycorrhiza and symbiotic rhizobia in the legume *Lotus japonicus*. PLOS Biology. https://doi.org/10.1371/journal. pbio.3002127

Dunken, N., Widmer, H., Balcke, GU., Straube, H., Langen, G., Charura, NM. Saake, P., De Quattro, C., Schön, J., Rövenich, H., Wawra, S., Khan, M., Djamei, A., Zurbriggen, MD., Tissier, A., Witte, CP., Zuccaro, A. (2024). A nucleoside signal generated by a fungal endophyte regulates host cell death and promotes root colonization. Cell Host and Microbe. https://doi.org/10.1016/j.chom.2024.10.020

Contents

Abstract

Plants are surrounded by a variety of microorganisms with commensal, mutualistic and pathogenic lifestyle. To monitor their environment, plants employ a multi-layered immune system consisting of extra- and intracellular receptors. Membrane-bound pattern recognition receptors (PRRs) detect conserved microbe-associated molecular patterns (MAMPs) outside of plant cells and activate pattern triggered immunity (PTI). Nucleotide-binding leucine-rich repeat receptors (NLRs) detect microbial effectors in the plant cytosol and activate effector triggered immunity (ETI). In the last decades, proteins, carbohydrates, nucelotides and lipids have been identified as MAMPs. Long-chain carbohydrates, or polysaccharides, are key structural components of microbial extracellular polysaccharide (EPS) matrices and cell walls (CWs), forming the outermost layers of microbial cells. Along with plasma membranes, which are predominantly composed of lipids, these structures constitute the interface for plant-microbe interactions. Consequently, EPS- and CW-derived polysaccharides and membrane lipids play a pivotal role in the establishment of plant-microbe associations. Here, we characterize their role as MAMPs and modulators of immunity in the interaction of the the model plant *A. thaliana* and crop barley (*Hordeum vulgare*) with the beneficial microbes *Flavobacterium* sp. Root935 and *Serendipita indica*, respectively. We provide evidence that EPS-matrices from both bacteria and fungi might function as oxidative shields or calcium chelators in addition to their function as MAMPs, thereby modulating the host immune response (Chapter 2.1, 2.2). This is likely attributed to the high branching or decoration frequency of the EPS. In addition, we identify β-glucan binding proteins as important compatibility factors in beneficial plant-microbe interactions (Chapter 2.3). Moreover, we provide a comprehensive overview of the PTI response, activated upon perception of lipids, isolated from *S. indica* mycelium, in barley roots. We identify ergosterol as the main immunogenic component of *S. indica* mycelium lipids and demonstrate activation of plant lipid signaling pathways, in particular phosphatidylinositol phosphate (PIP) signaling and diterpene biosynthesis, in response to fungal lipid treatment. This indicates that plant lipids mediate immune responses to fungal lipids in barley (Chapter 3.1). Finally local and systemic host responses to fungal lipids during *S. indica* colonization are further characterized (Chapter 3.2) and compared to colonization by the pathogenic fungus *Bipolaris sorokiniana* (Chapter 3.3). Altogether, the work depicted in this thesis expands our knowledge on the role of lipids and polysaccharides in plant immunity during beneficial plant-microbe interactions, which could be used to develop novel strategies to promote accommodation of beneficial microbes and enhance crop resistance.

Zusammenfassung

Pflanzen sind von einer Vielzahl von Mikroorganismen mit kommensalistischer, mutualistischer und pathogener Lebensweise umgeben. Um ihre Umwelt zu überwachen, verfügen Pflanzen über ein vielschichtiges Immunsystem, das aus extra- und intrazellulären Rezeptoren besteht. Membrangebundene PRR (pattern recognition receptors) Rezeptoren erkennen konservierte MAMPs (microbe-associated molecular patterns) außerhalb von Pflanzenzellen und aktivieren PTI (pattern triggered immunity). NLR (nucleotide-binding leucine-rich repeat receptors) Rezeptoren erkennen mikrobielle Effektoren im pflanzlichen Zytosol und aktivieren ETI (effector triggered immunity). In den letzten Jahrzehnten wurden Proteine, Polysaccharide, Nukleotide und Lipide als MAMPs identifiziert. Langkettige Kohlenhydrate, auch genannt Polysaccharide, bilden die Hauptbausteine extrazellulärer Polysaccharidmatrizen (EPS-Matrizen) und Zellwände, welche die äußersten Schichten der mikrobiellen Zellen bilden. Zusammen mit Plasmamembranen, welche haupstächlich aus Lipiden bestehen, bilden sie die Schnittstelle zwischen Pflanzen und Mikroben. Folglich spielen aus EPS und Zellwand gewonnene Polysaccharide und Membranlipide eine zentrale Rolle bei der Bildung von Pflanzen-Mikroben-Assoziationen. Hier charakterisieren wir dessen Rolle in der Aktivierung und Modulation des pflanzlichen Immunsystems während der Interaktion der Kulturpflanze Gerste (*Hordeum vulgare*) und der Modellpflanze *A. thaliana* mit den nützlichen Mikroben *Serendipita indica* bzw. *Flavobacterium* sp. Root935. Wir zeigen, dass bakterielle und Pilz-EPS-Matrizen, zusätzlich zu ihrer Funktion als MAMPs, als oxidative Schutzschilde oder Calcium Chelatoren fungieren und dadurch die Immunantwort des Wirtes modulieren könnten (Kapitel 2.1, 2.2). Dies wird wahrscheinlich durch eine hohe Verzweigungs- oder Dekorationsfrequenz der EPS bestimmt. Darüber hinaus identifizieren wir β-Glucan-bindende Proteine als wichtige Kompatibilitätsfaktoren in nützlichen Pflanzen-Mikroben Interaktionen (Chapter 2.3). Des Weiteren geben wir einen umfassenden Überblick über die PTI Reaktion, die bei der Wahrnehmung von Lipiden, isoliert aus *S. indica* Myzelium, in Gerstenwurzeln aktiviert wird. Wir identifizieren ergosterol als den haupt-immunogenen Bestandteil von *S. indica* Myzelium Lipiden und zeigen, dass pflanzliche Lipid-Signalwege, insbesondere Phosphatidylinositol phosphat (PIP)-Signalwege und die Diterpen-Biosynthese, als Reaktion auf die Wahrnehmung von Pilzlipiden aktiviert werden. Dies deutet darauf hin, dass pflanzliche Lipide die Immunantwort auf die Detektion von pilzlichen Lipiden vermitteln (Kapitel 3.1). Abschließend wird die lokale und systemische Immunantwort im Wirt auf pilzliche Lipide während *S. indica* Kolonisierung weitergehend charakterisiert (Chapter 3.2) und zu der Kolonisierung mit dem pathogenen Pilz *Bipolaris sorokiniana* verglichen (Chapter 3.3). Zusammengefasst, erweitern die in dieser Thesis vorgestellten Arbeiten unser Wissen über die Rolle von Lipiden und Polysacchariden in der pflanzlichen Immunantwort während nützlicher Interaktionen zwischen

Pflanzen und Mikroben. Dieses Wissen kann zur Entwicklung von neuartigen Strategien zur Förderung der Ansiedlung von nützlichen Mikroben und Verbesserung der Pflanzenresistenz, genutzt werden.

Chapter 1

Introduction

1.1 The plant microbiome and plant immunity

Plants are in constant contact with a variety of microorganisms both below- and above ground and accommodate a multitude of microbes living on (epiphytic) or inside (endophytic) their tissue. This adapted microbial community is called the microbiome and in case of the root, recruited from the soil (Lundberg et al., 2012; Bulgarelli et al., 2013; Duran et al., 2018; Wippel et al., 2021). Soil is an extremely organism-rich habitat containing approximately 60% of all species on earth (Anthony et al., 2023). Microbes such as bacteria, fungi and oomycetes resemble the largest proportion of soil organisms (Bakker et al., 2014). Plant-microbe interactions as well as plant-plant and microbe-microbe interactions in the soil directly influence the soil microbiome composition (Bakker et al., 2014; Duran et al., 2018; Wippel et al., 2021). The plant microbiome consists of commensal, beneficial and pathogenic microbes (Schlaeppi & Bulgarelli, 2015), which can significantly affect plant fitness, for instance by modulating resilience against abiotic stresses such as nutrient- and water deprivation (B. Bai et al., 2022). Moreover, the microbiome can protect the plant from pathogen infection. To monitor their environment, plants employ a multi-layered immune system consisting of plasma membrane resident receptors (pattern recognition receptors, PRRs) and intracellular receptors (nucleotide-binding leucine-rich repeat receptors, NLRs), which can perceive microbial molecules outside and inside the host cell, respectively. PRRs survey the apoplast, the aqueous space connecting host cells, where invading microbes proliferate and activate pattern triggered immunity (PTI) upon perception of microbe associated- or plant-derived damage associated molecular patterns (MAMPs or DAMPs). NLRs monitor the host cytoplasm and detect microbial effectors, leading to effector triggered immunity (ETI) (Zipfel & Oldroyd, 2017). Jones and Dangl, 2006 established the zig-zag model describing the consecutive activation of PTI and ETI during plant-microbe interactions. First, MAMPs are recognized by the plant and trigger PTI, restricting microbial colonization. Second, microbes secrete effectors, small molecules that interfere with the host immune response and thereby reduce plant defense responses (Presti et al., 2015; Todd et al., 2022), into the host cell, leading to effector triggered susceptibility (ETS). Third, microbial effectors are perceived by plant intracellular receptors (NLRs) leading to ETI and host resistance (Jones & Dangl, 2006). On an evolutionary scale this leads to an "arms-race" between plants and microbes in which microbes constantly evolve new effectors to overcome host immunity and

plants evolve new receptors to enhance resistance. In recent years increasing evidence was provided that PTI and ETI are interconnected and potentiate each other (Ngou et al., 2021; Pruitt et al., 2021; Chang et al., 2022). Upregulation of PTI components is important for an effective ETI response and regulated in a positive feedback loop by ETI signaling (H. Tian et al., 2021; Yuan et al., 2021). PTI and ETI act synergistically to effectively stop pathogen infection. In this thesis, we will focus on MAMP perception and subsequent PTI responses during beneficial plant-microbe interactions. Thus, PTI will be described in more detail in the following chapter while ETI will not be further discussed. For a detailed description of ETI, refer to Nguyen et al., 2021.

1.2 Pattern triggered immunity (PTI)

As described above, plants use PRRs to survey the apoplastic space for invading microbes. PRRs usually consist of a transmembrane domain, anchoring the protein in the plasma membrane (PM), an extracellular domain (ECD), which binds MAMPs or DAMPs, and a cytosolic domain, which activates downstream signaling targets. PRRs can be divided in receptor-like kinases (RLKs) and receptor-like proteins (RLPs). In RLKs the cytosolic domain contains a kinase domain, which is lacking in RLPs. Thus, RLPs associate with SUPPRESSOR OF BIR1 (SOBIR) adaptor RLKs for successful signal transduction (DeFalco and Zipfel, 2021, Figure 1A). PRRs are usually pre-associated to receptor-like cytoplasmic kinases (RLCKs). Upon ligand binding, co-receptor kinases are recruited to PRRs and phosphorylate the RLCKs (Figure 1A), which again propagate the signal. RLCKs phosphorylate several immunity signaling components, for instance the NADPH oxidase REACTIVE BURST OXIDASE HOMOLOG D (RBOHD), calcium influx channels or transcription factors, controlling immunity related genes. Ultimately, this results in apoplastic accumulation of reactive oxygen species (ROS), increase in cytosolic calcium (Ca^{2+}) concentrations, activation of MITOGEN ASSOCIATED PROTEIN KINASE (MAPK) phosphorylation cascades and differential gene expression, typical hallmarks of PTI (Couto and Zipfel, 2016; DeFalco and Zipfel, 2021, Figure 1B).

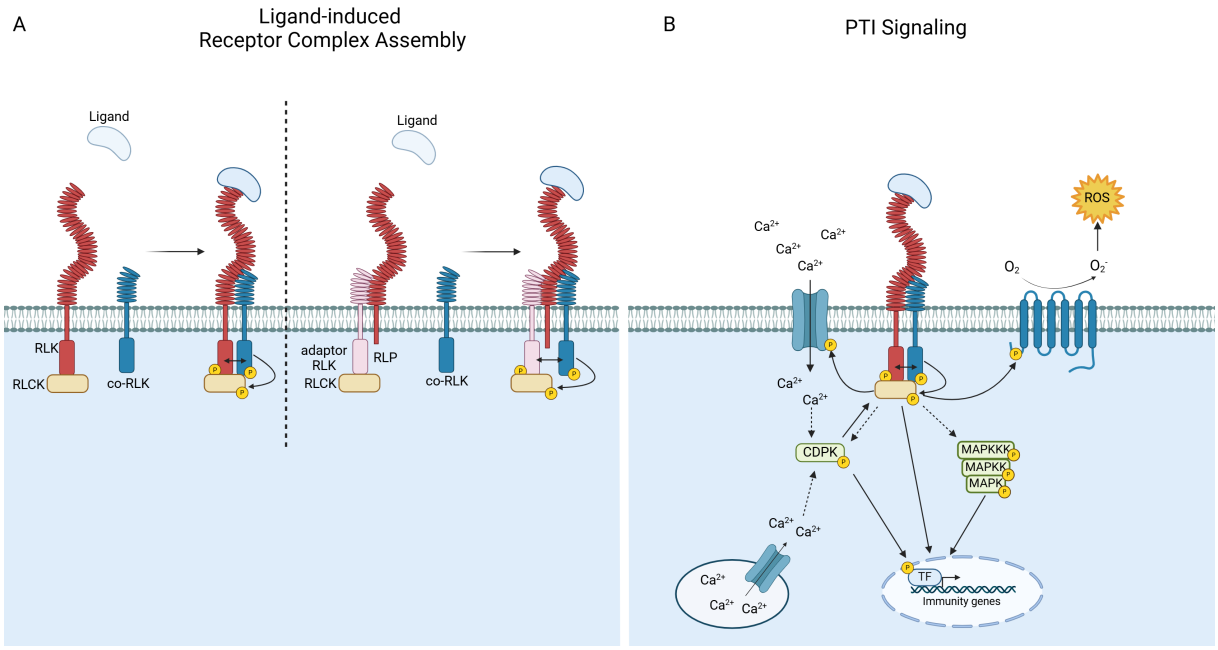

Figure 1: Ligand-induced receptor complex assembly and eary PTI signaling. A) PRRs (red) can be divided in RLKs (left), containing an intracellular kinase domain and RLPs (right), lacking this kinase domain. For ligand perception, RLPs associate with helper RLKs (pink). Additionally, PRRs are pre-associated to RLCKs (yellow) in the inactive state. Upon ligand binding, co-receptor kinases (blue) are recruited to the PRRs. This leads to transphosphorylation of the PRR and the co-receptor kinase and phosphorylation of the RLCKs. B) Phosphorylation of the RLCKs activates several downstream signaling pathways. RLCKs can directly phosphorylate calcium influx channels, the NADPH oxidase RBOHD and transcription factors, controlling immunity gene expression. Additionally, MAPKKKs are phosphorylated upon ligand binding, and calcium influx activates CDPKs. This results in apoplastic ROS accumulation, calcium influx into the cytosol, and differential gene expression. PRR = Pattern recognition receptor, RLK = Receptor-like kinase, RLP = Receptor-like protein, RLCK = Receptor-like cytoplasmic kinase, RBOHD = Respiratory burst oxidase homolog D, MAPKKK = mitogen associated protein kinase kinase kinase, CDPK = calcium dependent protein kinase, ROS = reactive oxygen species, TF = transcription factor. Adapted from Couto and Zipfel, 2016. The figure was created using Biorender.

1.3 The diversity of MAMPs and PRRs

MAMPs have been identified from all kingdoms of life and are found across all classes of major biomolecules from proteins, carbohydrates and lipids to nucleotides (Boutrot & Zipfel, 2017). The majority of MAMPS are highly conserved across genera and essential for survival, thus persist throughout evolution despite the high selective pressure due to perception by plant receptors. One of the most studied examples of a proteinaceous MAMP is flg22, a short peptide of the bacterial flagellin protein. Flg22 perception was first investigated in *A. thaliana*, where the perception mechanism and downstream signaling mechanisms were extensively studied. In *A. thaliana*, flg22 is perceived by the LRR-RLK FLAGELLIN SENSITIVE 2 (*At*FLS2) which is associated to the cytoplasmic RLCK BOTRYTIS-INDUCED KINASE 1 (*At*BIK1) (Chinchilla et al., 2006; Lu et al., 2010). Upon ligand binding, the co-receptor kinase BRASSINOSTEROID ASSOCIATED KINASE 1 (*At*BAK1) is recruited and phosphorylates *At*BIK1 to initiate downstream signaling (Heese et al., 2007; Y. Sun et al., 2013, Figure 2). In addition, *At*BIK1 can be phosphorylated by CALCIUM DEPENDENT PROTEIN KINASES (CDPKs) (Monaghan et al., 2014). *At*BIK1 subsequently phosphorylates calcium channels (W. Tian et al., 2019; Thor et al.,

2020) and *At*RBOHD (Kadota et al., 2014; L. Li et al., 2014), which mediate MAMP-induced apoplastic ROS production and calcium influx. Moreover, *At*BIK1 potentially phosphorylates *WRKY* transcription factors, thereby modulating expression of immunity-related genes (Lal et al., 2018, Figure 1B). The flagship MAMP for carbohydrates is the fungal cell wall (CW) component chitin, which consists of β-1,4 linked N-acetylglucosamine (GlcNAc) subunits (Brown et al., 2020). In *A. thaliana*, chitin oligomers are perceived by two LysM- containing RLKs *At*LYK5 and *At*LYK4, which recruit the co-receptor kinase *At*CERK1 (Cao et al., 2014, Figure 2). In rice, the LysM-RLK *Os*CEBiP forms a sandwich-type receptor complex with *Os*CERK1 to perceive chitin (Hayafune et al., 2014; Kouzai et al., 2014, Figure 2). Here, also several RLCKs are involved in downstream signaling (Boutrot & Zipfel, 2017). Additionally, oomycete-derived protein and lipid MAMPs were characterized. One example is the *Phytophtora infestans* ceramide D (*Pi*-Cer D), a sphingolipid, present in oomycete membranes. In *A. thaliana*, *Pi*-Cer D is cleaved by an apoplastic host ceramidase, NEUTRAL CERAMIDASE 2 (*At*NCER2), which releases a 9-methyl-branched sphingoid base (9-me-Spd) that is recognized by the *A. thaliana* lectin RLK, RESISTAND TO DFPM-INHIBITION of ABSCISIC ACID SINGALING 2 (*At*RDA2) and induces for instance expression of *WRKY* transcription factors (TFs) (Kato et al., 2022). Finally, plant-derived DAMPs also induce an immune response (Figure 2). One prominent example is adenosine triphosphate (ATP). ATP is released upon damage of host cells and perceived by two L-type lectin RLKs *At*LecRK-I.9, also called *At*P2K1 or *At*DORN1, and *At*LecRK-I.5, also called *At*P2K2 (Choi et al., 2014; Pham et al., 2020). Upon ATP perception, both receptors interact and cross-phosphorylate (Pham et al., 2020). An overview of the so far identified MAMPs and DAMPs and their respective RLKs, co-RLKs and RLCKs is depicted in Figure 2 (adapted from Ngou et al., 2022). This overview demonstrates that to date bacterial and fungal MAMPs make up the majority of identified MAMPs. While the perception of proteins and peptides is widely understood, information on receptors and co-receptors of carbohydrates, lipids or nucleotides is limited.

Knowledge on the characterized PRR-MAMP pairs and downstream signaling kinases involved in the immune response can help to identify PRRs and RLCKs of orphan MAMPs. Comparison of MAMPs and their corresponding PRR types revealed that the ECD of RLKs confers a binding preference for certain MAMP molecules. Generally, LRR-RLKs bind protein MAMPs, LysM-domain RLKs bind carbohydrate MAMPs, G-lectin domains bind lipid MAMPs, L-lectin RLKs nucleotides and EGF-type RLKs bind CW-derived oligogalacturonides (Couto and Zipfel, 2016; DeFalco and Zipfel, 2021, Figure 2). However, it should be noted that exceptions exist as for instance for the oomycete peptide *Pc*EXLX1 which is perceived by a G-type lectin receptor instead of a LysM-domain containing RLK (Figure 2). Often, co-receptor kinase recruitment is also regulated by the PRR ECD. In *A. thaliana*, the co-receptor kinase *At*BAK1 or closely related SOMATIC EMBRYOGENESIS RECEPTOR KINASES (SERKs) are involved in the perception of several peptides and associate mainly with LRR-RLKs (Figure 2). In contrast, CERK1 is involved in carbohydrate perception and recruited to various LysM containing RLKs (Couto & Zipfel, 2016). Further, it was demonstrated that these co-receptor kinases function not only in immunity but also symbiosis signaling or growth-related signaling pathways. This

indicates that a common molecular strategy is used by similar biochemical classes of RLKs for their ligand-induced activation (Zipfel & Oldroyd, 2017). In addition, plants harbour a great variety of RLCKs, allowing robustness and flexibility of their immune response. The same RLCKs can be involved in perception of several MAMPs, independent of the PRR type. *At*BIK1 and the closely related PBS1-like kinase (*At*PBL) proteins activate immune responses elicited by elf-18, *At*Pep1 and chitin (DeFalco & Zipfel, 2021). However, RLCKs can vary in their affinity to different PRRs and can activate distinct branches of PTI signaling (Couto & Zipfel, 2016).

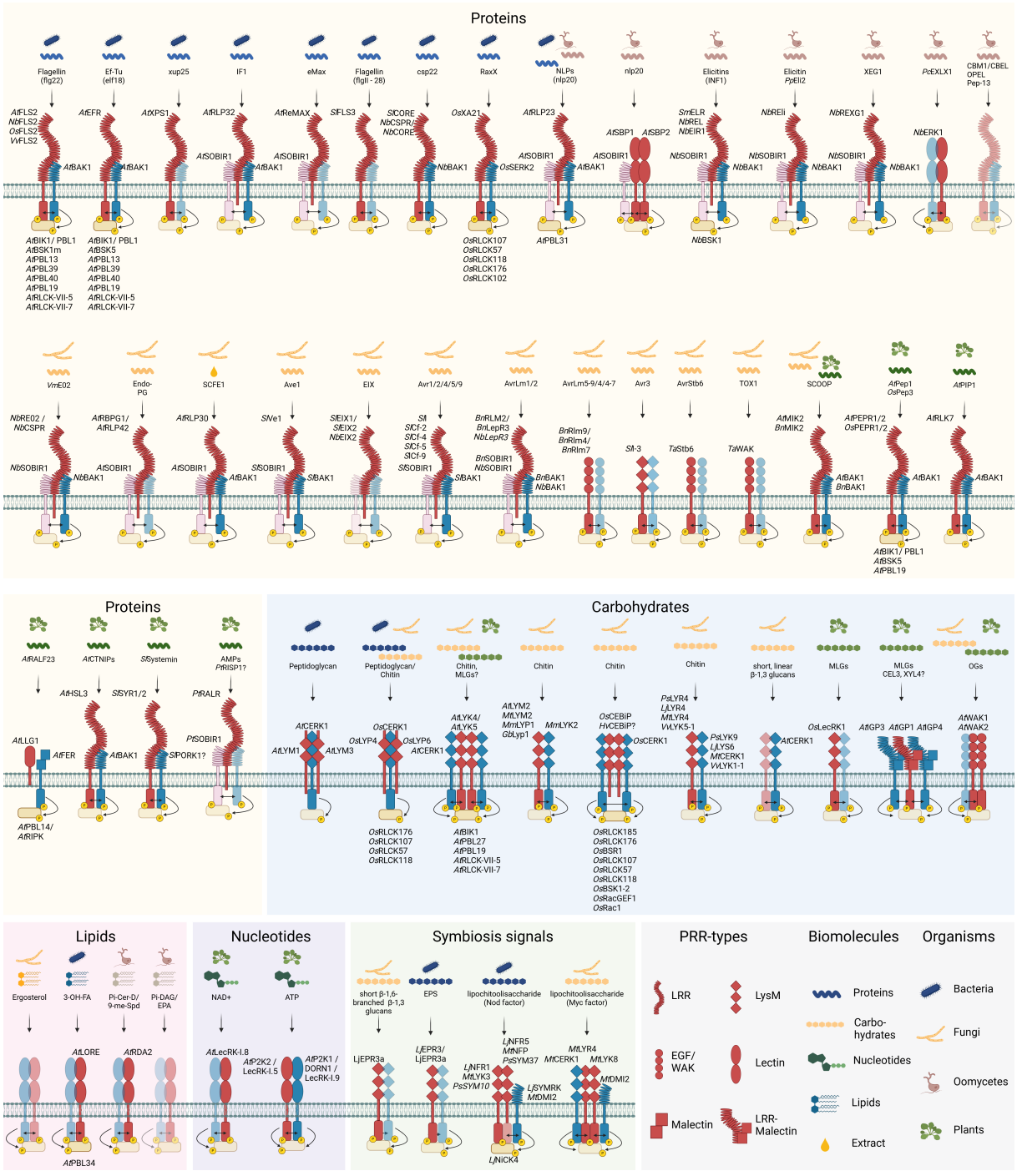

Figure 2: MAMPs / DAMPs and symbiosis signals and their respective receptor complexes. Characterized MAMPs / DAMPs and immunity signals from bacteria (blue), fungi (yellow), oomycete (pink) and plants (green) and their respective PRR complexes. Main receptors (RLKs or RLPs) are indicated in red, helper RLKs in pink, co-RLKs in blue and RLCKs in yellow. Unknown/missing components are depicted 50 % transparent. MAMPs / DAMPs are sorted by their molecule class into proteins, carbohydrates, lipids and nucleotides. Additionally, symbiosis signaling molecules are depicted. Abbreviations for plant species: *A. thaliana*, *At*; *B. napus*, *Bn*; *L. japonicus*, *Lj*; *M. truncatula*, *Mt*; *N. benthamiana*, *Nb*; *O. sativa*, *Os*; *P. sativum*, *Ps*; *S. lycopersicum*, *Sl*; *S. microdontum*, *Sm*; *T. aestivum*, *Ta*; *V. vinifera*, *Vv*. Adapted from Couto and Zipfel, 2016; Ngou et al., 2022. The figure was created using Biorender. A table containing all information depicted in this figure including references can be found in the Appendix.

1.4 Regulation of PTI

Activation of immunity is energetically costly for plants. Therefore, it must be tightly regulated to avoid constitutive activation. This regulation is integrated at several levels from recruitment of co-receptor kinases and signaling initiation at the PRR complex to cytoplasmic signal transduction pathways and transcriptional reprogramming (Couto & Zipfel, 2016). Kinases are essential components in plant immunity. However, approx. 10 % of all *A. thaliana* kinases are pseudokinases (Castells & Casacuberta, 2007), which do not phosphorylate substrates but function as allosteric activators of other kinases and promote or prevent protein-protein interactions (Zeqiraj & van Aalten, 2010; Shaw et al., 2014). Thereby, they can modulate recruitment of co-receptor kinases. Two examples are the pseudokinases *At*BIR1 and *At*BIR2 that associates with *At*BAK1 and thereby prevent *At*BAK1-*At*FLS2 complex formation (Gao et al., 2009; Blaum et al., 2014; Halter et al., 2014). Moreover, phosphatases are important negative regulators of kinases to avoid inadvertent immune responses. They affect immunity signaling at multiple levels. Protein phosphatases type 2C (PP2C) can dephosphorylate PRRs (Gómez-Gómez et al., 2001; Park et al., 2008; Diao et al., 2024) and protein phosphatase type 2A (PP2A) constitutively associates with and dephosphorylates BAK1 to negatively regulate its activity (Segonzac et al., 2014). RLCKs such as BIK1 are also regulated through their phosphorylation status (Couto et al., 2016) and dual specificity phosphatases (DUSPs) were shown to dephosphorylate MAPKs, thereby modulating their activity and subsequent transcription of immunity related genes (Caunt & Keyse, 2013). Transcription of immunity related genes is highly regulated by the activity of the respective TF. One prominent example are WRKY TFs, which are often retained in a protein complex in the inactive state but released upon ligand binding, allowing phosphorylation by MAPKs and subsequent activation of gene expression (J. L. Qiu et al., 2008; Mao et al., 2011; Javed & Gao, 2023). Finally, PTI signaling is incorporated in hormone- and endogenous peptide- signaling networks. The antagonistic immunity-related hormones salicylic acid (SA) and jasmonic acid (JA), positively and negatively regulate PTI, respectively (Pieterse et al., 2012; Yi et al., 2014; Aerts et al., 2021). Another major plant hormone, ethylene is especially involved in controlling the activation of gene expression via ethylene-responsive transcription factors and can act antagonistically or synergistically with both SA and JA (Boutrot et al., 2010; Pieterse et al., 2012). Plants need to meticulously manage allocation of their resources between immunity signaling and growth, leading to a so-called plant growth-defense trade-off. Thus, immunity is negatively regulated by growth-related hormones such as auxin. Auxin antagonizes SA signaling and auxin signaling is inhibited upon ligand perception. Furthermore, cytokinins and brassinosteroids also modulate PTI (C. Albrecht et al., 2012; T. Albrecht & Argueso, 2016). In addition to regulation via post-translational modifications, protein levels of immunity components are tightly regulated. Upon ligand-induced receptor complex formation, PRRs are endocytosed and degraded in the vacuole (Robatzek et al., 2006; Khaled et al., 2015; Ekanayake et al., 2021). This process, known as receptor-mediated endocytosis, serves as a regulatory mechanism to prevent constitutive activation of immune responses (Robatzek et al., 2006; Claus et al., 2018). At the same time, it might activate *de novo* biosynthesis of ligand-free receptor receptors replacing the activated ligand-bound receptors, allowing resensitization (Smith et al., 2014). Targeting for proteasomal degradation is mediated by ubiquitination *via*

PUB E3 ligases (Trujillo et al., 2008; Lu et al., 2011). In addition, RLCKs such as BIK1 are in constant turnover as well (Monaghan et al., 2014). Altogether, a tight regulation is critical to control resource allocation and avoid damage due to hyperactivation of immunity in plants. As the activation of immunity controls the accommodation of microbes, the plant regulatory mechanisms are valuable targets for many microbial effectors to interfere with host immunity.

1.5 PTI in mutualistic plant-microbe interactions

Arbuscular mycorrhizal fungi symbiosis (AMS) and *Rhizobia*-legume symbiosis or root nodule symbiosis (RNS) are the two major symbiotic relationships studied in plant roots. In addition, non-symbiotic beneficial endophytic interactions with plant growth promoting rhizobacteria (PGPR) and fungi (PGPF) confer beneficial effects to their host plants and share many signaling pathways with AMS and *Rhizobia* symbiosis (Nishad et al., 2020). The initial plant defence response to mutualistic microbes is similar as to biotrophic pathogens. Both induce a PTI response, although mutualistic microbes often to a lesser extent than pathogens, potentially due to reduction of MAMP production, diversification of MAMPs and chelation of host immune responses (Zamioudis & Pieterse, 2012; van Boerdonk et al., 2024). For example, ectomycorrhizal fungi encode less plant CW degrading or carbohydrate active enzymes (CAZymes) in their genome, which could be recognized by host plants as MAMPs, indicating an evolutionary adaptation to the symbiotic lifestyle (Martin et al., 2008; Martin et al., 2010). In contrast, genomic analyses of the beneficial root endophytes *Serendipita indica* and *Serendipita vermifera* revealed an expansion of CAZymes in both fungi (Lahrmann et al., 2015). *S. indica* and *S. vermifera* exhibit a specific biphasic colonization strategy characterized by an initial biotrophic phase followed by a saprotrophic cell-death associated phase (Lahrmann et al., 2013). The latter could explain the expanded repertoire of CAZymes as observed in many saprotrophic fungi (Jia et al., 2023). Diversification of MAMPs was for instance observed in the legume symbiont *Sinorhizobium meliloti*. Here, the usually well conserved flagellin epitope is exceptionally divergent and does not induce an immune response in the host plant *Lotus japonicus*. Likewise, flagellin from *Mesorhizobium loti* does not induce an immune response in the host *L. japonicus* (Lopez-Gomez et al., 2012) and *S. meliloti* lipopolysaccharides (LPS) only induced a minor response in the host *M. sativa*, while the response in non-host plants was stronger (Albus et al., 2001). This indicates that legumes evolved a sophisticated perception system to differentially respond to pathogens and symbionts. Finally, extracellular polysaccharides (EPS) of mutualistic bacteria were shown to chelate calcium and scavenge ROS in the apoplast, thereby reducing plant immunity and potentially promoting colonization (Scheidle et al., 2005; Aslam et al., 2008; Tiemblo-Martín et al., 2024).

Following the initial PTI activation, biotrophic pathogens and beneficial microbes need to overcome plant immunity. Therefore, microbes employ a variety of effectors which interfere with MAMP-induced immunity and its regulatory mechanisms described above. In the apoplast, effectors for example modulate host hydrolytic activity reducing the release of MAMPs and DAMPs or chelate immune responses such as ROS. Inside the host cell, effectors can modulate hormone biosynthesis, protein modification, trafficking or degradation and expression of

immunity- or susceptibility genes (Tanaka et al., 2015; Han & Kahmann, 2019; Ramachandran et al., 2021). Mutualistic microbes are sensitive to SA, thus they activate JA signaling and the production of growth-related phytohormones such as auxin and gibberillins to induce a negative cross-talk with SA signaling. Additionally, ethylene-dependent defense mechanisms are often targeted by microbial effectors. Other effectors such as the arbuscular mycorrhiza fungi (AMF) effector DMI3 target calcium influx channels, reducing calcium influx and downstream signaling processes. Further, effectors can influence the microbiome to successfully establish niche colonization (Plett & Plett, 2022; Eichfeld et al., 2024; Mesny et al., 2024). While effectors are widely studied for pathogens, only few effectors have been characterized in AMF and *Rhizobia* (Chacón et al., 2023; Chacón et al., 2024). To establish successful interactions and suppress SA-mediated defence responses, *Rhizobia* and AMF activate additional symbiosis (Sym) signaling pathways by secretion of Nod factors and Myc factors, respectively. Nod- and Myc factors are lipochitooligosaccharides (LCOs), perceived by host symbiosis receptors. Like other chito-oligosaccharides (COs), Nod-LCOs and Myc-LCOs are perceived by LysM-RLKs in legumes (Limpens et al., 2015; Feng et al., 2019; Gibelin-Viala et al., 2019; Krönauer and Radutoiu, 2021; Zhang et al., 2024; Figure 2). These associate with the regulatory malectin-like LRR RLKs *Lj*SYMRK in *L. japonicus* and *Mt*DMI2 in *M. truncatula* to activate downstream signaling (Zipfel and Oldroyd, 2017; Figure 2). Perception of Nod-factors not only activates symbiosis signaling, but also suppresses PTI responses, promoting accommodation. Nod factor perception induces FLS2 degradation and subsequently suppresses flg22 perception in *A. thaliana* and soybean (Liang et al., 2013), indicating a conserved function in legumes as well as nonlegume plants. Moreover, both AMF and host plants were shown to secrete LysM proteins to the apoplast to facilitate AMS (H. Yu et al., 2023). Nod- and Myc-LCOs are derivatives of immunogenic COs and perceived by similar receptors (Figure 2). To date, it is still not fully understood how plants distinguish between immunogenic and symbiotic signals. While the RLKs and co-RLKs *Mt*LYR4 and *Mt*CERK1 play a dual role in immunity and symbiosis signaling, recently *Mt*LYK8 was identified as essential component of the Myc-LCO receptor complex that is not involved in immunity signaling (Gibelin-Viala et al., 2019; Zhang et al., 2024, Figure 2). Moreover, it was proposed that a mix of both immunity and symbiosis signals promotes symbiotic interactions (Feng et al., 2019) and that calcium signatures induced by symbiotic and immunogenic COs overlap (Giovannetti et al., 2024). Thus, multiple factors besides COs might determine the plant response. Recently, two additional LysM-receptors *Lj*EPR3 and *Lj*EPR3a, which perceive short, β-1,6-branched β-1,3-glucans were demonstrated to modulate AMS and RNS, functioning as symbiotic β-glucan receptors, opening up a new field of research (Kawaharada et al., 2015; Kawaharada et al., 2017; S. Kelly et al., 2023).

Finally, colonization by mutualistic microbes induces an additional immune response to protect their host plant from pathogens or pests, called induced systemic resistance (ISR) or in the special case of AMF, mycorrhizal induced resistance (MIR) (S. C. Jung et al., 2012). Colonization by beneficial microbes shifts the plant into a primed state, allowing a faster and stronger response to pathogen infection, resulting in enhanced resistance (Conrath et al., 2006; Pieterse et al., 2014). Priming is commonly characterized by mild transcriptomic changes in the unchal-

langed plant. However, an elevated level of inactive TFs and MAPKs was observed, allowing a quicker response upon challenge (Pieterse et al., 2014). ISR was observed both locally and in spatially separated tissues, e.g. root & leaf (Wei et al., 1991) or split-root systems (L. Liu et al., 1995; Sarkar et al., 2019) and is often characterized by potentiated expression of JA/ET-regulated genes and enhanced cell wall apositions (CWAs) or callose depositions at pathogen infection sites to hinder entry of pathogens into the host cells (Ent et al., 2009).

While for a long time pathogenic and beneficial plant microbe interactions were studied separately, increasing evidence suggests that both types of microbes employ similar principles to establish successful interactions and are recognized by overlapping plant receptors. How plants recruit beneficial microbes while simultaneously fending off pathogens is still not fully understood and was postulated as number one of the top 10 unanswered questions in molecular plant microbe interactions at the IS-MPMI Congress in 2019 (Harris et al., 2020; Thoms et al., 2021). Further research, especially on the molecular dialogue between plants and beneficial microbes is essential to answer this question. Thus, the work presented in this thesis, focuses on MAMPs derived from beneficial microbes and mechanisms employed by these microbes to modulate the plant immune response. We used *Flavobacterium* sp. Root935, a mutualist, isolated from *A. thaliana* roots (Y. Bai et al., 2015)and *Serendipita indica*, a beneficial root endophytic fungus colonizing a broad spectrum of plant hosts (Lahrmann et al., 2013) as microbial model systems and *A. thaliana* and barley (*Hordeum vulgare*) as plant model systems. Moreover, the pathogenic fungus *Bipolaris sorokiniana* was used as model species to compare immunity modulating mechanisms of beneficial and pathogenic fungi.

1.6 Experimental systems

Flavobacterium sp. Root935

The genus *Flavobacterium* comprises gram-negative, rod-shaped bacteria, of pale to bright yellow colour that colonize various habitats such as water, soil and also plants (Whitman & Trust, 2015). Originally identified as fish pathogenic bacteria in salt- and freshwater, more recently, *Flavobacteria* were recognized as key taxa in plant microbiomes (Kwak et al., 2018). *Flavobacteria* are abundant in the rhizo- and phyllospheres of several plant species such as wheat and *A. thaliana* (Y. Bai et al., 2015; Kolton et al., 2016). Colonization by *Flavobacteria* often confers beneficial effects to their host plants including plant growth promotion and protection from biotic- and abiotic stresses (Seo et al., 2024). For instance, all 32 strains isolated from tomato rhizosphere showed growth promoting effects on tomato (Kwak et al., 2018; E. J. Jung et al., 2021). The molecular mechanisms on how *Flavobacteria* mediate these beneficial effects are not fully understood but some studies showed that *Flavobacteria* strains can produce antimicrobial volatile organic compounds (VOCs) to fend off pathogens. Further, *Flavobacteria* carry genes encoding nitrogen fixation proteins, alkaline phosphatases and siderophores. Thereby, they might provide their host plants with macro- and micronutrients, enhancing stress tolerance and plant growth (Seo et al., 2024). *Flavobacteria* are characterized by fast growth rates, a high abundance of genes involved in metabolism of plant cell wall carbohydrates and a unique form

of gliding motility, mediated by their type XI secretion system, potentially allowing them to successfully colonize plants and persist in the highly competitive rhizosphere (Kolton et al., 2016). *Flavobacterium* sp. Root935 is a mutualistic bacterium, isolated from *A. thaliana* roots (Y. Bai et al., 2015) and part of an *A. thaliana* root synthetic community (SynCom), used in multiple studies (Wippel et al., 2021; Mahdi et al., 2022). Here, we investigate how exopolysaccharides derived from *Flavobacterium* sp. Root935 impact plant immunity.

Serendipita indica

Serendipita indica belongs to the order of the Sebacinales (Agaricomycetes, Basidiomycota), which comprises mutualistic fungi that can establish highly diverse interactions with plants, ranging from saprotrophic to mycorrhizal associations (Weiß et al., 2016). Sebacinales are widely distributed and more than 1000 species are known, although many remain uncharacterised (Weiß et al., 2016). The order of Sebacinales contains the two families Sebacinaceae and Serendipitaceae. Sebacinaceae include mainly ectomycorrhizal and early saprotrophic species and Serendipitaceae encompass endophytes as well as ericoid-, orchid- and ecto-mycorrhizal fungi (Weiß et al., 2016). Two of the most studied Sebacinales from the Serendipitaceae family are the root endophytes *Serendipita indica* and *Serendipita vermifera*. As endophytes, they penetrate and proliferate inside cells of the epidermal- and outer cortex layers of the plant root. *Serendipita indica* follows a biphasic colonization strategy, with an initial biotrophic colonization of living epidermal cells, followed by a cell-death associated phase, where chlamydospores develop and secondary thin hyphae of *S. indica* colonize dead epidermal- and cortex cells (Deshmukh et al., 2006; Lahrmann et al., 2013). However, the cell death is restricted and does not lead to necrosis or reduced root growth. The shift from the biotrophic to the cell-death associated phase is accompanied by a shift in the *S. indica* transcriptome, characterized by induced expression of cell-death associated effectors, hydrolytic enzymes and ABC transporters, characteristic for a saprotrophic lifestyle (Lahrmann et al., 2013). Recently,it was demonstrated that synergistic activity of two fungal effectors, a nuclease *Si*NucA and ecto-5'-nucleotidase *Si*E5NT, in the host apoplast leads to the production of deoxyadenosine (dAdo), which is transported into the plant cells *via* the equilibrative nucleoside transporter ENT3 and subsequently induces host cell death (Nizam et al., 2019; Dunken et al., 2024). Colonization by *S. indica* confers several beneficial effects on its host plants such as enhanced root and shoot fresh weight or grain yield (Waller et al., 2005; Deshmukh et al., 2006), improved nutrient acquisition, especially nitrogen, phosphorus and potassium (V. Kumar et al., 2012), and enhanced tolerance to drought and salt stress (Waller et al., 2005). Moreover, *S. indica* confers resistance against several pathogens including *Verticillium dahliae*, *Bipolaris sorokiniana* and *Blumeria graminis* in multipartite interactions (Waller et al., 2005; C. Sun et al., 2014; Mahdi et al., 2022; Eichfeld et al., 2024). This protection can occur locally but also systemically in both root and leaf tissue (Weiß et al., 2016). Similar to other PGPF, *S. indica* initially induces a PTI response in its host plants, which is weaker than the response to pathogens, most likely due to suppression of MAMP perception and host immunity (Jacobs et al., 2011), allowing the establishment of a stable mutualistic interaction. Here, we investigate the role of *S. indica*- derived lipids and polysaccharides in modulation of

host immunity during barley root colonization.

Bipolaris sorokiniana

Bipolaris sorokiniana belongs to the order Pleosporales (Ascomycotina) and depicts a hemi-biotrophic pathogenic lifestyle (J. Kumar et al., 2002).In the biotrophic growth phase, the fungus penetrates host cells via appressoria like structures and invades a single epidermal host cell, whereas the necrotrophic growth phase is characterized by extensive invasion of the mesophyll tissue and host cell death in epidermal and mesophyll cells (J. Kumar et al., 2002). To induce host cell death, *B. sorokiniana* secretes a variety of sesquiterpenoid toxins such as prehelminthosporol, helminthosporol and helminthosporic acid and sorokinianin (Carlson et al., 1991; Jahani et al., 2014; Qader et al., 2017; Malviya et al., 2022). As the causal agent of foliar spot blotch, root rot and black point diseases on grains and head blight and seedling blight of wheat and barley, *B. sorokiniana* is an important thread in agriculture. Interestingly, *S. indica* and *S. vermifera* were shown to protect barley from *B. sorokiniana* infection, potentially due to direct fungal-fungal interactions outside the host (Mahdi et al., 2022; Eichfeld et al., 2024). Here, we use *B. sorokiniana* to compare the changes in the phytosterol composition and the ability to perceive fungal lipids of barley roots colonized by a pathogenic (*B. sorokiniana*) and a beneficial (*S. indica*) fungus.

Main Objectives and Thesis Outline

While research on MAMPs has yielded comprehensive information on protein-based MAMPs, the perception of carbohydrate- and lipid-based MAMPs is less well characterized, with few identified MAMP-PRR pairs (Figure 2). Although several PRRs recognizing carbohydrates have been discovered, research has largely concentrated on chitin and its derivatives. MAMP perception by plants is critical for mounting effective defenses against invaders. In contrast, beneficial microbes must overcome host immunity to establish stable interactions. Thus, they have evolved various strategies to evade and modulate the host immune response With the studies presented in this thesis, we sought to explore the role of polysaccharides and lipids as MAMPs and modulators of host immunity during beneficial plant-microbe interactions.

In Chapter 2.1 (Tiemblo-Martín et al., 2024), we investigate structure and properties of the extracellular polysaccharide (EPS) matrix, produced by *Flavobacterium* sp. Root935, a beneficial *Flavobacterium* strain isolated from *A. thaliana* roots, to elucidate its potential role during *A. thaliana* root colonization. We provide evidence that the structure and extensive decoration of *Flavobacterium* EPS potentially masks it for recognition by plant hosts and prevents binding to lectins. Further, the lack of calcium influx suggests a calcium chelating function.

In recent years, also in fungi, EPS matrices were identified as additional layer covering fungal cell walls (Wawra et al., 2016, 2019). In Chapter 2.2 (Chandrasekar et al., 2022), we structurally characterize the fungal EPS matrices of the beneficial root endophyte *Serendipita indica* and the pathogen *Bipolaris sorokiniana* and investigate their roles during *Hordeum vulgare* (barley) colonization. We demonstrate that the fungal EPS matrices are distinct compartments from the non-soluble cell walls with regards to their protein and carbohydrate composition and can protect microbes from oxidative stress upon plant colonization. The *S. indica* EPS matrix is mainly comprised of β-1,6-branched β-1,3-glucans and activity of the host endoglucanase *Hv*BGLUII releases a glucan decasaccharide β-GD, which scavenges ROS in the apoplast and subsequently enhances fungal accommodation. While we focus mainly on characterization of the EPS matrix of *S. indica*, the *B. sorokiniana* EPS matrix has similar properties, indicating that pathogenic fungi employ similar mechanisms to overcome plant immunity.

Chapter 2.3 (van Boerdonk et al., 2024) summarizes recent advances in the field of β-glucan perception and provides an overview of mechanisms evolved in mutualistic microbes to prevent- or modulate β-glucan-induced plant immunity. Moreover, Chapter 2.3 highlights two recent studies that were published in the framework of this thesis but are not included as separate

publications. These describe the host β-glucan binding proteins *Lj*EPR3a (S. Kelly et al., 2023) and *Hv*GBP1 (Wanke et al., 2023), which act as symbiosis receptors or compatibility factors and modulate colonization by beneficial microbes, presenting a novel role for β-glucan binding proteins beyond PRRs.

Chapter 3 discusses the perception of fungal-derived lipids and activation of plant lipid signaling pathways during plant-microbe interactions. As building blocks of plasma membranes, together with the cell wall, lipids build the interaction interface of plants with their surroundings. In addition, microbial lipids are perceived as MAMPs by plants. In Chapter 3.1, we characterize the barley immune response to lipids isolated from *S. indica* mycelium. We demonstrate that *S. indica* lipids induce a PTI response in barley, which is accompanied by activation of plant lipid signaling pathways involving phosphatidylinositolphosphate (PIP) signaling and leads to diterpene exudation. Moreover, we discuss additional data supporting and extending the findings of Chapter 3.1 such as the local and systemic responses to *S. indica* colonization in barley, activation of *Hv*MLO in response to lipid treatment (Chapter 3.2) and differences in *S. indica*- and *B. sorokiniana*-barley colonization with regards to changes in the barley phytosterol composition, as well as suppression of lipid MAMP perception (Chapter 3.3).

In Chapter 4 (Discussion), the findings of this thesis are placed into the broader context of the current literature. We identify frequent branching and decoration of EPS as an important structural feature in mutualistic plant-microbe interactions and discuss nanodomain formation and the potential role of oxysterol binding proteins in fungal lipid perception. We provide an overview of recent advances in lipid detection and quantification techniques and indicate future research directions. Finally, how plant-microbe research can contribute to overcoming the agricultural challenges we are currently facing with regards to climate change, is discussed.

Chapter 2

Extracellular polysaccharides and β-glucan binding proteins in immunity and symbiosis

2.1 Structure and properties of the exopolysaccharide isolated from *Flavobacterium* sp. Root935.

Tiemblo-Martín, M., Pistorio, V., Saake, P., Mahdi, LK., Asunción Campanero-Rhodes, M., Di Girolamo, R., Di Carluccio, C., Marchetti, R., Molinaro, A., Solís, D., Zuccaro, A., Silipo, A. (2024)
Carbohydrate Polymers. https://doi.org/10.1016 /j.carbpol.2024.122433

Author contributions

Marta Tiemblo-Martín: Writing – original draft, Methodology, Investigation, Formal analysis, Data curation. Valeria Pistorio: Methodology, Investigation. **Pia Saake:** Writing – original draft, Investigation, Formal analysis, Data curation. Lisa Mahdi: Writing – original draft, Investigation, Formal analysis, Data curation. María Asunci´on Campanero-Rhodes: Writing – original draft, Investigation, Formal analysis, Data curation, Conceptualization. Rocco Di Girolamo: Writing – original draft, Methodology, Investigation, Formal analysis. Cristina Di Carluccio: Methodology, Investigation, Formal analysis. Roberta Marchetti: Writing – original draft, Investigation, Funding acquisition, Formal analysis. Antonio Molinaro: Methodology, Investigation, Formal analysis. Dolores Solís: Writing – original draft, Methodology, Funding acquisition, Formal analysis, Data curation. Alga Zuccaro: Writing – original draft, Investigation, Funding acquisition, Formal analysis, Data curation. Alba Silipo: Writing – review & editing, Writing – original draft, Supervision, Project administration, Investigation, Funding acquisition, Data curation, Conceptualization.

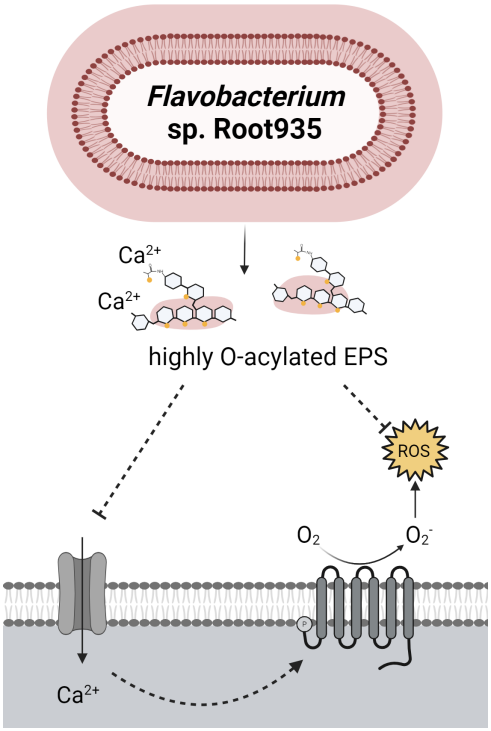

Carbohydrate Polymers 343 (2024) 122433

Contents lists available at ScienceDirect

Carbohydrate Polymers

journal homepage: www.elsevier.com/locate/carbpol

Structure and properties of the exopolysaccharide isolated from *Flavobacterium* sp. Root935

Marta Tiemblo-Martín [a], Valeria Pistorio [a,1], Pia Saake [b], Lisa Mahdi [b], María Asunción Campanero-Rhodes [c,d], Rocco Di Girolamo [a], Cristina Di Carluccio [a], Roberta Marchetti [a], Antonio Molinaro [a], Dolores Solís [c,d], Alga Zuccaro [b], Alba Silipo [a,*]

[a] Department of Chemical Sciences and Task Force for Microbiome Studies, University of Naples Federico II, Via Cinthia 4, 80126 Naples, Italy
[b] University of Cologne Cluster of Excellence on Plant Sciences (CEPLAS), Institute for Plant Sciences, D-50674 Cologne, Germany
[c] Instituto de Química Física Blas Cabrera, CSIC, Serrano 119, 28006 Madrid, Spain
[d] CIBER de Enfermedades Respiratorias (CIBERES), Avda Monforte de Lemos 3-5, 28029 Madrid, Spain

ARTICLE INFO

Keywords:
Exopolysaccharide (EPS)
Plant microbiota
Flavobacterium
Structure-function relationship
NMR

ABSTRACT

Flavobacterium strains exert a substantial influence on roots and leaves of plants. However, there is still limited understanding of how the specific interactions between *Flavobacterium* and their plant hosts are and how these bacteria thrive in this competitive environment. A crucial step in understanding *Flavobacterium* - plant interactions is to unravel the structure of bacterial envelope components and the molecular features that facilitate initial contact with the host environment. Here, we have revealed structure and properties of the exopolysaccharides (EPS) produced by *Flavobacterium* sp. Root935. Chemical analyses revealed a complex and interesting branched heptasaccharidic repeating unit, containing a variety of sugar moieties, including Rha, Fuc, GlcN, Fuc4N, Gal, Man and QuiN and an important and extended substitution pattern, including acetyl and lactyl groups. Additionally, conformational analysis using molecular dynamics simulation showed an extended hydrophobic interface and a distinctly elongated, left-handed helicoidal arrangement. Furthermore, properties of the saccharide chain, and likely the huge substitution pattern prevented interaction and recognition by host lectins and possessed a low immunogenic potential, highlighting a potential role of *Flavobacterium* sp. Root935 in plant-microbial crosstalk.

1. Introduction

The plant microbiota comprises an assorted community of microorganisms, including bacteria, viruses, fungi, protists and nematodes, and capable of thriving in various niches with plants. *Flavobacterium* sp. Root935 is a mesophilic, Gram-negative bacterium isolated from the roots of *Arabidopsis thaliana* ecotype Shakdara. Known for its ability to degrade complex organic compounds in diverse environments such as freshwater, marine, and soil, *Flavobacterium* is commonly identifiable by its characteristic yellow-orange colonies, attributed to carotenoid or flexirubin pigments (Bodenhausen et al., 2013; Bulgarelli et al., 2013). The family *Flavobacteriaceae*, along with other related families and taxa, is of a crucial importance in promoting plant growth and fitness by facilitating the mobilization of nutrients in the rhizosphere (Trivedi et al., 2020). Given these characteristics, there is growing interest in studying *Flavobacterium*, as harnessing beneficial bacteria for crop production could lead to more sustainable and environmentally friendly agricultural practices. Moreover, specific strains of *Flavobacterium*, if found to possess beneficial traits, could be utilized in biocontrol applications (Gunasinghe & Karunaratne, 2009; Kolton et al., 2014).

Despite *Flavobacterium* high capability to proliferate in root rhizosphere, little is known of mechanisms enabling their colonization of root surface, and consequently of their ability to proliferate and persist in such a competitive environment. Evasion or suppression of plant immune response is fundamental not only to pathogens to infect the host but also to commensals to variously colonize plant niches and establish symbiotic relationships. Nevertheless, mechanisms exploited i) by plant immune system to discriminate between advantageous and pathogenic species and ii) by beneficial microbes to evade plant recognition remain largely unknown.

* Corresponding author.
E-mail address: silipo@unina.it (A. Silipo).
[1] Present address: Centre de Recherche Saint Antoine (CRSA), Paris Ile-de-France, France

https://doi.org/10.1016/j.carbpol.2024.122433
Received 6 March 2024; Received in revised form 21 June 2024; Accepted 24 June 2024
Available online 26 June 2024

The initial steps of bacterial colonization are mediated by bacterial envelope components, including lipopolysaccharide (LPS) (Di Lorenzo et al., 2022, 2023), exopolysaccharide (EPS) (Vanacore, Forgione, et al., 2022) and adhesins. These bacteria-specific molecules, referred to as microbe-associated molecular patterns (MAMPs), undergo plant immune recognition through the action of pattern recognition receptors (Cook et al., 2015). In addition, EPSs, produced by both pathogenic and symbiotic bacteria during interaction with plants, have several functions, including sequestration of calcium ions, reactive oxygen species (ROS) scavenging, prevention of cellulose-mediated cell agglutination, tolerance to acidic pH, participation in biofilm formation, and host surface attachment (Laus et al., 2005; Lehman & Long, 2013; Vanacore, Forgione, et al., 2022; Wanke et al., 2021; Zipfel & Oldroyd, 2017). Interestingly, the immunosuppressive effect of EPSs occurs through the reduction of cytosolic calcium influx and the decrease of ROS generation, rather than through receptor-mediated signaling (Aslam et al., 2008).

Here we report on a comprehensive analysis of the structure, conformation, morphological characteristics and preliminary host recognition properties of the EPS isolated from *Flavobacterium* sp. Root935, member of the *Arabidopsis thaliana* root microbiota and isolated from roots of *Arabidopsis thaliana* ecotype Shakdara. To this aim we combined structural biology methodologies, NMR, biophysical and computational approaches, lectin microarray and preliminary immunological assays.

2. Material and methods

2.1. Bacteria isolation and growth

Flavobacterium sp. Root935 cells were grown in 10 l of succinate methanol medium at 28 °C, shaken at 150 rpm up to reach the end of the growth curve's exponential phase (4 days post inoculation). The cells were collected by centrifugation at 4000*g* for 30 min and the pellets lyophilized to produce approximately 8 g of dried cells.

2.2. Isolation, purification and compositional analysis of EPS from Flavobacterium sp. Root935

4 g of dried bacterial cells were extracted following the phenol/water procedure; the exopolysaccharide (EPS) was extracted in the phenol phase and further purified with enzymatic digestion with RNase (37 °C, Sigma-Aldrich, Darmstadt, Germany), DNase (37 °C, Sigma-Aldrich, Darmstadt, Germany), and Proteases (56 °C, Sigma-Aldrich, Darmstadt, Germany), ultracentrifugation (4 °C, 100,000 g, 16 h) and size-exclusion chromatography (Sephacryll S-100 column in ammonium bicarbonate 50 mM), with a final yield of 150 mg of EPS. An aliquot of EPS (30 mg) underwent a *O*-deacylation with ammonium hydroxide (2 mL, at 37 °C overnight). The monosaccharide content of the EPS was determined by analysis of the acetylated *O*-methyl glycoside derivatives, and the absolute configuration was defined by analysis of *O*-octylglycoside derivatives. Derivatization of sugar units in Partially Methylated Acetylated Alditols determined the substitution pattern of the saccharide units (details in the Supporting information section and in Di Lorenzo et al., 2022).

2.3. NMR spectroscopy

For structural assignments NMR spectra were recorded in D_2O at 298 K at pD 7 with a cryoprobe-equipped Bruker 600 AVANCE NEO. Total correlation spectroscopy (TOCSY), Rotating-frame Overhauser enhancement spectroscopy (ROESY), Nuclear Overhauser enhancement spectroscopy (NOESY) experiments were performed using data sets (t1 × t2) of 4096 × 800 points; Double-quantum-filtered phase-sensitive correlation spectroscopy (DQF-COSY) experiments were performed using data sets of 4096 × 912 points. Heteronuclear single-quantum coherence (HSQC) with multiplicity editing during the selection step. and Heteronuclear multiple-bond correlation (HMBC) experiments were performed using data sets of 2048 × 600 points. HMBC was optimized on long-range coupling constants (5–12 Hz), with a low-pass J filter to suppress one-bond correlations, using gradient pulses for selection. More details in the Supporting information section.

2.4. MM calculation and MD simulation

Maestro package (www.schrodinger.com/) was used to construct the adiabatic maps of OS (oligosaccharide) constituting disaccharides of *Flavobacterium* sp. Root935 EPS repeating unit, as a graphical representation of the conformational space of a glycosidic linkage. The map is generated by calculating the torsional angles of all possible conformations of the glycosidic linkage and plotting them on a 2D or 3D surface. MM3* forcefield, as included in MacroModel 8.0 was used, with a dielectric constant of 80, and extended nonbonded cut-off distances (a van der Waals cut-off of 8.0 % and an electrostatic cut-off of 20.0 %). AMBER 18 (Case, 2018) suite of programs were used to run MD simulations in explicit solvent. Parameters for non-standard residues (QuiN and substituted fucose), not included in the GLYCAM-web site, were generated by following a home-made protocol (manuscript in preparation) and used as building blocks to construct the OS repeating unit. Atom types and charges were assigned according to AMBER GLYCAM-06j-1 force field. The ligand was solvated in a periodic octahedral water box using the TIP3P model, containing water molecules 10 Å away from any atom, by using the LEaP module and also counter ions were added to neutralize the system. Sander and CUDA, which are distributed within the AMBER 18 package were used to minimize the system and to run MD simulations respectively. Further details in the supporting information section. MD simulation results were visualized with VMD molecular visualization program and analysed with the ptraj module included in the AMBER18 (Roe & Cheatham, 2013). Pymol 2.3 Sofware (https://pymol. org) and Discovery Studio Software were used to visualize and draw the molecules.

2.5. Scanning electron microscopy (SEM)

Field emission scanning electron microscope (SEM, FEI Nova NanoSEM450) was used to study the morphology of *Flavobacterium* sp. Root935 EPS. The sample was deposited on a carbon adhesive tab and then coated with a thin layer (5–7 nm) of gold-palladium alloy. The images were acquired at an accelerating voltage of 5 kV by collecting secondary electrons (SE) with an ETD detector.

2.6. Microarray binding assays

Flavobacterium sp. Root935 EPS and EPS_{deO} were printed as duplicates at six different concentrations (from 1 to 0.003 mg/ml) on 16-pad nitrocellulose-coated glass slides (Grace Biolabs ONCYTE NOVA) using a non-contact arrayer (Sprint, Arrayjet Ltd.), as described (details in the Supporting Information section). For testing the binding of human innate immune lectins, the arrays were overlaid with Fc- or His-tagged lectins at 20 μg/ml (tags, source of the lectins tested, and buffers used are listed in Tables S1-S2). After incubation for 1.5 h and subsequent washing steps, pads were incubated for 1 h with either biotinylated goat anti-human IgG antibody (Vector Labs, working dilution 1:10,000) or with mouse anti-His antibody pre-complexed with biotinylated goat anti-mouse IgG antibody (Sigma, final working dilutions 1:1000 and 3:1000, respectively), and then washed again 4 times with PBS. Finally, binding was monitored by incubation with AF647-streptavidin and scanning for AF647 signals, as above.

2.7. Plant cultivation

A. thaliana Col-0^{AEQ} seeds were surface sterilized with 70 % ethanol

for 10 min. RT, shaking at 900 rpm, followed by 7 min in 100 % ethanol at RT and shaking at 900 rpm. Afterwards, ethanol was discarded and seeds were dried in the sterile bench. Dry seeds were transferred to a 1/2 MS plate containing 1 % sucrose and stratified for 3 days in the dark at 4 °C. After germination, *Arabidopsis* seeds were transferred to the growth chamber with a day/night cycle of 16 h / 8 h (light intensity: 108 μmol m − 2 s − 1) and temperatures of 22 °C / 18 °C and cultivated for 7 days before being transferred to pots and grown for another 14 days for ROS assays or transferred to a 6-well plate containing 4 ml liquid ½ MS medium containing 1 % sucrose and grown for 5 more days.

2.8. ROS assay

Reactive oxygen species (ROS) are potent regulators of leaf development, here the leaf discs of the youngest adult leaf of 28 days old plants were transferred into white 96-well plates containing 200 μl water and incubated overnight in the growth chamber. On the next day, the water was exchanged for 100 μL of water containing 20 μM HRP and 20 μM L-012 (Sigma-Aldrich, Darmstadt, Germany). Following approx. 25 min incubation, 100 μL of two-fold concentrated elicitor solutions (or water mock control) were manually added to the wells. Measurements were started immediately and chemiluminescence was measured with an integration time of 450 msec using a TECAN SPARK 10 M microplate reader for 1 h. 1 mg/ml elicitor solutions were prepared and incubated for 4 h at 4 °C under gentle shaking before used in the assay.

2.9. Calcium assay

12 days old seedlings were transferred into white 96-well plates containing 200 μl water. Prior to overnight recovery in the dark, water was exchanged for 150 μl 10 μM coelenterazine solution. Next day, chemiluminescence was measured using a TECAN SPARK 10 M microplate plate reader. After the baseline measurement (5 min), 50 μL of four-fold concentrated elicitor solutions (or water mock control) were manually added to the wells after a baseline measurement for 5 min. Photon emission was constantly measured for 30 min. Over all selected wells. Subsequently, 100 μl of discharge solution (3 M $CaCl_2$ in 30 % EtOH) was injected into each well, followed by constant measurement for 1 min. All steps were performed with an integration time of 450 msec. In all assays, 2 columns (16 wells) were measured per run. 2 mg/ml elicitor solutions were prepared and incubated for 4 h at 4 °C under gentle shaking before used in the assay.

2.10. Preparation of Flavobacterium sp. Root935 pellet

Ten 100 ml ½ TSB (15 g/l) starter cultures were inoculated directly from the glycerol stock in a 250 ml Erlenmeyer flask and incubated ON at 28 °C, 120 rpm. On the next day, two cultures each were transferred into 5 l Erlenmeyer flask containing 1.8 l ½ TSB and incubated again ON at 28 °C, 110 rpm shaking. To harvest the bacterial cultures, 500 ml centrifuge bottles were filled with around 250–300 ml culture and centrifuged for 15 min at 4 °C, 5000 ×g. Supernatant was discarded and the procedure was repeated until all culture was pelleted. The pellets were washed two times with sterile milliQ water, and finally resuspended in milliQ water and transferred to 50 ml falcon tubes. Falcon tubes were centrifuged again at the 5000 ×*g*, 4 °C for 30 min. As much supernatant as possible was decanted. Samples were shockfrozen in liquid nitrogen and subsequently freeze-dried using a lyophilizer for about 74 h.

3. Results and discussion

3.1. Flavobacterium sp. Root935 EPS isolation and chemical analyses

Following the hot phenol-water extraction, *Flavobacterium* sp. Root935 exopolysaccharide (EPS) was isolated in the phenol phase and further purified by enzymatic treatments and gel filtration chromatography. Compositional and linkage analyses revealed the occurrence of terminal 4-amino-D-fucose (t-Fuc4N), 3-substituted L-rhamnose (3-Rha), 3,4-substituted D-glucosamine (3,4-GlcN), 3-substituted D-Galactose (3-Gal), 3-substituted D-Quinovosamine (3-QuiN), 3-substituted L-Fucose (3-Fuc), 6-substituted D-Mannose (6-Man) (Fig. S1B).

3.2. Flavobacterium sp. Root EPS structure determination and conformational analysis

3.2.1. NMR analysis EPS_{deO} and EPS

The high viscosity of the isolated EPS (Fig. 1 and S1D), ascribable to the extensive decoration of the glycan chain (see below), impaired a detailed NMR analysis on the intact saccharide chain. Therefore, a mild alkaline treatment was conducted to free the hydroxyl groups and increase solubility and tumbling in solution of *Flavobacterium* EPS (EPS_{deO}), that therefore underwent extensive NMR investigation (Speciale et al., 2022). The anomeric configuration of the monosaccharide units was assigned based on $^3J_{H1,H2}$ and $^1J_{C1,H1}$ coupling constants and confirmed by *intra*-residual NOE contacts; vicinal $^3J_{H,H}$ coupling constants and *intra* residual NOE contacts revealed the relative configuration of the sugar residues. Seven spin systems were identified (Figs. 1, S1 E-F, Table 1).

Residues A, D and F corresponded to *galacto* configured sugar units, as supported by $^3J_{H\text{-}3,H\text{-}4}$ and $^3J_{H\text{-}4,H\text{-}5}$ values below 1 Hz, both diagnostic of the equatorial orientation of H-4; their α-anomeric configuration was assigned by the $^1J_{CH}$ coupling constant value (above 170 Hz). Residue D matched with an α-Gal, while the scalar correlations of ring proton signals with a methyl group at position 6 allowed to identify residue F as an α-Fuc. Analogously, residue A was identified as an α-Fuc4N unit, according to the correlation of H-4 resonance to a nitrogen bearing carbon signal at 53.6 ppm, in turn bearing an N-lactyl residue (Fig. 1, Table 1). The *manno* configuration of residues B and G was established by $^3J_{H\text{-}1,H\text{-}2}$ and $^3J_{H\text{-}2,H\text{-}3}$, both below 2 Hz and diagnostic of the H-2 equatorial orientation. Residue G was identified as an α-Man while residue B was identified as a β-Rha, the anomeric configuration based on the $^1J_{CH}$ coupling constant value (160.0 Hz) and confirmed by the *intra*-residual NOE correlations between H-1 and H-3 and H-5. Residues C and E were identified as *gluco* configured sugar units, as indicated by the ring $^3J_{H,H}$ coupling constants (8–10 Hz). The *intra*-residual NOE contact of H-1 with H-3 and H-5, $^3J_{H1,H2}$ and $^1J_{CH}$ values were indicative of their β-anomeric configuration. Both residues C and E were identified as *N*-acetylated aminosugars, since in the HSQC spectrum H-2 resonance for both correlated to a nitrogen bearing carbon signal. Residue C matched with a β-GlcN sugar unit while residue E was identified as β-QuiN unit, as attested by the scalar correlations of ring protons to the methyl signal at position 6. The downfield shift of carbon resonances identified the following glycosylated positions: O-3 of B, D, E and F; O-3 and O-4 of C; and O-6 of G. Residue A was a terminal sugar unit. The *inter*-residual NOE contacts together with the long-range correlations derived from the HMBC spectrum (Fig. 1B), between A1 and B3; B1 and C4, E1 and C3; C1 and D3, D1 and G6, G1 and F3 and finally F1 and E3. The structure of EPS_{deO} is reported in Fig. S2.

Based on the structure obtained for the EPS_{deO}, the NMR spectra of intact EPS were evaluated and partially assigned in order to gain further information on the substitution pattern of this complex glycan chain. Therefore, the down-field shift of H-2 B and H-2 D and of the hydroxyl group of the lactyl residue were all diagnostic of *O*-acetylation at these positions (Table 1, Fig. S1D) and matched with *Flavobacterium* EPS structure as depicted in Fig. 2.

Molecular mechanics and dynamic simulations were employed to investigate the three-dimensional features of *Flavobacterium* sp. Root935 EPS. Initially, the conformational preferences of all the constituting disaccharide repeating units were determined by building their potential energy surfaces as a function of the glycosidic torsional angles Φ and

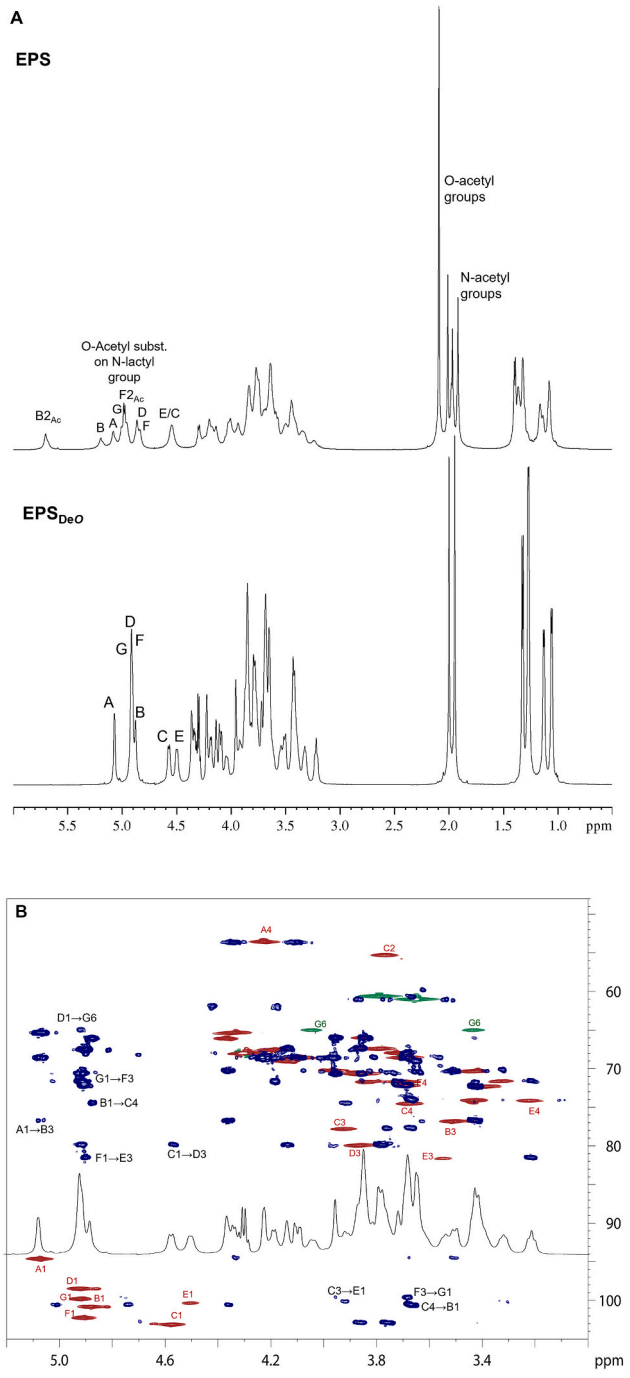

Fig. 1. A) DOSY NMR spectra of *Flavobacterium* sp. Root935 EPS and EPS_{deO}. B) Multiplicity edited HSQC (red and green) and HMBC (blue) NMR spectra of *Flavobacterium* sp. Root935 EPS_{deO}; the key *inter*-residual correlations were indicated; letters are as in Table S1.

Ψ. The calculated maps suggested that each disaccharide mainly adopted conformations according to the *exo*-anomeric orientation (Fig. S3). Subsequently, starting from the favorite global minima, a heptasaccharide fragment representing the EPS repeating unit was built and its conformational behavior was disclosed by using molecular dynamic simulations in explicit solvent with AMBER18. The results of the MD cluster analysis revealed that *Flavobacterium* EPS oligosaccharide adopted a defined Y-like shape, (Fig. 3A).

Modelling the structure of a longer *Flavobacterium* EPS, including three OS repeating units with two additional residues, one at the reducing- and one at the terminal- end, suggested that the polymer tends to adopt an extended conformation, characterized by a left-handed helicoidal structure, with 9 residues per turn and a pitch of around 31 Å. The Y-like arrangement found in the heptasaccharide fragment was maintained in the longer minimized polysaccharide (Figs. S3-S4). In addition, acetyl groups regularly surrounded the polymer backbone likely influencing the OS biophysical properties, and likely its interactions to the external environment (Figs. 3 and S4).

3.3. Morphological characterization via scanning electron microscopy (SEM)

Scanning electron microscopy (SEM) analysis of macromolecules represents a powerful tool to study surface morphology that can be correlated with microstructure of these materials. Many studies report the SEM morphological characterization of native *Flavobacterium* sp. Root935 EPS or other bacterial exopolysaccharides revealing shapes that include highly branched entangled porous structure, irregular highly porous spider web-like structure, morphologies with irregular lumps of different sizes, morphologies characterized by porous network structure with more uniform pore size distribution or compact, stiff and layer-like structure (Ayyash et al., 2020; Hu et al., 2020; Kansandee et al., 2019; Krishnamurthy et al., 2020; Prasanna et al., 2012).

Compared with the morphologies described above, the surface morphology of *Flavobacterium* EPS obtained by SEM analysis (Fig. 4) revealed a different shape, characterized by the presence of irregular flakes that reach lateral size up to 30–50 μm. This morphology can be due to presence of Y-like shape microstructure, in turn stabilized by *inter*-residual polar contacts and inter/intra-molecular hydrogen bonds that induce the formation of the large lamellae/flakes described above instead of filament networks. The morphology could be compatible with the high viscosity of EPS and its chemical nature, but rheological studies of these characteristics should be conducted.

3.4. Microarray assays and immunological studies

With the aim of evaluating lectin recognition of *Flavobacterium* sp. Root935 EPS and EPS_{deO}, these were printed onto microarray slides at a range of concentrations and two sets of binding assays were performed (Campanero-Rhodes et al., 2006, 2021). First, the binding of a panel of 41 model lectins with diverse carbohydrate-binding specificities (Table S1) was examined. As shown in Fig. 5, no meaningful binding signals to EPS and EPS_{deO} were observed, which can be ascribed to the particular structure and extensive decoration of the glycan chain, while the lectin-binding profile for control glycoproteins was the expected one (Vanacore, Vitiello, et al., 2022). Furthermore, the binding of 16 human innate immune lectins (Table S2) was examined, where different lectin-dependent signals were observed (Fig. 5). The lectin binding profile observed for *Flavobacterium* EPS was dominated by ficolins, innate immune receptors responsible for binding certain bacteria and opsonize them via the lectin pathway in mammals, in particular ficolin-1 (also called M-ficolin), followed by ficolin-2 (or L-ficolin) (Bidula et al., 2019). Recognition of GlcNAc, GalNAc, and various acetylated structures, including non-carbohydrate acetylated compounds as CysNAc, is a feature shared by all ficolins, although the architecture and even number of binding sites, and consequently their fine binding specificities, differ among the three lectins. Indeed, ficolin-1 is known to interact with sialic acid (in particular, 9-*O*-acetylated), ficolin-2 binds β-(1,3)-glucans and phosphocholine moieties of teichoic acids, and ficolin-3 recognizes Fuc.

Such differences in binding specificities may account, at least in part, for the different binding intensities here observed, and the extended *O*-acetylation pattern of *Flavobacterium* EPS might account for the high affinity toward Ficolin-1. In contrast, lectin binding profile observed for *Flavobacterium* EPS_{deO} depicted galectin-9 as dominant recognizing lectin (Solís et al., 2010). Although all galectins share galactoside-binding ability, their fine carbohydrate-binding specificity may differ

Table 1
^{1}H and ^{13}C NMR chemical shift values of *Flavobacterium* EPS_{deO}. Three further acetylated positions were identified in EPS and are annotated in italics.

Unit	1	2	3	4	5	6
A	5.07	3.69	4.10	4.22	4.34	1.05
t-α-Fuc4N	94.3	68.5	68.6	53.6	65.3	15.8
	$^{1}J_{C,H}$ = 173.4 Hz				N-lactyl residue CH_3-CHOH-C=O 1.32/20.4; 4.30/68.0; 178.5	
					Acetylated Lactyl residue in EPS: 4.98/70.34; 2.01/20.04	
B	4.88	4.36	3.50	3.42	3.39	1.28
3-β-Rha	100.4	66.1	76.6	70.2	72.2	16.7
	$^{1}J_{C,H}$ = 160.0 Hz					
	5.18/98.7	*5.69/67.5 in EPS, acetylated at O2; Acetyl group: 2.09/20.4*				
C	4.57	3.76	3.92	3.67	3.42	3.76/3.79
3,4-β-GlcN	102.8	55.4	77.7	74.4	73.9	60.6
	$^{1}J_{C,H}$ = 163.8 Hz	Acetyl CH_3-C=O 2.00/22.5; 173.8				
D	4.91	3.79	3.86	4.13	3.87	3.65
3-α-Gal	98.2	67.4	79.8	69.4	70.6	60.8
	$^{1}J_{C,H}$ = 172.5 Hz					
E	4.50	3.62	3.55	3.21	3.32	1.27
3-β-QuiN	100.1	56.5	81.5	74.0	71.6	17.2
	$^{1}J_{C,H}$ = 164.1 Hz	Acetyl CH_3-C=O 1.94/22.3; 173.8				
F	4.90	3.72	3.68	3.68	4.18	1.13
3-α-Fuc	102.0	68.0	72.1	71.6	67.5	15.3
	$^{1}J_{C,H}$ = 172.6 Hz					
	4.84/99.9	*4.98/67.4 in EPS, acetylated at O2; Acetyl group: 2.01/22.5*				
G	4.91	3.95	3.85	3.85	3.84	3.43
6-α-Man	99.4	70.2	71.6	66.0	65.9	64.8
	$^{1}J_{C,H}$ = 173.0 Hz					

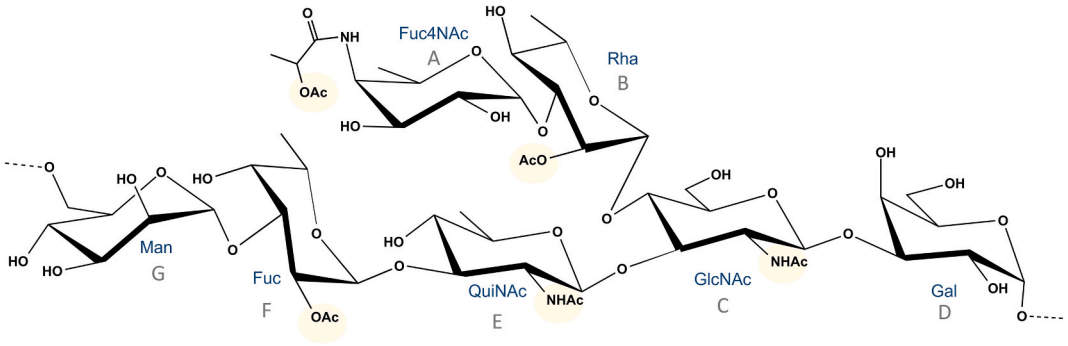

Fig. 2. The repeating unit of *Flavobacterium* sp. Root935 EPS structure.

significantly; this might explain why, among the tested, only galectin-9 recognized the epitope exposed after de-O-acylation in *Flavobacterium* EPS_{deO}.

To analyze the immunogenic potential of the natural EPS of *Flavobacterium* sp. Root935 and the impact of *O*-acylation, its ability to elicit early immune responses such as production of apoplastic reactive oxygen species (ROS) and cytosolic calcium influx in *Arabidopsis thaliana* was evaluated (see Fig. 6A). Whereas only low accumulation of ROS was observed with natural EPS, de-*O*-acylation resulted in significantly increased ROS accumulation in *Arabidopsis thaliana* leaves (see Fig. 6A), indicating that O-acylation reduces the lectin recognition of the EPS. Previously, we showed that *O*-acylation also reduced perception of LPS isolated from another member of the *Arabidopsis* microbiome, *Herbaspirillum* Root189 (Vanacore, Vitiello, et al., 2022). However, the ROS accumulation induced by de-*O*-acylated *Flavobacterium* sp. Root935 EPS was not as strong as with de-*O*-acylated *Herbaspirillum* Root189 LPS, suggesting a lower immunogenic potential for this carbohydrate structure. Furthermore, no cytosolic calcium influx was observed in *A. thaliana* leaves with either natural or de-O-acylated *Flavobacterium* sp. Root935 EPS (see Fig. 6B). In addition to EPS, lipooligosaccharide (LOS) isolated from *Flavobacterium* sp. Root935 was also tested, but did not induce ROS accumulation or calcium influx. The lack of cytosolic calcium influx in *A. thaliana* by *Flavobacterium* EPS indicates that it can sequester calcium ions and suppress calcium influx as was shown before for other EPS (Aslam et al., 2008), thereby leading to a weaker ROS response as compared to flg22 which induces both calcium influx and ROS accumulation in *A. thaliana*; conversely a significant ROS accumulation was observed with *Flavobacterium* EPS_{deO}.

4. Conclusion

Flavobacterium strains beneficially impact plant health and represent a significant fraction of root and leaf associated microbiomes in a broad range of plant species. Understanding how bacterial envelope glycans contribute to bacteria colonization, molecular features that mediate interactions with the host and allow bacteria to thrive in this competitive environment needs to be fully understood. Here, we revealed the chemical structure of the EPS produced by *Flavobacterium* sp. Root935, characterized by a branched, heptasaccharidic repeating unit, with an extended hydrophobic interface and an elongated, left-handed helicoidal arrangement that expose acetyl and lactic groups outward the saccharide chain, therefore tuning its properties and masking *Flavobacterium* sp. Root935 EPS to the host. The morphology was characterized by irregular flakes, which could be compatible with the high viscosity of EPS and its chemical nature, but rheological studies of these characteristics should be conducted. Furthermore, the related high intrinsic viscosity of *Flavobacterium* EPS could represent an opportunity to produce homogeneous films by solvent casting or other deposition

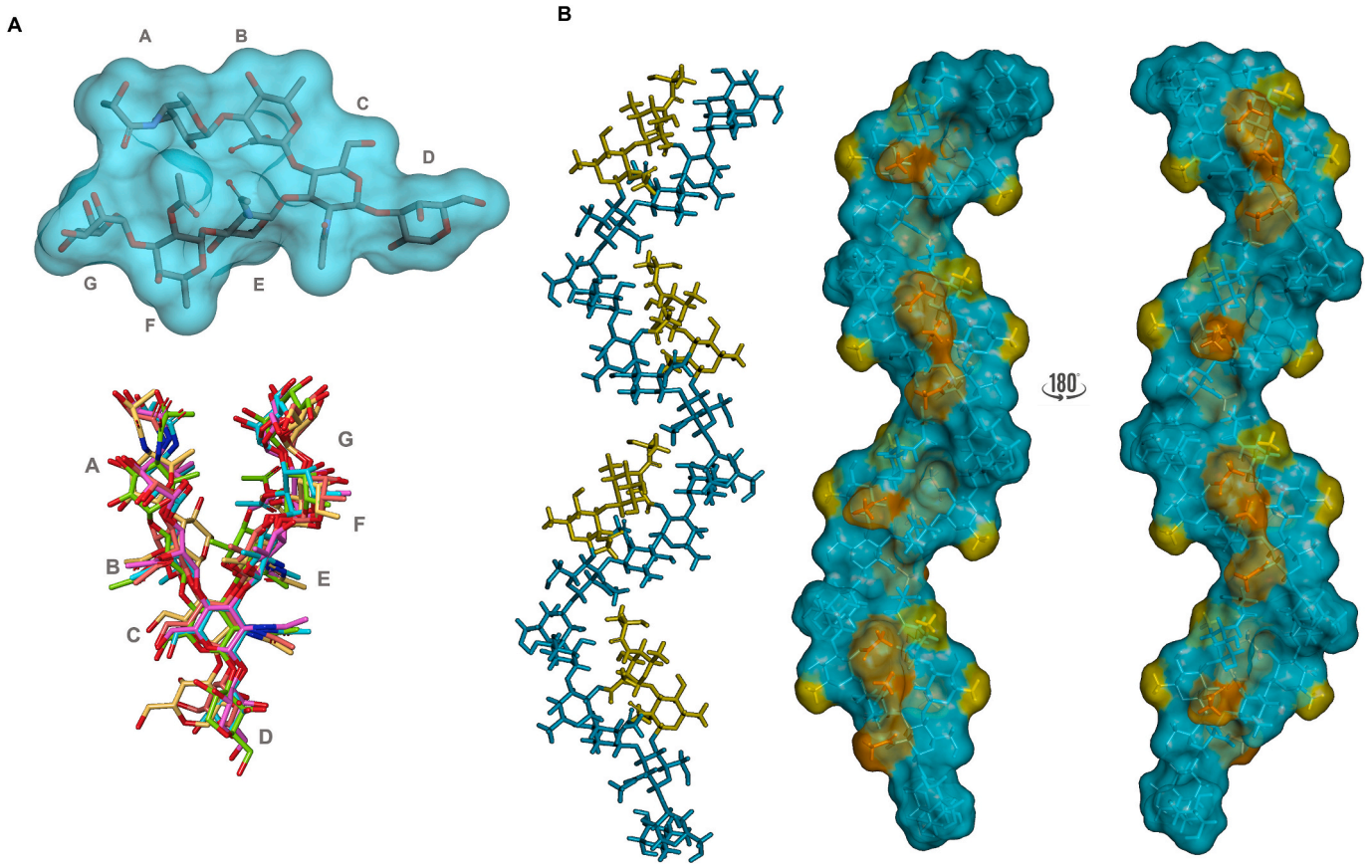

Fig. 3. Snapshots of *Flavobacterium* sp. Root935 oligosaccharide from simulated trajectories in explicit solvent with AMBER18. A) Superimposition of the main clusters from MD simulation on the heptasaccharide fragment representing the *Flavobacterium* sp. Root935 EPS repeating unit. B) 3D model of *Flavobacterium* sp. Root935 EPS, including four OS repeating units with two additional residues, one at the reducing- and one at the terminal- end. The extended conformation of *Flavobacterium* EPS is shown with the acetyl and methyl groups colored in orange and yellow, respectively.

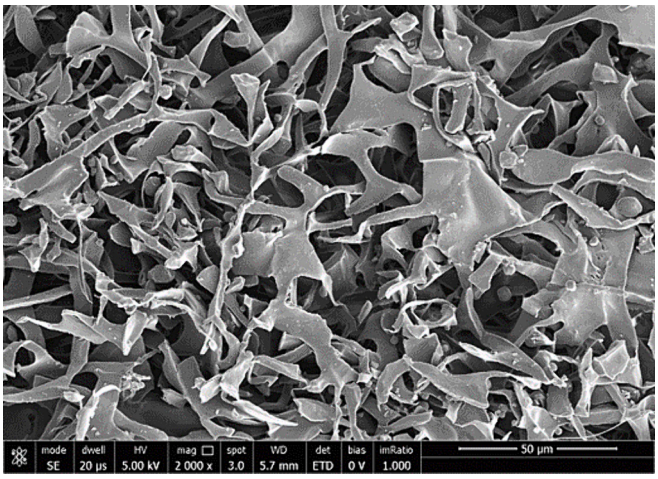

Fig. 4. Scanning electron micrograph (SEM) images of *Flavobacterium* sp. Root935 EPS.

techniques, which could be a good starting point to study its potential in the food and pharmaceutical industries. (Concórdio-Reis et al., 2022; Moradi et al., 2021).

Microarray binding assays revealed that most lectins had weak or negligible binding to *Flavobacterium* EPS, likely due to its complex structure and its decoration with multiple acetyl groups. Ficolins are known to bind to specific carbohydrate structures, and their interactions can provide insight into the structural composition of bacterial surfaces, including the presence of acetyl groups. Indeed, significant binding signals were almost exclusively restricted to the innate immune lectins ficolins 1 and 2, indicating the dominance of acetyl groups in lectin recognition. This highlights the importance of acetylation in masking eukaryotic recognition. Indeed, fully acetylated *Flavobacterium* EPS was a poor inducer of plant immune responses, differently from EPS_{deO}. The findings suggest that *Flavobacterium* EPS exerts a significant impact by suppressing the cytosolic calcium influx in *A. thaliana*, thereby affecting the plant immune response. This suppression is achieved through apoplastic calcium sequestration and reduction of subsequent signaling. This confirms previous observations in other plant associated bacterial species, like *Herbaspirillum*, *Rhizobia*, that indeed EPS acetylation acts as a shielding strategy, to tune immune recognition of the bacterial envelope by the plant immune system and mediate interactions with the host environment.

In conclusion, the study takes a multidisciplinary approach aimed at analyzing structure, properties, and immune recognition of *Flavobacterium* sp. Root935 EPS, to dissect the structure-to-function relationships of the active glycan constituents of *Flavobacterium*. This offers valuable information to harness the potential of beneficial bacteria and to exploit the unique characteristics of *Flavobacterium* for sustainable and environmentally friendly practices in plant-microbe interactions.

CRediT authorship contribution statement

Marta Tiemblo-Martín: Writing – original draft, Methodology, Investigation, Formal analysis, Data curation. **Valeria Pistorio:** Methodology, Investigation. **Pia Saake:** Writing – original draft,

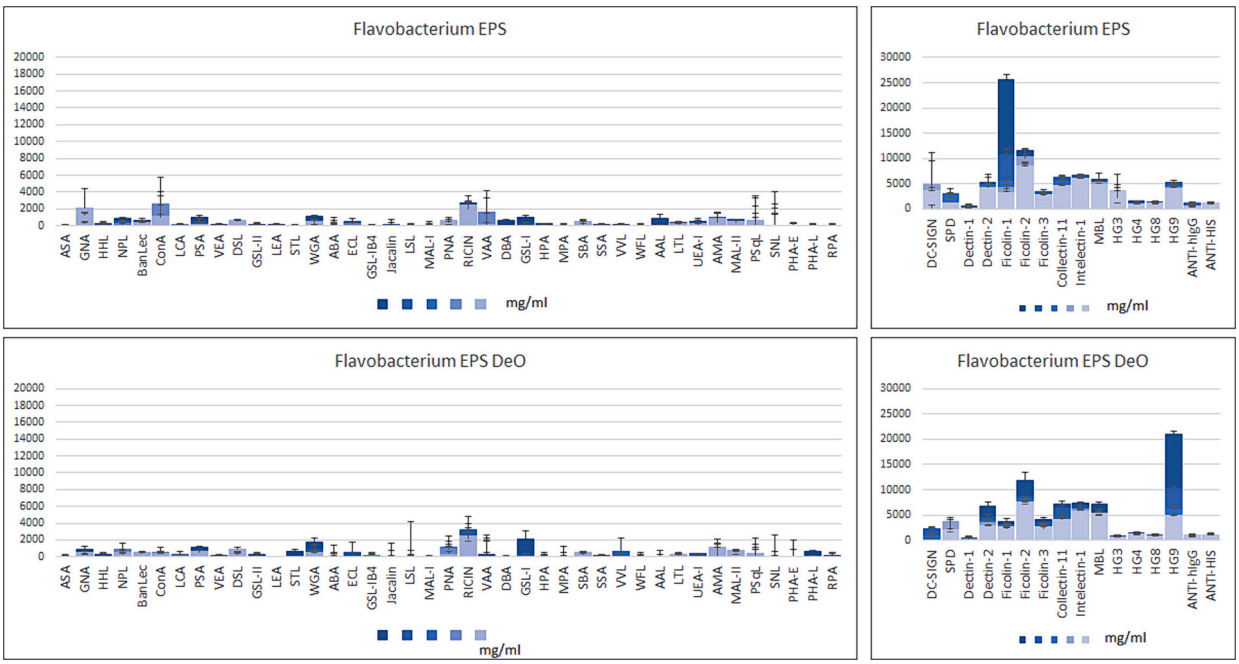

Fig. 5. Lectin binding to microarray-printed *Flavobacterium* sp. Root935 EPS and EPS_{deO}. The samples were printed as triplicates at different concentrations (highlighted from light to dark blue colors) and the binding of two different collections of lectins was assayed, using AF647-streptavidin for final detection. Left panels: Binding of biotin-labelled model lectins with diverse carbohydrate-binding specificities (see Table S1). Right panels: Binding of Fc- or His-tagged innate immune lectins (see Table S2). Blank experiments, in the absence of lectins, with biotinylated goat anti-human IgG antibody and with mouse anti-His antibody pre-complexed with biotinylated goat anti-mouse IgG antibody (see Materials and Methods) were run in parallel. Data shown correspond to the mean of the fluorescence signals obtained for samples printed at 1 (■), 0.3 (■), 0.1 (■), 0.03 (■) and 0.01 (■) mg ml^{-1} and error bars indicate the standard deviation of the mean.

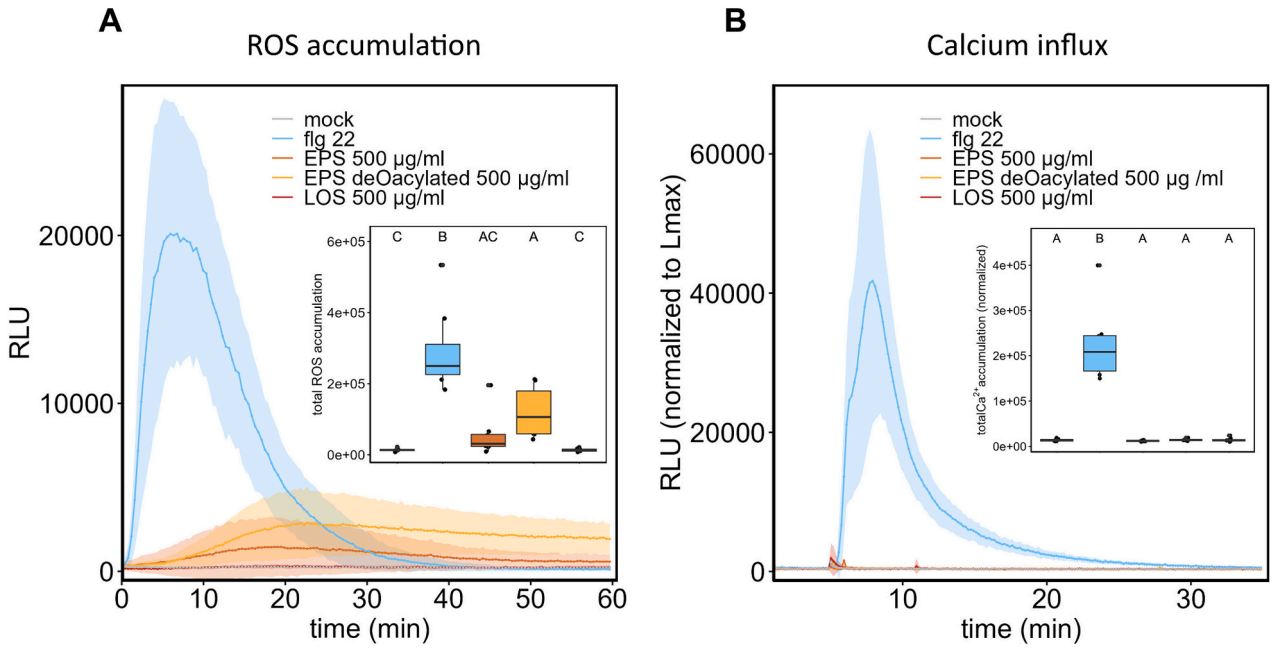

Fig. 6. ROS accumulation and calcium influx in *Arabidopsis thaliana* in response to *Flavobacterium* sp. Root935 EPS, LOS and de-O EPS. ROS accumulation and calcium influx in *Arabidopsis thaliana* in response to *Flavobacterium* sp. Root935 EPS, LOS and de-O EPS. Apoplastic ROS accumulation (A) and cytosolic calcium influx (B) after treatment of *A. thaliana* Col-0^{AEQ} leaf discs from 28-days old plants or 12 days old seedlings, respectively, with 500 µg/ml of LOS, EPS and de-O-acylated EPS. 2.5 mM MES pH 5.6 and 250 nM flg22 were used as negative and positive control, respectively. ROS accumulation was monitored via a luminol-based chemiluminescence assay. Ca^{2+} influx was monitored via a coelenterazine-based chemiluminescence assay. Values are normalized to maximum total luminescence induced by addition of discharge solution, representing the aequorin expression, for each replicate. Values represent mean ± SD from eight replicates. Boxplots display total ROS accumulation or calcium influx over the measured period of time. Different letters represent statistically significant differences in expression based on a one-way ANOVA and Tukey's post hoc test (significance threshold: $P \leq 0.05$). ROS, reactive oxygen species. RLU, relative luminescence units.

Investigation, Formal analysis, Data curation. **Lisa Mahdi:** Writing – original draft, Investigation, Formal analysis, Data curation. **María Asunción Campanero-Rhodes:** Writing – original draft, Investigation, Formal analysis, Data curation, Conceptualization. **Rocco Di Girolamo:** Writing – original draft, Methodology, Investigation, Formal analysis. **Cristina Di Carluccio:** Methodology, Investigation, Formal analysis. **Roberta Marchetti:** Writing – original draft, Investigation, Funding acquisition, Formal analysis. **Antonio Molinaro:** Methodology, Investigation, Formal analysis. **Dolores Solís:** Writing – original draft, Methodology, Funding acquisition, Formal analysis, Data curation. **Alga Zuccaro:** Writing – original draft, Investigation, Funding acquisition, Formal analysis, Data curation. **Alba Silipo:** Writing – review & editing, Writing – original draft, Supervision, Project administration, Investigation, Funding acquisition, Data curation, Conceptualization.

Declaration of competing interest

The authors declare that they have no known competing financial interests or personal relationships that could have appeared to influence the work reported in this paper.

Data availability

Data will be made available on request.

Acknowledgments

We gratefully acknowledge financial support from the Spanish Ministry of Science, Innovation, and Universities (RTI2018-099985-B-I00 and PID2022-143249OB-I00), and the CIBER of Respiratory Diseases (CIBERES), an initiative from the Spanish Institute of Health Carlos III (ISCIII). AS acknowledges PRIN MUR 2022 (2022ZEZS45) and PRIN MUR PNRR 2022 (P2022M457Z). AS and MTM acknowledge H2020-MSCA-ITN-2020 (contract n° 956758). RM acknowledges European Research Council (ERC) under the European Union's Horizon 2020 research and innovation program under grant agreement No 851356. AS and RM acknowledge PNRR, Missione 4 – Componente 2 – NextGenerationEU - Partenariato Esteso INF-ACT - One Health Basic and Translational Research Actions Addressing Unmet Needs on Emerging Infectious Diseases MUR: PE00000007. AZ, LM and PS acknowledge support from the Cluster of Excellence on Plant Sciences (CEPLAS) funded by the Deutsche Forschungsgemeinschaft (DFG, German Research Foundation) under Germany's Excellence Strategy–EXC 2048/1–Project ID: 390686111.

Appendix A. Supplementary data

Supplementary data to this article can be found online at https://doi.org/10.1016/j.carbpol.2024.122433.

References

Aslam, S. N., Newman, M. A., Erbs, G., Morrissey, K. L., Chinchilla, D., Boller, T., … Cooper, R. M. (2008). Bacterial polysaccharides suppress induced innate immunity by calcium chelation. *Current Biology, 18*(14), 1078–1083. https://doi.org/10.1016/j.cub.2008.06.061

Ayyash, M., Abu-Jdayil, B., Olaimat, A., Esposito, G., Itsaranuwat, P., Osaili, T., … Liu, S. Q. (2020). Physicochemical, bioactive and rheological properties of an exopolysaccharide produced by a probiotic Pediococcus pentosaceus M41. *Carbohydrate Polymers, 229*. https://doi.org/10.1016/j.carbpol.2019.115462

Bidula, S., Sexton, D. W., & Schelenz, S. (2019). Ficolins and the recognition of pathogenic microorganisms: An overview of the innate immune response and contribution of single nucleotide polymorphisms. In *, Vol. 2019. Journal of Immunology Research*. Hindawi Limited. https://doi.org/10.1155/2019/3205072.

Bodenhausen, N., Horton, M. W., & Bergelson, J. (2013). Bacterial communities associated with the leaves and the roots of Arabidopsis thaliana. *PLoS One, 8*(2). https://doi.org/10.1371/journal.pone.0056329

Bulgarelli, D., Schlaeppi, K., Spaepen, S., Van Themaat, E. V. L., & Schulze-Lefert, P. (2013). Structure and functions of the bacterial microbiota of plants. In. *Annual Review of Plant Biology, 64*, 807–838. https://doi.org/10.1146/annurev-arplant-050312-120106

Campanero-Rhodes, M. A., Childs, R. A., Kiso, M., Komba, S., Le Narvor, C., Warren, J., … Feizi, T. (2006). Carbohydrate microarrays reveal sulphation as a modulator of siglec binding. *Biochemical and Biophysical Research Communications, 344*(4), 1141–1146. https://doi.org/10.1016/j.bbrc.2006.03.223

Campanero-Rhodes, M. A., Kalograiaki, I., Euba, B., Llobet, E., Ardá, A., Jiménez-Barbero, J., … Solís, D. (2021). Exploration of galectin ligands displayed on gram-negative respiratory bacterial pathogens with different cell surface architectures. *Biomolecules, 11*(4). https://doi.org/10.3390/biom11040595

Case D.A, Ben-Shalom, I. Y., Brozell, S. R., Cerutti, D. S., Cheatham, T. E., & Cruzeiro, I. (n.d.). Amber 2018 Reference Manual Principal contributors to the current codes. http://ambermd.org/contributors.html.

Concórdio-Reis, P., Pereira, J. R., Alves, V. D., Nabais, A. R., Neves, L. A., Marques, A. C., … Freitas, F. (2022). Characterisation of films based on exopolysaccharides from Alteromonas strains isolated from French Polynesia marine environments. *Polymers, 14*(20). https://doi.org/10.3390/polym14204442

Cook, D. E., Mesarich, C. H., & Thomma, B. P. H. J. (2015). Understanding plant immunity as a surveillance system to detect invasion. In *, Vol. 53. Annual Review of Phytopathology* (pp. 541–563). Annual Reviews Inc.. https://doi.org/10.1146/annurev-phyto-080614-120114

Di Lorenzo, F., Duda, K. A., Lanzetta, R., Silipo, A., De Castro, C., & Molinaro, A. (2022). A journey from structure to function of bacterial lipopolysaccharides. In *, Vol. 122, Issue 20. Chemical reviews* (pp. 15767–15821). American Chemical Society. https://doi.org/10.1021/acs.chemrev.0c01321.

Di Lorenzo, F., Nicolardi, S., Marchetti, R., Vanacore, A., Gallucci, N., Duda, K., … Silipo, A. (2023). Expanding knowledge of methylotrophic capacity: Structure and properties of the rough-type lipopolysaccharide from Methylobacterium extorquens and its role on membrane resistance to methanol. *JACS Au, 3*(3), 929–942. https://doi.org/10.1021/jacsau.3c00025

Gunasinghe, W. K. R. N., & Karunaratne, A. M. (2009). Interactions of Colletotrichum musae and Lasiodiplodia theobromae and their biocontrol by Pantoea agglomerans and Flavobacterium sp. in expression of crown rot of "Embul" banana. *BioControl, 54*(4), 587–596. https://doi.org/10.1007/s10526-009-9210-4

Hu, X., Li, D., Qiao, Y., Wang, X., Zhang, Q., Zhao, W., & Huang, L. (2020). Purification, characterization and anticancer activities of exopolysaccharide produced by Rhodococcus erythropolis HX-2. *International Journal of Biological Macromolecules, 145*, 646–654. https://doi.org/10.1016/j.ijbiomac.2019.12.228

Kansandee, W., Moonmangmee, D., Moonmangmee, S., & Itsaranuwat, P. (2019). Characterization and Bifidobacterium sp. growth stimulation of exopolysaccharide produced by enterococcus faecalis EJRM152 isolated from human breast milk. *Carbohydrate Polymers, 206*, 102–109. https://doi.org/10.1016/j.carbpol.2018.10.117

Kolton, M., Frenkel, O., Elad, Y., & Cytryn, E. (2014). Potential role of flavobacterial gliding-motility and type IX secretion system complex in root colonization and plant defense. *Molecular Plant-Microbe Interactions, 27*(9), 1005–1013. https://doi.org/10.1094/MPMI-03-14-0067-R

Krishnamurthy, M., Jayaraman Uthaya, C., Thangavel, M., Annadurai, V., Rajendran, R., & Gurusamy, A. (2020). Optimization, compositional analysis, and characterization of exopolysaccharides produced by multi-metal resistant Bacillus cereus KMS3-1. *Carbohydrate Polymers, 227*. https://doi.org/10.1016/j.carbpol.2019.115369

Laus, M. C., Van Brussel, A. A. N., & Kijne, J. W. (2005). Role of cellulose fibrils and exopolysaccharides of rhizobium leguminosarum in attachment to and infection of Vicia sativa root hairs. */ 533. MPMI, 18*(6), 533–538. https://doi.org/10.1094/MPMI

Lehman, A. P., & Long, S. R. (2013). Exopolysaccharides from Sinorhizobium meliloti can protect against H2O2-dependent damage. *Journal of Bacteriology, 195*(23), 5362–5369. https://doi.org/10.1128/JB.00681-13

Moradi, M., Guimarães, J. T., & Sahin, S. (2021). Current applications of exopolysaccharides from lactic acid bacteria in the development of food active edible packaging. In *, Vol. 40. Current opinion in food science* (pp. 33–39). Elsevier Ltd.. https://doi.org/10.1016/j.cofs.2020.06.001

Prasanna, P. H. P., Bell, A., Grandison, A. S., & Charalampopoulos, D. (2012). Emulsifying, rheological and physicochemical properties of exopolysaccharide produced by Bifidobacterium longum subsp. infantis CCUG 52486 and Bifidobacterium infantis NCIMB 702205. *Carbohydrate Polymers, 90*(1), 533–540. https://doi.org/10.1016/j.carbpol.2012.05.075

Roe, D. R., & Cheatham, T. E. (2013). PTRAJ and CPPTRAJ: Software for processing and analysis of molecular dynamics trajectory data. *Journal of Chemical Theory and Computation, 9*(7), 3084–3095. https://doi.org/10.1021/ct400341p

Solís, D., Maté, M. J., Lohr, M., Ribeiro, J. P., López-Merino, L., André, S., … Gabius, H. J. (2010). N-domain of human adhesion/growth-regulatory galectin-9: Preference for distinct conformers and non-sialylated N-glycans and detection of ligand-induced structural changes in crystal and solution. *The International Journal of Biochemistry & Cell Biology, 42*, 1019–1029. https://doi.org/10.1016/j.biocel.2010.03.007

Speciale, I., Notaro, A., Garcia-Vello, P., Di Lorenzo, F., Armiento, S., Molinaro, A., … De Castro, C. (2022). Liquid-state NMR spectroscopy for complex carbohydrate structural analysis: A hitchhiker's guide. *Carbohydrate Polymers, 277*. https://doi.org/10.1016/j.carbpol.2021.118885

Trivedi, P., Leach, J. E., Tringe, S. G., Sa, T., & Singh, B. K. (2020). Plant–microbiome interactions: From community assembly to plant health. In *, Vol. 18, Issue 11. Nature Reviews Microbiology* (pp. 607–621). Nature Research https://doi.org/10.1038/s41579-020-0412-1.

Vanacore, A., Forgione, M. C., Cavasso, D., Nguyen, H. N. A., Molinaro, A., Saenz, J. P., … Silipo, A. (2022). Role of EPS in mitigation of plant abiotic stress: The case of

Methylobacterium extorquens PA1. *Carbohydrate Polymers, 295*. https://doi.org/10.1016/j.carbpol.2022.119863

Vanacore, A., Vitiello, G., Wanke, A., Cavasso, D., Clifton, L. A., Mahdi, L., … Silipo, A. (2022). Lipopolysaccharide O-antigen molecular and supramolecular modifications of plant root microbiota are pivotal for host recognition. *Carbohydrate Polymers, 277*. https://doi.org/10.1016/j.carbpol.2021.118839

Wanke, A., Malisic, M., Wawra, S., & Zuccaro, A. (2021). Unraveling the sugar code: The role of microbial extracellular glycans in plant-microbe interactions. In *, Vol. 72, Issue 1*. *Journal of Experimental Botany* (pp. 15–35). Oxford University Press. https://doi.org/10.1093/jxb/eraa414.

Zipfel, C., & Oldroyd, G. E. D. (2017). Plant signalling in symbiosis and immunity. In *, Vol. 543, Issue 7645*. *Nature* (pp. 328–336). Nature Publishing Group. https://doi.org/10.1038/nature22009.

Supporting information

The following Supporting Information is available for this article online:

- **Table S1:** Model lectins used in microarray binding assays.
- **Table S2:** Innate immune lectins.
- **Figure S1:** *Flavobacterium* sp. Root935 EPS SDS PAGE, linkage analysis and ^{1}H-NMR spectra.
- **Figure S2:** Structure of the repeating unit of *Flavobacterium* sp. Root935 EPS_{deO}.
- **Figure S3:** Adiabatic energy maps for the basic constituent disaccharides of EPS repeating unit.
- **Figure S4:** 3D model of *Flavobacterium* sp. Root935 EPS.

2.2 Fungi hijack a ubiquitous plant apoplastic endoglucanase to release a ROS scavenging β-glucan decasaccharide to subvert immune responses.

Chandrasekar, B.*, Wanke, A.*, Wawra, S.*, Saake, P., Mahdi, L., Charura, N., Neidert, M., Poschmann, G., Malisic, M., Thiele, M., Stuhler, K., Dama, M., Pauly, M., Zuccaro, A. (2022).
The Plant Cell. https://doi.org/10.1093/plcell/koac114

Author contributions

B.C., A.W., S.W., and A.Z. conceived the study. S.W. established the protocols for the CW and EPS matrix extraction and performed the proteomics of EPS, CW, and culture filtrates together with G.P. and K.S. B.C. performed carbohydrate analytics (glycosyl linkage analysis of EPS and CW, MALDI-TOF, purification of β-GD for 1H NMR, and ROS burst assay). A.W. performed DAB assays and gene expression analysis. A.W. and B.C. performed β-GD oxidation assays. A.W., S.W., **P.S.**, M.N., M.M., M.T., N.C. performed the ROS burst assays, EPS and CW preparations, and enzymatic digestions. L.M. performed the colonization assays. M.D. contributed to the ^{1}H NMR result interpretation. M.P. directed and supervised the carbohydrate analytics. A.Z. supervised the project, designed the experiments, and wrote the paper with contribution of all the authors.

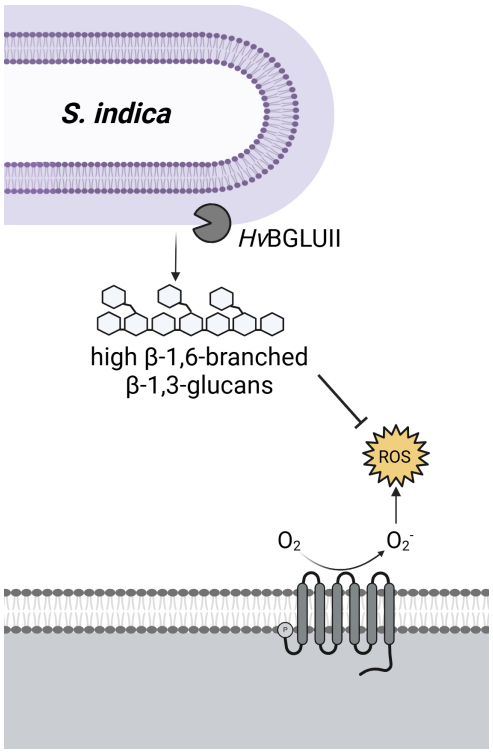

https://doi.org/10.1093/plcell/koac114

THE PLANT CELL

THE PLANT CELL 2022: 34: 2765–2784

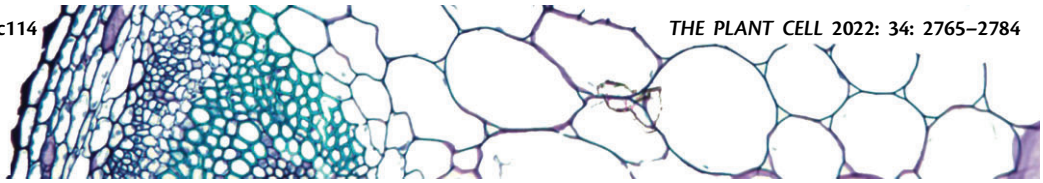

Research Article

Fungi hijack a ubiquitous plant apoplastic endoglucanase to release a ROS scavenging β-glucan decasaccharide to subvert immune responses

Balakumaran Chandrasekar ,[1,†] Alan Wanke ,[1,2] Stephan Wawra ,[1] Pia Saake ,[1] Lisa Mahdi ,[1,2] Nyasha Charura ,[1] Miriam Neidert ,[1] Gereon Poschmann ,[3] Milena Malisic ,[1] Meik Thiele ,[1] Kai Stühler,[4] Murali Dama ,[1] Markus Pauly [5] and Alga Zuccaro [1,*,‡]

1 Cluster of Excellence on Plant Sciences (CEPLAS), Institute for Plant Sciences, University of Cologne, 50679 Cologne, Germany
2 Max Planck Institute for Plant Breeding Research, 50829 Cologne, Germany
3 Institute of Molecular Medicine, Proteome Research, University Hospital and Medical Faculty, Heinrich-Heine University Düsseldorf, Universitätsstraße 1, 40225 Düsseldorf, Germany
4 Molecular Proteomics Laboratory, Biomedical Research Centre (BMFZ), Heinrich-Heine University Düsseldorf, Universitätsstraße 1, 40225 Düsseldorf, Germany
5 Institute of Plant Cell Biology and Biotechnology, Heinrich Heine University, 40225 Düsseldorf, Germany

*Author for correspondence: azuccaro@uni-koeln.de
These authors contributed equally (B.C., A.W. and S.W.).
†Present address: Department of Biological Sciences, Birla Institute of Technology & Science, Pilani (BITS Pilani), 333031, India.
‡Senior author.

B.C., A.W., S.W., and A.Z. conceived the study. S.W. established the protocols for the CW and EPS matrix extraction and performed the proteomics of EPS, CW, and culture filtrates together with G.P. and K.S. B.C. performed carbohydrate analytics (glycosyl linkage analysis of EPS and CW, MALDI-TOF, purification of β-GD for ^{1}H NMR, and ROS burst assay). A.W. performed DAB assays and gene expression analysis. A.W. and B.C. performed β-GD oxidation assays. A.W., S.W., P.S., M.N., M.M., M.T., N.C. performed the ROS burst assays, EPS and CW preparations, and enzymatic digestions. L.M. performed the colonization assays. M.D. contributed to the ^{1}H NMR result interpretation. M.P. directed and supervised the carbohydrate analytics. A.Z. supervised the project, designed the experiments, and wrote the paper with contribution of all the authors.

The author responsible for distribution of materials integral to the findings presented in this article in accordance with the policy described in the Instructions for Authors (https://academic.oup.com/plcell) is: Alga Zuccaro (azuccaro@uni-koeln.de).

Abstract

Plant pathogenic and beneficial fungi have evolved several strategies to evade immunity and cope with host-derived hydrolytic enzymes and oxidative stress in the apoplast, the extracellular space of plant tissues. Fungal hyphae are surrounded by an inner insoluble cell wall layer and an outer soluble extracellular polysaccharide (EPS) matrix. Here, we show by proteomics and glycomics that these two layers have distinct protein and carbohydrate signatures, and hence likely have different biological functions. The barley (*Hordeum vulgare*) β-1,3-endoglucanase *Hv*BGLUII, which belongs to the widely distributed apoplastic glycoside hydrolase 17 family (GH17), releases a conserved β-1,3;1,6-glucan decasaccharide (β-GD) from the EPS matrices of fungi with different lifestyles and taxonomic positions. This low molecular weight β-GD does not activate plant immunity, is resilient to further enzymatic hydrolysis by β-1,3-endoglucanases due to the presence of three β-1,6-linked glucose branches and can scavenge reactive oxygen species. Exogenous application of β-GD leads to enhanced fungal colonization in barley, confirming its role in the fungal counter-defensive strategy to subvert host immunity. Our data highlight the hitherto undescribed capacity of this often-overlooked EPS matrix from plant-associated fungi to act as an outer protective barrier important for fungal accommodation within the hostile environment at the apoplastic plant–microbe interface.

Received September 15, 2021. Accepted March 31, 2022. Advance access publication April 20, 2022

2766 | *THE PLANT CELL* 2022: 34; 2765–2784 Chandrasekar et al.

IN A NUTSHELL

Background: Plants secrete various hydrolytic enzymes into the apoplastic space to protect themselves against invading microbes. Some of these enzymes target the fungal cell wall polymer chitin. This enzymatic attack leads to the release of chitin oligomers, which can be perceived by the plant immune system, informing the plant to activate its defense machinery. However, chitin accounts for only a small part of most fungal cell walls. Recent studies have highlighted a largely uncharacterized, β-glucan-rich extracellular polysaccharide matrix (EPS) surrounding the cell wall of various plant-colonizing fungi.

Question: This EPS matrix is made of glucose and abundantly produced during colonization. As its secretion into the extracellular environment is costly for the fungus, we explored how this EPS matrix affects plant immunity and fungal colonization.

Findings: We demonstrated that EPS matrices from a symbiotic and pathogenic plant-colonizing fungus are distinct from the nonsoluble fungal cell walls with respect to their protein and carbohydrate composition. Enzymatic digests revealed that a secreted plant hydrolase from barley (*Hv*BGLUII) acts on these EPS matrices and releases a highly branched β-glucan decasaccharide (β-GD) fragment. This fragment is not perceived by the plant immune system but instead detoxifies reactive oxygen species produced by the plant host as a defense mechanism and contributes to host colonization. We thus have shown that the outermost fungal EPS layer represents a protective shield against oxidative stress.

Next steps: The diversity of linkage types and branching patterns of β-glucans not only accounts for their different biochemical properties, but also makes them important messengers for the plant, potentially encoding specific information on the approaching fungal invader. Future studies should aim to identify other plant hydrolases and the elusive glucan receptors, to disentangle the contribution of β-glucans to the communication between plant hosts and fungi.

Introduction

The fungal cell wall (CW) consists of repeatedly branched glycan polymers and proteins that adjust according to cell type, environmental conditions, and lifestyle phases (Geoghegan et al., 2017; Gow et al., 2017). The CW of animal pathogenic fungi is commonly surrounded by a soluble gel-like extracellular polysaccharide (EPS) matrix that can contain β-glucans, a heterogeneous group of glucose polymers (Gravelat et al., 2013; Gow et al., 2017; Kang et al., 2018). Commonly, fungal β-glucans have a structure comprising a main chain of β-1,3 and/or β-1,4-glucopyranosyl units, decorated by side-chains with various branches and lengths (Han et al., 2020). The immunomodulatory properties of β-glucans derived from animal pathogens have been long recognized (Goodridge et al., 2009). β-glucans exhibit a broad spectrum of biological activities and have a dual role with respect to host immunity that depends on their chemophysical characteristics. On the one hand, β-glucans are important microbe-associated molecular patterns (MAMPs) that are detected upon fungal colonization to trigger host immune responses in both vertebrates and invertebrates (Brown and Gordon, 2005). On the other hand, certain soluble β-glucans do not possess high immunogenic properties but are implicated in antioxidant activities and scavenging of reactive oxygen species (ROS; Han et al., 2020). Their immunological or antioxidant properties are rather complex and could be influenced by modifications in their structural characteristics such as molecular weight, substitution pattern, solubility, polymer charge, and conformation in solution (Han et al., 2020).

In plant–fungal interactions, carbohydrate metabolic processes mediated by carbohydrate-active enzymes (CAZymes) in the apoplast play a crucial role. Surface-exposed and accessible fungal polysaccharides are hydrolyzed by apoplastic CAZymes, such as chitinases and glucanases and the resulting oligosaccharides can act as elicitors to trigger a plant immune response known as pattern-triggered immunity (Silipo et al., 2010; Rovenich et al., 2016; Van Holle and Van Damme, 2018; Wanke et al., 2020, 2021; Buscaill and van der Hoorn, 2021; Ngou et al., 2021; Rebaque et al., 2021; Yuan et al., 2021). Recently, we described a soluble extracellular β-glucan matrix produced by endophytic fungi during root colonization of *Arabidopsis thaliana* (hereafter Arabidopsis) and *Hordeum vulgare* (hereafter barley; Wawra et al., 2019). Little is known about the biochemical properties, composition, and function of this EPS matrix, but its detection in beneficial and pathogenic fungi strongly suggests a conserved role in counteracting environmental and immunological challenges during fungal growth and plant colonization (El Oirdi et al., 2011; Mahdi et al., 2021; Wanke et al., 2021). It is therefore crucial to investigate the structure and function of these soluble β-glucans and the hydrolytic events

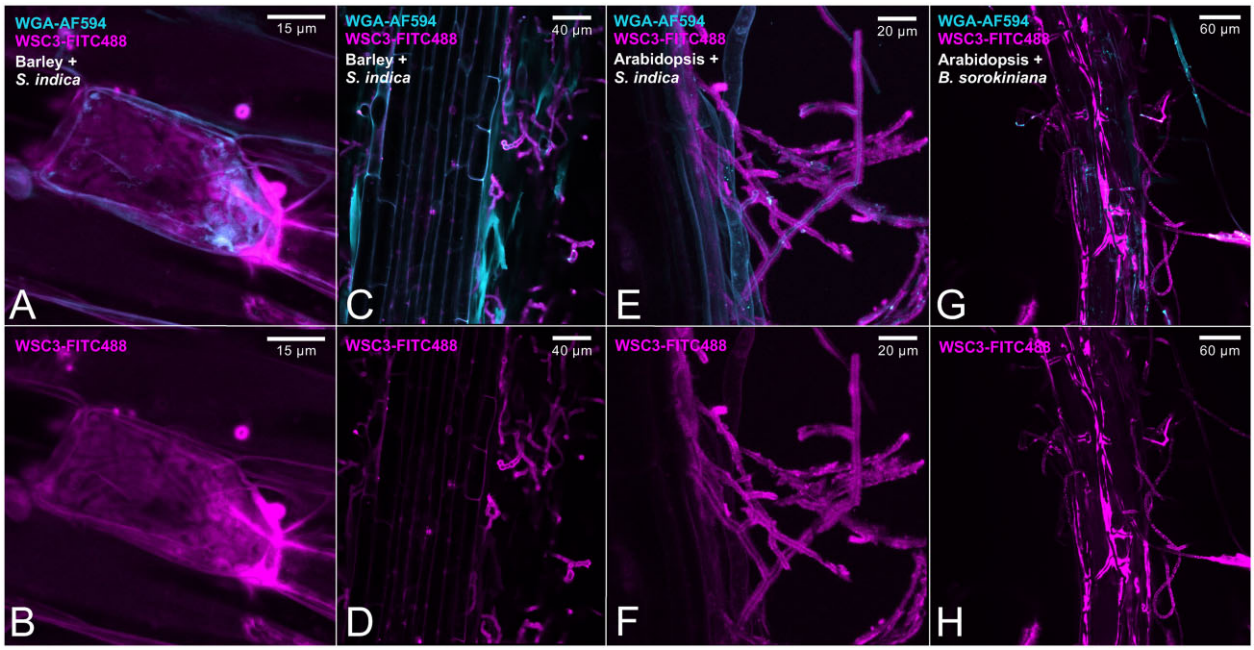

Figure 1 Fungal EPS matrix revealed by the fluorescently labeled β-glucan binding lectin *Si*WSC3-His-FITC488 during root colonization. The β-glucan-binding *Si*WSC3-His and the chitin-binding WGA lectins were used as molecular probes to visualize the fungal EPS matrix and CW of *S. indica* and *B. sorokiniana*, respectively. Magenta pseudocolor corresponds to FITC488-labeled *Si*WSC3-His. Cyan pseudocolor corresponds to WGA-AF594. (A), (C), (E), and (G) are merged confocal microscopy images of *Si*WSC3-His-FITC488 and WGA-AF594. (B), (D), (F), and (H) display the EPS matrix of *S. indica* or *B. sorokiniana* stained by *Si*WSC3-His-FITC488 during colonization of Arabidopsis or barley roots. (A) and (B) show *S. indica* intracellular colonization of a barley root cell with abundant production of the β-glucan EPS matrix. The microscopy was repeated at least 10 times with two independent *Si*WSC3-His-FITC488 batches and independent Arabidopsis or barley plants colonized by *S. indica* or *B. sorokiniana*. The fungal matrix was not a sporadic observation but regularly observed with both fungi. WGA, wheat germ agglutinin.

mediated by host apoplastic CAZymes during plant–fungal interactions. In this study, we have characterized the CW and the soluble EPS matrix produced by two distantly related fungi, the beneficial root endophyte *Serendipita indica* (Basidiomycota), and the pathogenic fungus *Bipolaris sorokiniana* (Ascomycota), separated by over 649 million years of evolution (Taylor and Berbee, 2006; Lutzoni et al., 2018). Proteomics and glycomics revealed that β-glucan-binding proteins with cell wall integrity and stress response component (WSC) domains and β-1,3;1,6-glucan polysaccharides are enriched in the soluble EPS matrix compared to the CW layer. Treatment of the fungal EPS matrices with the apoplastic barley β-1,3-endoglucanase *Hv*BGLUII released a β-1,3;1,6-glucan decasaccharide (β-GD) with a mass/charge (m/z) of 1661 Da. Proton nuclear magnetic resonance (^{1}H NMR) of β-GD is consistent with a heptameric β-1,3-glucan backbone substituted with three monomeric β-glucosyl residues at O-6. The β-GD is resilient to further enzymatic digestion by glycoside hydrolase 17 (GH17) family members and is immunologically inactive in a β-1,6-glucan side-branch-dependent manner. This low molecular weight soluble β-GD is able to efficiently scavenge ROS and to enhance colonization, corroborating its role as a previously undescribed fungal carbohydrate-class effector. The release of a conserved β-GD from the β-glucan-rich EPS matrix of a beneficial and a pathogenic fungus indicates that the utilization of this outermost soluble polysaccharide layer as a protective shield against oxidative stress and ROS-mediated host signaling is a common fungal strategy to withstand apoplastic defense responses during plant colonization.

Results

Beneficial and pathogenic fungi produce a gel-like β-glucan EPS matrix surrounding their CWs

We recently reported on a gel-like EPS matrix surrounding the hyphae of different fungi during colonization of plant hosts (Wawra et al., 2019; Wanke et al., 2021), suggesting that the secretion of soluble glycans is a common feature of plant-associated fungi independent of their lifestyle and taxonomy. This finding motivated us to investigate the biochemical characteristics, composition, and function of this matrix in the beneficial root endophyte *S. indica* and in the pathogenic fungus *B. sorokiniana*. To this end, we labeled the β-1,3-glucan-binding lectin PIIN_05825 (*Si*WSC3-His-FITC488) from *S. indica* by applying an improved FITC488 conjugation protocol (see "Materials and methods") and used it as a molecular probe for localization studies of the fungal EPS matrix in planta. *Si*WSC3-His-FITC488 signal accumulated around the wheat germ agglutinin-stained chitin layer in both fungi (Figure 1), strongly indicating that β-1,3-glucans are abundant in the outer EPS matrix. This expands the repertoire of fungal β-glucan-binding lectins that can be

used as molecular probes to fluorescently label the fungal EPS matrix during live cell imaging (Wawra et al., 2016).

The *S. indica* EPS matrix, CW, and culture filtrate represent three functionally distinct but interconnected compartments

To identify secreted proteins associated with the EPS matrix, the CW, and/or the culture filtrate, we performed quantitative proteomics with protein extracts from these three compartments from *S. indica* axenically grown in three different media (complete medium [CM], yeast-extract peptone dextrose [YPD], tryptic soy broth [TSB]; Supplemental Figure S1). We identified 1,724 proteins from all media and compartments (Supplemental Data Set S1; Figure 2A). Among those, 220 proteins carrying a predicted signal peptide were further analyzed for their domain architecture using the Pfam database (Supplemental Data Set S2; Figure 2A). Glucan-binding proteins with at least one WSC domain were more abundant or uniquely present in the EPS matrix compared to the CW (enrichment score 0.96, Benjamini–Hochberg corrected $P = 0.00003$) or the culture filtrate (enrichment score 0.6, Benjamini–Hochberg corrected $P = 0.02$), irrespective of the medium used (Figure 2B; Supplemental Figure S2 and Supplemental Data Set S3). Four of them, including *Si*WSC3 (PIIN_08474, PIIN_06786, PIIN_03979, and PIIN_05825), were among the most abundant proteins consistently found in this compartment (Figure 2B; Supplemental Figure S2), thereby confirming our in planta localization study (Figure 1). Gene expression analyses revealed an induction of these genes during *S. indica* colonization of barley and Arabidopsis over time (Wawra et al., 2019; Supplemental Figure S3). Additionally, several *S. indica* proteases and CAZymes were more abundant in the EPS matrix and culture filtrate compared to the CW (Supplemental Figure S2 and Supplemental Data Set S3), suggesting that the matrix may serve as a transient storage depot for these enzymes. In the CW fraction, we identified two chitin-binding LysM proteins (PIIN_02172 and PIIN_02169) and several other lectin-like proteins, including the β-1,6-glucan-binding effector *Si*FGB1 (Wawra et al., 2016; PIIN_03211) and the ricin B lectin (PIIN_01237). Most of these lectins were also present in the culture filtrate, indicating that besides their ability to bind to CW components, such as chitin and glucan, they also function as soluble lectins in the extracellular environment (Figure 2B; Supplemental Figure S2). This is in agreement with the function of *Si*FGB1, which has the potential to alter fungal CW composition and properties as well as suppress β-glucan-triggered immunity in the apoplast of different plant hosts (Wawra et al., 2016). Proteins containing cellulose-binding CBM_1 or starch-binding CBM_20 domains were found at higher abundances in the culture filtrate (Supplemental Figure S2). Based on the distribution and nature of the carbohydrate-binding proteins, we propose that the EPS matrix, the CW, and the culture filtrate represent three functionally distinct but interconnected compartments.

Serendipita indica EPS matrix and CW have different sugar compositions

The different amount of glycan-binding proteins within the EPS matrix and CW layer prompted us to investigate the glycan composition of these two compartments. Protein-free EPS matrix and CW preparations from *S. indica* grown in TSB medium were subjected to glycosyl linkage analysis for neutral sugars (Ciucanu, 2006; Liu et al., 2015). About 85% of the detected glycosidic linkages could be annotated based on the retention times and the mass spectra profile of the sugar residues (Supplemental Data Sets S4 and S5). Terminal glucose, 3-glucose, and 3,6-glucose were the dominant glycosidic linkages (∼35%) observed in the EPS matrix compared to other glycosidic sugar residues (Figure 2C; Supplemental Figure S4 and Supplemental Data Set S4). In contrast, in the CW fraction, 4-linked glucose was more abundant (∼45%, Figure 2C; Supplemental Figure S4 and Supplemental Data Set S5) than in the EPS matrix. Further analyses are required to clarify the type of glycosidic linkages that can be α-, β-, or mixed type.

Next, we treated the EPS matrix and CW with β-glucanases from *T. harzianum* (TLE) and *H. pomatia* and analyzed the digested products by thin-layer chromatography (TLC) and matrix-assisted laser desorption ionization time-of-flight mass (MALDI-TOF; Figure 3A). Several glucan fragments with various degrees of polymerization could be detected in the digested fraction confirming that β-glucans are present in both layers (Figure 3B; Supplemental Figure S5). Altogether, these data demonstrate that the EPS matrix and the CW of *S. indica* display major differences in the linkage compositions of their neutral sugars.

A β-glucan decasaccharide is released from the *S. indica* EPS matrix by a barley glucanase

We recently reported that several β-glucanases belonging to the GH17 family accumulate in the apoplast of barley roots during colonization by *S. indica* (Wawra et al., 2016). Among them, the β-glucanase *Hv*BGLUII (P15737) was consistently found at different colonization stages but also in mock-treated plants (Wawra et al., 2016; Supplemental Data Set S6), suggesting that this may be an ubiquitous apoplastic enzyme in root tissues. To investigate the activity of *Hv*BGLUII on the fungal CW and/or on the EPS matrix, we analyzed the digested fraction by TLC analysis after enzymatic incubation. Treatment of the EPS matrix with *Hv*BGLUII led to the release of a glucan fraction found at the sample origin spot that could not be further resolved under the TLC separation conditions used (Figure 3B). The corresponding band was not detected in the CW digestion (Figure 3B), indicating that *Hv*BGLUII is only active on the EPS matrix. Other β-1,3-glucanases (TLE and *H. pomatia* β-1,3-glucanase) were able to release oligosaccharides from both EPS and CW preparations, indicating that both preparations contain β-glucans

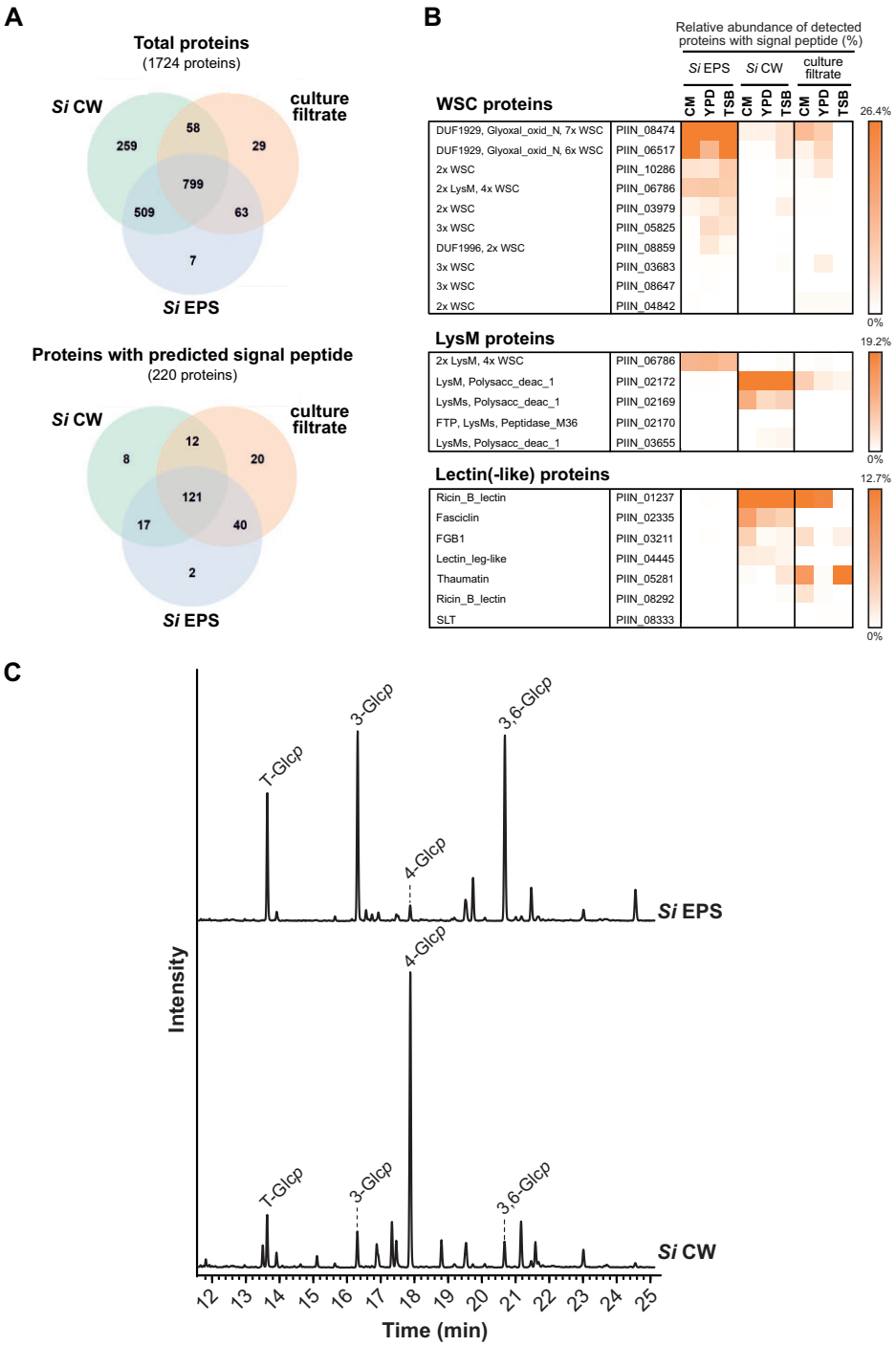

Figure 2 Proteomics and glycosyl linkage analysis of *S. indica* EPS matrix and CW. A, Venn diagram of proteins identified in the EPS matrix, CW, and/or culture filtrate from three cultivation media (CM, YPD, and TSB). B, Proteins with WSC domain/s show higher abundances in the EPS matrix of *S. indica* (see also Supplemental Figure S2 and Supplemental Data Sets S1, S2, and S3). The relative abundance of each protein was calculated using LFQ intensity values and is depicted in percentage. C, Glycosidic linkage analysis of *S. indica* EPS and CW preparations. 3-glucose and 3,6-glucose are abundant in the EPS matrix, whereas 4-glucose is abundant in the CW of *S. indica*. The experiment was performed with four independent biological replicates of *Si* EPS and *Si* CW and the TIC of one of the replicates is represented. TIC, total ion chromatogram; LysM, lysine motif; *p*, pyranose; *Si*, *Serendipita indica*.

that are enzyme accessible (Figure 3B; Supplemental Figure S5).

To further characterize the structure of the compound released by *Hv*BGLUII from the EPS matrix, we performed MALDI-TOF and glycosyl linkage analyses. An oligosaccharide with a *m/z* of 1,661 Da, corresponding to 10 hexoses (referred to as β-glucan decasaccharide [β-GD] fragment) with 3- and 3,6-linked glucoses was detected in high

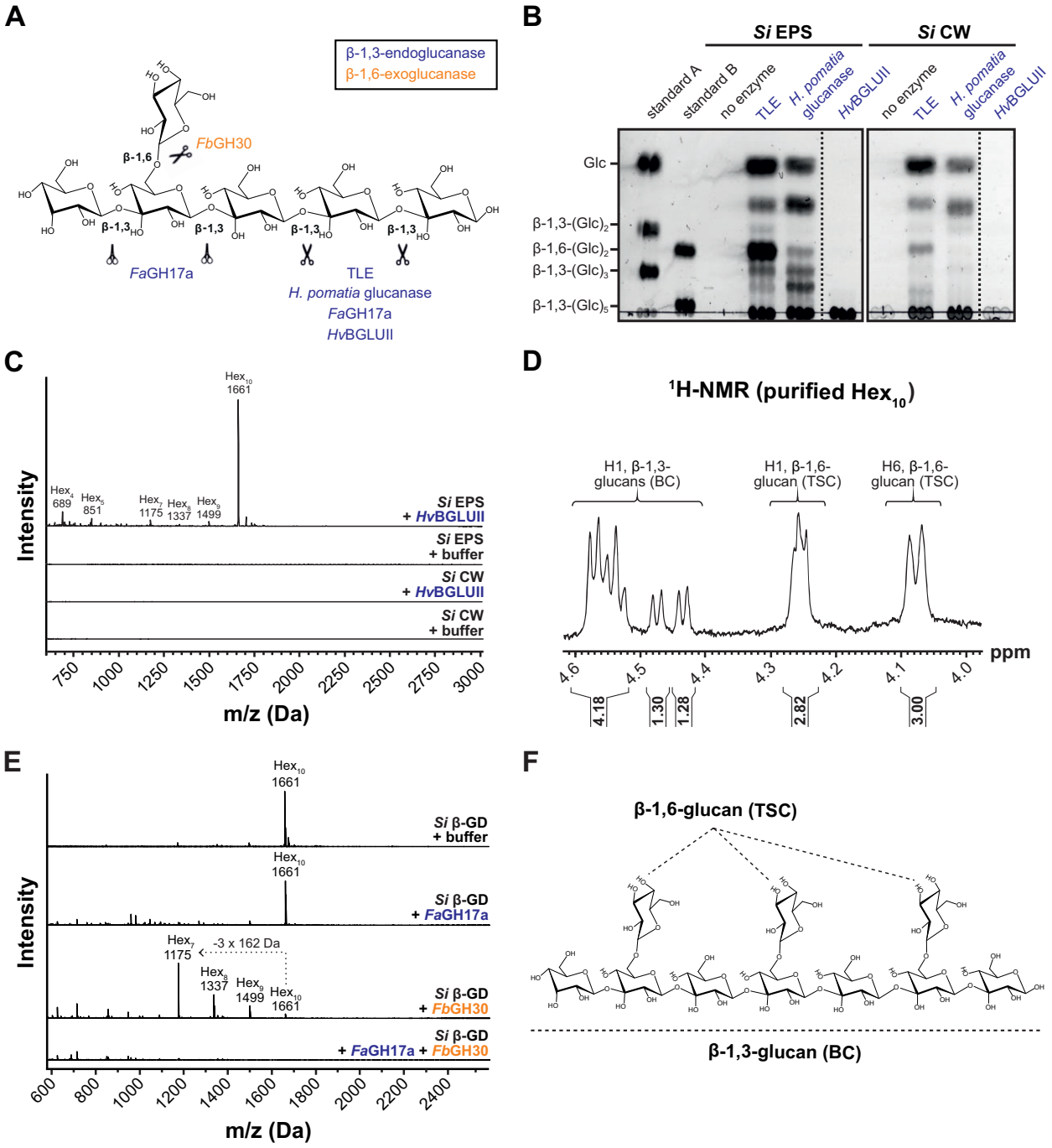

Figure 3 The β-1,3;1,6-glucan decasaccharide β-GD is released from the *S. indica* EPS matrix upon treatment with the barley apoplastic glycosyl hydrolase *Hv*BGLUII. A, Glycosyl hydrolases specific for β-1,3;1,6-glucans were used for the characterization of the EPS matrix, CW, and β-GD. The β-1,3-endoglucanases from *T. harzianum* (TLE) and *H. pomatia* as well as *Fa*GH17a and *Hv*BGLUII are shown as open scissors (in blue). *Fa*GH17a is represented as closed scissors because it does not hydrolyze glycosidic bonds of β-1,3-glucosyl residues substituted with β-1,6-glucosyl residues (in blue). *Fb*GH30 is a β-1,6-exoglucanase (in orange). B, Analysis of digested EPS matrix or CW fractions by TLC. Several glucan fragments with different lengths are released from the EPS matrix and CW by the action of TLE and *H. pomatia* β-1,3-glucanase. *Hv*BGLUII releases a glucan fraction from the β-glucan-containing EPS matrix but not from the CW. The experiment was repeated twice with *Si* EPS and *Si* CW isolated under different medium conditions (YPD and CM) and similar results were obtained. C, Analysis of digested EPS or CW fractions by MALDI-TOF mass spectrometry. The 1,661 Da β-GD corresponding to 10 hexoses is released from the EPS matrix but not from the CW of *S. indica*. The representative DP of hexoses is indicated on top of the *m/z* $(M + Na)^+$ masses of oligosaccharides. The digestion of *Si* EPS with *Hv*BGLUII was repeated independently more than three times with a similar result and the digestion of *Si* CW with *Hv*BGLUII was performed two times with a similar result. D, ^{1}H NMR spectrum of HPLC purified β-GD. E, Treatment of β-GD with various hydrolases followed by MALDI-TOF analysis of the products. The loss of three hexoses (−3 × 162 Da) as a result of treatment with *Fb*GH30 is indicated with a dotted arrow. The experiment was performed two times with a similar result. F, Structure of the β-GD based on the ^{1}H NMR spectrum. β-GD consists of a linear β-1,3-glucan backbone substituted with β-1,6-glucosyl moieties. *Si*, *Serendipita indica*; DP, degree of polymerization; Hex_n, oligosaccharides with the indicated hexose composition; BC, backbone chain; TSC, terminal side-chain.

abundance compared to other oligosaccharides with various degrees of polymerization (DP4–DP9, Figure 3C; Supplemental Figure S6A). Neither the β-GD nor the other oligosaccharides were detected in the supernatant of the digested CW preparation (Figure 3C), confirming the TLC result (Figure 3B). Furthermore, the β-GD was also released from the EPS matrix of *S. indica* grown in CM medium (Supplemental Figure S6B), suggesting that the growth conditions do not notably influence the release of the β-GD.

To further asses the structure of β-GD, the fragment was purified using reverse-phase chromatography (Supplemental Figure S7) and subjected to ^{1}H NMR spectroscopy (Figure 3D). ^{1}H NMR analysis displayed characteristic proton signals for β-1,3;1,6-glucan (Kim et al., 2000; Tada et al., 2009; Lowman et al., 2011). Since β-GD was reduced prior to the NMR analysis, only nine anomeric carbohydrate signals were present. The anomeric ^{1}H NMR signals of the six internal β-1,3-glucan backbone moieties were identified at 4.4–4.6 ppm (Figure 3D). They appear as a multiplet due to overlapping proton doublet signals at 4.5–4.6 ppm (four protons), a doublet at 4.48 ppm (J 7.8 Hz, one proton) representing the second glucose unit next to the reducing end and a doublet at 4.44 ppm (J 7.8 Hz, one proton) representing the non-reducing end of the oligosaccharide backbone. Anomeric NMR signals were also observed for the β-1,6-D-side-chain substituents at 4.26 ppm (three protons), indicating that the oligosaccharide contains three individual monomeric substituents. This is confirmed by the H6 NMR signal of β-1,6-D-glucose substituents at 4.08 ppm (three protons). In conclusion, the ^{1}H NMR analysis indicates that β-GD consists of seven β-1,3-linked D-glucose backbone units substituted with three terminal β-1,6-glucose units. The order of the substituents on the backbone could not be established by the NMR analysis performed here.

To validate the ^{1}H NMR results, we took advantage of the two well-characterized glycosyl hydrolases, *Fa*GH17a and *Fb*GH30 (Becker et al., 2017; Wanke et al., 2020). *Fa*GH17a is an endoglucanase specifically active on unsubstituted β-1,3-glucans and *Fb*GH30 is an exoglucanase specific for β-1,6-glycosidic linkages (Figure 3A). The β-GD was treated with *Fa*GH17a or *Fb*GH30 or a combination of the two enzymes and the digested samples were analyzed using MALDI-TOF mass spectrometry (Figure 3E). Digestion with *Fb*GH30 resulted in ion signals that represent the enzymatic removal of one (*m/z* 1,499), two (*m/z* 1,337), or most pronounced three glucosyl moieties (m/z 1,175), confirming the presence of three β-1,6-glucose units in β-GD. Digestion with *Fa*GH17a alone did not alter the molecular weight of β-GD indicating that potential enzyme hydrolysis sites are blocked by its side-chain substituents. In contrast, the combined treatment with both enzymes led to complete hydrolysis of the β-GD (Figure 3E). Taken together, these results demonstrate that the β-GD released from the EPS matrix by the action of *Hv*BGLUII is a decasaccharide with seven β-1,3-glucosyl units substituted with three β-1,6-glucosyl units as depicted in Figure 3F.

The apoplastic *Hv*BGLUII fosters MAMP-triggered immunity that is counteracted by the uncleavable β-GD

Since β-glucans represent an important class of microbial cell surface glycans able to trigger plant immune responses (Fesel and Zuccaro, 2016; Wanke et al., 2020), we performed ROS burst assays with *S. indica* CW and EPS matrix as well as with the enzymatically released β-GD to test their immunogenic potential on barley roots. Whereas the application of the fungal MAMP chitohexaose (positive control) triggered apoplastic ROS accumulation, incubation with *S. indica* CW and EPS matrix only marginally induced ROS accumulation (Supplemental Figure S8). Applications of the β-GD led to significantly lower ROS levels compared to the mock treatment (Figure 4A; Supplemental Figure S9). This prompted us to test the ability of this fragment to affect ROS levels during co-treatment with different MAMPs (Figure 4A; Supplemental Figures S10 and S11). The combined application of chitohexaose and β-GD led to a decreased accumulation of ROS with increasing concentrations of added β-GD (Figure 4A; Supplemental Figures S9 and S10). Combined digestion of the β-GD with the endoglucanases *Fa*GH17a and *Fb*GH30 restored the chitohexaose-triggered ROS burst (Figure 4B), thereby highlighting that the decreased accumulation of apoplastic ROS is linked to the presence of an—at least largely—intact β-GD. Impaired ROS accumulation was not observed with *S. indica* CW or EPS matrix preparations (Figure S8). Additionally, the application of the β-GD significantly reduced apoplastic ROS accumulation in barley roots treated with the β-1,3;1,6-glucan laminarin and in Arabidopsis seedlings treated with the flagellin-derived peptide flg22 (Supplemental Figure S11), substantiating a general function of the β-GD irrespective of plant species or elicitor.

To clarify whether the β-GD interferes with the MAMP perception machinery or detoxifies ROS, we tested its effect on further early and late immune responses triggered by chitohexaose. In barley, *HvWRKY2* has been demonstrated to act as a reliable marker for the onset of early immune responses among a wide range of elicitors applied to barley (Shen et al., 2007; Liu et al., 2014; Wanke et al., 2020). Despite the reduction of the oxidative burst, chitohexaose-triggered *HvWRKY2* expression was not reduced by the application of the β-GD (Figure 4C; Supplemental Figure S10C). This shows that the β-GD does not prevent MAMP perception but acts on the released ROS. Furthermore, treatment with the β-GD alone did not lead to a significant increase in *HvWRKY2* expression, supporting the notion that this β-glucan fragment does not exhibit an immunogenic

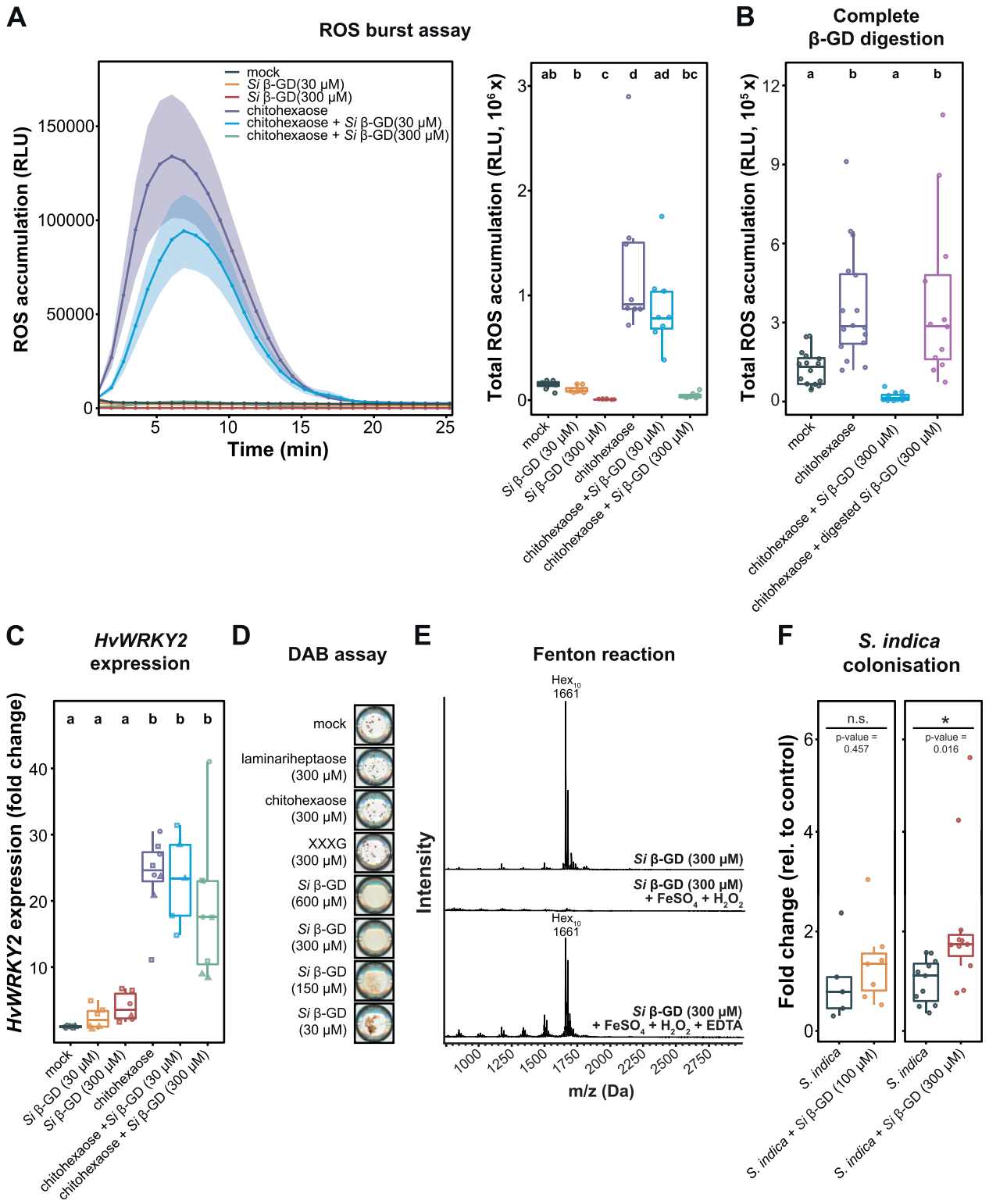

Figure 4 The β-GD released from *S. indica* EPS matrix scavenges ROS and enhances host colonization. A, Apoplastic ROS accumulation after treatment of barley roots of 8-day-old plants with 25-µM chitohexaose and/or purified β-GD from *S. indica*. ROS accumulation was monitored via a luminol-based chemiluminescence assay. Treatment with Milli-Q water was used as mock control. Boxplot represents total ROS accumulation over the measured time period. Values represent mean ± SEM from eight wells, each containing four root pieces. In total, roots from 16 individual barley plants were used per experiment. The assay was performed at least four times with independent β-GD preparations. Letters represent statistically significant differences in expression based on a one-way ANOVA and Tukey's post hoc test (significance threshold: $P \leqslant 0.05$). B, Prior to treatment of barley root pieces with the elicitors, β-GD was digested overnight (25°C, 500 rpm in heat block) with the glucanases *Fa*GH17a and *Fb*GH30, which led to complete digestion of β-GD (see also Figure 3E). As control, β-GD without the addition of enzymes (but instead with an equal volume of Milli-Q water) was treated similarly. Barley root pieces were treated with Milli-Q water (n = 16) and 25-µM

activity in barley roots. In support of this, treatments of Arabidopsis seedlings with β-GD did not induce rapid intracellular calcium fluxes (Supplemental Figure S12), an early hallmark of plant immune responses (Boller and Felix, 2009). These results are surprising due to the structural similarity of β-GD to laminarihexaose and laminarin, two potent ROS elicitors in different plant species, including barley and Arabidopsis (Wanke et al., 2020). Thus, the frequency and position of β-1,6-glucose substituents may define both their immunomodulatory potential as MAMP as well as their biochemical activity as ROS scavengers. To confirm this hypothesis, we treated laminariheptaose, the β-1,3-backbone of β-GD, with *Hv*BGLUII for 1 h or overnight and tested those preparations in ROS burst assays. Barley BGLUII was capable of digesting the laminariheptaose to glucose and laminaribiose (Supplemental Figure S13). The activity of *Hv*BGLUII on the laminariheptaose led to higher ROS accumulation compared to incubation with undigested laminariheptaose (Supplemental Figure S13). This demonstrates that *Hv*BGLUII is a host defense enzyme that releases potent MAMPs from unbranched β-1,3-glucan oligomers likely derived from the fungus (Figure 2C), playing a role in host glycan perception.

The β-GD scavenges apoplastic ROS

Numerous studies have highlighted the capability of sugars and specifically of β-glucans to act as ROS scavengers, contributing to the intracellular antioxidant system in different eukaryotes (Benaroudj et al., 2001; Nishizawa et al., 2008; Valluru and Van den Ende, 2008; Peshev et al., 2013; Lei et al., 2015; Boulos and Nystrom, 2017). To test whether the β-GD can directly act as an antioxidant, we performed an in vitro 3,3′-diaminobenzidine (DAB) assay. In the presence of hydrogen peroxide and horseradish peroxidase as catalyst, DAB is oxidized and polymerizes, ultimately leading to the formation of a brown, water-insoluble precipitate (Figure 4D). At low concentrations of β-GD (30–150 μM), DAB still oxidizes but forms less precipitates compared to the mock control. Formation of precipitates was completely inhibited at higher concentrations of β-GD (300–600 μM; Figure 4D). The inhibition of DAB precipitation can be explained by the ability of β-GD to scavenge ROS in a concentration dependent manner. Other CW-associated sugars such as chitohexaose, laminariheptaose, and a xyloglucan heptasaccharide (XXXG) did not interfere with DAB precipitation (Figure 4D). Mechanistically, nonenzymatic scavenging of hydroxyl radicals by sugars is based on their oxidation, which can lead to cleavage of glycosidic linkages and the formation of less reactive sugar radicals that further cross-react with themselves or other sugars (Matros et al., 2015). To validate if the oxidation of the decasaccharide contributes to ROS scavenging, we performed a Fenton reaction-based assay with the β-GD followed by MALDI-TOF analysis. In the presence of the Fenton reagents, the peak at 1,661 Da, corresponding to the β-GD, was no longer detected, suggesting that the fragment might have undergone oxidative degradation and/or have changed its chemo-physical properties by the activity of hydroxyl radicals produced by the Fenton reaction (Figure 4E). The oxidative degradation of the β-GD could be rescued in the presence of ethylenediaminetetraacetic acid (EDTA), which chelates the catalytic iron involved in the formation of hydroxyl radicals. Complete degradation was not observed for the structurally related laminariheptaose, chitohexaose, and XXXG (Supplemental Figure S14). Altogether, these results demonstrate that the activity of *Hv*BGLUII on the *S. indica* EPS matrix does not release a MAMP that initiates plant defense responses, but a fragment that can detoxify apoplastic ROS possibly via oxidative degradation. These results highlight a hitherto undescribed function of the fungal EPS matrix as a protective layer to mitigate oxidative stress during plant–microbe interaction.

To explore whether the β-GD can facilitate root colonization during early interaction, we performed colonization assays on barley roots in the presence of various β-GD concentrations (Figure 4F). The addition of β-GD slightly

Figure 4 (continued)
chitohexaose alone (n = 16) or in combination with digested or undigested β-GD (300 μM, n = 12). The experiment was performed twice with similar results. Statistically significant differences are indicated by different letters based on a one-way ANOVA and Tukey's post hoc test (significance threshold: $P \leqslant 0.05$). C, Barley root pieces were collected 1 h after elicitor treatment and further processed for RNA extraction and cDNA synthesis. Expression changes of the elicitor-responsive gene *HvWRKY2* were analyzed by RT-qPCR. Fold change expression were calculated by normalization to housekeeping gene expression (*HvUBI*) and mock treatment. Data from three independent experiments are indicated by different dot shapes. Letters represent statistically significant differences in expression based on two-way ANOVA (additive model, treatment + experiment) and Tukey's post hoc test (significance threshold: $P \leqslant 0.05$). Significant differences were associated with different treatments (F = 11.629, $P = 1.58 \times 10^{-6}$), but not with independent experiments (F = 2.227, P = 0.124). D, The capability of different carbohydrates to prevent hydrogen peroxide-based and horseradish peroxidase-catalyzed oxidation and precipitation of DAB was monitored. Respective sugars (or Milli-Q water as mock control) were pre-incubated with 1-mM H_2O_2 and 0.05-μM horseradish peroxidase before DAB (50 μM) was added. Scans of wells from 96-well plates were performed 16 h after DAB addition. The experiment was performed three times with similar results. E, Oxidative degradation of *S. indica* EPS matrix-derived β-GD (300 μM) by H_2O_2 was detected with an overnight Fenton reaction (1-mM H_2O_2, 100-μM $FeSO_4$) followed by MALDI-TOF mass spectroscopic analysis. As controls, either sugar alone or the samples supplemented with 100-μM EDTA were used. F, Colonization of barley roots by *S. indica* upon daily application of sterile Milli-Q water (mock) or β-GD (100 or 300 μM). Fungal colonization in each biological replicate was assessed by RT-qPCR comparing the expression of the fungal housekeeping gene *SiTEF* and the plant gene *HvUBI* (n = 5–11). Boxplot elements in this figure: center line, median; box limits, upper and lower quartiles; whiskers, 1.5× interquartile range. Statistical significance was determined on the nontransformed values (before normalization to *S. indica* control treatment) using a two-tailed Student's t test (*$P \leqslant 0.05$). *Si*, *Serendipita indica*; RLU, relative light units; XXXG, xyloglucan heptasaccharide.

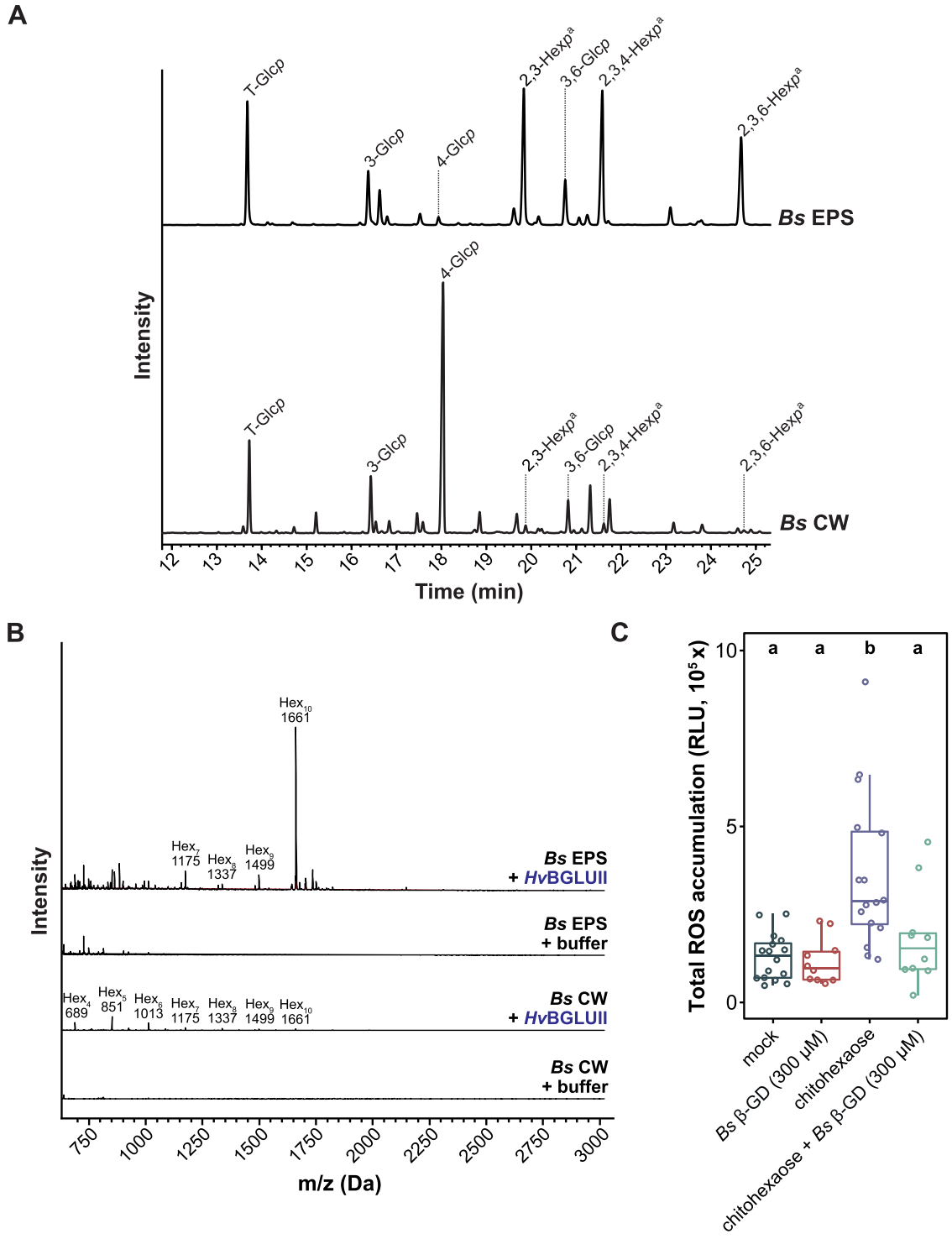

Figure 5 The β-GD derived from the hydrolysis of *B. sorokiniana* EPS matrix exhibits antioxidative properties. A, Glycosidic linkage analysis of *B. sorokiniana* EPS matrix and CW preparations. 2,3-hexopyranose, 2,3,4- hexopyranose, and 2,3,6- hexopyranose are abundant in the EPS matrix, whereas 4-glucose is abundant in the CW of *B. sorokiniana*. The experiment was performed with three independent biological replicates of *Bs* EPS and *Bs* CW and the TIC from one of the replicates is represented. B, Analysis of digested EPS or CW fractions by MALDI-TOF mass spectrometry. The 1,661-Da β-GD corresponding to 10 hexoses is released from the EPS matrix but not from the CW of *B. sorokiniana*. The representative DP of hexoses is indicated on top of the *m/z* $(M + Na)^+$ masses of oligosaccharides. The digestion of *Bs* EPS with *Hv*BGLUII was repeated independently three times with a similar result and the digestion of *Bs* CW with *Hv*BGLUII was performed once. C, ROS burst assay was performed on barley roots treated with Milli-Q water (mock), chitohexaose (25 μM), *Bs* β-GD (300 μM), or a combination of chitohexaose and *Bs* β-GD. Boxplots represent total cumulative ROS accumulation over a measured time interval of 25 min. Each data point in the boxplot represents the integrated value from an individual well (center line, median; box limits, upper and lower quartiles; whiskers, 1.5× interquartile range). The experiment was performed three times with similar results. Statistically significant differences are indicated by different letters based on a one-way ANOVA and Tukey's post hoc test (significance threshold: $P \leqslant 0.05$). *Bs*, *Bipolaris sorokiniana*; DP, degree of polymerization; *p*, pyranose. [a]exact sugar moiety unknown; overrepresentation of linkages due to undermethylation cannot be excluded.

increased colonization at 100 μM and led to an on average 2.15-fold increase of fungal colonization at 300 μM after 3 days post inoculation (dpi). This demonstrates that an EPS matrix-resident decasaccharide that is released by a plant glucanase can act as a carbohydrate-class effector enhancing fungal colonization.

The antioxidative properties of the β-GD are conserved among pathogenic and beneficial fungi

To clarify whether the observed properties of the β-GD are conserved among fungi with different lifestyles and taxonomic positions, we performed glycosyl linkage analysis of the CW and EPS matrix of *B. sorokiniana* grown in YPD medium. As observed for *S. indica*, the relative abundance of 4-linked glucose in the *B. sorokiniana* CW was higher compared to other sugar residues (Figure 5A; Supplemental Figure S15 and Supplemental Data Set S7). In the *B. sorokiniana* EPS matrix, 3-glucose and 3,6-glucose represented only a minor fraction (∼10%) compared to 2,3-hexose, 2,3,4-hexose, and 2,3,6-hexose (∼40%) and this is different from the EPS matrix of *S. indica* (Figure 5A; Supplemental Figure S15 and Supplemental Data Set S8). However, the presence of 3- and 3,6-linked glucose suggests that β-glucans with similar structures to *S. indica* glucans are also present in the EPS matrix of *B. sorokiniana*. Indeed several glucan fragments with various degrees of polymerization (DP3–DP10) could be release from digestion with the TLE but not from the buffer control (Supplemental Figure S16), indicating that β-glucans are present in the EPS matrix.

Since *Hv*BGLUII was detected in the apoplastic fluid of *B. sorokiniana* challenged barley roots and the gene is highly induced during *B. sorokiniana* root colonization (Supplemental Data Sets S6 and S9), we investigated whether *Hv*BGLUII can also release oligosaccharides from the *B. sorokiniana* EPS matrix. We detected a 1,661 Da fragment in high abundance representing a decasaccharide (Figure 5B). To characterize the structure of the 1,661 Da fragment from *B. sorokiniana*, we incubated it with *Fa*GH17a or *Fb*GH30 or a combination of the two enzymes. MALDI-TOF analysis revealed that this fragment has the same digestion profile and thus most likely the same structure as *S. indica* β-GD (Supplemental Figure S17), demonstrating that β-GD is conserved among distantly related fungi.

Next, to investigate the immunogenic properties of *B. sorokiniana* β-GD, we tested it in ROS burst assays using barley roots. Consistent with the data obtained from *S. indica*, the enzymatically released *B. sorokiniana* β-GD, but not crude EPS matrix or CW preparations, displayed a decrease in ROS accumulation when co-applied with chitohexaose (Figure 5C; Supplemental Figure S18). Collectively, our results indicate that the antioxidative property of the β-GD is a common feature among plant-associated fungi.

Discussion

Fungi synthetize and secrete a wide range of glycans, which are crucial determinants of microbe–microbe and microbe–host interactions. Despite variations in glycan structures and composition of the CW and the surrounding EPS matrix between fungal species, β-glucans are generally the most abundant and complex structural components. Their recognition by host receptors activates immune responses, such as accumulation of ROS and CAZymes in the extracellular apoplastic space, which hamper host colonization (El Oirdi et al., 2011; Wanke et al., 2020, 2021; Rebaque et al., 2021). In order to overcome or bypass such responses, fungi employ different extracellular strategies (Buscaill and van der Hoorn, 2021). Common fungal countermeasures to prevent recognition and hydrolysis of their surface exposed glycans involve converting, depleting or masking highly immunoactive CW components. Although effective, these countermeasures may not always be employed because some of these glycan structures mediate important processes that are beneficial to the fungus. This explains why some glycan structures are highly conserved and cannot be extensively modified. Thus, fungi have additionally evolved apoplastic glycan-binding effector proteins that either sequester immunoactive CW-derived elicitors from the apoplast to prevent their recognition or shield them from hydrolysis. Additionally, fungi secrete CAZyme inhibitors and proteases that cleave host hydrolytic enzymes (Ham et al., 1997; Rovenich et al., 2016; Rocafort et al., 2020). Less is known about fungal cytoplasmic effector proteins targeting the disruption of glycan signaling inside plant cells.

Here, we identified a previously undescribed extracellular fungal counterdefensive strategy to subvert host immunity that involves the hijacking of widely distributed plant apoplastic endoglucanases to release a conserved β-1,3;1,6-glucan decasaccharide with ROS scavenging properties from the extracellular polysaccharide matrix of different fungi (Figure 6). Several classes of plant proteins, called pathogenesis-related (PR) proteins, are induced in response to fungal colonization. Among these proteins the family of PR-2 proteins, which are β-1,3-endo-type glucanases, is long known (Stintzi et al., 1993; Leubner-Metzger and Meins, 1999). In seed plants, β-1,3-glucanases are widely distributed, highly regulated and abundant in the apoplast or vacuoles. Besides their role in the plant response to microbial pathogens and wounding, these enzymes are also implicated in diverse physiological and developmental processes in the uninfected plant. The GH17 family member BGLUII is present in the apoplast of uninfected and infected barley roots and highly induced upon challenge with the pathogen *B. sorokiniana*. The activity of BGLUII on the fungal EPS matrix indicates that its substrate is available/exposed in this layer, the first physical site of contact with the plant defense components. The released β-GD is not immunoactive in barley and Arabidopsis and has some specific properties, which include resilience to further digestion by GH17 family members as well as ROS scavenging abilities. These properties seem to depend on the presence of β-1,6-linked glucosyl substituents. In fact, the structurally related laminariheptaose, which has the same structure as the backbone of β-

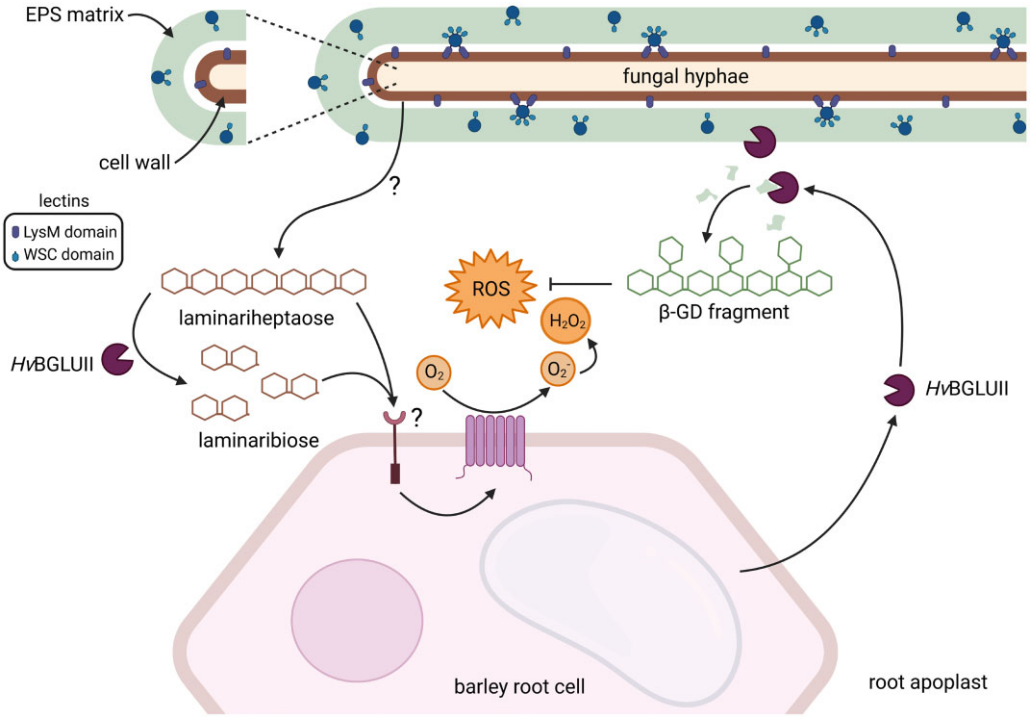

Figure 6 Model for the production and function of the conserved fungal EPS-derived β-1,3;1,6-glucan decasaccharide. The fungal-responsive GH17 family member *Hv*BGLUII is found in the apoplast of barley roots and acts on β-1,3-glucan. Digestion of linear β-1,3-glucan (laminariheptaose) with *Hv*BGLUII enhances ROS accumulation in barley roots, corroborating its role as a host defense enzyme with a function in β-glucan perception. To counteract the activity of *Hv*BGLUII, plant-colonizing fungi produce a β-1,3;1,6-glucan-rich EPS matrix. The activity of *Hv*BGLUII on the EPS matrix releases a conserved β-GD, which is resilient to further digestion by GH17 family members. The β-GD acts as a carbohydrate-class effector by scavenging ROS and enhancing fungal colonization. Lectins containing WSC domains are enriched in the outer EPS matrix and lectins containing LsyM domains are enriched in the CW of *S. indica*. Graphical illustration was designed with the BioRender online tool.

GD, is highly sensitive to digestion by *Hv*BGLUII and other GH17 family members, is immunoactive in barley, is not significantly degraded/modified in the Fenton reaction and does not display ROS scavenging capabilities (Figure 4D; Supplemental Figures S13 and S14). The removal of the side-branches from the β-GD by a microbial-derived β-1,6-glucanase makes it sensitive to further digestion by GH17 family members, confirming the protective effect displayed by the side-branches. In planta, the β-GD most likely corresponds to a host glucanase-resistant structure because plants are not known to produce β-1,6-glucanases (Fliegmann et al., 2004; Nars et al., 2013).

Additionally, the branching frequency might also be crucial for the immunomodulating activities of β-glucans. In animal systems, glucans are sensed by the well-characterized receptor Dectin-1. The minimal glucan subunit structure for Dectin-1 activation is a β-1,3-glucan oligosaccharide containing a backbone with at least seven glucose subunits and a single β-1,6-linked side-chain branch at the nonreducing end (Adams et al., 2008). We recently have shown that in plants β-1,3-glucan oligomers are perceived in a host species and length-dependent manner. While the monocots barley and *Brachypodium distachyon* can recognize longer (laminarin) and shorter (laminarihexaose) β-1,3-glucans with responses of varying intensity, duration and timing, the dicot *Nicotiana benthamiana* activates immunity in response to long β-1,3-glucans, whereas Arabidopsis and *Capsella rubella* perceive short β-1,3-glucans. The hydrolysis of the β-1,6 side-branches of laminarin did not affect recognition, demonstrating that not the glycosidic decoration but rather the degree of polymerization plays a pivotal role in the recognition of long-chain β-glucans in plants. Our data do not unambiguously demonstrate the glucosyl position of the substituents on the heptasaccharide backbone of the β-GD, but a possible explanation to the observed differences between the immune properties of laminarin (1:10 branching) and the β-GD (1:2.3 branching) might be that in barley roots β-glucans with a higher degree of branching could stereochemically interfere with each other, leading to less binding by specific receptors. It could well be that the β-GD has different immune properties depending on the plant species and this requires further investigation. However, here we show that upon incubation of β-GD with two unrelated plant species, Arabidopsis and barley, no accumulation of ROS was detected. It should also be mentioned that the antioxidant value of β-GD seems to be strictly "single use" and the β-GD pool may be easily depleted in planta. Nevertheless, a temporary dampening of the oxidative burst may be all that is required to support colonization and/or hamper ROS signaling. The immunomodulatory properties of the β-GD resemble those of

fungal effector proteins, suggesting that carbohydrate-class effectors also play an important role in fungal accommodation.

In conclusion, our data demonstrate that the fungal EPS matrix is a source of soluble β-glucans that leads to ROS scavenging properties important for host colonization and represents a distinct outer fungal layer with well-defined protein and carbohydrate signatures. B-glucans can form complex higher order structures depending on the conformation of sugar residues, molecular weight, inter- and intra-chain hydrogen bonding, and environmental conditions—all effecting their properties. This is different to the immune perception of the MAMP chitin, which is solely based on the length of the released oligomers by, for instance, the activity of chitinases. In plants, β-glucans are considered "orphan MAMPs" as their direct immune receptors have so far not been unambiguously identified. One of the remaining challenges is to fully elucidate the β-glucans' functions and receptors. Information on the structure, solubility, molecular weight, side-chain branching frequency, and conformation is of paramount importance and should be provided in studies dealing with fungal β-glucans and their effects on the plant immune system.

Materials and methods

Biological assays were performed with barley (*H. vulgare* L. cv Golden Promise) and *A. thaliana* Col-0 or aequorin-expressing Col-0 lines (Choi et al., 2014). Barley seeds were surface sterilized with 6% bleach for 1 h, followed by five washing steps with 30 mL of sterile Milli-Q water (each 30 min, two quick rinses for a couple of seconds between longer incubation steps). Sterilized seeds were germinated for 3 days on wet filter paper at room temperature in the dark under sterile conditions. Seedlings were transferred to sterile jars containing solid 1/10 plant nutrition medium (PNM), 0.4% gelrite (Duchefa, Haarlem, the Netherlands) Lahrmann et al., 2013) and cultivated in a growth chamber with a day/night cycle of 16 h/8 h (light intensity, 108 µmol m^{-2} s^{-1}) and temperatures of 22°C/18°C. Seedlings were grown for 4 more days before being used for immunity assays.

Arabidopsis seeds were surface sterilized (10 min 70% ethanol, 7 min 100% ethanol) and sown on half-strength Murashige and Skoog (MS) medium (pH 5.7) supplemented with 0.5% sucrose and 0.4% Gelrite (Duchefa, Haarlem, the Netherlands). Plates were transferred to climate chambers with 8-h/16-h light/dark regime (light intensity of 110 µmol m^{-2} s^{-1}) at 22°C/18°C. Seven-day-old seedlings were transferred into petri dishes filled with 30-mL fresh half-strength MS liquid medium and grown for 7 additional days under the same conditions.

Commercial enzymes

The commercial β-glucanases used in this study are the *Trichoderma harzianum* lysing enzymes (TLE, Sigma L1412), the *Helix pomatia* β-1,3-glucanase (Sigma 67138) and the *H. vulgare* β-1,3-endoglucanase (GH17 family *Hv*BGLUII, E-LAMHV in 50% (v/v) glycerol, Megazyme). TLE or *H. pomatia* β-1,3-glucanase were prepared in a stock concentration of 1.25 mg·mL^{-1} in respective buffers: TLE (2-mM sodium acetate, pH 5.0), *H. pomatia* β-1,3-glucanase (2-mM MES, pH 5.0). The GH17A family β-1,3-endoglucanase from *Formosa agariphila* (*Fa*GH17a) and the GH30 family β-1,6-exoglucanase from *Formosa* sp. nov strain Hel1_33_131 (*Fb*GH30) were obtained from Prof. Dr Jan-Hendrik Hehemann (Center for Marine Environmental Sciences, University of Bremen, Germany) at a concentration of 5 µg·mL^{-1} in water (Becker et al., 2017). For testing residual glycogen, α-amylase (E-BAASS, Megazyme) was prepared in a stock concentration of 1.25 mg·mL^{-1} using 50% (v/v) glycerol.

FITC488 labeling and confocal microscopy

FITC488 labeling of *Si*WSC3 and *Si*FGB1 and confocal laser scanning microscopy was done as described previously (Wawra et al., 2019) using the KPL SureLink Fluorescein-X (FAM-X) labeling kit (#82-00-02) by Sera Care with the following modification for *Si*WSC3 labeling: 20-min incubation time at 20°C with half of the recommended concentration. The reaction was stopped by adding 1-M TRIS (pH 7.5) to a final concentration of 50 mM and then dialyzed overnight against 3 L of Milli-Q water. Modifications to the standard labeling protocol were necessary because over labeling reduced the ability of the *Si*WSC3 to bind to its substrate (Wawra et al., 2019).

Microbial strains and culture conditions for EPS matrix production in *S. indica* and *B. sorokiniana*

The EPS matrix was isolated from the *S. indica* strain expressing GFP in the dikaryotic wild-type background DSM11827 (Wawra et al., 2016) and from the *B. sorokiniana* wild-type strain ND90r. *Serendipita indica* spores were isolated from 3-week-old cultures grown on solid complex medium (*Si*_CM) using 0.002% (v/v) Tween water (Zuccaro et al., 2011). For the preculture, 2 mL of *S. indica* spores at a concentration of 500,000 mL^{-1} were inoculated in 100 mL of TSB medium containing 1% (w/v) sucrose and shaking at 120 rpm at 28°C. After 48 h, the pre-cultures were transferred to 400 mL of TSB containing 1% sucrose and shaken at 120 rpm at 28°C for 72 h. *Bipolaris sorokiniana* spores were isolated from 10-day-old cultures grown on solid complete medium (*Bs*_CM), using 0.002% (v/v) Tween water (Sarkar et al., 2019). The spores were inoculated at a final concentration of 250 spores·mL^{-1} in 250 mL of YPD medium and these samples were shaken at 28°C for 36 h.

Isolation of EPS matrix from *S. indica* and *B. sorokiniana* culture supernatant

Culture supernatants from axenically grown *S. indica* or *B. sorokiniana* were collected by filtering the mycelia using Miracloth (Merck Millipore). The EPS matrix was isolated from the culture media using cryogelation. Briefly, the culture media were frozen overnight at −20°C and slowly thawed at room temperature for 16 h. The precipitated EPS

matrix (Supplemental Figure S1) present in the culture medium was isolated using a pipette controller and washed four times with 30 mL of Milli-Q water and either used for proteome analyses (see section "Proteome analysis of *S.indica* EPS matrix, CW, and culture filtrate") or washed one more time with 30 mL of 8.3-mM EDTA (pH 8.0) to remove metal ions potentially present in the EPS. The proteins present in the EPS matrix were removed by treatment with 30 mL of protein denaturation solution (containing 8-M urea, 2-M thiourea, 4% [w/v] sodium dodecyl sulfate [SDS], 100-mM Tris–HCl, pH 7.5) and boiling at 95°C for 15 min. The SDS present in the EPS matrix was removed by boiling the material with 30 mL of Milli-Q water at 95°C for 10 min and centrifuging at 10,000*g* for 10 min at room temperature. The latter step was repeated approximately 15 times until no further foaming occurred. The resulting protein-free EPS matrix was lyophilized and used for glycosyl linkage, TLC or MALDI-TOF analyses.

Proteome analysis of *S. indica* EPS matrix, CW, and culture filtrate

The proteins were isolated from the EPS matrix, CW, and the culture filtrate obtained from axenic cultures of *S. indica* strain expressing GFP grown in different media (CM, YPD, and TSB).

Protein isolation from the CW

Mycelium collected from the *S. indica* GFP strain was ground in liquid N_2 and resuspended in PBS buffer containing 1-mM PMSF and 1% (v/v) NP-40 using an ULTRA-TURRAX (IKA, Staufen, Germany). The resuspended mixture was incubated at 4°C in a rotating wheel for 30 min. The pellet obtained after centrifugation at 8,000*g* for 15 min at 4°C was resuspended in PBS buffer containing 1-mM PMSF and 0.1% (v/v) IGEPAL using an ULTRA-TURRAX. The pellet obtained after centrifugation at 8,000*g* for 15 min at 4°C was washed three times with Milli-Q water. Finally, the pellet was resuspended in Laemmli buffer containing 8-M urea, 2-M thiourea, and β-mercaptoethanol and boiled at 95°C for 10 min.

Protein isolation from the EPS matrix

The EPS matrix obtained from the culture media by cryogelation was washed four times with Milli-Q water and was directly boiled in Laemmli buffer containing 8-M urea, 2-M thiourea, and β-mercaptoethanol at 95°C for 10 min.

Protein isolation from the culture filtrate

The culture supernatant left over from the EPS matrix isolation step was first filtered using a Whatman filter paper and then using a 0.22-μM syringe filter. Approximately 30 mL of EPS matrix depleted culture supernatant was treated with 5 mL of 95% (v/v) trichloroacetic acid and incubated overnight at 4°C. The precipitated proteins were collected by centrifugation (10,000*g*) for 1 h at 4°C. The isolated proteins were washed at least three times with 100% (v/v) acetone. The dried protein pellet was resuspended in Laemmli buffer containing 8-M urea, 2-M thiourea, and β-mercaptoethanol and boiled at 95°C for 10 min.

Liquid chromatography coupled mass spectrometric protein identification and quantification

The proteins isolated from the EPS matrix, CW and culture filtrate were separated using a 10% (v/v) SDS–polyacrylamide gel electrophoresis gel for 15 min and subsequently stained with Coomassie Brilliant Blue. Protein-containing bands from Coomassie-stained gels were prepared for mass spectrometric analysis as described elsewhere (Poschmann et al., 2014). Briefly, bands were destained and the proteins were reduced with dithiothreitol and alkylated with iodoacetamide and subjected to tryptic digestion. The resulting peptides were extracted and reconstituted in 0.1% (v/v) trifluoroacetic acid in water. Peptides were separated on an Ultimate 3000 Rapid Separation Liquid Chromatography system (Thermo Fisher Scientific) on a 25-cm length C18 column using a 1-h gradient and subsequently analyzed by a QExactive Plus mass spectrometer (Thermo Fisher Scientific) as described with minor modifications (Poschmann et al., 2014). First, survey scans were carried out at a resolution of 140,000 and up to 22- and 3-fold charged precursors selected by the quadrupole (4 *m/z* isolation window), fragmented by higher energy collisional dissociation and fragment spectra recorded at a resolution of 17,500. Mass spectrometric data were further processed by MaxQuant 1.6.12.0 (Max-Planck Institute for Biochemistry, Planegg, Germany) with standard parameters if not otherwise stated. Label-free quantification, "match between runs" and iBAQ quantification were enabled. Searches were carried out based on *S. indica* reference protein entries (UP000007148), downloaded on 15 May 2020 from the UniProt Knowledge Base. Carbamidomethylation at cysteines was considered as fixed and methionine oxidation and proteins N-terminal acetylation as variable modifications. Peptides and proteins were accepted at a false discovery rate of 1% and only proteins further considered were identified with at least two different peptides. The identified proteins were grouped into families using the Pfam database (Mistry et al., 2021). The mass spectrometry proteomics data have been deposited to the ProteomeXchange Consortium via the PRIDE partner repository with the dataset identifier PXD025640.

Proteome analysis of *S. indica* EPS matrix, CW, and culture filtrate

Further calculations were done on label-free quantification (LFQ) intensity values. Only proteins were considered showing at least two valid intensity values at least in one group. LFQ intensity values were log2 transformed and missing values imputed with values drawn from a downshifted normal distribution (width 0.3, downshift 1.8) before statistical and enrichment analysis. Statistical analysis was done for selected protein groups using the significance analysis of microarrays method (Tusher et al., 2001; 5% false discovery rate,

S0 = 0.1) and Student's *t* test. To identify proteins containing certain domains showing a higher abundance in the EPS matrix, we performed an annotation enrichment analysis (Cox and Mann, 2012) based on the differences of mean values of log2 transformed LFQ intensities.

The percentage relative abundance of signal peptide containing proteins detected in the three components (EPS matrix, CW, and culture filtrate) was calculated using LFQ intensities.

Large scale digestion and enrichment of the β-GD released from the EPS matrix of *S. indica* and *B. sorokiniana*

Five milligram of freeze-dried EPS matrix obtained from *S. indica* or *B. sorokiniana* were ground with two stainless steel beads (5 mm) using a TissueLyser (Qiagen, Hilden, Germany) at 30 Hz for 1 min at room temperature and soaked in 1 mL of 100-mM sodium acetate buffer (pH 5.0) at 70°C overnight. The soaked material was incubated with 20 µL (50 U) of *Hv*BGLUII in a total reaction volume of 1 mL using 100-mM sodium acetate buffer (pH 5.0). The digestion was performed at 40°C with shaking at 500 rpm for 48 h. The supernatant containing the β-GD was collected by centrifugation at 10,000*g* for 5 min at room temperature. The digested pellet was additionally suspended in 1 mL of water and heated at 80°C for 10 min to solubilize additional β-GD. The resulting supernatant was combined with the initial digested material and boiled at 95°C for 15 min. The precipitated proteins were removed by centrifugation at 10,000*g* for 20 min at room temperature and the debris were removed using a 0.45-µM syringe filter. The clear supernatant fraction was freeze-dried. The freeze-dried material was dialyzed against 3 L of Milli-Q water at 4°C using a 1-kDa cutoff dialysis tubing (Repligen Spectra/Por 6 Pre-Wetted Regenerated Cellulose, cat. no. 888-11461). The dialyzate was lyophilized before further use.

Preparation of alcohol insoluble residue and protein-free CW from *S. indica* and *B. sorokiniana*

The mycelium collected from axenic cultures of *S. indica* or *B. sorokiniana* was washed twice with Milli-Q water and freeze-dried overnight. The freeze-dried material was powdered in liquid N_2 using a pestle and mortar and stored at −20°C until use. Twenty milligrams of the material was resuspended in 1 mL of 70% (v/v) aqueous ethanol with a stainless steel bead (5 mm) using a TissueLyser at 30 Hz for 1 min. After centrifugation at 10,000*g* for 20 min at room temperature, the pellet was washed with chloroform/methanol (1:1), then acetone and subsequently air-dried. Protein-free fungal wall material was prepared as mentioned previously (Wawra et al., 2016).

Glycosyl linkage analysis of EPS matrices and CW preparations

EPS matrix (2 mg) or CW preparation of *S. indica* or *B. sorokiniana* were ground with a stainless steel bead (5 mm) using a TissueLyser mill at 30 Hz for 1 min. The powdered material was subjected to glycosyl linkage analysis as described (Liu et al., 2015). Briefly, a methylation reaction was performed using NaOH/DMSO. The methylated compounds were hydrolyzed in 1 M trifluoroacetic acid, reduced using sodium borodeuteride (ACROS Organics, cat.no. 194950050) and per-o-acetylated. The resulting partially methylated alditol acetates were analyzed using an Agilent 5977A GC/MSD System equipped with a SP-2380 Fused Silica Capillary Column (Supelco). The glycosidic linkages were assigned based on retention time and mass spectrum fragmentation patterns compared to the CCRC spectral database (https://www.ccrc.uga.edu/specdb/ms/pmaa/pframe.html).

Digestion of EPS matrix and CW and TLC analysis

Freeze-dried EPS matrix (1 mg) or CW preparation (1 mg) from *S. indica* or *B. sorokiniana* were suspended in 400 µL of 2-mM sodium acetate (pH 5.0; for TLE), 2-mM MES (pH 5.0; for *H. pomatia* β-1,3-glucanase), or 100-mM sodium acetate (pH 5.0; for *Hv*BGLUII) at 70°C overnight. The excess buffer was removed and the suspended material was treated with 5 µL of the glucanase enzymes (0.125 $mg{\cdot}mL^{-1}$ or 12.5 U for *Hv*BGLUII) in the respective buffers, containing 1 µL of BSA (100 $mg{\cdot}mL^{-1}$) in a total reaction volume of 50 µL and incubated at 40°C by shaking at 500 rpm for 16 h. The digestion reaction was stopped by incubating the samples at 95°C for 10 min. An aliquot was subjected to TLC using a silica gel 60 F254 aluminum TLC plate (Merck Millipore, cat. no. 105554), with a running buffer containing ethyl acetate/acetic acid/methanol/formic acid/water in a ratio of 80:40:10:10:10 (v/v). D-glucose, laminaribiose β-1-3-$(Glc)_2$, laminaritriose β-1-3-$(Glc)_3$, gentiobiose β-1-6-$(Glc)_2$, and laminaripentaose β-1-3-$(Glc)_5$ with a concentration of 1.5 $mg{\cdot}mL^{-1}$ were used as standards. The glucan fragments were visualized by spraying the TLC plate with glucan developer solution (containing 45-mg N-naphthol, 4.8-mL H_2SO_4, 37.2-mL ethanol, and 3-mL water) and heating the TLC plate to 100°C until the glucan bands were visible (∼4–5 min).

MALDI-TOF analysis

Analysis of the β-GD from S. indica

Freeze-dried β-GD was solubilized in water at 70°C for 10 min.

Structural characterization of the β-GD from S. indica and B. sorokiniana

Ten microliters of β-GD (2 $mg{\cdot}mL^{-1}$) was treated with 2 µL of *Fa*GH17a or 2-µL *Fb*GH30 or 1 µL of *Fa*GH17a + 1 µL *Fb*GH30 in 50 µL of Milli-Q water. The digestion reaction was carried out at 40°C for 16 h and the reaction was stopped by incubation at 95°C for 5 min.

Analysis of oligosaccharides released from the EPS matrix and CW of S. indica

Freeze-dried EPS matrix (1 mg) or CW preparation (1 mg) isolated from *S. indica* were suspended in 400 µL of a 2-mM

sodium acetate buffer, pH 5.0 (TLE), 2-mM MES buffer, pH 5.0 (*H. pomatia* β-1,3-glucanase), or 25-mM sodium acetate buffer, pH 5.0 (*Hv*BGLUII) and incubated at 70°C overnight. The suspended material was treated with 2.5 µL of TLE, 2.5 µL of *H. pomatia* β-1,3-glucanase, or 1 µL of *Hv*BGLUII in the respective buffers, as described before, in a total reaction volume of 50 µL. The digestion was performed at 40°C with shaking at 500 rpm for 16 h. The digestion reaction was stopped at 95°C for 10 min and centrifuged at 11,000*g* for 5 min at room temperature.

Analysis of oligosaccharides released from the EPS matrix and CW of B. sorokiniana

Freeze-dried EPS matrix (1 mg) or CW preparation (1 mg) isolated from *B. sorokiniana* were solubilized in 400 µL of 2-mM sodium acetate, pH 5.0 (TLE) or 25-mM sodium acetate, pH 5.0 (*Hv*BGLUII). The solubilized material was treated with 1 µL of TLE or 1 µL of *Hv*BGLUII in a total reaction volume of 50 µL. The digestion was performed at 40°C with shaking at 500 rpm for 16 h. The digestion reaction was stopped at 95°C for 10 min.

Mass spectrometrical analysis

The oligosaccharides present in the prepared samples were analyzed by Oligosaccharide Mass Profiling as described (Günl et al., 2011). Briefly, the samples were spotted onto a dried spot of dihydroxy benzoic acid matrix (10 mg·mL^{-1}) and analyzed by MALDI-TOF mass spectrometry (Bruker rapifleX instrument). The machine was set to linear, positive reflectron mode with an accelerating voltage of 20,000 V. The spectra from the samples were analyzed using flexanalysis software 4.0 (Bruker Daltonics).

Reduction and purification of *S. indica* β-GD

Enriched β-GD (40 mg) was reduced with sodium borodeuteride (20 mg·mL^{-1}; ACROS Organics, cat.no. 194950050) in 1-M ammonium hydroxide for 90 min at room temperature. The reaction was neutralized by addition of glacial acetic acid and 9:1 (v:v) methanol:acetic acid. The solvents were evaporated under N_2 gas. The dried material was washed once with 9:1 (v:v) methanol:acetic acid and three times with methanol. In each washing step, the methanol:acetic acid or methanol were evaporated under N_2 gas. The dried material was dissolved in 6% (v/v) aqueous methanol, vortexed, and centrifuged at 4,000*g* for 15 min at room temperature, to remove any occurring debris. The supernatant (50 µL) was subjected to reverse-phase chromatography using a Vydac 238 TP C18 column (Vydac, Hesperia, CA, USA) eluting with a linear gradient from 6% (v/v) to 12% (v/v) methanol in 10 min, followed by 12% (v/v) to 50% (v/v) methanol in 10 min and equilibrated back to 6% (v/v) methanol in 10 min with a flow rate of 0.5 mL·min^{-1}. The eluting compounds were detected by an evaporative light scattering detector (ERC GmbH, Munich, Germany) at 38°C and simultaneously collected for MALDI-TOF analyses. Collected fractions containing the β-GD were pooled and freeze-dried.

^{1}H NMR analysis

Reduced β-GD (1 mg) was dissolved in D_2O (100% atom D, ACROS Organics, 320700075) at 80°C for 10 min and subsequently freeze-dried overnight. The freeze-dried material was dissolved in 300 µL of 6:1 (v/v) of methyl sulphoxide D6 (99.9% atom D + 1% tetramethylsilane, ACROS Organics):D_2O (100% atom D, ACROS Organics, 320700075) at 80°C for 10 min. The ^{1}H NMR spectrum of the reduced β-GD was measured using a 600 MHz Bruker NMR spectrometer at 80°C (Kim et al., 2000). The chemical shift signal was referred to the internal standard tetramethylsilane at 0 ppm and the ^{1}H NMR spectrum was processed using Bruker's Topspin software.

Purification of native β-GD for the ROS burst assay

Enriched β-GD (40 mg) was dissolved in 6% (v/v) aqueous methanol, vortexed, and centrifuged to remove any debris. The β-GD was purified as described above but without reduction and used for the ROS burst assays if not otherwise stated in the legend.

Preparation of crude fungal CW substrates for immunity assays

For crude extraction of soluble fragments from the fungal CW and EPS matrix, 5 mg of the respective fungal substrate was transferred to a 2-mL Eppendorf tube with three stainless steel beads (5 mm), snap-frozen in liquid nitrogen and ground with a TissueLyser (1 min, 30 Hz). The ground substrate was resuspended in 2 mL of Milli-Q water, incubated at 70°C for 16 h (700 rpm), and then boiled at 95°C for 10 min. The volume was filled up to 5 mL for a final concentration of 1 mg·mL^{-1}. The suspension was centrifuged at 13,000*g* for 10 min at room temperature and the supernatant was further used in plant immunity assays.

Plant immunity assays

Preparation of immunity assays

For immunity assays using barley, roots were separated from 7-day-old seedlings (cut 2 cm below seed), root tips were removed (first 1 cm), and residual roots were cut into 5-mm pieces. Each assay was performed with randomized root pieces from 16 barley seedlings. Four root pieces were transferred into each well of a 96-well plate microtiter plate containing Milli-Q water. For immunity assays with Arabidopsis (wild-type or aequorin-expressing lines), intact 14-day-old seedlings were transferred into a 96-well plate (one seedling/well) filled with Milli-Q water.

Elicitors

Chitohexaose was purchased from Megazyme (Bray, Ireland), flg22 from GenScript (Piscataway, NJ, USA), and laminarin from Sigma-Aldrich (Taufkirchen, Germany). All commercial substrates were dissolved in Milli-Q water without additional treatment. Substrates derived from fungal CW and EPS were prepared as described earlier. The elicitor solutions had the following pH ± SD (n = 3): Milli-Q water = 7.20 ± 0.125; EPS

matrix prep1 = 7.30 ± 0.322; EPS matrix prep2 = 7.37 ± 0.167; β-GD = 6.96 ± 0.212; Chit6 = 7.32 ± 0.106.

Cytosolic calcium influx measurements

The solution in the 96-well plates containing the plant material (Arabidopsis seedlings expressing aequorin, see above) was exchanged for 100 µL of a 10-µM coelenterazine solution (Roth, Karlsruhe, Germany). After overnight incubation in the dark, the plates were transferred to a TECAN SPARK 10M multi-well plate reader. After baseline measurement (5 min), 50 µL of a three-fold concentrated elicitor solution was manually added to the wells and luminescence was measured for 30 min. Residual aequorin was discharged with 100 µL of 2.5-m $CaCl_2$ (in 25% [v/v] ethanol) and luminescence was detected for 1 min. All measurements were performed with an integration time of 300 ms. Baseline luminescence and elicitor-triggered luminescence were normalized according to the maximal integrated discharge value obtained from individual wells.

ROS assay

The ROS assay is based on previously published protocols (Felix et al., 1999; Wanke et al., 2020; Ngou et al., 2021). In detail, 96-well plate with plant material (see above) were incubated overnight at room temperature on the bench to remove ROS and other contaminants originating from the mechanical damage of the tissue during preparation. The next day, water was replaced by 100 µL of fresh Milli-Q water containing 20 $\mu g \cdot mL^{-1}$ horseradish peroxidase (Sigma-Aldrich, Taufkirchen, Germany) and 20-µM L-012 (Wako Chemicals, Neuss, Germany). Following a short incubation time (~15 min), 100 µL of double-concentrated elicitor solutions were added to the wells. Measurements of elicitor-triggered apoplastic ROS production were started immediately and taken continuously with an integration time of 450 ms using a TECAN SPARK 10 M multi-well plate reader. Horseradish peroxidase catalyzes the oxidation of the luminol derivate L-012 by the plant-produced ROS species upon elicitation with MAMPs. This leads to a chemiluminescent signal that is detected by the plate reader.

Gene expression analysis

After the ROS burst assay (1 h after elicitor addition), plant material from three to four wells was pooled, dried on tissue paper and snap-frozen in liquid nitrogen for further analysis of gene expression changes. Total RNA was extracted using TRIzol reagent (Invitrogen, Karlsruhe, Germany) and contaminating gDNA was digested during a DNaseI treatment (Thermo Fisher Scientific, Schwerte, Germany) according to manufacturers' instructions. Synthesis of cDNA was carried out using the First Strand cDNA Synthesis Kit (Thermo Fisher Scientific, Schwerte, Germany) without changes to the manufacturer's protocol. Target gene expression was analyzed by reverse transcription-quantitative polymerase chain reaction (RT-qPCR) as described previously (Wawra et al., 2019). Relative expression of elicitor-responsive *HvWRKY2* gene (Shen et al., 2007) compared to *H. vulgare* ubiquitin gene (Sarkar et al., 2019) was determined using the following primer pairs: *HvUBI*_F (5′-ACCCTCGCCGACTACAACAT-3′) with *HvUBI*_R (5′-CAGTAGTGGCGGTCGAAGT-3′) and *HvWRKY2*_F (5′-AACAACCACCACCAGTCGTT-3′) with *Hv*WRKY2_R (5′-TCACCTTCTGCCCGTACTTC-3′). Gene expression levels in elicitor-treated samples were normalized to the expression levels in mock-treated samples.

In vitro DAB oxidation assay

DAB assay was performed as previously described (Nostadt et al., 2020). Sugar substrates (concentrations as indicated) were mixed with 0.05-µM horseradish peroxidase (Sigma-Aldrich, Taufkirchen, Germany) and 1-mM H_2O_2 (Sigma-Aldrich, Taufkirchen, Germany) in reaction buffer (50-mM sodium acetate, 150-mM NaCl, pH 5) and incubated for 10 min at room temperature in a 96-well plate. Then, an equal volume of a 200-µM DAB solution was added to the wells. After 16 h of incubation in the dark, plates were scanned on a flatbed scanner (transmissive light mode).

Fenton reaction-based oxidation of sugars

The assay was performed as previously described (Matros et al., 2015). Carbohydrate samples (300 µM) were mixed with Fenton reagents (1-mM H_2O_2 [Sigma], 100-µM $FeSO_4$ [Sigma]) and incubated overnight at 30°C. Control samples with an additional 100-µM EDTA (Sigma) or without Fenton reagents were treated in the same way. Samples were centrifuged at 13,000*g* for 10 min at room temperature and the supernatant was further analyzed by MALDI-TOF.

Colonization assay with β-GD

Roots of 4-day-old barley seedlings were inoculated with 3 mL of *S. indica* spores at a concentration of 500,000 mL^{-1} and grown at a day/night cycle of 16 h/8 h at 22°C/18°C, 60% humidity, and 108 µmol m^{-2} s^{-1} light intensity. At 1 and 2 dpi, 1 mL of sterile water as a control or 100- or 300-µM β-GD were added to the jars which contained four seedlings each. The seedlings of each jar were pooled and harvested at 3 dpi. The roots were washed in ice water to remove extraradical hyphae, cut as previously described (Nizam et al., 2019), frozen in liquid nitrogen and used for RNA extraction. RNA extraction for fungal colonization, cDNA generation, and RT-qPCR was performed as previously described (Sarkar et al., 2019). For quantification of endophytic fungal colonization by RT-qPCR, the following primers were used: 5′-GCAAGTTCTCCGAGCTCATC-3′ and 5′-CCAAGTGGTGGGTACTCGTT-3′ for *S. indica* translation-elongation factor (*SiTEF*) and 5′-ACCCTCGCCGAC TACAACAT-3′ and 5′CAGTAGTGGCGGTCGAAGTG3′ for barley ubiquitin (*HvUbi*).

Expression analysis of selected genes with WSC domains

Gene expression of *S. indica* WSC domain-containing proteins during root colonization of barley and Arabidopsis was monitored via RT-qPCR as previously described (Wawra

et al., 2019) at 3, 7, and 14 dpi. For each biological replicate (n = 3), roots from several individual plants were pooled (Arabidopsis: 60 plants; barley: 4 plants).

Statistical analyses

A summary of statistical analyses is given in Supplemental Data Set S10.

Accession numbers

Hordeum vulgare **BGLU2**: P15737 (UniProt), HORVU.MOREX.r3.3HG0319100.1 (MorexV3_pseudomolecules_assembly, EnsemblePlants).

Supplemental data

The following materials are available in the online version of this article.

Supplemental Figure S1. EPS matrix isolated from *S. indica* grown in CM medium using a cryogelation approach.

Supplemental Figure S2. Proteome analysis of *S. indica* EPS matrix, CW, and culture filtrate.

Supplemental Figure S3. Expression analysis of selected genes with WSC domains in *S. indica* during plant colonization at 3, 7, and 14 dpi.

Supplemental Figure S4. Glycosyl linkage analysis of *Si* EPS and *Si* CW.

Supplemental Figure S5. Analysis of oligosaccharides released from the EPS or protein-free CW of *S. indica* by the action of β-1,3-glucanases.

Supplemental Figure S6. Glycosyl linkage and MALDI-TOF analysis of the glucan fraction (β-GD) released from the EPS matrix of *S. indica*.

Supplemental Figure S7. Purification of the β-GD fragment for ^{1}H NMR analysis.

Supplemental Figure S8. Mechanically released fragments from *S. indica* EPS matrix and CW layer do not exhibit ROS scavenging activity.

Supplemental Figure S9. Chitohexaose-triggered ROS accumulation is decreased by *S. indica* β-GD treatment in a concentration-dependent manner.

Supplemental Figure S10. Purification of native β-GD and immunogenic characterization.

Supplemental Figure S11. Detoxification of apoplastic ROS by *S. indica* β-GD is independent of elicitor treatment and plant species.

Supplemental Figure S12. *Serendipita indica* β-GD treatment does not trigger cytosolic calcium influx in *A. thaliana* seedlings.

Supplemental Figure S13. Digestion of laminariheptaose with *Hv*BGLUII enhances ROS production in barley roots.

Supplemental Figure S14. Glycan controls are not degraded by hydrogen peroxide during Fenton reaction.

Supplemental Figure S15. Glycosyl linkage analysis of *B. sorokiniana* EPS matrix and CW.

Supplemental Figure S16. Analysis of oligosaccharides released from the EPS of *B. sorokiniana* by the action of *Trichoderma harzianum* lysing enzymes.

Supplemental Figure S17. The β-GD released from the EPS matrix of *B. sorokiniana* consists of a seven unit β-1,3-linked glucan backbone substituted with three β-1,6-glucosyl residues.

Supplemental Figure S18. Mechanically released fragments from *B. sorokiniana* EPS matrix or CW do not scavenge ROS.

Supplemental Data Set S1. Total proteins detected in the proteome analysis of the EPS matrix, CW, and culture filtrate isolated from *S. indica* grown in CM, TSB, or YPD liquid media.

Supplemental Data Set S2. Relative abundance of signal peptide (SP) containing proteins detected in the EPS matrix, CW, and culture filtrate isolated from the *S. indica* under three culture mediums: CM, TSB, and YPD. LFQ intensities of the proteins were used to calculate their relative abundance.

Supplemental Data Set S3. Statistics, enrichment score, Benjamini–Hochberg corrected *P*-value.

Supplemental Data Set S4. Glycosyl sugar residues detected in the total ion chromatogram of EPS matrix isolated from *S. indica*, n = 4 independent biological replicates.

Supplemental Data Set S5. Glycosyl sugar residues detected in the total ion chromatogram of alcohol insoluble residue (cell wall) isolated from *S. indica*, n = 4 independent biological replicates.

Supplemental Data Set S6. List of Barley CAZymes detected in the root apoplastic fluids (AFs) of barley after mock, *S. indica* or *B. sorokiniana* treatments.

Supplemental Data Set S7. Glycosyl sugar residues detected in the total ion chromatogram of alcohol insoluble residue (cell wall) isolated from *B. sorokiniana*, n = 3 independent biological replicates.

Supplemental Data Set S8. Glycosyl sugar residues detected in the total ion chromatogram of EPS matrix isolated from *B. sorokiniana*, n = 3 independent biological replicates.

Supplemental Data Set S9. List of Barley CAZymes differentially regulated during *B. sorokiniana* infection.

Supplemental Data Set S10. Summary of statistical analyses.

Acknowledgments

The authors would like to thank Katharina Lufen, Institute for Plant Cell Biology and Biotechnology, Heinrich Heine University, Düsseldorf for excellent technical assistance and Alba Silipo Department of Chemical Sciences, University of Napoli Federico II for initial support with the sugar analyses. We thank Gereon Poschmann, Anja Stefanski, Thomas Lenz and Kai Stühler, Institute of Molecular Medicine, Proteome research facility, Medical Faculty and University Hospital Düsseldorf for excellent proteomics. NMR analysis was performed at the Center for Molecular and Structural Analytics at the Heinrich Heine University, Düsseldorf. We further thank Jan-Hendrik Hehemann for providing aliquots of *Fa*GH17a and *Fb*GH30.

Funding

A.Z. and L.M. acknowledge support from the Cluster of Excellence on Plant Sciences (CEPLAS) funded by the Deutsche Forschungsgemeinschaft (DFG, German Research Foundation) under Germany's Excellence Strategy–EXC 2048/1–Project ID: 390686111 and projects ZU 263/11-1 (SPP 2125 DECRyPT).

Conflict of interest statement. The authors have no conflicts of interest.

References

Adams EL, Rice PJ, Graves B, Ensley HE, Yu H, Brown GD, Gordon S, Monteiro MA, Papp-Szabo E, Lowman DW, et al. (2008) Differential high-affinity interaction of dectin-1 with natural or synthetic glucans is dependent upon primary structure and is influenced by polymer chain length and side-chain branching. J Pharmacol Exp Therap **325**: 115–123

Becker S, Scheffel A, Polz MF, Hehemann J-H (2017) Accurate quantification of laminarin in marine organic matter with enzymes from marine microbes. Appl Environ Microbiol **83**: e03389–16

Benaroudj N, Lee DH, Goldberg AL (2001) Trehalose accumulation during cellular stress protects cells and cellular proteins from damage by oxygen radicals. J Biol Chem **276**: 24261–24267

Boller T, Felix G (2009) A renaissance of elicitors: perception of microbe-associated molecular patterns and danger signals by pattern-recognition receptors. Annu Rev Plant Biol **60**: 379–406

Boulos S, Nystrom L (2017) Complementary sample preparation strategies for analysis of cereal beta-glucan oxidation products by UPLC-MS/MS. Front Chem 5: 90

Brown GD, Gordon S (2005) Immune recognition of fungal β-glucans. Cell Microbiol **7**: 471–479

Buscaill P, van der Hoorn RAL (2021) Defeated by the nines: nine extracellular strategies to avoid MAMP recognition in plants. Plant Cell (in press)

Choi J, Tanaka K, Cao Y, Qi Y, Qiu J, Liang Y, Lee SY, Stacey G (2014) Identification of a plant receptor for extracellular ATP. Science **343**: 290–294

Ciucanu I (2006) Per-O-methylation reaction for structural analysis of carbohydrates by mass spectrometry. Analyt Chim Acta **576**: 147–155

Cox J, Mann M (2012) 1D and 2D annotation enrichment: a statistical method integrating quantitative proteomics with complementary high-throughput data. BMC Bioinform **13 (Suppl 16)**: S12

El Oirdi M, El Rahman TA, Rigano L, El Hadrami A, Rodriguez MC, Daayf F, Vojnov A, Bouarab K (2011) Botrytis cinerea manipulates the antagonistic effects between immune pathways to promote disease development in tomato. Plant Cell **23**: 2405–2421

Felix G, Duran JD, Volko S, Boller T (1999) Plants have a sensitive perception system for the most conserved domain of bacterial flagellin. Plant J **18**: 265–276

Fesel PH, Zuccaro A (2016) β-glucan: crucial component of the fungal cell wall and elusive MAMP in plants. Fungal Genet Biol **90**: 53–60

Fliegmann J, Mithofer A, Wanner G, Ebel J (2004) An ancient enzyme domain hidden in the putative beta-glucan elicitor receptor of soybean may play an active part in the perception of pathogen-associated molecular patterns during broad host resistance. J Biol Chem **279**: 1132–1140

Geoghegan I, Steinberg G, Gurr S (2017) The role of the fungal cell wall in the infection of plants. Trends Microbiol **25**: 957–967

Goodridge HS, Wolf AJ, Underhill DM (2009) Beta-glucan recognition by the innate immune system. Immunol Rev **230**: 38–50

Gow NAR, Latge JP, Munro CA (2017) The fungal cell wall: structure, biosynthesis, and function. Microbiol Spectr **5**

Gravelat FN, Beauvais A, Liu H, Lee MJ, Snarr BD, Chen D, Xu W, Kravtsov I, Hoareau CM, Vanier G, et al. (2013). Aspergillus galactosaminogalactan mediates adherence to host constituents and conceals hyphal beta-glucan from the immune system. PLoS Pathog **9**: e1003575

Günl M, Kraemer F, Pauly M (2011) Oligosaccharide mass profiling (OLIMP) of cell wall polysaccharides by MALDI-TOF/MS. Methods Mol Biol **715**: 43–54

Ham K-S, Wu S-C, Darvill AG, Albersheim P (1997) Fungal pathogens secrete an inhibitor protein that distinguishes isoforms of plant pathogenesis-related endo-β-1,3-glucanases. Plant J **11**: 169–179

Han B, Baruah K, Cox E, Vanrompay D, Bossier P (2020) Structure-functional activity relationship of β-glucans from the perspective of immunomodulation: a mini-review. Front Immunol **11**: 658

Kang X, Kirui A, Muszynski A, Widanage MCD, Chen A, Azadi P, Wang P, Mentink-Vigier F, Wang T (2018) Molecular architecture of fungal cell walls revealed by solid-state NMR. Nat Commun **9**: 2747

Kim YT, Kim EH, Cheong C, Williams DL, Kim CW, Lim ST (2000) Structural characterization of beta-D-(1 –> 3, 1 –> 6)-linked glucans using NMR spectroscopy. Carbohydr Res **328**: 331–341

Lahrmann U, Ding Y, Banhara A, Rath M, Hajirezaei MR, Döhlemann S, Wirén Nv, Parniske M, Zuccaro A (2013) Host-related metabolic cues affect colonization strategies of a root endophyte. Proc Natl Acad Sci USA **110**: 13965–13970

Lei N, Wang M, Zhang L, Xiao S, Fei C, Wang X, Zhang K, Zheng W, Wang C, Yang R, Xue F (2015) Effects of low molecular weight yeast beta-glucan on antioxidant and immunological activities in mice. Int J Mol Sci **16**: 21575–21590

Leubner-Metzger G, Meins F (1999) Functions and regulation of plant ß-1,3-glucanases (PR-2): pathogenesis-related proteins in plants. *In* SK Datta, S Muthukrishnan, eds, Pathogenesis-related Proteins in Plants. CRC Press LLC, Boca Raton, FL, pp 49–76

Liu D, Leib K, Zhao P, Kogel K-H, Langen G (2014) Phylogenetic analysis of barley WRKY proteins and characterization of HvWRKY1 and -2 as repressors of the pathogen-inducible gene HvGER4c. Mol Genet Genomics **289**: 1331–1345

Liu L, Paulitz J, Pauly M (2015) The presence of fucogalactoxyloglucan and its synthesis in rice indicates conserved functional importance in plants. Plant Physiol **168**: 549–560

Lowman DW, West LJ, Bearden DW, Wempe MF, Power TD, Ensley HE, Haynes K, Williams DL, Kruppa MD (2011) New insights into the structure of (1→3,1→6)-β-D-glucan side chains in the Candida glabrata cell wall. PLoS One **6**: e27614

Lutzoni F, Nowak MD, Alfaro ME, Reeb V, Miadlikowska J, Krug M, Arnold AE, Lewis LA, Swofford DL, Hibbett D, et al. (2018) Contemporaneous radiations of fungi and plants linked to symbiosis. Nat Commun **9**: 5451

Mahdi LK, Miyauchi S, Uhlmann C, Garrido-Oter R, Langen G, Wawra S, Niu Y, Guan R, Robertson-Albertyn S, Bulgarelli D, et al. (2021) The fungal root endophyte Serendipita vermifera displays inter-kingdom synergistic beneficial effects with the microbiota in Arabidopsis thaliana and barley. ISME J (in press)

Matros A, Peshev D, Peukert M, Mock H-P, Ende WVd (2015) Sugars as hydroxyl radical scavengers: proof-of-concept by studying the fate of sucralose in Arabidopsis. Plant J **82**: 822–839

Mistry J, Chuguransky S, Williams L, Qureshi M, Salazar GA, Sonnhammer ELL, Tosatto SCE, Paladin L, Raj S, Richardson LJ, et al. (2021) Pfam: the protein families database in 2021. Nucleic Acids Res **49**: D412–D419

Nars A, Lafitte C, Chabaud M, Drouillard S, Mélida H, Danoun S, Le Costaouëc T, Rey T, Benedetti J, Bulone V, et al. (2013) Aphanomyces euteiches cell wall fractions containing novel glucan-chitosaccharides induce defense genes and nuclear calcium

oscillations in the plant host Medicago truncatula. PloS One **8**: e75039

Ngou BPM, Ahn HK, Ding P, Jones JDG (2021) Mutual potentiation of plant immunity by cell-surface and intracellular receptors. Nature **592**: 110–115

Nishizawa A, Yabuta Y, Shigeoka S (2008) Galactinol and raffinose constitute a novel function to protect plants from oxidative damage. Plant Physiol **147**: 1251–1263

Nizam S, Qiang X, Wawra S, Nostadt R, Getzke F, Schwanke F, Dreyer I, Langen G, Zuccaro A (2019) Serendipita indica E5′NT modulates extracellular nucleotide levels in the plant apoplast and affects fungal colonization. EMBO Rep **20**: e47430

Nostadt R, Hilbert M, Nizam S, Rovenich H, Wawra S, Martin J, Küpper H, Mijovilovich A, Ursinus A, Langen G, et al. (2020) A secreted fungal histidine- and alanine-rich protein regulates metal ion homeostasis and oxidative stress. New Phytol **227**: 1174–1188

Peshev D, Vergauwen R, Moglia A, Hideg É, Van den Ende W (2013) Towards understanding vacuolar antioxidant mechanisms: a role for fructans? J Exp Bot **64**: 1025–1038

Poschmann G, Seyfarth K, Besong Agbo D, Klafki H-W, Rozman J, Wurst W, Wiltfang J, Meyer HE, Klingenspor M, Stühler K (2014) High-fat diet induced isoform changes of the Parkinson's disease protein DJ-1. J Proteome Res **13**: 2339–2351

Rebaque D, Del Hierro I, Lopez G, Bacete L, Vilaplana F, Dallabernardina P, Pfrengle F, Jorda L, Sanchez-Vallet A, Perez R, et al. (2021) Cell wall-derived mixed-linked beta-1,3/1,4-glucans trigger immune responses and disease resistance in plants. Plant J (in press)

Rocafort M, Fudal I, Mesarich CH (2020) Apoplastic effector proteins of plant-associated fungi and oomycetes. Curr Opin Plant Biol **56**: 9–19

Rovenich H, Zuccaro A, Thomma BPHJ (2016) Convergent evolution of filamentous microbes towards evasion of glycan-triggered immunity. New Phytol **212**: 896–901

Sarkar D, Rovenich H, Jeena G, Nizam S, Tissier A, Balcke GU, Mahdi LK, Bonkowski M, Langen G, Zuccaro A (2019) The inconspicuous gatekeeper: endophytic Serendipita vermifera acts as extended plant protection barrier in the rhizosphere. New Phytol **224**: 886–901

Shen Q-H, Saijo Y, Mauch S, Biskup C, Bieri S, Keller B, Seki H, Ulker B, Somssich IE, Schulze-Lefert P (2007) Nuclear activity of MLA immune receptors links isolate-specific and basal disease-resistance responses. Science (New York, N.Y.) **315**: 1098–1103

Silipo A, Erbs G, Shinya T, Dow JM, Parrilli M, Lanzetta R, Shibuya N, Newman MA, Molinaro A (2010) Glyco-conjugates as elicitors or suppressors of plant innate immunity. Glycobiology **20**: 406–419

Stintzi A, Heitz T, Prasad V, Wiedemann-Merdinoglu S, Kauffmann S, Geoffroy P, Legrand M, Fritig B (1993) Plant 'pathogenesis-related' proteins and their role in defense against pathogens. Biochimie **75**: 687–706

Tada R, Adachi Y, Ishibashi K-i, Ohno N (2009) An unambiguous structural elucidation of a 1,3-beta-D-glucan obtained from liquid-cultured Grifola frondosa by solution NMR experiments. Carbohydr Res **344**: 400–404

Taylor JW, Berbee ML (2006) Dating divergences in the Fungal Tree of Life: review and new analyses. Mycologia **98**: 838–849

Tusher VG, Tibshirani R, Chu G (2001) Significance analysis of microarrays applied to the ionizing radiation response. Proc Natl Acad Sci USA **98**: 5116–5121

Valluru R, Van den Ende W (2008) Plant fructans in stress environments: emerging concepts and future prospects. J Exp Bot **59**: 2905–2916

Van Holle S, Van Damme EJM (2018) Signaling through plant lectins: modulation of plant immunity and beyond. Biochem Soc T **46**: 217–233

Wanke A, Malisic M, Wawra S, Zuccaro A (2021) Unraveling the sugar code: the role of microbial extracellular glycans in plant-microbe interactions. J Exp Bot **72**: 15–35

Wanke A, Rovenich H, Schwanke F, Velte S, Becker S, Hehemann J-H, Wawra S, Zuccaro A (2020) Plant species-specific recognition of long and short β-1,3-linked glucans is mediated by different receptor systems. Plant J **102**: 1142–1156

Wawra S, Fesel P, Widmer H, Neumann U, Lahrmann U, Becker S, Hehemann J-H, Langen G, Zuccaro A (2019) FGB1 and WSC3 are in planta-induced β-glucan-binding fungal lectins with different functions. New Phytol **222**: 1493–1506

Wawra S, Fesel P, Widmer H, Timm M, Seibel J, Leson L, Kesseler L, Nostadt R, Hilbert M, Langen G, et al. (2016) The fungal-specific β-glucan-binding lectin FGB1 alters cell-wall composition and suppresses glucan-triggered immunity in plants. Nat Commun **7**: 13188

Yuan M, Jiang Z, Bi G, Nomura K, Liu M, Wang Y, Cai B, Zhou JM, He SY, Xin XF (2021) Pattern-recognition receptors are required for NLR-mediated plant immunity. Nature **592**: 105–109

Zuccaro A, Lahrmann U, Güldener U, Langen G, Pfiffi S, Biedenkopf D, Wong P, Samans B, Grimm C, Basiewicz M, et al. (2011) Endophytic life strategies decoded by genome and transcriptome analyses of the mutualistic root symbiont Piriformospora indica. PLOS Pathogens **7**: e1002290

Supporting information

The following Supporting Information is available for this article online:

- **Supplemental Figure S1.** EPS matrix isolated from *S. indica* grown in CM medium using a cryogelation approach.
- **Supplemental Figure S2.** Proteome analysis of *S. indica* EPS matrix, CW, and culture filtrate.
- **Supplemental Figure S3.** Expression analysis of selected genes with WSC domains in *S. indica* during plant colonization at 3, 7, and 14 dpi.
- **Supplemental Figure S4.** Glycosyl linkage analysis of *Si* EPS and *Si* CW.
- **Supplemental Figure S5.** Analysis of oligosaccharides released from the EPS or protein-free CW of *S. indica* by the action of β-1,3-glucanases.
- **Supplemental Figure S6.** Glycosyl linkage and MALDITOF analysis of the glucan fraction (β-GD) released from the EPS matrix of *S. indica*.
- **Supplemental Figure S7.** Purification of the β-GD fragment for ^{1}H NMR analysis.
- **Supplemental Figure S8.** Mechanically released fragments from *S. indica* EPS matrix and CW layer do not exhibit ROS scavenging activity.
- **Supplemental Figure S9.** Chitohexaose-triggered ROS accumulation is decreased by *S. indica* β-GD treatment in a concentration-dependent manner.
- **Supplemental Figure S10.** Purification of native β-GD and immunogenic characterization.
- **Supplemental Figure S11.** Detoxification of apoplastic ROS by *S. indica* β-GD is independent of elicitor treatment and plant species.
- **Supplemental Figure S12.** *Serendipita indica* β-GD treatment does not trigger cytosolic calcium influx in *A. thaliana* seedlings.
- **Supplemental Figure S13.** Digestion of laminariheptaose with *Hv*BGLUII enhances ROS production in barley roots.
- **Supplemental Figure S14.** Glycan controls are not degraded by hydrogen peroxide during Fenton reaction.
- **Supplemental Figure S15.** Glycosyl linkage analysis of *B. sorokiniana* EPS matrix and CW.
- **Supplemental Figure S16.** Analysis of oligosaccharides released from the EPS of *B. sorokiniana* by the action of *Trichoderma harzianum* lysing enzymes.

- **Supplemental Figure S17.** The β-GD released from the EPS matrix of *B. sorokiniana* consists of a seven unit β-1,3- linked glucan backbone substituted with three β-1,6-glucosyl residues.
- **Supplemental Figure S18.** Mechanically released fragments from *B. sorokiniana* EPS matrix or CW do not scavenge ROS.
- **Supplemental Data Set S1.** Total proteins detected in the proteome analysis of the EPS matrix, CW, and culture filtrate isolated from *S. indica* grown in CM, TSB, or YPD liquid media.
- **Supplemental Data Set S2.** Relative abundance of signal peptide (SP) containing proteins detected in the EPS matrix, CW, and culture filtrate isolated from the *S. indica* under three culture mediums: CM, TSB, and YPD. LFQ intensities of the proteins were used to calculate their relative abundance.
- **Supplemental Data Set S3.** Statistics, enrichment score, Benjamini–Hochberg corrected P-value.
- **Supplemental Data Set S4.** Glycosyl sugar residues detected in the total ion chromatogram of EPS matrix isolated from *S. indica*, n = 4 independent biological replicates.
- **Supplemental Data Set S5.** Glycosyl sugar residues detected in the total ion chromatogram of alcohol insoluble residue (cell wall) isolated from *S. indica*, n = 4 independent biological replicates.
- **Supplemental Data Set S6.** List of Barley CAZymes detected in the root apoplastic fluids (AFs) of barley after mock, *S. indica* or *B. sorokiniana* treatments.
- **Supplemental Data Set S7.** Glycosyl sugar residues detected in the total ion chromatogram of alcohol insoluble residue (cell wall) isolated from *B. sorokiniana*, n = 3 independent biological replicates.
- **Supplemental Data Set S8.** Glycosyl sugar residues detected in the total ion chromatogram of EPS matrix isolated from *B. sorokiniana*, n = 3 independent biological replicates.
- **Supplemental Data Set S9.** List of Barley CAZymes differentially regulated during *B. sorokiniana* infection.
- **Supplemental Data Set S10.** Summary of statistical analyses.

2.3 β-Glucan-binding proteins are key modulators of immunity and symbiosis in mutualistic plant–microbe interactions.

van Boerdonk, S., Saake, P., Wanke, A., Neumann, U and Zuccaro, A. (2024). Current Opinion in Plant Biology. https://doi.org/10.1016/j.pbi.2024.102610

Author contributions

SvB: Conceptualization, Investigation, Writing-original draft preparation. **PS:** Conceptualization, Writing-original draft preparation. AW: Writing-reviewing and editing. UN: Investigation, Supervision, Writing-reviewing and editing. AZ: Conceptualization, Supervision, Writing-reviewing and editing, Funding acquisition

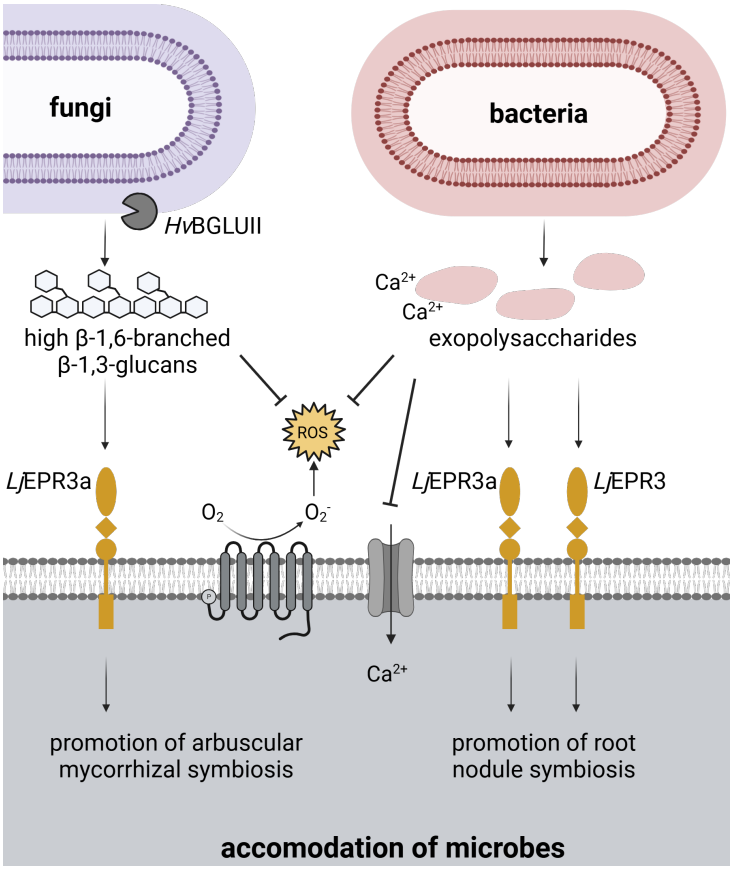

Available online at www.sciencedirect.com

ScienceDirect

Current Opinion in Plant Biology

β-Glucan-binding proteins are key modulators of immunity and symbiosis in mutualistic plant–microbe interactions

Sarah van Boerdonk[1,2], Pia Saake[1,3], Alan Wanke[4], Ulla Neumann[2] and Alga Zuccaro[1,3]

Abstract

In order to discriminate between detrimental, commensal, and beneficial microbes, plants rely on polysaccharides such as β-glucans, which are integral components of microbial and plant cell walls. The conversion of cell wall-associated β-glucan polymers into a specific outcome that affects plant-microbe interactions is mediated by hydrolytic and non-hydrolytic β-glucan-binding proteins. These proteins play crucial roles during microbial colonization: they influence the composition and resilience of host and microbial cell walls, regulate the homeostasis of apoplastic concentrations of β-glucan oligomers, and mediate β-glucan perception and signaling. This review outlines the dual roles of β-glucans and their binding proteins in plant immunity and symbiosis, highlighting recent discoveries on the role of β-glucan-binding proteins as modulators of immunity and as symbiosis receptors involved in the fine-tuning of microbial accommodation.

Addresses

[1] Institute for Plant Sciences, University of Cologne, Cologne, Germany
[2] Max Planck Institute for Plant Breeding Research, Cologne, Germany
[3] Cluster of Excellence on Plant Sciences (CEPLAS), Cologne, Germany
[4] Sainsbury Laboratory, University of Cambridge, Cambridge, United Kingdom

Corresponding author: Zuccaro, Alga (azuccaro@uni-koeln.de)

Current Opinion in Plant Biology 2024, **81**:102610

This review comes from a themed issue on **VSI: Biotic Interactions 2025**

Edited by **Dr. Mariana Schuster** and **Dr. Lay-Sun Ma**

For a complete overview see the Issue and the Editorial

Available online xxx

https://doi.org/10.1016/j.pbi.2024.102610

Introduction

The ability for plants to differentiate between beneficial and detrimental microbes in their environment is important for their survival. β-Glucans comprise a structurally highly diverse group of β-linked D-glucose polysaccharides, varying in linkage, chain length and branching patterns. Among other polysaccharides, β-glucans are conserved components of cell walls of both microbes and plants. For example, β-glucans contribute to a large proportion of the polysaccharide content of fungal cell walls [1,2]. In contrast to chitin, which often forms a rigid inner layer of the cell wall, β-glucans are mainly present in the outer, flexible layer, predominantly in the form of β-1,3-linked glucans with β-1,6-linked side branches or as β-1,3- and β-1,4- mixed-linked glucans (MLGs) in varying ratios [3,4]. Additionally, high molecular weight β-1,3/β-1,6-glucans are present in the mobile gel-like extracellular polysaccharide (EPS) matrix which is loosely attached to the outer cell wall layer [4–6]. In bacteria, β-glucans are found in the EPS matrix [7,8]. In plants, the β-1,4-linked glucan cellulose is the major β-glucan of the cell wall, while the β-1,3-linked glucan callose, though a minor component, plays a functionally important role. MLGs are found in several plant species, especially abundant in the cell walls of grasses like barley, oats, and wheat, where they contribute to cell wall flexibility and growth [9–12]. As building blocks of cell walls, β-glucans are present at the first contact sites of plants and microbes, the apoplast. Here, fragments/oligomers can be released by plant- or microbe-derived hydrolytic enzymes (glucanases) [11]. These fragments, derived from microbes or plants, act as microbe-associated molecular patterns (MAMPs) or damage-associated molecular patterns (DAMPs), respectively. They are detected by pattern recognition receptors (PRRs) on the plant plasma membrane. Receptor binding can activate various hallmarks of pattern-triggered immunity (PTI), such as apoplastic reactive oxygen species (ROS) accumulation, cytosolic calcium influx, or phosphorylation of mitogen-associated protein kinases (MAPK) [13–16]. Recent studies have shown that certain β-glucans can bind to symbiosis receptors that do not induce plant immunity but are involved in the accommodation of beneficial microbes. In mutant lines lacking those symbiosis receptors, establishment of arbuscular mycorrhizal symbiosis (AMS) and bacterial root nodule symbiosis (RNS) is restricted [5]. Here, we discuss established and emerging roles of β-glucan-binding

proteins in plant–microbe interactions and highlight several recent studies that identified novel β-glucan-binding proteins which, rather than promoting resistance, act as compatibility factors by enhancing microbial accommodation.

β-Glucan-binding proteins as immunity receptors

In the past years, β-glucans have been identified as major microbial cell wall MAMPs, providing a gateway for studying the mechanisms of β-glucan perception in plants and the receptors involved. Recent studies demonstrated that recognition of linear β-1,3-glucans varies between plant species and depends largely on the degree of polymerization (DP) [14,15]. While both longer (laminarin) and shorter (laminarihexaose [hereafter lam6]) β-1,3-glucans can be perceived in leaves of the monocotyledons *Hordeum vulgare* (hereafter barley) and *Brachypodium distachyon*, leaves of the dicotyledon *Nicotiana benthamiana* perceive only the long β-1,3-glucan laminarin. In barley, *Nicotiana tabacum* and *N. benthamiana* leaves, perception of laminarin was independent of the presence of β-1,6-branches, emphasizing that the DP is important for laminarin perception in these plant species. Branch length and DP can also influence supramolecular structure formation (i.e. aggregation into helical bundles of individual β-glucan strands) which might be relevant for β-glucan protein binding [6,15,17,18]. In *N. tabacum*, sulfation was additionally found to impact laminarin perception and activate a different, SA-dependent signaling pathway [19]. In leaves of the dicotyledons *Arabidopsis thaliana* (hereafter Arabidopsis) and *Capsella rubella*, short lam6 but not the long laminarin was perceived [15]. In Arabidopsis, this perception depends on the co-receptor kinase CHITIN ELICITOR RECEPTOR KINASE 1 (*At*CERK1) [14,20] (Figure 1), while perception of laminarin in rice and *N. benthamiana* is independent of *Os*CERK1 and *Nb*CERK1, respectively [15]. However, *in silico* analysis and isothermal titration calorimetry binding assays did not predict a direct interaction of *At*CERK1 and lam6 [20], suggesting that *At*CERK1 might act as a co-receptor. Therefore, other immune receptors must be present which can directly bind to β-1,3-glucans. One example of a soluble β-glucan receptor is the β-glucan-binding protein (*Gm*GBP) from *Glycine max* L. (soybean), which binds to a β-1,6-linked, β-1,3-branched heptaglucoside (HG) of the oomycete *Phytophthora sojae*. Treatment of soybean tissue with the HG induces phytoalexin production [21]. Additionally, *Gm*GBP has been shown to possess bifunctional properties, exhibiting both binding and endoglycosidic activity on β-1,3-oligoglucosides. This dual functionality allows *Gm*GBP to potentially release fragments from microbial cell walls that it can recognize, thereby initiating defense responses [21,22]. Besides linear β-1,3-glucans, MLGs can trigger PTI in both monocots and dicots [23,24] (Figure 1). MLGs, consisting of linear, unsubstituted chains of β-1,3- and β-1,4-linked glucan subunits, are widely distributed in the cell walls of monocot plants (e.g., Poaceae), fungi, and oomycetes. These MLGs can be recognized as either DAMPs or MAMPs [23,24]. The trisaccharide β-D-cellobiosyl-1,3-β-D-glucose is currently the smallest known MLG structure capable of triggering immunity in Arabidopsis, resulting in enhanced disease resistance to the oomycete pathogen *Hyaloperonospora arabidopsidis* [24]. During *Magnaporthe oryzae* infection, two hemicellulose-derived oligosaccharides are released from rice, 3^1-β-D-cellobiosyl-glucose and 3^1-β-D-cellotriosyl-glucose, and are perceived as DAMPs by an immune complex containing *Os*CERK1 and *Os*CEBiP [25].

Besides MLGs, the β-1,4-linked cellulose derivatives cellobiose and cellotriose are perceived as DAMPs in Arabidopsis [26,27]. Recently, it was found that activation of plant immunity by MLG43 and cellotriose depends on the LRR-MAL-RKs *At*IGP1/CORK1, *At*IGP3 and *At*IGP4 in Arabidopsis [28,29]. Cross-elicitation experiments of cellotriose with the xylo-oligosaccharide DAMPs β-1,4-D-xylotetraose (XYL4) and the pentasaccharide 3^3-alpha-l-arabinofuranosyl-xylotetraose (XA3XX) showed refractory responses in the respective combinations, suggesting shared perception mechanisms [30]. Therefore, the LRR-MAL-RKs *At*IGP1/CORK1, *At*IGP3 and *At*IGP4 might function as common receptors for DAMPs with β-1,4-linked sugar backbones. A more detailed description of plant, fungal or oomycete glycan structures inducing PTI responses in plants and the respective glucan-binding proteins involved in DAMP/MAMP perception, is provided in recent reviews [4,31].

Microbial evasion of β-glucan-triggered immunity

To successfully colonize the host, microbes have evolved various mechanisms to suppress perception and activation of plant immunity [37] (Figure 2). One strategy is downregulating MAMP biosynthesis to avoid MAMP exposure. For example, the hemibiotroph *Colletotrichum graminicola* downregulates the β-1,6-glucan biosynthesis pathway genes, *KRE5* and *KRE6*, in biotrophic hyphae [38] (Figure 2a). Overexpression of *KRE5* and *KRE6* in biotrophic hyphae led to activation of broad-spectrum plant defense responses, including papilla and H_2O_2 formation, as well as transcriptional activation of several defense-related genes [38]. Another strategy to avoid MAMP release is through secretion of inhibitors of plant hydrolytic enzymes. The oomycete pathogen *P. sojae* secretes the Glucanase Inhibiting Protein1 (GIP1), which inhibits the activity of the plant-secreted endoglucanase EGaseA to avoid the release of β-1,3/1,6-glucan MAMPs from the fungal cell wall [39] (Figure 2b).

Figure 1

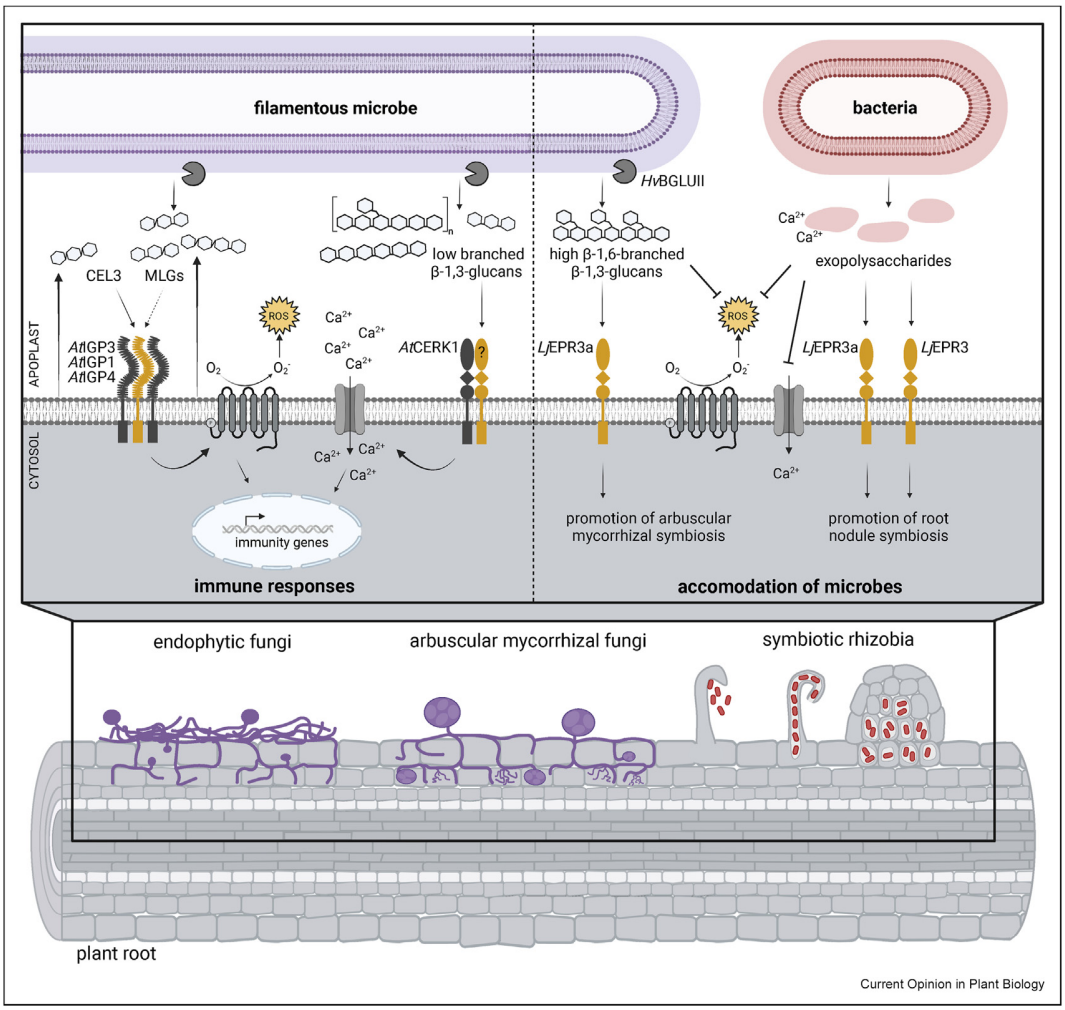

β-Glucan-binding proteins are involved in activation of plant innate immunity or accommodation of microbes as symbiosis receptors. Activation of plant immune responses: Cellotriose (CEL3) and MLGs can be released from plant and fungal cell walls through hydrolytic enzymes (gray circles) and are perceived in Arabidopsis by the LRR-MAL-RKs *Atl*GP1/CORK1, *Atl*GP3 and *Atl*GP4 [28]. CEL3 directly binds to *Atl*GP1, while no direct binding of MLG43 could be shown. However, plant immunity activation in response to MLG43 was reduced in *igp1*, *igp3* and *igp4* mutants [28]. Perception leads to cytosolic calcium influx, apoplastic ROS accumulation and subsequently transcriptional activation of plant immunity genes. In addition, low branched β-1,3-glucans can be released from fungal or oomycete cell walls or EPS matrices and bind to an unknown receptor. In Arabidopsis, *At*CERK1 is involved in laminarihexaose perception as a co-receptor (black) [14,15]. Accommodation of microbes: The plant-derived endoglucanase *Hv*BGLUII releases a β-1,6-branched β-1,3-glucan decasaccharide (β-GD) from fungal EPS matrix which scavenges ROS [32]. β-GD was also shown to bind to the *Lotus japonicus* symbiosis receptor *Lj*EPR3a which promotes arbuscular mycorrhizal symbiosis (AMS) [5]. Similarly, bacterial EPS can chelate calcium ions to prevent cytosolic calcium influx and scavenge apoplastic ROS to suppress plant immunity [33,34]. Furthermore, binding of bacterial EPS to the symbiosis receptors *Lj*EPR3 and *Lj*EPR3a in *L. japonicus* promotes root nodule symbiosis (RNS) [5,35,36]. Receptors that directly bind to ligands are indicated in gold, co-receptors in black. Lower box: Beneficial fungi and bacteria colonizing the plant root epidermis and cortex layer (light gray outermost layers). Endodermis (white) and central cylinder (dark gray innermost layers) are not colonized.

A third strategy, acting further downstream from MAMP release, is the degradation of the released MAMPs to avoid their perception. The rice blast fungus *M. oryzae* secretes a glycoside hydrolase family 17 (GH17) exo-β-1,3-glucanase (Ebg1), which hydrolyzes the β-1,3-glucans released from the fungal cell wall and/or EPS matrix into monomeric glucose to prevent PTI responses [40]. Ebg1 itself can be perceived as a MAMP. Therefore, *M. oryzae* secretes another protein, elongation factor 1 alpha (EF1α), which binds to Ebg1, thereby preventing its recognition [40] (Figure 2c). Similar to Ebg1, the xylo- and β-glucanase XEG1 of *P. sojae* can be recognized as a MAMP in *N. benthamiana* and induce immunity [41]. This response can be suppressed by *P. sojae* RXLR effectors, indicating the use of similar strategies to avoid

Figure 2

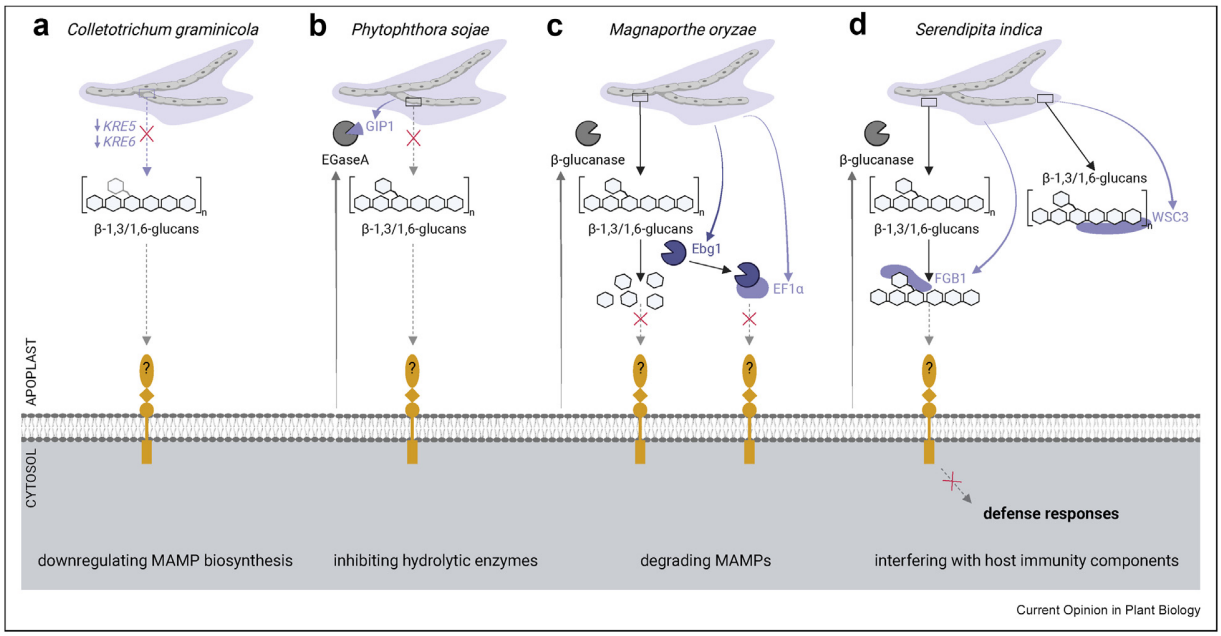

Microbial strategies to evade β-glucan-triggered immunity. a) Downregulating MAMP biosynthesis: To avoid MAMP exposure during infection, the hemibiotroph *Colletotrichum graminicola* downregulates the β-1,6-glucan biosynthesis pathway genes, *KRE5* and *KRE6*, in biotrophic hyphae [38]. **b)** Inhibiting hydrolytic enzymes: To avoid the release of β-glucan MAMPs from the cell wall, the oomycete pathogen *Phytophthora sojae* secretes the Glucanase Inhibitor Protein1 (GIP1), which inhibits the activity of the plant-secreted endoglucanase EGaseA [39]. **c)** Degrading MAMPs: The rice blast fungus *Magnaporthe oryzae* secretes a GH17 exo-β-1,3-glucanase (Ebg1), which hydrolyzes the β-1,3-glucans released from the fungal cell wall and/or EPS matrix (light purple) into single glucose units to prevent PTI responses [40]. Ebg1 itself can be perceived as a MAMP, therefore *M. oryzae* secretes a second protein, elongation factor 1 alpha (EF1α), which sequesters Ebg1. **d)** Interfering with host immunity components: The beneficial root endophytic fungus *Serendipita indica* releases the lectin Fungal Glucan-Binding 1 (FGB1) which binds to β-1,3/1,6-glucans [42]. This lectin localizes on the fungal cell wall and is also extensively secreted into the environment. Substoichiometric amounts of FGB1 were sufficient to significantly reduce glucan perception, indicating that FGB1 might interfere with host immunity components to prevent perception. In addition, *S. indica* secretes the lectin WSC3, which is highly induced during both plant- and microbe-interactions [6]. WSC3 specifically binds to β-1,3-linked glucans of the fungal EPS matrix where it accumulates [6], and potentially functions in adhesion between hyphal cells and strengthening of the cell wall against external stresses. Adapted from Buscaill et al., 2021 [37].

perception of β-glucanases as MAMPs. Alternatively, a fourth strategy is interfering with downstream host immunity components, that activate defense responses upon β-glucan perception (Figure 2d). The beneficial root endophytic fungus *Serendipita indica* secretes the lectin Fungal Glucan-Binding 1 (FGB1) which can bind to the β-1,6-linkages of various β-glucans including laminarin and the disaccharide gentiobiose (D-glucose subunits with β-1,6-linkage) (Figure 2d). Substoichiometric amounts of FGB1 were sufficient to significantly reduce laminarin-induced ROS production in both barley and Arabidopsis, indicating that FGB1 might interfere with host immunity components e.g. through competing for receptor binding and/or blocking of receptor assembly [42]. Moreover, *S. indica* colonization was significantly higher in barley when FGB1 was added, suggesting that this effector promotes fungal colonization in the host [6,42]. *S. indica* additionally expresses the lectin WSC3, which is highly induced *in planta* and in confrontation with other fungi [6,43]. WSC3 is associated with the EPS matrix of *S. indica* [32] and contains three Wall Stress Component (WSC) domains which can each bind to long β-1,3-linked glucans (Figure 2d). While WSC domains were initially described as cell surface sensors for cell wall integrity in yeast [44,45], *S. indica* WSC3 promotes adhesion between hyphal cells and potentially strengthens the cell wall against external stresses. This is likely achieved through the formation of helical bundles involving three β-1,3-linked glucan polymers [6]. WSC-domain-containing proteins are prominent among carbohydrate binding proteins of fungi of various lifestyles [46] and are found to be induced in other plant-fungal systems during colonization [47,48], suggesting a function beyond cell wall stress sensing. These findings suggest that fungal lectins such as FGB1 and WSC3 can bind β-glucans present in the fungal cell wall, EPS matrices and released fragments in the apoplast and might interfere with host immunity signaling components. Further research is needed to investigate the potential role of these lectins in intermicrobial interactions.

Plant-derived β-glucanases modulate immune responses

Downstream of the release and perception of microbial MAMPs during host colonization, several mechanisms evolved that can fine-tune the degree in which plant immunity affects microbial accommodation. Previous reports indicated that some microbial β-glucans (e.g. bacterial EPS) can suppress plant immune responses due to their physicochemical properties, for instance, by sequestration of calcium ions or ROS scavenging [33,34]. A more recent study demonstrated how the interplay between the microbial EPS matrix and plant hydrolases has led to the emergence of a similar principle in fungi [32]. During colonization by *S. indica*, barley secretes an endoglucanase, *Hv*BGLUII, of the family GH17 into the apoplastic space. This enzyme acts on the EPS matrix of the fungus, and releases a specific fragment, a β-1,3/1,6-glucan decasaccharide (β-GD) which does not activate plant immunity (Figure 1). Moreover, β-GD was resistant to further degradation by host glucanases due to the presence of its β-1,6-branches and found to actively scavenge ROS in the apoplast (Figure 1). *S. indica* colonization of barley was enhanced by exogenous application of β-GD, confirming the role of this β-glucan fragment and *Hv*BGLUII in accommodation of beneficial fungi [32]. In addition, *Hv*BGLUII releases β-GD from the cell wall of the pathogenic fungus *Bipolaris sorokiniana* which also possesses immunity-suppressive function [32]. This confirms that the outer microbial EPS layer of fungi and bacteria function as a protective shield against oxidative stress.

An additional response in plant immunity is the production of cell wall appositions (CWA) to restrict fungal and oomycete colonization [49–51]. A recent study identified a previously undescribed barley β-glucanase via a pulldown approach using laminarin as bait. This GH81 member, named β-glucan-binding protein (*Hv*GBP1), hydrolyzes the β-1,3-linkages of laminarin. Barley double mutant lines of the only two GBP paralogs (*gbp1 gbp2*) were significantly less colonized by fungi of various lifestyles compared to the control line (Golden Promise Fast) and relative expression of *HvPR10*, a barley defense marker gene, was significantly higher in the *gbp* mutant lines compared to the control line, implying that *Hv*GBP acts as a compatibility factor in barley by attenuating immune signaling. *Hv*GBP1 was not active on the EPS of *S. indica*, indicating a degree of specificity. Further investigation revealed that when colonized by *S. indica*, the *gbp* mutant lines displayed significantly more CWA compared to the control lines [52]. Since CWA are composed of callose (a β-1,3-glucan), it was inferred that *Hv*GBP likely operates on

Figure 3

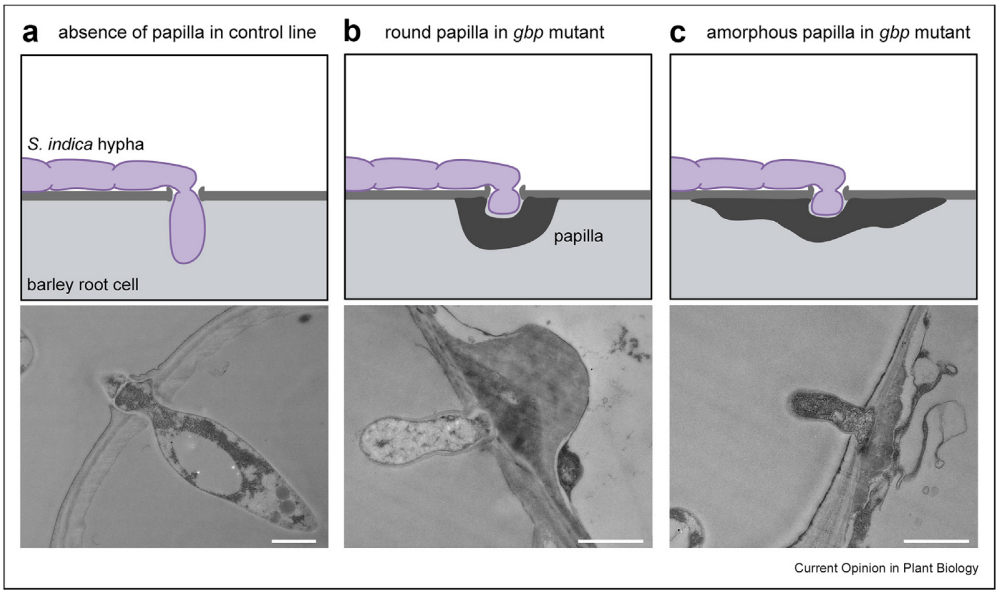

Barley β-glucan-binding protein (GBP) affects the barley cell wall responses at *Serendipita indica* hyphae penetration sites. a) Example of the absence of papilla formation during hyphal penetration in the barley control line Golden Promise Fast [53]. **b)** During hyphal penetration, round, compact papilla structures can be deposited at the barley cell wall such as in the roots of the barley *gbp* mutant line [52]. **c)** In addition to round papilla structures, also spatially unrestricted, amorphous papilla were detected in barley *gbp* roots lacking GBP [52]. These amorphous papillae were not observed in the control line Golden Promise Fast. Top panel: graphical representations of the images below. Bottom panel: transmission electron micrographs of cross-sections of chemically fixed barley roots colonized by *S. indica* at 6 dpi. Scale bars = 1 μm.

the plant cell wall, hydrolyzing callose, thereby enabling fungal penetration of the plant cells [52]. Transmission electron microscopy analysis suggests that both round-shaped, as well as spatially unrestricted, amorphous papillae can be found in *gbp* mutant barley roots at fungal hyphae penetration sites (Figure 3). Amorphous papillae were never found in the control line Golden Promise Fast (Figure 3). This implies that apoplastic β-glucanases can not only target microbial substrates but also modify the plant cell wall to enhance microbial accommodation. Taken together, these findings suggest that β-glucanases can facilitate the colonization of both beneficial and pathogenic fungi by modulating/attenuating the effect of activated defense responses. This indicates a potential homeostatic mechanism to prevent hyperactivation of immunity, which is particularly important in the context of beneficial plant—microbe associations, where an overly aggressive immune response could be detrimental.

β-Glucan symbiosis receptors promote accommodation of beneficial microbes

In contrast to the extensive knowledge of β-glucan receptors in animals, plant β-glucan receptors are relatively understudied, with only a few linked to microbial accommodation. Recent reports have identified two β-glucan receptors from *Lotus japonicus*. One of these is EXOPOLYSACCHARIDE RECEPTOR 3 (*Lj*EPR3), a LysM receptor kinase that plays a crucial role in promoting root nodule symbiosis during rhizobia accommodation in *L. japonicus* [35,36,54] (Figure 1). In a more recent study, *Lj*EPR3a, another LysM receptor kinase, was shown to promote arbuscular mycorrhizal fungus accommodation in *L. japonicus* [5] (Figure 1). *epr3a* mutants exhibited significantly reduced intracellular arbuscule formation compared to the wild-type. Characterization by microscale thermophoresis revealed that both *Lj*EPR3 and *Lj*EPR3a bind the immunosuppressive β-GD released from EPS of endophytic fungi. ROS accumulation upon β-glucan treatment was not affected in *epr3* and *epr3a* mutant plants, indicating β-glucan perception by *Lj*EPR3 and *Lj*EPR3a is not involved in immunity signaling. Instead, *Lj*EPR3 and *Lj*EPR3a act as symbiosis receptors [5,36] (Figure 1). Symbiosis receptor kinases are known from legume-rhizobia symbiosis, where they are important in symbiosis initiation through perception of lipochitooligosaccharides (LCOs) from bacteria (Nodulation-factors) [55,56]. Similarly, perception of LCOs as well as other chitin oligomers from arbuscular mycorrhizal fungi (Myc-factors) by symbiosis receptor kinases plays a key role in AM symbiosis establishment in the host [55—57]. These recent reports about EPR3/EPR3a show for the first time that symbiosis receptors also exist for β-glucan-type ligands, opening up an exciting field of research.

Conclusions

β-Glucans are a diverse group of polysaccharides that can be released by plant- or microbe-derived glucanases and perceived as MAMPs or DAMPs, triggering plant immunity. However, recent studies identified β-glucan-binding proteins which prevent activation of host immunity. Host-derived β-glucanases were also shown to modulate plant immune responses after MAMP perception, for instance by releasing β-glucan fragments which scavenge ROS or by reducing callose deposition along the plant cell wall. A growing amount of evidence suggests that the β-glucan-rich EPS matrix surrounding the cell wall of microbes acts as a protective shield against oxidative stress and that components of the EPS matrix are recognized by symbiosis receptors, which are important in the establishment of mutualistic plant—microbe interactions including AMS and RNS. Similar to the well-studied contrasting roles of chitin-oligosaccharides in immunity and symbiosis establishment [58—61], these findings collectively show that β-glucans play important roles beyond immunity activation in microbial accommodation. The β-glucans themselves, as well as their interacting β-glucan-binding proteins, can be considered as compatibility factors operating at different stages of colonization. These recent advances highlight the unexplored potential for β-glucans of different lengths and branching patterns as symbiosis messengers, shifting our attention to the search for β-glucan ligand/receptor pairs to unravel their mechanisms during beneficial plant—microbe interactions.

Author contributions

SvB: Conceptualization, Investigation, Writing-original draft preparation. PS: Conceptualization, Writing-original draft preparation. AW: Writing-reviewing and editing. UN: Investigation, Supervision, Writing-reviewing and editing. AZ: Conceptualization, Supervision, Writing-reviewing and editing, Funding acquisition.

Declaration of competing interest

The authors declare that they have no known competing financial interests or personal relationships that could have appeared to influence the work reported in this article.

Data availability

Data will be made available on request.

Acknowledgments

SvB and UN acknowledge support by the Max Planck Society. SvB acknowledges support from the International Max Planck Research School (IMPRS) and from project ZU 263/11-2 (SPP 2125 DECRyPT). AZ and PS acknowledge support from the Cluster of Excellence on Plant Sciences (CEPLAS) funded by the Deutsche Forschungsgemeinschaft (DFG, German Research Foundation) under Germany's Excellence Strategy-EXC 2048/1-Project ID: 390686111. AW acknowledges support from the Gatsby

Charitable Foundation, the Leverhulme Trust (Leverhulme Trust Early Career Fellowship) and Darwin College (Cambridge). Figures were created using BioRender.

References

Papers of particular interest, published within the period of review, have been highlighted as:

* of special interest
** of outstanding interest

1. Bowman SM, Free SJ: **The structure and synthesis of the fungal cell wall**. *Bioessays* 2006, **28**:799–808.

2. Ruiz-Herrera J, Ortiz-Castellanos L: **Cell wall glucans of fungi. A review**. *The Cell Surf* 2019, **5**, 100022.

3. Kang X, Kirui A, Muszyński A, Widanage MCD, Chen A, Azadi P, Wang P, Mentink-Vigier F, Wang T: **Molecular architecture of fungal cell walls revealed by solid-state NMR**. *Nat Commun* 2018, **9**:2747.

4. Wanke A, Malisic M, Wawra S, Zuccaro A: **Unraveling the sugar code: the role of microbial extracellular glycans in plant-microbe interactions**. *J Exp Bot* 2021, **72**:15–35.

5. ** Kelly S, Hansen SB, Rübsam H, Saake P, Pedersen EB, Gysel K, Madland E, Wu S, Wawra S, Reid D, *et al.*: **A glycan receptor kinase facilitates intracellular accommodation of arbuscular mycorrhiza and symbiotic rhizobia in the legume Lotus japonicus**. *PLoS Biol* 2023, **21**, e3002127.
This study biochemically characterized a LysM receptor kinase, EPR3a, which binds β-1,3/β-1,6-glucans, and is widely conserved in eudicot and monocot plant species. They showed EPR3a is a symbiosis receptor important for arbuscular mycorrhizal accommodation in *Lotus japonicus*.

6. Wawra S, Fesel P, Widmer H, Neumann U, Lahrmann U, Becker S, Hehemann JH, Langen G, Zuccaro A: **FGB1 and WSC3 are in planta-induced β-glucan-binding fungal lectins with different functions**. *New Phytol* 2019, **222**:1493–1506.

7. McIntosh M, Stone BA, Stanisich VA: **Curdlan and other bacterial (1→3)-β-d-glucans**. *Appl Microbiol Biotechnol* 2005, **68**:163–173.

8. Chawla PR, Bajaj IB, Survase SA, Singhal RS: **Microbial cellulose: fermentative production and applications**. *Food Technol Biotechnol* 2009, **47**.

9. Vega-Sánchez ME, Verhertbruggen Y, Scheller HV, Ronald PC: **Abundance of mixed linkage glucan in mature tissues and secondary cell walls of grasses**. *Plant Signal Behav* 2013, **8**, e23143.

10. Burton RA, Fincher GB: **(1,3;1,4)-β-D-Glucans in cell walls of the Poaceae, lower plants, and fungi: a tale of two linkages**. *Mol Plant* 2009, **2**:873–882.

11. * Perrot T, Pauly M, Ramírez V: **Emerging roles of β-glucanases in plant development and adaptative responses**. *Plants* 2022, **11**.
This review summarizes the different activities of plant β-glucanases, their evolutionary origin, and their roles during physiological processes in growth and development, as well as in plant-microbial interactions.

12. Delmer D, Dixon RA, Keegstra K, Mohnen D: **The plant cell wall—dynamic, strong, and adaptable—is a natural shape-shifter**. *Plant Cell* 2024, **36**:1257–1311.

13. Fesel PH, Zuccaro A: **β-Glucan: crucial component of the fungal cell wall and elusive MAMP in plants**. *Fungal Genet Biol* 2016, **90**:53–60.

14. Mélida H, Sopeña-Torres S, Bacete L, Garrido-Arandia M, Jordá L, López G, Muñoz-Barrios A, Pacios LF, Molina A: **Non-branched β-1,3-glucan oligosaccharides trigger immune responses in Arabidopsis**. *Plant J* 2018, **93**:34–49.

15. Wanke A, Rovenich H, Schwanke F, Velte S, Becker S, Hehemann J-H, Wawra S, Zuccaro A: **Plant species-specific recognition of long and short β-1,3-linked glucans is mediated by different receptor systems**. *Plant J* 2020, **102**:1142–1156.

16. DeFalco TA, Zipfel C: **Molecular mechanisms of early plant pattern-triggered immune signaling**. *Mol Cell* 2021, **81**:3449–3467.

17. Okobira T, Miyoshi K, Uezu K, Sakurai K, Shinkai S: **Molecular dynamics studies of side chain effect on the beta-1,3-D-glucan triple helix in aqueous solution**. *Biomacromolecules* 2008, **9**:783–788.

18. Pluvinage B, Fillo A, Massel P, Boraston AB: **Structural analysis of a family 81 glycoside hydrolase implicates its recognition of β-1,3-glucan quaternary structure**. *Structure* 2017, **25**:1348–1359.e1343.

19. Ménard R, Alban S, de Ruffray P, Jamois F, Franz G, Fritig B, Yvin JC, Kauffmann S: **Beta-1,3 glucan sulfate, but not beta-1,3 glucan, induces the salicylic acid signaling pathway in tobacco and Arabidopsis**. *Plant Cell* 2004, **16**:3020–3032.

20. del Hierro I, Mélida H, Broyart C, Santiago J, Molina A: **Computational prediction method to decipher receptor–glycoligand interactions in plant immunity**. *Plant J* 2021, **105**:1710–1726.

21. Fliegmann J, Mithofer A, Wanner G, Ebel J: **An ancient enzyme domain hidden in the putative beta-glucan elicitor receptor of soybean may play an active part in the perception of pathogen-associated molecular patterns during broad host resistance**. *J Biol Chem* 2004, **279**:1132–1140.

22. Fliegmann J, Montel E, Djulić A, Cottaz S, Driguez H, Ebel J: **Catalytic properties of the bifunctional soybean β-glucan-binding protein, a member of family 81 glycoside hydrolases**. *FEBS Lett* 2005, **579**:6647–6652.

23. Barghahn S, Arnal G, Jain N, Petutschnig E, Brumer H, Lipka V: **Mixed linkage β-1,3/1,4-glucan oligosaccharides induce defense responses in *Hordeum vulgare* and *Arabidopsis thaliana***. *Front Plant Sci* 2021, **12**, 682439.

24. Rebaque D, Del Hierro I, López G, Bacete L, Vilaplana F, Dallabernardina P, Pfrengle F, Jordá L, Sánchez-Vallet A, Pérez R, *et al.*: **Cell wall-derived mixed-linked β-1,3/1,4-glucans trigger immune responses and disease resistance in plants**. *Plant J* 2021, **106**:601–615.

25. Yang C, Liu R, Pang J, Ren B, Zhou H, Wang G, Wang E, Liu J: **Poaceae-specific cell wall-derived oligosaccharides activate plant immunity via OsCERK1 during Magnaporthe oryzae infection in rice**. *Nat Commun* 2021, **12**:2178.

26. Souza CA, Li S, Lin AZ, Boutrot F, Grossmann G, Zipfel C, Somerville SC: **Cellulose-derived oligomers act as damage-associated molecular patterns and trigger defense-like responses**. *Plant Physiol* 2017, **173**:2383–2398.

27. Johnson JM, Thürich J, Petutschnig EK, Altschmied L, Meichsner D, Sherameti I, Dindas J, Mrozinska A, Paetz C, Scholz SS, *et al.*: **A poly(A) ribonuclease controls the cellotriose-based interaction between *Piriformospora indica* and its host Arabidopsis**. *Plant Physiol* 2018, **176**:2496–2514.

28. * Martín-Dacal M, Fernández-Calvo P, Jiménez-Sandoval P, López G, Garrido-Arandía M, Rebaque D, del Hierro I, Berlanga DJ, Torres MÁ, Kumar V, *et al.*: **Arabidopsis immune responses triggered by cellulose- and mixed-linked glucan-derived oligosaccharides require a group of leucine-rich repeat malectin receptor kinases**. *Plant J* 2023, **113**:833–850.
This work identified a group of LRR-MAL receptor kinases in Arabidopsis, essential for perception of cellulose- and mixed-linked glucan-derived oligosaccharides as DAMPs or MAMPs. Isothermal titration calorimetry (ITC) assays with purified extracellular domains of the receptor kinases demonstrated direct binding to cellulose oligosaccharides.

29. Tseng Y-H, Scholz SS, Fliegmann J, Krüger T, Gandhi A, Furch ACU, Kniemeyer O, Brakhage AA, Oelmüller R: **CORK1, A LRR-malectin receptor kinase, is required for cellooligomer-induced responses in Arabidopsis thaliana**. *Cells* 2022, **11**:2960.

30. Fernández-Calvo P, López G, Martín-Dacal M, Aitouguinane M, Carrasco-López C, González-Bodí S, Bacete L, Mélida H, Sánchez-Vallet A, Molina A: **Leucine rich repeat-malectin receptor kinases IGP1/CORK1, IGP3 and IGP4 are required for Arabidopsis immune responses triggered by β-1,4-D-Xylo-oligosaccharides from plant cell walls**. *Cell Surf* 2024, **11**, 100124.

31. ** Molina A, Jordá L, Torres M, Martín-Dacal M, Berlanga DJ, Fernández-Calvo P, Gómez-Rubio E, Martín-Santamaría S: **Plant**

cell wall-mediated disease resistance: current understanding and future perspectives. *Mol Plant* 2024, **17**:699–724.
This review provides an overview of the perception mechanisms of known carbohydrate-based molecular patterns, and their relevance during disease resistance in plants.

32. * Chandrasekar B, Wanke A, Wawra S, Saake P, Mahdi L, Charura N, Neidert M, Poschmann G, Malisic M, Thiele M, *et al.*: **Fungi hijack a ubiquitous plant apoplastic endoglucanase to release a ROS scavenging β-glucan decasaccharide to subvert immune responses**. *Plant Cell* 2022, **34**:2765–2784.
In this study, the authors identified a ROS-scavenging, β-1,3/β-1,6 decasaccharide, which is released from the EPS matrices of fungi of different lifestyles by the plant GH17 β-1,3-endoglucanase and promotes fungal colonization in barley.

33. Aslam SN, Newman M-A, Erbs G, Morrissey KL, Chinchilla D, Boller T, Jensen TT, De Castro C, Ierano T, Molinaro A, *et al.*: **Bacterial polysaccharides suppress induced innate immunity by calcium chelation**. *Curr Biol* 2008, **18**:1078–1083.

34. Silipo A, Erbs G, Shinya T, Dow JM, Parrilli M, Lanzetta R, Shibuya N, Newman MA, Molinaro A: **Glyco-conjugates as elicitors or suppressors of plant innate immunity**. *Glycobiology* 2010, **20**:406–419.

35. Kawaharada Y, Kelly S, Nielsen MW, Hjuler CT, Gysel K, Muszyński A, Carlson RW, Thygesen MB, Sandal N, Asmussen MH, *et al.*: **Receptor-mediated exopolysaccharide perception controls bacterial infection**. *Nature* 2015, **523**:308–312.

36. Kawaharada Y, Nielsen MW, Kelly S, James EK, Andersen KR, Rasmussen SR, Füchtbauer W, Madsen LH, Heckmann AB, Radutoiu S, *et al.*: **Differential regulation of the Epr3 receptor coordinates membrane-restricted rhizobial colonization of root nodule primordia**. *Nat Commun* 2017, **8**, 14534.

37. Buscaill P, van der Hoorn RAL: **Defeated by the nines: nine extracellular strategies to avoid microbe-associated molecular patterns recognition in plants**. *Plant Cell* 2021, **33**:2116–2130.

38. Oliveira-Garcia E, Deising HB: **Attenuation of PAMP-triggered immunity in maize requires down-regulation of the key β-1,6-glucan synthesis genes KRE5 and KRE6 in biotrophic hyphae of *Colletotrichum graminicola***. *Plant J* 2016, **87**:355–375.

39. Rose JK, Ham KS, Darvill AG, Albersheim P: **Molecular cloning and characterization of glucanase inhibitor proteins: coevolution of a counterdefense mechanism by plant pathogens**. *Plant Cell* 2002, **14**:1329–1345.

40. * Liu H, Lu X, Li M, Lun Z, Yan X, Yin C, Yuan G, Wang X, Liu N, Liu D, *et al.*: **Plant immunity suppression by an exo-β-1,3-glucanase and an elongation factor 1α of the rice blast fungus**. *Nat Commun* 2023, **14**:5491.
This study characterized a *Magnaporthe oryzae*-derived exo-glucanase, which suppresses β-1,3-glucan-triggered PTI but itself is recognized as a MAMP. Therefore, they show that a second effector EF1α, is required to shield its perception and allow virulence of this rice pathogen.

41. Ma Z, Song T, Zhu L, Ye W, Wang Y, Shao Y, Dong S, Zhang Z, Dou D, Zheng X, *et al.*: **A Phytophthora sojae glycoside hydrolase 12 protein is a major virulence factor during soybean infection and is recognized as a PAMP**. *Plant Cell* 2015, **27**:2057–2072.

42. Wawra S, Fesel P, Widmer H, Timm M, Seibel J, Leson L, Kesseler L, Nostadt R, Hilbert M, Langen G, *et al.*: **The fungal-specific β-glucan-binding lectin FGB1 alters cell-wall composition and suppresses glucan-triggered immunity in plants**. *Nat Commun* 2016, **7**, 13188.

43. Eichfeld R, Mahdi LK, Quattro CD, Armbruster L, Endeshaw AB, Miyauchi S, Hellmann MJ, Cord-Landwehr S, Grigoriev I, Peterson D, *et al.*: **Time-resolved transcriptomics reveal a mechanism of host niche defense: beneficial root endophytes deploy a host-protective antimicrobial GH18-CBM5 chitinase**. *bioRxiv* 2023. 2023.2012.2029.572992.

44. Lodder AL, Lee TK, Ballester R: **Characterization of the Wsc1 protein, a putative receptor in the stress response of Saccharomyces cerevisiae**. *Genetics* 1999, **152**:1487–1499.

45. Verna J, Lodder A, Lee K, Vagts A, Ballester R: **A family of genes required for maintenance of cell wall integrity and for the stress response in Saccharomyces cerevisiae**. *Proc Natl Acad Sci U S A* 1997, **94**:13804–13809.

46. Lahrmann U, Zuccaro A: **Opprimo ergo sum – evasion and suppression in the root endophytic fungus *Piriformospora indica***. *Mol Plant Microbe Interact* 2012, **25**:727–737.

47. Kohler A, Kuo A, Nagy LG, Morin E, Barry KW, Buscot F, Canbäck B, Choi C, Cichocki N, Clum A, *et al.*: **Convergent losses of decay mechanisms and rapid turnover of symbiosis genes in mycorrhizal mutualists**. *Nat Genet* 2015, **47**:410–415.

48. Doré J, Perraud M, Dieryckx C, Kohler A, Morin E, Henrissat B, Lindquist E, Zimmermann SD, Girard V, Kuo A, *et al.*: **Comparative genomics, proteomics and transcriptomics give new insight into the exoproteome of the basidiomycete *Hebeloma cylindrosporum* and its involvement in ectomycorrhizal symbiosis**. *New Phytol* 2015, **208**:1169–1187.

49. Hückelhoven R: **Cell wall–associated mechanisms of disease resistance and susceptibility**. *Annu Rev Phytopathol* 2007, **45**:101–127.

50. Chowdhury J, Henderson M, Schweizer P, Burton RA, Fincher GB, Little A: **Differential accumulation of callose, arabinoxylan and cellulose in nonpenetrated versus penetrated papillae on leaves of barley infected with *Blumeria graminis* f. sp. hordei**. *New Phytol* 2014, **204**:650–660.

51. Albersheim P, Darvill A, Roberts K, Sederoff R, Staehelin A: *Plant cell walls*. Garland Science; 2010.

52. ** Wanke A, van Boerdonk S, Mahdi LK, Wawra S, Neidert M, Chandrasekar B, Saake P, Saur IML, Derbyshire P, Holton N, *et al.*: **A GH81-type β-glucan-binding protein enhances colonization by mutualistic fungi in barley**. *Curr Biol* 2023, **33**:5071–5084.e5077.
Using a biochemical pull-down, the authors identified a novel plant-derived glycoside hydrolase from barley which enhances colonization of mutualistic fungi of varying lifestyles.

53. Gol L, Haraldsson EB, von Korff M: **Ppd-H1 integrates drought stress signals to control spike development and flowering time in barley**. *J Exp Bot* 2021, **72**:122–136.

54. Wong JEMM, Gysel K, Birkefeldt TG, Vinther M, Muszyński A, Azadi P, Laursen NS, Sullivan JT, Ronson CW, Stougaard J, *et al.*: **Structural signatures in EPR3 define a unique class of plant carbohydrate receptors**. *Nat Commun* 2020, **11**:3797.

55. Yoshida S, Parniske M: **Regulation of plant symbiosis receptor kinase through serine and threonine phosphorylation**. *J Biol Chem* 2005, **280**:9203–9209.

56. Antolín-Llovera M, Petutsching EK, Ried MK, Lipka V, Nürnberger T, Robatzek S, Parniske M: **Knowing your friends and foes – plant receptor-like kinases as initiators of symbiosis or defence**. *New Phytol* 2014, **204**:791–802.

57. Zhang J, Sun J, Chiu CH, Landry D, Li K, Wen J, Mysore KS, Fort S, Lefebvre B, Oldroyd GED, *et al.*: **A receptor required for chitin perception facilitates arbuscular mycorrhizal associations and distinguishes root symbiosis from immunity**. *Curr Biol* 2024, **34**:1705–1717.e1706.

58. Feng F, Sun J, Radhakrishnan GV, Lee T, Bozsóki Z, Fort S, Gavrin A, Gysel K, Thygesen MB, Andersen KR, *et al.*: **A combination of chitooligosaccharide and lipochitooligosaccharide recognition promotes arbuscular mycorrhizal associations in Medicago truncatula**. *Nat Commun* 2019, **10**:5047.

59. Fukuda H, Mamiya R, Akamatsu A, Takeda N: **Two LysM receptor-like kinases regulate arbuscular mycorrhiza through distinct signaling pathways in *Lotus japonicus***. *New Phytologist* 2024, **243**:519–525.

60. Shinya T, Nakagawa T, Kaku H, Shibuya N: **Chitin-mediated plant–fungal interactions: catching, hiding and handshaking**. *Curr Opin Plant Biol* 2015, **26**:64–71.

61. Liang Y, Tóth K, Cao Y, Tanaka K, Espinoza C, Stacey G: **Lipochitooligosaccharide recognition: an ancient story**. *New Phytol* 2014, **204**:289–296.

Chapter 3

Lipids in plant-microbe interactions

3.1 Plant Lipids Mediate Immune Responses to Fungal Lipids in Barley

Saake, P., **Brands, M.**, **Endeshaw, A.**, **Stolze, SC.**, **Westhoff,P.**, **Balcke, GU.**, **Tissier, A.**, **Hensel, G.**, **Nakagami, H.**, **Zuccaro, A.** (2024). Accepted in New Phytologist with minor revisions.

Author contributions

PS, MB and AZ designed the research, conceptualized and edited the manuscript. **PS**, MB and ABE performed the research and analyzed the data. SCS and HN performed the phosphoproteome analysis. PW performed the GC-TOF-MS analysis. GB performed LC-MS/MS analysis. GH generated the AEQ expressing barley lines. NH and CZ generated the tomato *serk3a/b* mutants. All authors were involved in editing the paper. AZ provided funding for the experiments.

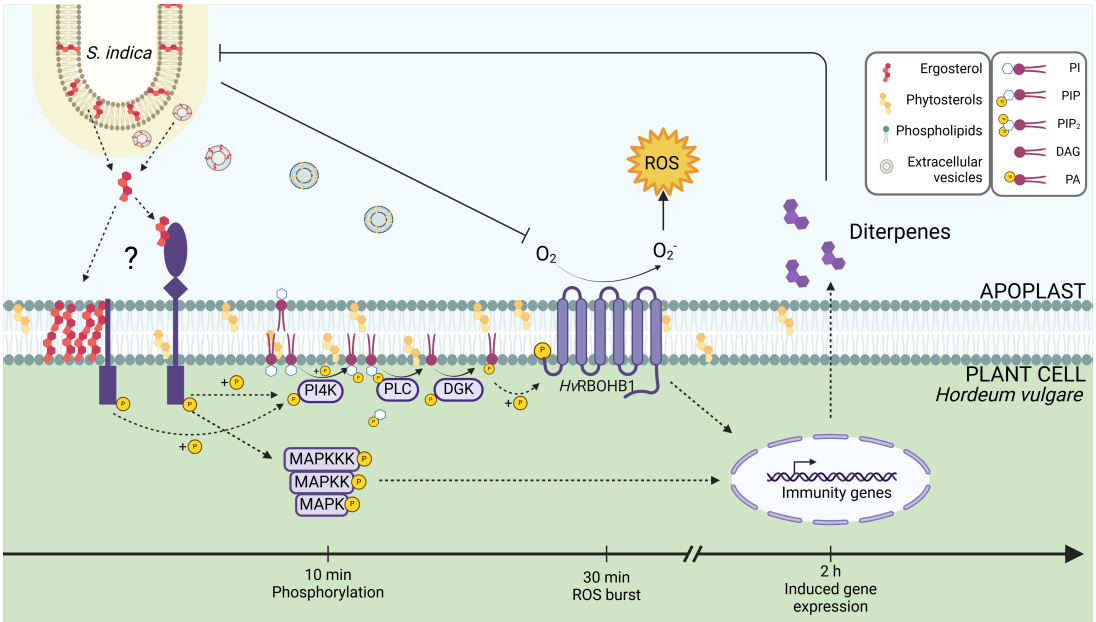

New Phytologist

Plant Lipids Mediate Immune Responses to Ergosterol in Barley

Journal:	*New Phytologist*
Manuscript ID	NPH-MS-2024-49112.R1
Manuscript Type:	Full Paper
Date Submitted by the Author:	10-Jan-2025
Complete List of Authors:	Saake, Pia; University of Cologne, Institute for Plant Sciences; CEPLAS, Cluster of Excellence on Plant Sciences Brands, Mathias; University of Cologne, Institute for Plant Sciences Endeshaw, Asmamaw; University of Cologne, Institute for Plant Sciences Stolze, Sara Christina; Max Planck Institute for Plant Breeding Research, Protein Mass Spectrometry Westhoff, Philipp; Heinrich Heine University Düsseldorf, Institute of Plant Biochemistry; CEPLAS, Cluster of Excellence on Plant Sciences Balcke, Gerd; Leibniz-Institut für Pflanzenbiochemie, Cell and Metabolic Biology Hensel, Goetz; Heinrich Heine University Düsseldorf, Institute of Plant Biochemistry; CEPLAS, Cluster of Excellence on Plant Sciences Holton, Nicholas; Sainsbury Laboratory, University of East Anglia Zipfel, Cyril; University of Zurich, Department of Plant and Microbial Biology; Sainsbury Laboratory, University of East Anglia Tissier, Alain; Leibniz-Institut für Pflanzenbiochemie, Cell and Metabolic Biology Nakagami, Hirofumi; Max-Planck-Institut fur Pflanzenzuchtungsforschung, Basic Immune System of Plants / Protein Mass Spectrometry Zuccaro, Alga; University of Cologne, Institute for Plant Sciences; University of Cologne, Institute for Plant Sciences
Key Words:	Serendipita indica, Ergosterol, Phosphatidylinositol phosphate, Phosphatidic acid, Lipid signaling, Pattern-triggered immunity
Suggested Handling Editor:	Francis Martin

Data Availability Statement

Our Mandates Data Policy requires data to be shared and a Data Availability Statement, so please enter one in the space below. Sample statements can be found here. Please note that this statement will be published alongside your manuscript, if it is accepted for publication.

The RNA-Seq data generated in this paper will be available at the National Center for Biotechnology Information (NCBI) Gene Expression Omnibus (GEO), under the GEO accession number GSE280369 (https://www.ncbi.nlm.nih.gov/geo/query/acc.cgi?acc=GSE280369). The mass spectrometry proteomics data have been deposited to the ProteomeXchange Consortium via the PRIDE partner repository (Perez-Riverol et al., 2022) with the dataset identifier PXD056788.

All data supporting the findings of this study are available within the article and supporting information (Fig. S1-S9; Tables S1-S3; Methods S1).

Plant Lipids Mediate Immune Responses to Ergosterol in Barley

Authors:

Pia Saake[1,2], Mathias Brands[1], Asmamaw Bidru Endeshaw[1], Sara Christina Stolze[4], Philipp Westhoff[2,3], Gerd Ulrich Balcke[5], Götz Hensel[2,3], Nicholas Holton[6], Cyril Zipfel[6,7], Alain Tissier[5], Hirofumi Nakagami[4], Alga Zuccaro[1,2]

[1] University of Cologne, Institute for Plant Sciences, Cologne, Germany.

[2] Cluster of Excellence on Plant Sciences (CEPLAS), Cologne, Germany.

[3] Heinrich-Heine University Düsseldorf, Institute for Plant Biochemistry, Düsseldorf, Germany.

[4] Max Planck Institute for Plant Breeding Research, Protein Mass Spectrometry, Cologne, Germany.

[5]Leibnitz Institute for Plant Biochemistry, Halle (Saale), Germany.

[6]The Sainsbury Laboratory, University of East Anglia, Norwich, United Kingdom.

[7]Institute of Plant and Microbial Biology, Zurich-Basel Plant Science Center, University of Zurich, Zurich, Switzerland.

Corresponding author: Alga Zuccaro; azuccaro@uni-koeln.de

ORCIDs

Pia Saake	0000-0002-1776-8580
Mathias Brands	0000-0001-6548-1448
Asmamaw Bidru Endeshaw	0000-0002-9406-4245
Sara Christina Stolze	0000-0002-1421-9703
Philipp Westhoff	0000-0002-3494-9420
Gerd Ulrich Balcke	0000-0002-0475-0672
Götz Hensel	0000-0002-5539-3097
Nicholas Holton	0000-0002-7674-2794
Cyril Zipfel	0000-0003-4935-8583
Alain Tissier	0000-0002-9406-4245
Hirofumi Nakagami	0000-0003-2569-7062
Alga Zuccaro	0000-0002-8026-0114

Total word count (include only Introduction, Materials and Methods, Results and Discussion)	7996	Acknowledgements:	117
Summary:	184	Author contributions:	68
Introduction:	701	No. of figures:	7
Materials and Methods:	2351	No. of Tables:	0
Results:	2886	No. of Supporting information files:	4
Discussion:	2028		

Summary

- Lipids play crucial roles in plant-microbe interactions, functioning as structural components, signaling molecules, and microbe-associated molecular patterns (MAMPs). However, the mechanisms underlying lipid perception and signaling in plants remain largely unknown.
- Here, we investigate the immune responses activated in barley (*Hordeum vulgare* L.) by lipid extracts from the beneficial root endophytic fungus *Serendipita indica* and compare them to responses elicited by chitohexaose and the fungal sterol ergosterol. We demonstrate that *S. indica* lipid extract induces hallmarks of pattern-triggered immunity (PTI) in barley. Ergosterol emerged as the primary immunogenic component and was detected in the apoplastic fluid of *S. indica*-colonized barley roots. Notably, *S. indica* colonization suppresses the ergosterol-induced burst of reactive oxygen species (ROS) in barley.
- By employing a multi-omics approach, which integrates transcriptomics, phosphoproteomics, and metabolomics, we provide evidence for the activation of phosphatidylinositol phosphate (PIP) signaling and diterpene biosynthesis upon exposure to fungal lipids. Furthermore, we show that phosphatidic acid (PA) enhances lipid-mediated apoplastic ROS production in barley.
- These findings indicate that plant lipids facilitate immune responses to fungal lipids in barley, providing new insights into lipid-based signaling mechanisms in plant-microbe interactions.

Highlights

- Fungal lipids activate pattern-triggered immunity, phosphatidylinositol phosphate signaling and diterpene synthesis in barley.
- Phosphatidic acid enhances lipid-mediated ROS production, indicating a role for plant lipids in immune responses.
- Ergosterol is the main immunogenic component of *S. indica* lipid extract and present in the apoplastic fluid of *S. indica*-colonized roots.
- *S. indica* colonization suppresses the ergosterol-induced ROS burst in barley roots.

Key words

Serendipita indica, ergosterol, phosphatidylinositol phosphate, phosphatidic acid, lipid signaling, pattern-triggered immunity

Introduction

Lipids are a diverse group of molecules that play crucial roles in plant nutrition, development and plant-microbe interactions. As major constituents of the plasma and organelle membranes, they work in conjunction with the cell wall to establish the interface for environment interactions. Here, they act as structural elements, modulate physicochemical membrane properties, function as (stress) signaling molecules and influence subcellular protein localization through lipid-protein interactions (Noack & Jaillais, 2020; Macabuhay *et al.*, 2022; Zarreen *et al.*, 2023).

Lipids are categorized into three main classes based on their chemical structures: sphingolipids, sterols, and (glycero)phospholipids (Moreau & Bayer, 2023). Among these, phosphoinositides stand out as crucial, low-abundance signaling molecules, which are derived from phosphatidylinositol (PI), a ubiquitous phospholipid containing *myo*-inositol in its head group. PI can be phosphorylated at various positions by phosphatidylinositol kinases (PIKs) to produce phosphatidylinositol phosphates (PIPs). In plants, phosphatidylinositol 4-phosphate (PI4P) is the most abundant phosphoinositide, although PI3P, PI5P and diphosphorylated forms, such as PI(4,5)P_2 and PI(3,5)P_2 have also been detected (Munnik & Vermeer, 2010).

During abiotic and biotic stress, PIPs can be interconverted and hydrolyzed to produce the signaling lipid phosphatidic acid (PA). PIPs are also associated with disease resistance (Xing *et al.*, 2019; Qin *et al.*, 2020), cytoskeletal rearrangements (Sinha *et al.*, 2024), endo- and exocytosis (Synek *et al.*, 2021; Marković & Jaillais, 2022), and the formation of membrane nanodomains (Gronnier *et al.*, 2017; Jaillais & Ott, 2020). Nanodomains, accommodating membrane-associated kinases and receptor-like kinases can act as signaling hubs during

plant-microbe interactions to enable perception of microbe- or damage-associated molecular patterns (MAMPs or DAMPs) and subsequent immune signaling (Couto & Zipfel, 2016; Jaillais & Ott, 2020).

MAMP recognition initiates a signaling cascade often involving an increase in cytosolic calcium concentration ($[Ca^{2+}]_{cyt}$), production of reactive oxygen species (ROS) and phosphorylation of mitogen activated protein (MAP) kinases. This cascade ultimately leads to altered gene expression and secretion of chemically diverse antimicrobial compounds, such as phytoalexins (Siebers *et al.*, 2016; DeFalco & Zipfel, 2021). Altogether, this response is known as pattern-triggered immunity (PTI). While plant lipids are important signaling molecules, microbial lipids can also be detected by plants as MAMPs. Lipid MAMPs can be directly recognized by plant receptors, as in the case of the medium-chain-3-hydroxy fatty acids from *Pseudomonas syringae* lipopolysaccharides (Kutschera *et al.*, 2019) or processed by secreted enzymes prior to recognition, such as ceramide D from *Phytophora infestans* (Kato *et al.*, 2022).

The fungal sterol lipid ergosterol, a 5,7-diene oxysterol, has also been shown to be perceived as a MAMP by plants (Kasparovsky *et al.*, 2003). Sterols are core membrane components that regulate membrane organization, stability, and permeability (Macabuhay *et al.*, 2022; Der *et al.*, 2024). Ergosterol is the main sterol in most fungal membranes (Jordá & Puig, 2020) and is absent from plant membranes. It has been shown to induce early immune responses in various plant species. These responses include ROS accumulation in *Beta vulgaris* (Rossard *et al.*, 2010), increase in $[Ca^{2+}]_{cyt}$ in *Nicotiana tabacum* (Kasparovsky *et al.*, 2003; Vatsa *et al.*, 2011), medium alkalinization in *Beta vulgaris* and *Nicotiana tabacum* (Rossard *et al.*, 2010; Vatsa *et al.*, 2011) and induced expression of immunity related genes such as pathogenesis related (*PR*) genes and *WRKY* transcription factors in *Vitis vinifera*, *Nicotiana tabacum* and *Solanum lycopersicum* (Laquitaine *et al.*, 2006; Lochman & Mikes, 2006; Lindo *et al.*, 2020). Despite being known as a MAMP for over two decades, the perception and signaling pathway of ergosterol remains largely unknown. This study investigates the molecular signaling mechanisms activated in barley (*Hordeum vulgare*) in response to lipid extracts, containing a mixture of lipids from the mycelium of the beneficial root endophytic fungus *Serendipita indica* (Sebacinales, Basidiomycota). Our data demonstrate that fungal lipids induce immunity in barley, with ergosterol identified as the primary immunogenic component of *S. indica* lipids and detected in the apoplast, the aqueous space between the host cells, of *S. indica*-colonized barley roots. By integrating transcriptomics, phosphoproteomics, and metabolomics, we provide evidence that PIP signaling and diterpene biosynthesis are activated upon exposure to fungal lipids. Furthermore, we demonstrate that PA enhances lipid-mediated apoplastic ROS production in barley. Notably, fungal colonization alters the host's phytosterol content and

suppresses the ergosterol-induced ROS burst, suggesting a counterstrategy against lipid-mediated host immunity.

Materials and Methods

Plant material and growth conditions

Seeds of *Hordeum vulgare* L. cv Golden Promise were surface sterilized with 6% sodium-hypochlorite for 1 h and washed six times for 30 min with sterile milliQ-water. Seed coats were removed gently and seeds were germinated on wet filter paper for three days in the dark at 21 °C. Germinated seedlings were transferred to sterile WECK jars containing 100 ml solid 1/10 PNM (plant nutrition medium, pH 5.6) and 0.4 % (w/v) Gelrite for MAMP treatments and 1.2 % (w/v) Gelrite for fungal colonization and grown under long-day conditions (day/night cycle of 16/8 h, 22 °C/18 °C, light intensity of 108 µmol/m^2*s) for an additional four days for MAMP treatment, and 3-, 7- and 14- days for fungal colonization assays. For Ca^{2+}-influx assays, barley lines expressing apoaequorin (Hv^{AEQ}) were generated (see Methods S1).

Solanum lycopersicum L. cv Moneymaker wildtype (WT) and *serk3a serk3b* mutant seeds (see Methods S1) were sown on soil and grown for ~2-3 weeks in the greenhouse under long-day conditions (day/night cycle of 17/7 h, 25-28 °C, ~35-40% humidity). For ROS assays, 3 mm leaf discs of the two youngest, adult leaves of three weeks old tomato plants were used.

Seeds of a *Nicotiana benthamiana* D. line expressing aequorin (Nb^{AEQ}) (Wanke *et al.*, 2020) were sown on soil and grown for ~3 weeks in the greenhouse under long-day conditions (day/night cycle of 16/8 h, 22–25°C, light intensity of ~140 µmol/m^2*s, maximal humidity of 60%). For ROS and Ca^{2+}-influx assays, 3 mm leaf discs of the youngest, adult leaf of 3 weeks old plants were used.

Seeds of *Arabidopsis thaliana* L. Col-0 plants expressing cytosolic apoaequorin (At^{AEQ}) were surface sterilized with EtOH and subsequently dried under the clean bench. Dried seeds were placed on ½ MS (Murashige-Skoog-Medium, with vitamins, pH 5.7) plates containing 0.5 % sucrose and 0.4 % (w/v) Gelrite and stratified for 2-5 days at 4 °C in the dark. Subsequently, plants were grown in short day conditions (8 h light, 16 h dark, with 130 µmol/ m^2*s of light and 22 °C/18 °C) for 7-8 days. For ROS assays, one seedling was transferred into each well of a 96 well plate. For Ca^{2+}-assays, seedlings were transferred to 24 well plates containing 1 ml ½ MS medium + sucrose and grown for another 4 days prior to use in the assay.

Cultivation of *S. indica* and plant colonization

Cultivation and chlamydospore isolation of *Serendipita indica* (DSM11827) was done as previously described (Wawra *et al.*, 2016; Sarkar *et al.*, 2019).

Germinated barley seedlings were prepared as described above and inoculated with 3 ml of either sterile water as control or *S. indica* chlamydospores (500,000 spores/ml). Roots were harvested at 3-, 7- and 14 days post inoculation (dpi), washed thoroughly in ice-cold water to remove extraradical fungal hyphae, briefly dried on tissue paper and frozen in liquid nitrogen. Four barley plants were used per jar and pooled per biological replicate.

ROS accumulation assay

ROS assays were performed as described previously (Chandrasekar *et al.*, 2022). Preparation of *N. benthamiana*, tomato and *A. thaliana* material is described above. For barley, roots and shoots of seven days old seedlings were separated. Three root pieces (0.5 cm) or one 3 mm leaf disc were transferred to each well of a 96-well microtiter plate (white, flat bottom) containing 200 µl of 2.5 mM MES buffer, pH 5.6. The plate was incubated ON at 21°C for recovery. The next day, the buffer was replaced with 100 µl 2.5 mM MES buffer containing 20 µM LO-12 and 20 µg/ml HRP. After 25 min incubation in the dark, 100 µl two-fold concentrated elicitor solution or solvent control was added to each well and chemiluminescence was measured using a TECAN SPARK 10M microplate reader over all wells for 2h with an integration time of 450 msec.

Calcium influx *assay*

Preparation of *N. benthamiana* and *A. thaliana* material is described above. For barley, roots and shoots were prepared as described for ROS accumulation assays but Hv^{AEQ} plants were used. Prior to ON recovery, the buffer in the wells was replaced with 100 µl 2.5 mM MES buffer containing 10 µM coelenterazine and 10 mM $CaCl_2$ per well and plates were incubated ON in the dark at 21°C. On the next day, chemiluminescence was measured using a TECAN SPARK 10M microplate plate reader. After the baseline measurement (5 min), 100 µl of two-fold concentrated elicitor solution was added manually. Photon emission was constantly measured for 30 minutes. Subsequently, 100 µl of discharge solution (3M $CaCl_2$ in 50 % EtOH) was injected into each well, followed by constant measurement for 1 minute. All steps were performed with an integration time of 450 msec. In all assays, 2 columns (16 wells) were measured per run.

MAPK phosphorylation

Barley root segments and leaf discs were prepared as described above for ROS and Ca^{2+}-influx assays. Twenty-four randomly selected pieces were transferred into each well of a 24-well plate containing 1 ml 2.5 mM MES buffer. Plates were incubated ON at 21°C for recovery. On the next day, 500 µl buffer of each well were removed and replaced with two-fold concentrated elicitor solution and gently mixed. At 5-, 10-, 20- or 30-min post treatment, roots

were removed from the treatment solution, gently dried on tissue paper and snap frozen in liquid nitrogen and homogenized with glass beads in the TissueLyserII (Qiagen) for 4 times 30 sec, 30 Hz in ice-cold holders. Phosphorylated proteins were isolated using phosphoprotein extraction buffer (50 mM Tris-HCl (pH 7.5), 2 mM DTT, 5 mM EDTA, 5 mM EGTA, 10 mM NaF, 50 mM β-glycerolphosphate, 10 % glycerol, 1 tablet each of Roche Complete Mini – EDTA free and PhosStop phosphatase inhibitor per 10 ml). Protein concentration was determined using Bradford Assay following the manufacturer's instructions and 4 µg protein of each sample were separated on SDS-PAGEs and subsequently transferred to nitrocellulose membranes. Membranes were blocked for 1h with 2.5 % TBS-T BSA and incubated ON with the primary antibody (anti-p44/p42, 1:1500) in 2.5 % TBS-T BSA at 4 °C. The next day, the membranes were washed with 1xTBS-T and the secondary antibody (anti-rabbit IgG, 1:50.000) was added for 1h. After washing with 1xTBS-T and 1x TBS, blots were developed using 1ml SuperSignal™West Femto (Thermo Scientific) solution per membrane. Western Blots were imaged using the Fujifilm LAS 4000 mini camera.

Elicitor preparations

The following chemicals were used as elicitors, pre- or cotreatments. Chitohexaose (Megazyme, O-CHI6), flg22 peptide (GenScript, RP19986), ergosterol pharmaceutical standard (Supelco, PHR1512), L-α-phosphatidylinositol (soy PI, Avanti, 840044), L-α-phosphatidic acid (egg PA, Avanti, 840101), L-α-phosphatidylcholine (soy PC, Avanti, 441601), L-α-phosphatidylinositol 4-monophosphate (Sigma-Aldrich, P9638), L-α-phosphatidylinositol 4,5-diphosphate (Sigma-Aldrich, P9763). Stock solutions of lipids were prepared in methanol and used to prepare elicitor solutions of appropriate concentrations in aqueous MES buffer as described below. Self-produced lipid extracts and lipid fractions were evaporated with N_2 gas and resuspended in MeOH as solvent. As control, the respective solvent was processed in the same way. All elicitor and control solutions were prepared as two-fold concentrated solutions in 2.5 mM MES buffer, pH 5.6 containing 1:20 (v/v %) MeOH. For liposomes, PA was evaporated under N_2 gas and the lipid film hydrated with buffer (25 mM HEPES, pH=7.5, 50 mM KCL, 1 mM $MgCL_2$) at 4°C, rapidly vortexed for 30 seconds and sonicated on ice 5 times for 10 sec with each 10 sec pause prior to use in cotreatment ROS assay with ergosterol.

RNA-seq and qRT-PCR

For RNA-seq and qRT-PCR, barley roots were prepared as described for the MAPK phosphorylation assay. RNA extraction, cDNA synthesis and qRT-PCR were performed as described previously (Sarkar *et al.*, 2019).

For RNA sequencing, 25 µl RNA with a concentration of 100 ng/µl was used. For Illumina-compatible RNAseq libraries at first an enrichment for poly-A RNAs was performed (NEBNext® Poly(A) mRNA Magnetic Isolation Module; New England Biolabs), followed by library generation with NEBNext Ultra™II Directional RNA Library Prep Kit for Illumina (New England Biolabs). Next, sequencing-by-synthesis was done on a NextSeq 2000 device in 2 x 150 bp paired-end read mode Library construction and sequencing was performed at the Genome Centre of the Max Planck Institute for Plant Breeding, Cologne. For information on processing of the sequencing data see Methods S1.

Apoplastic fluid isolation of barley roots

Barley seedlings were grown and inoculated with *S. indica* on 1/10 PNM medium as described above. Per replicate, 110 barley seedlings were used, which yielded approximately ~1 ml apoplastic fluid per replicate. For extraction of apoplastic fluid, the roots were washed thoroughly in ice-cold water to remove external fungal hyphae and cut into 2 cm pieces. Root pieces were submitted to five cycles of vacuum infiltration (15 min 250 mbar, 1.5 min ATM) in ice cold water. Subsequently, roots were dried on tissue paper and transferred into a 20 ml syringe inside a 50 ml falcon tube and centrifuged for 15 min at 4 °C, 2000 rpm, lowest de- and acceleration to collect apoplastic fluid (approx. 1-2 ml per replicate) in the bottom of the falcon tube. Apoplastic fluid was stored on ice at 4 °C until further use. Roots were flash-frozen in liquid nitrogen and stored at -80 °C until further use.

Lipid extraction and fractionation by solid phase extraction

Lipid extraction was done according to the method described (Bligh & Dyer, 1959) using chloroform:methanol:formic acid (1:1:0.2 v/v). To extract lipids from *S. indica* mycelium or colonized or mock-inoculated barley roots, frozen material was ground in liquid nitrogen into a very fine powder using mortar and pestle. Per sample, ~200 mg of homogenized plant or fungal tissue was used. For fractionation of crude lipids, the lipid extract was separated by two consecutive solid phase extractions (SPE) using Strata®SI-1 (55 µm, 70 Å, 1 ml) silica columns. In the first SPE, lipids were separated via elution with chloroform ($CHCL_3$) and MeOH into neutral ($CHCL_3$) and polar lipids (MeOH). The $CHCL_3$ fraction was evaporated under N_2 gas and used for further fractionation of the neutral lipids using a hexane:diethylether gradient on a second silica column as described previously (vom Dorp *et al.*, 2013) (Methods S1). All fractions that were used in immunity assays were dried under N_2 and resuspended in 4 ml MeOH prior to usage.

Phosphoproteomics

To analyze phosphorylated proteins in response to elicitor treatments, barley roots were treated as described for the MAPK phosphorylation assay and root material was harvested 10 min post treatment. Root material was ground into a very fine powder and phospho-enriched proteins were extracted using 1 ml extraction buffer (8M urea, 20 µl/ml Phosphatase Inhibitor Cocktail 2 (Sigma, P5726-5ML), 20 µl/ml Phosphatase Inhibitor Cocktail 3 (Sigma, P0044-5ML), 5 mM DTT), alkylated with CAA (550 mM stock, 14 mM final) and the reaction was quenched with DTT (5 mM final). An equivalent of 500 µg total protein per sample was diluted to 1 M urea with 100 mM Tris-HCl pH 8.5, 1 mM $CaCl_2$ and samples were digested with 5 µg LysC (stock: 1 µg/µl Lys-C (WAKO) in 50 mM NH_4HCO_3) for 4h at RT and 5 µg trypsin (stock: 1 µg/µl in 1 mM HCl) ON at 37 °C. After incubation, samples were acidified with TFA to 0.5% final concentration and samples were desalted using C18 SepPaks (1cc cartridge, 100 mg (WAT023590). Phosphopeptide enrichment was performed by hydroxy acid-modified metal-oxide chromatography (HAMMOC) (adapted from:(Nakagami, 2014)). Finally, the samples were dried in a vacuum evaporator, and dissolved in 10 µl 2% ACN, 0.1% TFA (A* buffer) for MS analysis.

Samples were analyzed using an Ultimate 3000 RSLC nano (Thermo Fisher) coupled to an Orbitrap Exploris 480 mass spectrometer equipped with a FAIMS Pro interface for Field asymmetric ion mobility separation (Thermo Fisher). Raw data were processed using MaxQuant software (version 1.6.3.4) (Cox & Mann, 2008) with label-free quantification (LFQ) and iBAQ enabled (Tyanova *et al.*, 2016). For more details on sample- and data processing see Methods S1.

Measurements of sterols via GC-TOF-MS

For sterol measurement via GC-TOF-MS, 5 nmol stigmastanol was added as internal standard in a $CHCL_3$:MeOH (2:1) mix prior to lipid extraction. Lipid extraction and SPE was performed as described above. Dried free sterol fractions (50µl) were directly derivatized with 100 µl MSTFA for 30 min at 80 °C. Subsequently the samples were transferred to glass vials and measured with split ratio of 1:10. To measure crude lipid extracts of apoplastic fluid, dried lipid extracts were resuspended in 300 µl hexane and split in 2x 150 µl samples. One 150 µl sample each was evaporated under N_2 gas. Dried samples were derivatized with MSTFA for 30 min at 80°C automatically prior to measurement using a Multipurpose Autosampler (Gerstel). 1 µl of sample was injected with an automatic liner exchange system in conjunction with a cold injection system in splitless mode (ramping from 50 °C to 250 °C at 12 °C s-1) into the GC with a helium flow of 1 ml/min. Chromatography was performed using a 7890B GC system (Agilent Technologies) with a HP-5MS column with 5 % phenyl methyl siloxane film (Agilent 19091S-

433, 30 m length, 0.25 mm internal diameter, 0.25 µM film). Compounds were identified via MassHunter Qualitative (v b08.00, Agilent Technologies) by comparison of spectra to the NIST14 Mass Spectral Library. Ergosterol was verified using a pharmaceutical standard (Supelco, PHR1512) and stigmastanol was used as an internal standard. Peaks were integrated using MassHunter Quantitative (v b08.00, Agilent Technologies). For relative quantification, all metabolite peak areas were normalized to the corresponding peak area of the internal standard stigmastanol and the sample fresh weight (mycelium, roots) or volume (AF).

Diterpene measurements via LC-MS

Germinated barley seedlings were treated with solvent control, 250 nM ergosterol or inoculated with *Bipolaris sorokiniana* spores (5000 spores/ml, 5ml) and grown for 6 days as described above. To harvest root exudates, plants were removed from the medium and washed gently in 25 ml water to wash off residual diterpenes attached on the outside of the roots. The medium was collected with the wash water from the roots and flash-frozen in liquid nitrogen. Diterpenes were extracted as described previously (Liu *et al.*, 2024). For information on LC-MS measurement see Methods S1.

Figure preparation

Figure 1 C and Figure 7 were created using Biorender.

Results

Lipids from the beneficial endophyte *S. indica* induce immunity in barley.

To investigate the immune response of barley to fungal lipids, root and leaf tissues were treated with a crude lipid extract from *S. indica* mycelium grown in axenic culture. MAPK activation, *PR* gene induction and Ca^{2}- and ROS burst production were monitored. The fungal MAMP chitohexaose (Chit6) served as a positive control, while a solvent control (Sc) was used as the negative control. Treatment with *S. indica* lipid extract (*Si*) induced MAPK phosphorylation in barley roots 10-20 minutes post treatment with the highest signal after 20 minutes (Figure 1 A). This induction was weaker and occurred later than with chitohexaose treatment, which resulted in MAPK phosphorylation as early as 5 minutes post treatment (Figure 1 A). The expression of the immunity-related gene *HvPR10* (Mahdi *et al.*, 2022) was induced to a similar extent upon treatment with *S. indica* lipid extract and chitohexaose 2 hours post treatment (hpt) (Figure 1 B). While *HvPR10* expression in chitohexaose-treated roots returned to baseline levels after 24 hours, expression in *S. indica* lipid extract-treated roots remained high at this time point (Figure 1 B). In barley leaves, both chitohexaose and *S. indica* lipid extract treatments induced *HvPR10* expression at 24 hpt (Fig. S1 B). In response to MAMP treatment,

the level of apoplastic ROS increases rapidly, followed by a rapid decline. Treatment with the lipid extract of *S. indica* induced a ROS burst in barley roots and leaves, which reached a maximum approximately 20 minutes post elicitor treatment. In contrast, the chitohexaose-induced ROS burst showed a more rapid increase, reaching a maximum at about 8 minutes, followed by a steep decline (Figure 1 D, Fig. S1 A).

To identify the immunogenic components of the *S. indica* lipid extract, we fractionated the crude lipid extract by solid phase extraction (Figure 1 C). We found that the ROS burst correlated with the fraction containing free sterols, as all other fractions did not induce ROS bursts in barley roots (Figure 1 D). The timing and shape of the ROS burst induced by the sterol fraction closely matched those induced by the total lipid extract of *S. indica* and a pharmaceutical ergosterol standard (Figure 1 D, yellow and orange) and differed from the ROS burst induced by chitohexaose (Figure 1 D, light blue). Consistent with this, ergosterol treatment also induced MAPK phosphorylation in barley roots with the highest signal obtained at 20 minutes post treatment (Fig. S2).

Another hallmark of early immune signaling is increase in cytosolic Ca^{2+} concentration ($[Ca^{2+}]_{cyt}$). While chitohexaose induced a strong and rapid Ca^{2+}-burst, only a slight increase in $[Ca^{2+}]_{cyt}$ was observed when barley roots were treated with ergosterol or *S. indica* lipids (Figure 1 E).

To investigate whether the perception of *S. indica* lipids occurs in other plant species, ROS- and Ca^{2+}-burst assays were performed in *Nicotiana benthamiana* and *Arabidopsis thaliana*. In *N. benthamiana* leaves, *S. indica* lipids induced a pronounced ROS burst accompanied by a minor yet distinct increase in $[Ca^{2+}]_{cyt}$ (Fig. S3 A-B). Timing and shape of the *S. indica* lipids-induced ROS burst overlapped with ergosterol-induced ROS burst (Fig. S3 C) In *A. thaliana* seedlings, total ROS accumulation increased after treatment with *S. indica* lipids or ergosterol, however no pronounced peak was observed (Fig. S3 D) and only a slight increase in $[Ca^{2+}]_{cyt}$ was detected (Fig. S3 E).

Taken together, these results indicate that *S. indica* lipid extract induces MAPK phosphorylation, *PR*-gene expression and ROS burst in barley, which are typical hallmarks of PTI. In addition, the perception of fungal lipids is conserved between barley and *N. benthamiana*, in leaves. In contrast to chitohexaose, *S. indica* lipid-induced ROS accumulation is not accompanied by a strong Ca^{2+}-burst, but rather appears to be independent of it.

Ergosterol is the primary immunogenic component of *S. indica* lipid extract and is present in the apoplast of colonized barley roots.

Since the free sterol fraction in barley elicited a comparable ROS burst as the crude *S. indica* lipid extract (Figure 1 D), we analyzed this fraction by GC-TOF-MS to identify the major sterols

potentially triggering the immune response. We found that ergosterol was the major lipid in this fraction. In addition, smaller amounts of related sterols, presumably ergosta-7,22-dien-3-ol and ergost-8(14)-en-3-ol, were detected (Figure 2 A).

Microbes often employ different strategies to avoid MAMP recognition by the host. For example, reducing abundance or shielding of the MAMP during colonization (van Boerdonk *et al.*, 2024). To investigate whether ergosterol is present during endophytic root colonization, total lipids were isolated from mock-treated or *S. indica*-colonized barley roots at 3-, 7- and 14-days post inoculation (dpi). Subsequently, free sterols were isolated using solid-phase extraction, following the protocol previously described for extracting lipids from *S. indica* mycelium (Figure 1 C). Consequently, samples from mock-treated roots contained free sterols derived exclusively from plant roots, whereas samples from colonized roots comprised a mixture of plant and fungal free sterols. Roots were thoroughly washed prior to extraction to remove extraradical mycelium. The free sterol fractions were then tested for their potential to elicit ROS production in barley roots (Figure 2 B). Free sterols isolated from colonized barley roots, but not from mock-treated barley roots, induced a ROS burst with similar timing to that obtained with *S. indica* mycelial lipids (Figure 2 B). GC-TOF-MS analysis confirmed the presence of ergosterol in colonized barley roots (Figure 2 C). Since mock-inoculated roots lack ergosterol (Figure 2 C), and no other major qualitative differences in identified free sterols were observed using our method (Figure 2 B), the ROS burst associated with free sterols isolated from *S. indica*-colonized roots is most likely attributable to ergosterol. The relative amount of ergosterol increased from 3 to 7 dpi, followed by a decrease at 14 dpi (Figure 2 D). Intraradical *S. indica* colonization, as determined by expression of the fungal housekeeping gene *SiTEF*, followed a comparable trend (Figure 2 G). In addition, the amount of the phytosterol stigmasta-5,22-dien-3β-ol (hereafter stigmasterol) increased upon colonization with *S. indica* and over time, while the amount of 24β-ethylcholest-5-en-3β-ol (hereafter β-sitosterol) remained unchanged (Fig. S4 A-B). Thus, the ratio of stigmasterol to β-sitosterol increased in *S. indica*-colonized roots at 14 dpi (Fig. S4 C). Stigmasterol, which is synthesized by desaturation of β-sitosterol, has been shown to accumulate in several plant-microbe interactions (Griebel & Zeier, 2010; Wang *et al.*, 2012; Huang *et al.*, 2022). This data demonstrates that the plant modifies its phytosterol content in response to *S. indica* colonization.

Having detected immunogenic ergosterol in colonized roots (Figure 2 C-D), we next analyzed the lipid content of apoplastic fluid of *S. indica*-colonized and mock-treated barley roots. Ergosterol was detected in the apoplastic fluid of colonized roots but was absent in mock-inoculated samples (Figure 2 E-F), demonstrating its relevance during the *S. indica*-barley interaction.

394 Ergosterol pretreatment desensitizes barley roots to fungal lipid-induced immune responses.

395 MAMP perception triggers complex signaling cascades in plants, including the internalization
396 and degradation of receptor complexes. This process, known as receptor-mediated
397 endocytosis, serves as a regulatory mechanism to prevent constitutive activation of immune
398 responses (Robatzek *et al.*, 2006; Claus *et al.*, 2018). Simultaneously, it may trigger *de novo*
399 biosynthesis of ligand-free receptors to replace the activated ligand-bound receptors, thereby
400 enabling resensitization (Smith *et al.*, 2014). Consequently, subsequent exposure to the same
401 MAMP or MAMPs that share receptor complexes results in a diminished or completely
402 abolished immune response. This phenomenon, termed desensitization or refractory period,
403 is crucial for maintaining cellular homeostasis and preventing excessive energy expenditure
404 on continuous immune activation. Subsequent exposure experiments can be used to
405 distinguish whether different MAMPs share the same receptor and signaling components.
406 Here, barley roots were either pretreated with a solvent control, chitohexaose, ergosterol or
407 stigmasterol for 16 hours and subsequently treated with solvent control, chitohexaose,
408 ergosterol or *S. indica* lipids. In chitohexaose pretreated roots, the chitohexaose-induced ROS
409 burst was abolished, whereas ergosterol and *S. indica* lipids induced a ROS burst similar to
410 ergosterol and *S. indica* lipid treatment of solvent control- or stigmasterol pretreated roots
411 (Figure 3 A, B, D). The opposite was observed in ergosterol pretreated roots. Here, no ROS
412 burst was elicited by ergosterol and *S. indica* lipids, whereas chitohexaose treatment induced
413 ROS accumulation (Figure 3 C). Pretreatment with stigmasterol neither affected the
414 chitohexaose-induced ROS burst nor the ergosterol- or *S. indica* lipids-induced ROS burst
415 (Figure 3 D). These data suggest that ergosterol and *S. indica* lipids share common signaling
416 components but are perceived by a distinct receptor from chitohexaose.

417 Distinct receptor complexes were shown to recruit similar co-receptor kinases such as the
418 receptor like kinase BRASSINOSTEROID-INSENSITIVE 1-ASSOCIATED KINASE 1 (BAK1)/
419 SOMATIC EMBRYOGENESIS RECEPTOR KINASE 3 (SERK3), a co-receptor involved in
420 several PTI signaling pathways, predominantly those associated with leucine-rich repeat (LRR)
421 receptor-like kinases (Couto & Zipfel, 2016). To determine whether BAK1/SERK3 is linked to
422 ergosterol perception, we assessed ROS production in leaves of *Solanum lycopersicum* cv.
423 Moneymaker wildtype (WT) and *serk3a serk3b* mutant plants in response to ergosterol or flg22
424 as control (Fig. S5). Previously, flg22-induced ROS burst was shown to be reduced in *S.*
425 *lycopersicum serk3b* mutants (Peng & Kaloshian, 2014). As expected, the flg22-induced ROS
426 burst was reduced in *serk3a serk3b* mutant leaves compared to WT (Fig. S5). However, the
427 ergosterol-induced ROS burst was unaltered in *serk3a serk3b* leaves. This indicates that
428 BAK1/SERK3 is not involved in ergosterol perception in tomato, suggesting that LRR-type
429 receptor-like kinases are not involved in ergosterol perception.

Previous studies showed that *S. indica* colonization suppresses ROS bursts induced by flg22 and chitooctaose in *A. thaliana* (Jacobs *et al.*, 2011) and by laminarin in barley (Wawra *et al.*, 2016). Therefore, we analyzed whether *S. indica* colonization alters the perception of chitohexaose, *S. indica* lipids and ergosterol in barley. In *S. indica*-colonized roots, the peak height of the chitohexaose-induced ROS burst was only slightly reduced compared to mock-inoculated roots, whereas the ROS bursts induced by *S. indica* lipids and ergosterol were completely abolished (Figure 3 E-F). These findings suggest that *S. indica* more effectively inhibits the perception of ergosterol and fungal lipids than chitohexaose in barley at this stage of colonization.

Phosphatidylinositol phosphate signaling components are phosphorylated upon fungal lipid treatment.

Phosphorylation plays a pivotal role in immunity signaling as one of the primary post-translational modifications used to rapidly propagate signals within cells. This reversible process allows for quick and dynamic responses to external stimuli. To elucidate the early signal transduction events triggered by fungal lipids and identify key proteins involved in the initial steps of the signaling cascade activated by different elicitors, we conducted a comprehensive analysis of the phosphoproteome in barley roots. Samples were treated for 10 minutes with ergosterol, *S. indica* lipid extract, chitohexaose, or solvent control as a negative control (Figure 4). A total of 4502 phosphorylated peptides were detected across all treatments (Table S1 A). Of those, 271 were absent from the solvent control treatment but present in at least one of the three elicitor treatments in the unimputed data, and therefore contained candidates for proteins involved in MAMP-mediated signal transduction (Table S1 B). Based on Gene Ontology (GO) terms, candidate proteins were selected and grouped into functional categories (Table S1 C). 66% of the treatment-specific phosphorylated peptides were shared between all three treatments, indicating a conserved response in phosphorylation in response to chitohexaose, ergosterol and fungal lipids, while 20% were shared between ergosterol and *S. indica* lipid treatment alone (Figure 4 A). A large portion of the phosphorylated candidate peptides refer to proteins that are predicted to be involved in responses to (a)biotic stress or signal transduction, such as MAP kinases, calcium-dependent protein kinases and WRKY transcription factors. Interestingly, an MLO-like protein was phosphorylated specifically upon lipid treatment (Figure 4 B, Table S1 B). Mildew resistance locus O (MLO) proteins were first identified in barley, where their mutations confer resistance against the pathogen *Blumeria graminis* f. sp. *hordei* (Piffanelli *et al.*, 2002) and recently also shown to be involved in *S. indica* colonization (Hilbert *et al.*, 2020). We further detected proteins potentially involved in vesicle trafficking and transmembrane transport, processes known to be important in PTI (Figure 4 B, Table S1 B). Moreover, we identified phosphorylation of proteins, that are predicted to be

involved in lipid metabolism and function in plant defense responses, namely a patatin and a sphingosine-1-phosphate lyase (Figure 4 B). Patatins have lipid acyl hydrolase function (Rydel *et al.*, 2003) and patatin-like phospholipase As are involved in phospholipid signaling (Ryu, 2004; Canonne *et al.*, 2011) and pathogen response (La Camera *et al.*, 2005; Kim *et al.*, 2014; Jang *et al.*, 2020). Sphingosine-1-phosphate lyases are involved in sphingosine-1-phosphate metabolism, an important signaling molecule in the regulation of drought stress, plant disease resistance and programmed cell death (Michaelson et al., 2016; Seo et al., 2021; Zhang et al., 2014). Additionally, a phosphatidylinositol 4-kinase (PI4K), 1-phosphatidylinositol-3-phosphate 5-kinase-like (PI3P5K), diacylglycerol kinase (DGK) and Sac1-like domain containing protein, four proteins potentially involved in PIP-mediated signaling, were phosphorylated (Figure 4 B). PI4K and PI3P5K can phosphorylate PI and PI3P, respectively, producing PI4P and PI(3,5)P_2, which again can be substrates for other PIP-kinases or phospholipase C (PLC) to produce diacylglycerol (DAG). DAG can be phosphorylated by DGKs to produce PA (Figure 4 C). In addition, PA can also be produced from unspecific hydrolysis of all phospholipids by phospholipase D (PLD) (Figure 4 C). The Sac1-like or suppressor of actin (SAC) domain containing family of proteins are phosphoinositide phosphatases, which dephosphorylate PIPs and therefore are involved in PIP turnover (Mao & Tan, 2021) (Figure 4 C). Taken together, these findings suggest a rapid activation of PIP- signaling in response to fungal elicitors as part of the barley root immune response.

PA enhances the ergosterol-induced ROS burst.

DGK phosphorylation suggests that barley might synthesize PA from DAG in response to ergosterol and *S. indica* lipid treatment. PLC-DGK-derived PA was recently shown to enhance the MAMP-induced ROS burst in *A. thaliana* (Zhang *et al.*, 2009; Kalachova *et al.*, 2022; Kong *et al.*, 2024; Qi *et al.*, 2024). Apoplastic ROS is primarily produced by NADPH-oxidases, also known as respiratory burst oxidase homologs (RBOHs), which are activated through phosphorylation. In our phosphoproteome analysis, we detected phosphorylation of HvRBOHI3 (4HG0409670.1) and HvRBOHB1 (4HG0414140.2) - annotation based on (Mahalingam *et al.*, 2021) - in samples treated with chitohexaose, ergosterol, or *S. indica* lipid extract (Figure 4 B). We therefore tested the influence of PA, PI and PI4P on the chitohexaose- and ergosterol-induced ROS bursts in barley roots. As an additional control, we used the phospholipid phosphatidylcholine (PC). Addition of PC, PI or PI4P did not affect the chitohexaose- or ergosterol-induced ROS burst in barley roots (Figure 5 A-C, Fig. S7 A-C). In contrast, co-treatment with PA significantly enhanced the ergosterol-induced ROS burst, resulting in both higher peak maxima and an overall increase in total ROS production (Figure 5 D). Furthermore, cotreatment with PA liposomes, which are believed to facilitate uptake of PA, yielded similar results (Fig. S6). Conversely, addition of PA did not enhance chitohexaose-

induced ROS production in barley roots (Fig. S7 D). To exclude a chitohexaose concentration-dependent effect, we tested a range of chitohexaose concentrations and confirmed that PA did not enhance the chitohexaose-induced ROS burst across all tested concentrations (Fig. S8). These results reveal a differential impact of phospholipids on MAMP-induced ROS production in barley, with PA specifically enhancing the ergosterol-triggered ROS burst but not the chitohexaose-induced response, further suggesting distinct signaling pathways for these MAMPs.

Diterpene biosynthesis is activated upon fungal lipid treatment.

In addition to changes in the phosphoproteome, we investigated transcriptomic changes upon treatment with ergosterol or *S. indica* lipids at 2 hpt to identify candidate genes involved in downstream responses. The analysis revealed that 244 genes were significantly differentially expressed upon ergosterol or *S. indica* lipid treatment (log2FC ≥ 1, ≤ -1; q-value ≤ 0.05) (Table S2 B). Among the most upregulated genes were two genes encoding 1-deoxy-xylulose-5-phosphate synthases (*DXS*) and one gene encoding a 1-deoxy-d-xylulose 5-phosphate reductoisomerase (*DXR*), the enzymes that perform the committing steps of the 2-C-methylerythritol 4-phosphate (MEP or non-mevalonate) pathway (Table S2, Figure 6 A). In addition, expression of multiple genes, potentially involved in the MEP pathway was induced, whereas expression of genes potentially involved in the mevalonate (MVA) pathway was downregulated or not detected at all (Figure 6 A). The MEP pathway leads to the production of isoprenoid intermediates, which can be converted to hordedanes, a class of diterpene phytoalexins produced in barley in response to fungal treatment (Figure 6 A) (Liu *et al.*, 2024). Indicative of an induction of diterpene synthesis, we found homologs of geranylgeranyl diphosphate synthase (*GGPPS*), *ent*-copalyl diphosphate synthase 2 (*CPS2*), kaurene synthase-like 4 (*KSL4*) and cytochrome P450 oxygenases (*CYPs*) among the strongest induced genes upon fungal lipid treatment (Figure 6 A, Table S2). We verified the induction of *HvCPS2*, *HvKSL4* and *HvCYP89E31* upon addition of ergosterol via qRT-PCR (Figure 6 B).

To investigate whether diterpenes are synthesized in response to ergosterol treatment, we analyzed root exudates of barley roots treated with either ergosterol or roots infected by *B. sorokiniana* as positive control, by LC-MS. We detected two major diterpenes with mass-to-charge ratio (*m*/*z*) of 315.196 and 317.211 -previously identified in root exudates of *B. sorokiniana*-colonized roots (Liu *et al.*, 2024) - in both root exudates of ergosterol-treated and *B. sorokiniana*-colonized barley roots (Figure 6 C, Fig. S9). These findings confirm that ergosterol perception by barley triggers the biosynthesis and exudation of antimicrobial phytoalexin diterpenes.

Discussion

S. indica colonization modulates pattern-triggered immunity during fungal lipid perception.

In this study we demonstrate that ergosterol and total lipids isolated from the beneficial root endophyte *S. indica* induce hallmarks of PTI in barley (Figure 1, Fig. S1-S2). Apoplastic ROS production and increase in $[Ca^{2+}]_{cyt}$ are recognized as two of the earliest and often interlinked signaling mechanisms activated in plants in response to MAMP perception (Ranf *et al.*, 2011; Qi *et al.*, 2017; Marcec *et al.*, 2019). In addition to the Ca^{2+}-independent activation of *A. thaliana* RBOHD by phosphorylation *via* the cytosolic kinase BIK1 (Kadota *et al.*, 2015), intracellular Ca^{2+} was shown to activate *A. thaliana* RBOHD through direct binding of Ca^{2+} to EF hand motifs (Ogasawara *et al.*, 2008; Kimura *et al.*, 2012) and phosphorylation by Ca^{2+}-dependent protein kinases (Dubiella *et al.*, 2013; Seybold *et al.*, 2014). In addition, increase in $[Ca^{2+}]_{cyt}$ is required for initiation of the flg22-induced ROS burst in *A.thaliana* (Marcec & Tanaka, 2022). In our experiments, chitohexaose treatment induced both a strong Ca^{2+}- and ROS burst in barley roots (Figure 1 D-E) as previously reported (Chandrasekar *et al.*, 2022). In contrast, ergosterol and *S. indica* lipids induced no or only minor increase in $[Ca^{2+}]_{cyt}$ but a distinct ROS burst in barley roots (Figure 1 D-E), suggesting that Ca^{2+}-influx might not be required for the lipid-induced ROS burst in barley roots.

Given that plants encode various RBOH isoforms with distinct functions (Suzuki *et al.*, 2011; Zhang *et al.*, 2023), the perception of different MAMPs in barley may activate specific RBOH isoforms, some of which might not require Ca^{2+} for activation (Mahalingam *et al.*, 2021). Phosphoproteome analysis of barley roots revealed minor phosphorylation of *Hv*RBOHB1 (4HG0414140.2) and *Hv*RBOHI3 (4HG0409670.1), indicating they might be involved in MAMP perception in barley. Further identification and characterization of the barley RBOHs is needed to clarify their specific functions in fungal lipid perception and MAMP-induced responses.

Desensitization of MAMP-induced immunity in barley revealed that barley roots employ distinct receptors for chitohexaose and ergosterol perception (Figure 3 A-D). Similarly, membrane hyperpolarization induced by ergosterol in *Mimosa pudica* cells was abolished upon subsequent exposure with ergosterol but not chitosan or cholesterol (Amborabé *et al.*, 2003). Further evidence in tomato indicates that BAK1/SERK3 is not involved in ergosterol recognition (Fig. S5). Moreover, colonization by *S. indica* more effectively suppressed the perception of ergosterol compared to chitohexaose perception (Figure 3 E-F) and the activation of early immune responses was delayed with fungal lipids compared to chitohexaose treatment (Figure 1, Fig. S1).

The distinct perception of ergosterol compared to other MAMPs may be attributed to their differing physicochemical properties. Unlike water-soluble MAMPs such as flg22 and

chitohexaose, ergosterol is hydrophobic and poorly soluble in water. Ergosterol is present in the membrane of fungal extracellular vesicles (EVs) (Rodrigues, 2018) and animal pathogens such as *Cryptococcus neoformans* or *Candida albicans* were shown to secrete ergosterol-containing EVs to transport macromolecules across the cell wall (Rodrigues *et al.*, 2007; Vargas *et al.*, 2015). The amount of ergosterol in liposomes correlated with the ability to induce pyroptosis (Wellington *et al.*, 2014; Koselny *et al.*, 2018). Plant colonizing fungi can also release EVs into the apoplast to secrete antimicrobial compounds, small-interfering RNAs, or effector proteins (An *et al.*, 2006; Lo Presti & Kahmann, 2017; Rutter & Innes, 2018; Garcia-Ceron *et al.*, 2021; Li *et al.*, 2022; Oliveira-Garcia *et al.*, 2023). Recently, it was reported that ergosterol-induced nanodomains are required for activation of clathrin-mediated endocytosis to translocate fungal effectors into the host during the *Magnaporthe oryzae* – rice interaction (Guo *et al.*, 2023; Oliveira-Garcia *et al.*, 2023).

Thus, upon plant colonization, ergosterol could be released into the apoplast via EVs, making it accessible for perception by the plant. Ergosterol is able to integrate into membranes, potentially inducing the formation of nanodomains that significantly alter the structure and fluidity of the membrane (Xu *et al.*, 2001; Klemptner *et al.*, 2014). In plant plasma membranes, such perturbations could activate membrane-embedded mechanosensors or other receptors sensitive to structural changes in the lipid bilayer, as observed with the lipopeptide surfactin from root-associated rhizobacteria (Pršić *et al.*, 2023).

This complex process could explain the delayed ROS burst observed with ergosterol compared to chitohexaose perception. The time required for membrane integration and subsequent signaling cascades may exceed that of direct recognition by apoplastic receptors, accounting for the differences in timing of the immune response between these MAMPs. Still perception via direct binding to a membrane receptor is not excluded.

S. indica colonization led to an increase in stigmasterol in barley roots (Fig. S4). Stigmasterol is synthesized via C22 desaturation of β-Sitosterol (Aboobucker & Suza, 2019) and was shown to have a higher ordering effect on the membrane than β-sitosterol (Grosjean *et al.*, 2015). Changes in the stigmasterol-to-β-sitosterol content affect microbial colonization and nutrient exchange, probably by influencing membrane rigidity (Griebel & Zeier, 2010; Wang *et al.*, 2012; Huang *et al.*, 2022). Furthermore, sterols regulate the spatial distribution of membrane lipids e.g. PIPs and certain proteins, such as transporters, RBOHs (Der *et al.*, 2024) or callose-modifying enzymes (Grison *et al.*, 2015), potentially modulating plant immune responses or receptor availability. Therefore, the increase in stigmasterol during *S. indica* colonization could lead to rigidified membranes and modified spatial distribution of membrane proteins, altering nutrient transport, fungal penetration and immunity activation.

606 Fungal lipid treatment induces phosphorylation of proteins and expression of genes involved
607 in plant lipid signaling components.

608 Next to canonical signaling components such as MAPK and receptor-like cytoplasmic kinases,
609 we found PI4K, PI3P5K, DGK and a Sac1-like domain containing protein to be phospho-
610 regulated upon fungal lipid treatment (Figure 4). These enzymes could be involved in the
611 synthesis and homeostasis of the plant lipids PI4P, PI(3,5)P_2 and PA. In *A. thaliana*, *At*PI4Kα1
612 (At1g49340), *At*FAB1A (At4g33240) and *At*PLC2 (At3g08510), involved in PIP signaling, were
613 detected in the plasma membrane associated proteome after ergosterol treatment (Khoza *et*
614 *al.*, 2019).

615 Barley PI4K (2HG0208880.1, Figure 4 C) shows highest sequence similarity to *A. thaliana*
616 PI4Kγ7 (At2g03890), and wheat PI4Kγ6-like (XP_044459596), which was shown to be
617 involved in salt- and drought stress tolerance (Liu *et al.*, 2013) and barley PI3P5K
618 (7HG0697890.1, Figure 4 C) is most similar to *A. thaliana* FORMATION OF APLOID AND
619 BINUCLEATE CELLS1 A (FAB1A, At4g33240) and FAB1B (At3g14270), involved in
620 endosome maturation and microtubule association, controlling protein trafficking (Hirano *et al.*,
621 2011, 2015). While PI4K and PI3P5K phosphorylate PIPs, the barley Sac1-like domain
622 containing protein (5HG0422410.1, Figure 4 C) is the homolog of Arabidopsis SAC9, a plant-
623 specific PI(4,5)P_2-5 phosphatase that likely dephosphorylates PI(4,5)P_2 to PI4P (Williams *et*
624 *al.*, 2005; Lebecq *et al.*, 2022). The interplay of PIP kinases and the Sac1-like protein in barley
625 likely regulates the formation of membrane regions enriched in PI4P and PI(4,5)P_2. These
626 could serve as signaling hubs for membrane receptors (Antignani *et al.*, 2015) involved in plant
627 immunity during colonization of barley with *S. indica* and control vesicle trafficking (Synek *et*
628 *al.*, 2021) and fungal accommodation (Ivanov & Harrison, 2019; Qin *et al.*, 2020).

629 In addition, DGK phosphorylation suggests that barley might synthesize PA from DAG in
630 response to ergosterol and *S. indica* lipid treatment. Barley DGK (5HG0440700.1, Figure 4 C)
631 showed highest sequence similarity to *A. thaliana* DGK1 and 2 (At5g07920, At5g63770), which
632 were shown to be involved in cold stress tolerance in *A. thaliana* (Arisz *et al.*, 2013). PLC and
633 PA were described as important modulators of ROS levels under biotic stress (D'Ambrosio *et*
634 *al.*, 2017; Seth *et al.*, 2024) and PA was shown to accumulate in a burst-like fashion, similar to
635 ROS, in response to microbial infection (Andersson *et al.*, 2006; Zhang & Xiao, 2015).
636 Moreover, earlier studies demonstrated ROS production upon PA treatment of tobacco cells,
637 *A. thaliana* guard cells or PA infiltration in *A. thaliana* leaves (Sang *et al.*, 2001; Park *et al.*,
638 2004; De Jong *et al.*, 2004; Zhang *et al.*, 2009). PA interacts with many different proteins in *A.*
639 *thaliana*, targeting them to membranes and activating or inhibiting their enzymatic functions
640 (Testerink & Munnik, 2005; Pokotylo *et al.*, 2018; Yao & Xue, 2018). Thus, PA can regulate

the availability of receptors and signaling components involved in MAMP perception, as recently demonstrated for *A. thaliana* RBOHD. PLC2-DGK5β-derived PA inhibited vacuolar degradation of RBOHD in response to flg22 and chitin treatment, thereby enhancing RBOHD mediated ROS production in *A. thaliana* leaves (D'Ambrosio *et al.*, 2017; Kong *et al.*, 2024; Qi *et al.*, 2024). Cotreatment of barley roots with PA enhanced the ergosterol-induced ROS burst (Figure 5 D), indicating PA might stabilize RBOH in barley roots in response to MAMP treatment as well. However, we did not observe an enhanced ROS burst upon chitohexaose treatment with PA cotreatment in barley roots or a ROS burst triggered by PA alone (Figure 5, Fig. S7-S8). PA synthesis was shown to be activated by *S. indica* colonization and involved in *S. indica* mediated growth promotion of *A. thaliana*, via a pathway involving a PLD, 3-phosphoinositide-dependent protein kinase1 (PDK1) and oxidative signal inducible1 (OXI1) cascade (Camehl *et al.*, 2011). Expression of *PDK1*, which is activated by PA (Anthony *et al.*, 2004), and *OXI1*, which is necessary for ROS burst-mediated signaling in *A. thaliana* (Rentel *et al.*, 2004), is upregulated during *S. indica* colonization, supporting a connection between PA and ROS signaling upon *S. indica* colonization (Camehl *et al.*, 2011). It remains unknown how *S. indica* colonization suppresses the lipid-induced ROS burst (Figure 3 F) but since PA enhances the ergosterol-induced ROS burst (Figure 5), modulating PA synthesis could be one way to also modulate lipid-induced host immunity. However, since addition of PA is not required for the ergosterol-induced ROS burst, other pathways are likely also targets of *S. indica* for suppression of host immunity.

Additionally, we have observed that the perception of *S. indica* lipids and ergosterol induces the expression of the diterpene biosynthesis genes, *HvCPS2*, *HvKSL4* and *HvCYP89E31* (Figure 6 A-B). Recently, these genes were shown to be highly induced in response to colonization by the pathogenic fungus *B. sorokiniana* but also slightly by the beneficial root endophyte *Serendipita vermifera*. Diterpenes synthesized by these enzymes have been shown to be exuded by barley roots upon fungal colonization and inhibit germination of several root colonizing fungi including *S. indica* (Sarkar *et al.*, 2019; Mahdi *et al.*, 2022; Liu *et al.*, 2024).

Taken together these data demonstrate that perception of fungal lipids activates several plant lipid signaling pathways involved in both rapid and downstream immune responses.

Conclusion

Ergosterol, the predominant sterol in fungal membranes, serves as a MAMP in barley-fungus interactions. During root colonization, *S. indica* hyphae proliferate in the apoplast where ergosterol is present. Although typically confined within fungal membranes, ergosterol could become accessible for plant perception through the release of EVs into the apoplast.

Two mechanisms may underlie plant perception of ergosterol. First, ergosterol may bind to the extracellular domain of membrane-bound receptors in the apoplast. Alternatively, ergosterol could integrate into the plant plasma membrane, subsequently activating membrane-embedded mechanosensors or other receptors responsive to structural changes in the lipid bilayer. Additionally, the integrated ergosterol may directly interact with specific ergosterol-binding receptors within the membrane (Figure 7).

Upon ergosterol perception, a signaling cascade is initiated that leads to the phosphorylation of PI4K, PI3P5K and DGK, potentially promoting PA synthesis, which in turn, enhances RBOH activation and stabilization, amplifying the ROS burst in barley. Furthermore, phosphoinositides generated from PI4K and PI3P5K contribute to the formation of membrane contact sites that may facilitate vesicle fusion, receptor recruitment or internalization. This series of signaling events activates MAPK cascades, leading to increased expression of immunity genes and diterpene biosynthesis genes. The culmination of these events results in diterpene exudation, a protective response that deters microbial invaders sensitive to this diterpene class. Notably, *S. indica* has adapted to root colonization and can suppress the fungal-lipid-induced ROS burst and thus limit diterpene biosynthesis.

Despite ergosterol's important role in plant-microbe interactions and its use as a marker for fungal colonization in crops like barley and corn, it has received limited research attention in recent years. This study provides evidence that fungal-lipid perception in barley roots is mediated through plant-lipid signaling pathways. Further investigation into the specific receptors involved could offer valuable insights into plant-fungal interactions and the mechanisms employed by fungi to overcome plant immune responses.

Acknowledgements

We thank Gabriel Schaaf, Oliver Ebenhöh and Takaki Maekawa for the helpful discussions and input. We thank Elisabeth Klemp, Maria Graf and Katrin Weber for the great help with processing of the samples and analysis of the sterol GC-MS measurements. We thank Anne Harzen for the phosphoproteomics sample preparation. PS, GH, PW and AZ acknowledge support from the Cluster of Excellence on Plant Sciences (CEPLAS) funded by the Deutsche Forschungsgemeinschaft (DFG, German Research Foundation) under Germany's Excellence Strategy-EXC 2048/1-Project ID: 390686111. HN and SCS acknowledge support by the Max Planck Society. GB, AT and AZ acknowledge support from project ZU 263/11-1 (SPP 2125 DECRyPT). CZ acknowledges support from the Gatsby Charitable Foundation and the University of Zurich.

Competing interest

The authors declare no competing interest.

Author contributions

PS, MB and AZ designed the research, conceptualized and edited the manuscript. PS, MB and ABE performed the research and analyzed the data. SCS and HN performed the phosphoproteome analysis. PW performed the GC-TOF-MS analysis. GB performed LC-MS/MS analysis. GH generated the AEQ expressing barley lines. NH and CZ generated the tomato *serk3a serk3b* mutants. All authors were involved in editing the paper. AZ provided funding for the experiments.

Data availability

The RNA-Seq data generated in this paper will be available at the National Center for Biotechnology Information (NCBI) Gene Expression Omnibus (GEO), under the GEO accession number GSE280369 (https://www.ncbi.nlm.nih.gov/geo/query/acc.cgi?acc=GSE280369). Reviewers can access the data using the access token: sbyjiicmzjifrkp. The mass spectrometry proteomics data have been deposited to the ProteomeXchange Consortium via the PRIDE partner repository (Perez-Riverol *et al.*, 2022) with the dataset identifier PXD056788 and can be accessed on the PRIDE website using the following account details: Username: reviewer_pxd056788@ebi.ac.uk; Password: T9HRaIWDZqQH.

All data supporting the findings of this study are available within the article and supporting information (Fig. S1-S9; Tables S1-S3; Methods S1).

References

Aboobucker SI, Suza WP. **2019**. Why do plants convert sitosterol to stigmasterol? *Frontiers in Plant Science* **10**.

Amborabé BE, Rossard S, Pérault JM, Roblin G. **2003**. Specific perception of ergosterol by plant cells. *Comptes Rendus Biologies* **326**: 363–370.

An Q, Ehlers K, Kogel KH, Van Bel AJE, Hückelhoven R. **2006**. Multivesicular compartments proliferate in susceptible and resistant MLA12-barley leaves in response to infection by the biotrophic powdery mildew fungus. *New Phytologist* **172**: 563–576.

Andersson MX, Kourtchenko O, Dangl JL, Mackey D, Ellerström M. **2006**. Phospholipase-dependent signalling during the AvrRpm1- and AvrRpt2-induced disease resistance responses in Arabidopsis thaliana. *The Plant journal : for cell and molecular biology* **47**: 947–959.

Anthony RG, Henriques R, Helfer A, Mészáros T, Rios G, Testerink C, Munnik T, Deák M, Koncz C, Bögre L. **2004**. A protein kinase target of a PDK1 signalling pathway is involved in root hair growth in Arabidopsis. *EMBO Journal* **23**: 572–581.

Antignani V, Klocko AL, Bak G, Chandrasekaran SD, Dunivin T, Nielsen E. **2015**. Recruitment of PLANT U-BOX13 and the PI4Kβ1/β2 phosphatidylinositol-4 kinases by the small GTPase RabA4B plays important roles during salicylic acid-mediated plant defense signaling in arabidopsis. *Plant Cell* **27**: 243–261.

Arisz SA, van Wijk R, Roels W, Zhu JK, Haring MA, Munnik T. **2013**. Rapid phosphatidic acid accumulation in response to low temperature stress in Arabidopsis is generated through diacylglycerol kinase. *Frontiers in Plant Science* **4**.

Bligh EG, Dyer WJ. **1959**. A Rapid Method of Total Lipid Extraction and Purification. *Canadian Journal of Biochemistry and Physiology* **37**.

van Boerdonk S, Saake P, Wanke A, Neumann U, Zuccaro A. **2024**. β-Glucan-binding proteins are key modulators of immunity and symbiosis in mutualistic plant–microbe interactions. *Current Opinion in Plant Biology* **81**: 102610.

Camehl I, Drzewiecki C, Vadassery J, Shahollari B, Sherameti I, Forzani C, Munnik T, Hirt H, Oelmüller R. **2011**. The OXI1 kinase pathway mediates Piriformospora indica-induced growth promotion in Arabidopsis. *PLoS Pathogens* **7**.

La Camera S, Geoffroy P, Samaha H, Ndiaye A, Rahim G, Legrand M, Heitz T. **2005**. A pathogen-inducible patatin-like lipid acyl hydrolase facilitates fungal and bacterial host colonization in Arabidopsis. *The Plant Journal* **44**: 810–825.

Canonne J, Froidure-Nicolas S, Rivas S. **2011**. Phospholipases in action during plant defense signaling. *Plant Signaling and Behavior* **6**: 13–18.

Chandrasekar B, Wanke A, Wawra S, Saake P, Mahdi L, Charura N, Neidert M, Poschmann G, Malisic M, Thiele M, *et al.* 2022. Fungi hijack a ubiquitous plant apoplastic endoglucanase to release a ROS scavenging b-glucan decasaccharide to subvert immune responses. *The Plant Cell*.

Claus LAN, Savatin D V., Russinova E. **2018**. The crossroads of receptor-mediated signaling and endocytosis in plants. *Journal of Integrative Plant Biology* **60**: 827–840.

772 **Couto D, Zipfel C**. **2016**. Regulation of pattern recognition receptor signalling in plants.
773 *Nature Reviews Immunology* **16**: 537–552.

774 **Cox J, Mann M**. **2008**. MaxQuant enables high peptide identification rates, individualized
775 p.p.b.-range mass accuracies and proteome-wide protein quantification. *Nature*
776 *Biotechnology* **26**: 1367–1372.

777 **D'Ambrosio JM, Couto D, Fabro G, Scuffi D, Lamattina L, Munnik T, Andersson MX,**
778 **Álvarez ME, Zipfel C, Laxalt AM**. **2017**. Phospholipase C2 Affects MAMP-Triggered
779 Immunity by Modulating ROS Production. *Plant Physiology* **175**: 970–981.

780 **DeFalco TA, Zipfel C**. **2021**. Molecular mechanisms of early plant pattern-triggered immune
781 signaling. *Molecular Cell* **81**: 3449–3467.

782 **Der C, Courty PE, Recorbet G, Wipf D, Simon-Plas F, Gerbeau-Pissot P**. **2024**. Sterols,
783 pleiotropic players in plant–microbe interactions. *Trends in Plant Science* **29**: 524–534.

784 **vom Dorp K, Dombrink I, Dörmann P**. **2013**. Quantification of Diacylglycerol by Mass
785 Spectrometry. In: Munnik T, Heilmann I, eds. Plant Lipid Signaling Protocols. Springer.

786 **Dubiella U, Seybold H, Durian G, Komander E, Lassig R, Witte CP, Schulze WX,**
787 **Romeis T**. **2013**. Calcium-dependent protein kinase/NADPH oxidase activation circuit is
788 required for rapid defense signal propagation. *Proceedings of the National Academy of*
789 *Sciences of the United States of America* **110**: 8744–8749.

790 **Garcia-Ceron D, Lowe RGT, McKenna JA, Brain LM, Dawson CS, Clark B, Berkowitz O,**
791 **Faou P, Whelan J, Bleackley MR, *et al.* 2021**. Extracellular vesicles from fusarium
792 graminearum contain protein effectors expressed during infection of corn. *Journal of Fungi* **7**.

793 **Griebel T, Zeier J**. **2010**. A role for β-sitosterol to stigmasterol conversion in plant-pathogen
794 interactions. *Plant Journal* **63**: 254–268.

795 **Grison MS, Brocard L, Fouillen L, Nicolas W, Wewer V, Dörmann P, Nacir H, Benitez-**
796 **Alfonso Y, Claverol S, Germain V, *et al.* 2015**. Specific Membrane Lipid Composition Is
797 Important for Plasmodesmata Function in Arabidopsis. *The Plant Cell* **27**: 1228–1250.

798 **Gronnier J, Crowet JM, Habenstein B, Nasir MN, Bayle V, Hosy E, Platre MP, Gouguet**
799 **P, Raffaele S, Martinez D, *et al.* 2017**. Structural basis for plant plasma membrane protein
800 dynamics and organization into functional nanodomains. *eLife* **6**.

801 **Grosjean K, Mongrand S, Beney L, Simon-Plas F, Gerbeau-Pissot P**. **2015**. Differential
802 effect of plant lipids on membrane organization specificities of phytosphingolipids and
803 phytosterols. *Journal of Biological Chemistry* **290**: 5810–5825.

804 **Guo Z, Liu X, Wang N, Mo P, Shen J, Liu M, Zhang H, Wang P, Zhang Z**. **2023**.
805 Membrane component ergosterol builds a platform for promoting effector secretion and
806 virulence in Magnaporthe oryzae. *New Phytologist* **237**: 930–943.

807 **Hilbert M, Novero M, Rovenich H, Mari S, Grimm C, Bonfante P, Zuccaro A**. **2020**. MLO
808 Differentially Regulates Barley Root Colonization by Beneficial Endophytic and Mycorrhizal
809 Fungi. *Frontiers in Plant Science* **10**: 490627.

810 **Hirano T, Matsuzawa T, Takegawa K, Sato MH**. **2011**. Loss-of-function and gain-of-
811 function mutations in FAB1A/B impair endomembrane homeostasis, conferring pleiotropic
812 developmental abnormalities in Arabidopsis. *Plant physiology* **155**: 797–807.

Hirano T, Munnik T, Sato MH. **2015**. Phosphatidylinositol 3-Phosphate 5-Kinase, FAB1/PIKfyve Kinase Mediates Endosome Maturation to Establish Endosome-Cortical Microtubule Interaction in Arabidopsis. *Plant Physiology*.

Huang L, Li G, Wang Q, Meng Q, Xu F, Chen Q, Liu F, Hu Y, Luo M. **2022**. GhCYP710A1 Participates in Cotton Resistance to Verticillium Wilt by Regulating Stigmasterol Synthesis and Plasma Membrane Stability. *International Journal of Molecular Sciences* **23**: 8437.

Ivanov S, Harrison MJ. **2019**. Accumulation of phosphoinositides in distinct regions of the periarbuscular membrane. *New Phytologist* **221**: 2213–2227.

Jacobs S, Zechmann B, Molitor A, Trujillo M, Petutschnig E, Lipka V, Kogel K-H, Schäfer P. **2011**. Broad-Spectrum Suppression of Innate Immunity Is Required for Colonization of Arabidopsis Roots by the Fungus Piriformospora indica. *Plant Physiology* **156**: 726–740.

Jaillais Y, Ott T. **2020**. The nanoscale organization of the plasma membrane and its importance in signaling: A proteolipid perspective. *Plant Physiology* **182**: 1682–1696.

Jang JH, Nguyen NQ, Légeret B, Beisson F, Kim YJ, Sim HJ, Lee OR. **2020**. Phospholipase pPLAIIIα Increases Germination Rate and Resistance to Turnip Crinkle Virus when Overexpressed. *Plant Physiology* **184**: 1482–1498.

De Jong CF, Laxalt AM, Bargmann BOR, De Wit PJGM, Joosten MHAJ, Munnik T. **2004**. Phosphatidic acid accumulation is an early response in the Cf-4/Avr4 interaction. *The Plant Journal* **39**: 1–12.

Jordá T, Puig S. **2020**. Regulation of Ergosterol Biosynthesis in Saccharomyces cerevisiae. *Genes*.

Kadota Y, Shirasu K, Zipfel C. **2015**. Regulation of the NADPH Oxidase RBOHD during Plant Immunity. *Plant and Cell Physiology* **56**: 1472–1480.

Kalachova T, Skrabálková E, Pateyron S, Soubigou-Taconnat L, Djafi N, Collin S, Sekereš J, Burketová L, Potocký M, Pejchar P, *et al.* 2022. DIACYLGLYCEROL KINASE 5 participates in flagellin-induced signaling in Arabidopsis. *Plant Physiology* **190**: 1978–1996.

Kasparovsky T, Milat ML, Humbert C, Blein JP, Havel L, Mikes V. **2003**. Elicitation of tobacco cells with ergosterol activates a signal pathway including mobilization of internal calcium. *Plant Physiology and Biochemistry* **41**: 495–501.

Kato H, Nemoto K, Shimizu M, Abe A, Asai S, Ishihama N, Matsuoka S, Daimon T, Ojika M, Kawakita K, *et al.* 2022. Recognition of pathogen-derived sphingolipids in Arabidopsis. *Science* **376**: 857–860.

Khoza T, Dubery I, Piater L. **2019**. Identification of Candidate Ergosterol-Responsive Proteins Associated with the Plasma Membrane of Arabidopsis thaliana. *International Journal of Molecular Sciences* **20**: 1302.

Kim DS, Jeun Y, Hwang BK. **2014**. The pepper patatin-like phospholipase CaPLP1 functions in plant cell death and defense signaling. *Plant Molecular Biology* **84**: 329–344.

Kimura S, Kaya H, Kawarazaki T, Hiraoka G, Senzaki E, Michikawa M, Kuchitsu K. **2012**. Protein phosphorylation is a prerequisite for the Ca2+-dependent activation of Arabidopsis NADPH oxidases and may function as a trigger for the positive feedback

regulation of Ca2+ and reactive oxygen species. *Biochimica et Biophysica Acta (BBA) - Molecular Cell Research* **1823**: 398–405.

Klemptner RL, Sherwood JS, Tugizimana F, Dubery IA, Piater LA. **2014**. Ergosterol, an orphan fungal microbe-associated molecular pattern (MAMP). *Molecular Plant Pathology* **15**: 747–761.

Kong L, Ma X, Zhang C, Kim S-I, Li B, Xie Y, Yeo I-C, Thapa H, Chen S, Devarenne TP, *et al.* 2024. Dual phosphorylation of DGK5-mediated PA burst regulates ROS in plant immunity. *Cell* **187**: 609-623.e21.

Koselny K, Mutlu N, Minard AY, Kumar A, Krysan DJ, Wellington M. **2018**. A Genome-Wide Screen of Deletion Mutants in the Filamentous Saccharomyces cerevisiae Background Identifies Ergosterol as a Direct Trigger of Macrophage Pyroptosis. *mBio* **9**.

Kutschera A, Dawid C, Gisch N, Schmid C, Raasch L, Gerster T, Schäffer M, Smakowska-Luzan E, Belkhadir Y, Corina Vlot A, *et al.* 2019. Bacterial medium-chain 3-hydroxy fatty acid metabolites trigger immunity in Arabidopsis plants. *Science* **364**: 178–181.

Laquitaine L, Gomès E, François J, Marchive C, Pascal S, Hamdi S, Atanassova R, Delrot S, Coutos-Thévenot P. **2006**. Molecular basis of ergosterol-induced protection of grape against Botrytis cinerea: Induction of type I LTP promoter activity, WRKY, and stilbene synthase gene expression. *Molecular Plant-Microbe Interactions* **19**: 1103–1112.

Lebecq A, Doumane M, Fangain A, Bayle V, Leong JX, Rozier F, Del Marques-Bueno M, Armengot L, Boisseau R, Simon ML, *et al.* 2022. The Arabidopsis SAC9 enzyme is enriched in a cortical population of early endosomes and restricts PI(4,5)P2 at the plasma membrane. *eLife* **11**.

Li D, Li Z, Wu J, Tang Z, Xie F, Chen D, Lin H, Li Y. **2022**. Analysis of Outer Membrane Vesicles Indicates That Glycerophospholipid Metabolism Contributes to Early Symbiosis Between Sinorhizobium fredii HH103 and Soybean. *Molecular Plant-Microbe Interactions* **35**: 311–322.

Lindo L, Cardoza RE, Lorenzana A, Casquero PA, Gutiérrez S. **2020**. Identification of plant genes putatively involved in the perception of fungal ergosterol-squalene. *Journal of Integrative Plant Biology* **62**: 927–947.

Liu Y, Esposto D, Mahdi LK, Porzel A, Stark P, Hussain H, Scherr-Henning A, Isfort S, Bathe Ulschan, Acosta IF, *et al.* 2024. Hordedane diterpenoid phytoalexins restrict Fusarium graminearum infection but enhance Bipolaris sorokiniana colonization of barley roots. *Molecular Plant* **17**: 1307–1327.

Liu P, Xu Z-S, Lu P-P, Hu D, Chen M, Li L-C, Ma Y-Z. **2013**. A wheat PI4K gene whose product possesses threonine autophophorylation activity confers tolerance to drought and salt in Arabidopsis. *Journal of Experimental Botany* **64**: 2915–2927.

Lochman J, Mikes V. **2006**. Ergosterol treatment leads to the expression of a specific set of defence-related genes in tobacco. *Plant Molecular Biology* **62**: 43–51.

Macabuhay A, Arsova B, Walker R, Johnson A, Watt M, Roessner U, Macabuhay A. **2022**. Modulators or facilitators? Roles of lipids in plant root-microbe interactions Plant Science. *Trends in Plant Science* **27**.

Mahalingam R, Graham D, Walling JG. **2021**. The Barley (Hordeum vulgare ssp. vulgare) Respiratory Burst Oxidase Homolog (HvRBOH) Gene Family and Their Plausible Role on Malting Quality. *Frontiers in plant science* **12**.

Mahdi LK, Miyauchi S, Uhlmann C, Garrido-Oter R, Langen G, Wawra S, Niu Y, Guan R, Robertson-Albertyn S, Bulgarelli D, *et al.* 2022. The fungal root endophyte Serendipita vermifera displays inter-kingdom synergistic beneficial effects with the microbiota in Arabidopsis thaliana and barley. *ISME* **16**: 876–889.

Mao Y, Tan S. **2021**. Functions and Mechanisms of SAC Phosphoinositide Phosphatases in Plants. *Frontiers in Plant Science* **12**: 803635.

Marcec MJ, Gilroy S, Poovaiah BW, Tanaka K. **2019**. Mutual interplay of Ca2+ and ROS signaling in plant immune response. *Plant Science* **283**: 343–354.

Marcec MJ, Tanaka K. **2022**. Crosstalk between calcium and ros signaling during flg22-triggered immune response in arabidopsis leaves. *Plants* **11**.

Marković V, Jaillais Y. **2022**. Phosphatidylinositol 4-phosphate: a key determinant of plasma membrane identity and function in plants. *New Phytologist* **235**: 867–874.

Michaelson L V., Napier JA, Molino D, Faure JD. **2016**. Plant sphingolipids: Their importance in cellular organization and adaption. *Biochimica et Biophysica Acta - Molecular and Cell Biology of Lipids* **1861**: 1329–1335.

Moreau H, Bayer EM. **2023**. Lipids: plant biology's slippery superheroes. *Frontiers in Plant Physiology* **1**: 1–8.

Munnik T, Vermeer JEM. **2010**. Osmotic stress-induced phosphoinositide and inositol phosphate signalling in plants. *Plant, Cell and Environment* **33**: 655–669.

Nakagami H. **2014**. StageTip-based HAMMOC, an efficient and inexpensive phosphopeptide enrichment method for plant shotgun phosphoproteomics. *Methods in molecular biology* **1072**: 595–607.

Noack LC, Jaillais Y. **2020**. Functions of Anionic Lipids in Plants. *Annual Review of Plant Biology* .

Ogasawara Y, Kaya H, Hiraoka G, Yumoto F, Kimura S, Kadota Y, Hishinuma H, Senzaki E, Yamagoe S, Nagata K, *et al.* 2008. Synergistic Activation of the Arabidopsis NADPH Oxidase AtrbohD by Ca2+ and Phosphorylation. *Journal of Biological Chemistry* **283**: 8885–8892.

Oliveira-Garcia E, Tamang TM, Park J, Dalby M, Martin-Urdiroz M, Herrero CR, Vu AH, Park S, Talbot NJ, Valent B. **2023**. Clathrin-mediated endocytosis facilitates the internalization of Magnaporthe oryzae effectors into rice cells. *Plant Cell* **35**: 2527–2551.

Park J, Gu Y, Lee Y, Yang Z, Lee Y. **2004**. Phosphatidic Acid Induces Leaf Cell Death in Arabidopsis by Activating the Rho-Related Small G Protein GTPase-Mediated Pathway of Reactive Oxygen Species Generation. *Plant Physiology* **134**: 129–136.

Peng HC, Kaloshian I. **2014**. The tomato leucine-rich repeat receptor-like kinases SlSERK3A and SlSERK3B have overlapping functions in bacterial and nematode innate immunity. *PLoS ONE* **9**.

Perez-Riverol Y, Bai J, Bandla C, García-Seisdedos D, Hewapathirana S, Kamatchinathan S, Kundu DJ, Prakash A, Frericks-Zipper A, Eisenacher M, *et al.* 2022. The PRIDE database resources in 2022: a hub for mass spectrometry-based proteomics evidences. *Nucleic Acids Research* **50**: D543.

Piffanelli P, Zhou F, Casais C, Orme J, Jarosch B, Schaffrath U, Collins NC, Panstruga R, Schulze-Lefert P. **2002**. The Barley MLO Modulator of Defense and Cell Death Is Responsive to Biotic and Abiotic Stress Stimuli. *Plant Physiology* **129**: 1076–1085.

Pokotylo I, Kravets V, Martinec J, Ruelland E. **2018**. The phosphatidic acid paradox: Too many actions for one molecule class? Lessons from plants. *Progress in Lipid Research* **71**: 43–53.

Lo Presti L, Kahmann R. **2017**. How filamentous plant pathogen effectors are translocated to host cells. *Current Opinion in Plant Biology* **38**: 19–24.

Pršić J, Gilliard G, Ibrahim H, Argüelles-Arias A, Crowet J-M, Genva M, Patricio Luzuriaga-Loaiza W, Nail Nasir M, Lins L, Mathelie-Guinlet M, *et al.* 2023. Mechanosensing and Sphingolipid-Docking Mediate Lipopeptide-Induced Immunity in Arabidopsis. *bioRxiv*.

Qi F, Li J, Ai Y, Shangguan K, Li P, Lin F, Liang Y. **2024**. DGK5β-derived phosphatidic acid regulates ROS production in plant immunity by stabilizing NADPH oxidase. *Cell Host and Microbe*: 1–16.

Qi J, Wang J, Gong Z, Zhou JM. **2017**. Apoplastic ROS signaling in plant immunity. *Current Opinion in Plant Biology* **38**: 92–100.

Qin L, Zhou Z, Li Q, Zhai C, Liu L, Quilichini TD, Gao P, Kessler SA, Jaillais Y, Datla R, *et al.* 2020. Specific recruitment of phosphoinositide species to the plant-pathogen interfacial membrane underlies Arabidopsis susceptibility to fungal infection. *Plant Cell* **32**: 1665–1688.

Ranf S, Eschen-Lippold L, Pecher P, Lee J, Scheel D. **2011**. Interplay between calcium signalling and early signalling elements during defence responses to microbe- or damage-associated molecular patterns. *The Plant Journal* **68**: 100–113.

Rentel MC, Lecourieux D, Ouaked F, Usher SL, Petersen L, Okamoto H, Knight H, Peck SC, Grierson CS, Hirt H, *et al.* 2004. OXI1 kinase is necessary for oxidative burst-mediated signalling in Arabidopsis. *Nature* **427**: 858–861.

Robatzek S, Chinchilla D, Boller T. **2006**. Ligand-induced endocytosis of the pattern recognition receptor FLS2 in Arabidopsis. *Genes and Development* **20**: 537–542.

Rodrigues ML. **2018**. The Multifunctional Fungal Ergosterol. *mbio*: 1–5.

Rodrigues ML, Nimrichter L, Oliveira DL, Frases S, Miranda K, Zaragoza O, Alvarez M, Nakouzi A, Feldmesser M, Casadevall A. **2007**. Vesicular polysaccharide export in Cryptococcus neoformans is a eukaryotic solution to the problem of fungal trans-cell wall transport. *Eukaryotic Cell* **6**: 48–59.

Rossard S, Roblin G, Atanassova R. **2010**. Ergosterol triggers characteristic elicitation steps in Beta vulgaris leaf tissues. *Journal of Experimental Botany* **61**: 1807–1816.

Rutter BD, Innes RW. **2018**. Extracellular vesicles as key mediators of plant–microbe interactions. *Current Opinion in Plant Biology* **44**: 16–22.

Rydel TJ, Williams JM, Krieger E, Moshiri F, Stallings WC, Brown SM, Pershing JC, Purcell JP, Alibhai MF. **2003**. The crystal structure, mutagenesis, and activity studies reveal that patatin is a lipid acyl hydrolase with a Ser-Asp catalytic dyad. *Biochemistry* **42**: 6696–6708.

Ryu SB. **2004**. Phospholipid-derived signaling mediated by phospholipase A in plants. *Trends in Plant Science* **9**: 229–235.

Sang Y, Cui D, Wang X. **2001**. Phospholipase D and Phosphatidic Acid-Mediated Generation of Superoxide in Arabidopsis. *Plant Physiology* **126**: 1449.

Sarkar D, Rovenich H, Jeena G, Nizam S, Tissier A, Balcke GU, Mahdi LK, Bonkowski M, Langen G, Zuccaro A. **2019**. The inconspicuous gatekeeper: endophytic Serendipita vermifera acts as extended plant protection barrier in the rhizo-sphere. *New Phytologist* **224**: 886–901.

Seth T, Asija S, Umar S, Gupta R. **2024**. The intricate role of lipids in orchestrating plant defense responses. *Plant Science* **338**: 111904.

Seybold H, Trempel F, Ranf S, Scheel D, Romeis T, Lee J. **2014**. Ca 2+ signalling in plant immune response: from pattern recognition receptors to Ca 2+ decoding mechanisms. *New Phytologist* **204**: 782–790.

Siebers M, Brands M, Wewer V, Duan Y, Hölzl G, Dörmann P. **2016**. Lipids in plant–microbe interactions. *Biochimica et Biophysica Acta - Molecular and Cell Biology of Lipids* **1861**: 1379–1395.

Sinha J, Singh Y, Kumar Verma P. **2024**. Cytoskeleton remodeling: a central player in plant-fungus interactions. *Journal of Experimental Botany* **75**: 3269–3286.

Smith JM, Salamango DJ, Leslie ME, Collins CA, Heese A. **2014**. Sensitivity to Flg22 Is modulated by ligand-induced degradation and de novo synthesis of the endogenous flagellin-receptor FLAGELLIN-SENSING2. *Plant Physiology* **164**: 440–454.

Suzuki N, Miller G, Morales J, Shulaev V, Torres MA, Mittler R. **2011**. Respiratory burst oxidases: the engines of ROS signaling. *Current Opinion in Plant Biology* **14**: 691–699.

Synek L, Pleskot R, Sekereš J, Serrano N, Vukašinovi N, Ortmannová J, Klejchová M, remysl Pejchar P, Batystová K, Gutkowska M, *et al.* 2021. Plasma membrane phospholipid signature recruits the plant exocyst complex via the EXO70A1 subunit. *PNAS* **118**.

Testerink C, Munnik T. **2005**. Phosphatidic acid: a multifunctional stress signaling lipid in plants. *Trends in Plant Science* **10**: 368–375.

Tyanova S, Temu T, Cox J. **2016**. The MaxQuant computational platform for mass spectrometry-based shotgun proteomics. *Nature Protocols* **11**: 2301–2319.

Vargas G, Rocha JDB, Oliveira DL, Albuquerque PC, Frases S, Santos SS, Nosanchuk JD, Gomes AMO, Medeiros LCAS, Miranda K, *et al.* 2015. Compositional and immunobiological analyses of extracellular vesicles released by Candida albicans. *Cellular Microbiology* **17**: 389–407.

Vatsa P, Chiltz A, Luini E, Vandelle E, Pugin A, Roblin G. **2011**. Cytosolic calcium rises and related events in ergosterol-treated Nicotiana cells. *Plant Physiology and Biochemistry* **49**: 764–773.

Wang K, Senthil-Kumar M, Ryu CM, Kang L, Mysore KS. **2012**. Phytosterols play a key role in plant innate immunity against bacterial pathogens by regulating nutrient efflux into the apoplast. *Plant Physiology* **158**: 1789–1802.

Wanke A, Rovenich H, Schwanke F, Velte S, Becker S, Hehemann JH, Wawra S, Zuccaro A. **2020**. Plant species-specific recognition of long and short β-1,3-linked glucans is mediated by different receptor systems. *Plant Journal* **102**: 1142–1156.

Wawra S, Fesel P, Widmer H, Timm M, Seibel J, Leson L, Kesseler L, Nostadt R, Hilbert M, Langen G, *et al.* 2016. The fungal-specific β-glucan-binding lectin FGB1 alters cell-wall composition and suppresses glucan-triggered immunity in plants. *Nature Communications 2016 7:1* **7**: 1–11.

Wellington M, Koselny K, Sutterwala FS, Krysan DJ. **2014**. Candida albicans triggers NLRP3-mediated pyroptosis in macrophages. *Eukaryotic Cell* **13**: 329–340.

Williams ME, Torabinejad J, Cohick E, Parker K, Drake EJ, Thompson JE, Hortter M, DeWald DB. **2005**. Mutations in the Arabidopsis phosphoinositide phosphatase gene SAC9 lead to overaccumulation of PtdIns(4,5)P2 and constitutive expression of the stress-response pathway. *Plant Physiology* **138**: 686–700.

Xing J, Li X, Wang X, Lv X, Wang L, Zhang L, Zhu Y, Shen Q, Baluska F, Samaj J, *et al.* 2019. Secretion of phospholipase Dδ functions as a regulatory mechanism in plant innate immunity. *The Plant Cell* **31**: 3015–3032.

Xu X, Bittman R, Duportail G, Heissler D, Vilcheze C, London E. **2001**. Effect of the Structure of Natural Sterols and Sphingolipids on the Formation of Ordered Sphingolipid/Sterol Domains (Rafts). *Journal of Biological Chemistry* **276**: 33540–33546.

Yao HY, Xue HW. **2018**. Phosphatidic acid plays key roles regulating plant development and stress responses. *Journal of Integrative Plant Biology* **60**: 851–863.

Zarreen F, Kumar K, Chakraborty S. **2023**. Phosphoinositides in plant-pathogen interaction: trends and perspectives. *Stress Biology* **3**.

Zhang H, Jin X, Huang L, Hong Y, Zhang Y, Ouyang Z, Li X, Song F, Li D. **2014**. Molecular characterization of rice sphingosine-1-phosphate lyase gene OsSPL1 and functional analysis of its role in disease resistance response. *Plant Cell Reports* **33**: 1745–1756.

Zhang H, Wang X, Yan A, Deng J, Xie Y, Liu S, Liu D, He L, Weng J, Xu J. **2023**. Evolutionary Analysis of Respiratory Burst Oxidase Homolog (RBOH) Genes in Plants and Characterization of ZmRBOHs. *International Journal of Molecular Sciences* **24**: 3858.

Zhang Q, Xiao S. **2015**. Lipids in Salicylic acid-mediated defense in plants: Focusing on the roles of phosphatidic acid and phosphatidylinositol 4-phosphate. *Frontiers in Plant Science* **6**: 141695.

Zhang Y, Zhu H, Zhang Q, Li M, Yan M, Wang R, Wang L, Welti R, Zhang W, Wang X. **2009**. Phospholipase Dα1 and Phosphatidic Acid Regulate NADPH Oxidase Activity and Production of Reactive Oxygen Species in ABA-Mediated Stomatal Closure in Arabidopsis. *The Plant Cell* **21**: 2357.

Supporting information

Fig. S1: Lipids from the beneficial root endophyte *S. indica* induce immunity in barley leaves.

Fig. S2: Ergosterol induces MAPK phosphorylation in barley roots.

Fig. S3: *S. indica* lipids are differentially perceived in different plant species.

Fig.S4: *S. indica* colonization induces modulation of the phytosterol pool in barley.

Fig. S5: BAK1/SERK3 is not involved in *S. indica* lipid perception in *S. lycopersicum* leaves.

Fig. S6: Cotreatment with PA liposomes enhances the ergosterol-induced ROS burst in barley roots.

Fig.S7: Phospholipid cotreatment does not enhance the chitohexaose-induced ROS burst in barley roots.

Fig. S8: PA cotreatment does not enhance chitohexaose-induced ROS burst in barley roots

Fig. S9: Diterpene exudation in response to ergosterol treatment and *B. sorokiniana* colonization.

Table S1: Phosphoproteomics data

A. Imputed data of all phosphorylated peptides
B. MNAR data of all peptides absent from the control but present in any treatment + groups based on GO terms
C. Data presented in Figure 5B (Selected groups from Table S1B, imputed data)

Table S2: RNAseq data

A. Log2FC and tpm of all genes
B. Significantly differentially expressed genes

Table S3: Primers used in this study

Methods S1: Detailed description of materials and methods

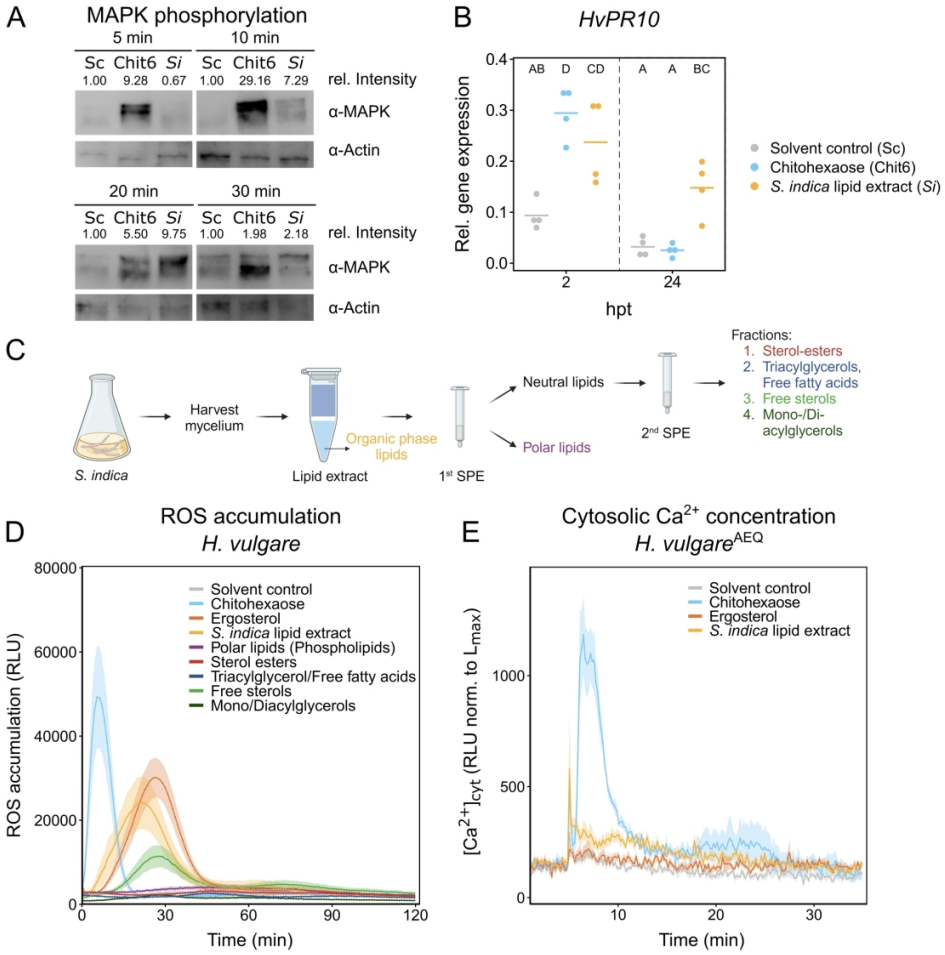

Figure 1: Lipids from the beneficial root endophyte *Serendipita indica* induce immunity in barley roots. A) MAPK phosphorylation in roots of seven days old barley plants, treated with the indicated MAMPs or solvent control for 5-, 10-, 20- or 30- min. 1st antibody: Phospho-p44/42 MAPK (upper) or α-Actin as loading control (lower), 2nd antibody: anti-rabbit IgG. Sc = solvent control [1:160], Chit6 = chitohexaose [250 nM], *Si* = *S. indica* lipid extract [1:160]. Relative Intensity depicts the MAPK signal intensity normalized to the Actin signal intensity of the same treatment and to the solvent control for each timepoint. The experiment was repeated four times with similar results (see Fig. S2). B) Gene expression of *HvPR10* relative to the housekeeping gene *HvUBI* in barley roots determined by qRT-PCR. Roots were treated with the indicated MAMPs or solvent control for 2 or 24 h. Letters indicate significant differences based on ANOVA + post hoc Tukey test ($p \leq 0.05$). C) Lipid fractionation method. D-E) ROS accumulation (D) and cytosolic Ca^{2+} concentration ($[Ca^{2+}]_{cyt}$) (E) in roots of seven days old barley plants, treated with the indicated lipid fractions or solvent control as negative control. Values represent means (normalized to maximum luminescence over all wells for Ca^{2+}) ± SEM from six to eight wells, each containing three root pieces. The following concentrations and dilutions were used: *S. indica* total lipid extract and fractions: 1:160 (v/v), ergosterol: 250 nM, chitohexaose: 25 µM. All treatments contained a final amount of 1:40 (v/v) methanol.

189x191mm (300 x 300 DPI)

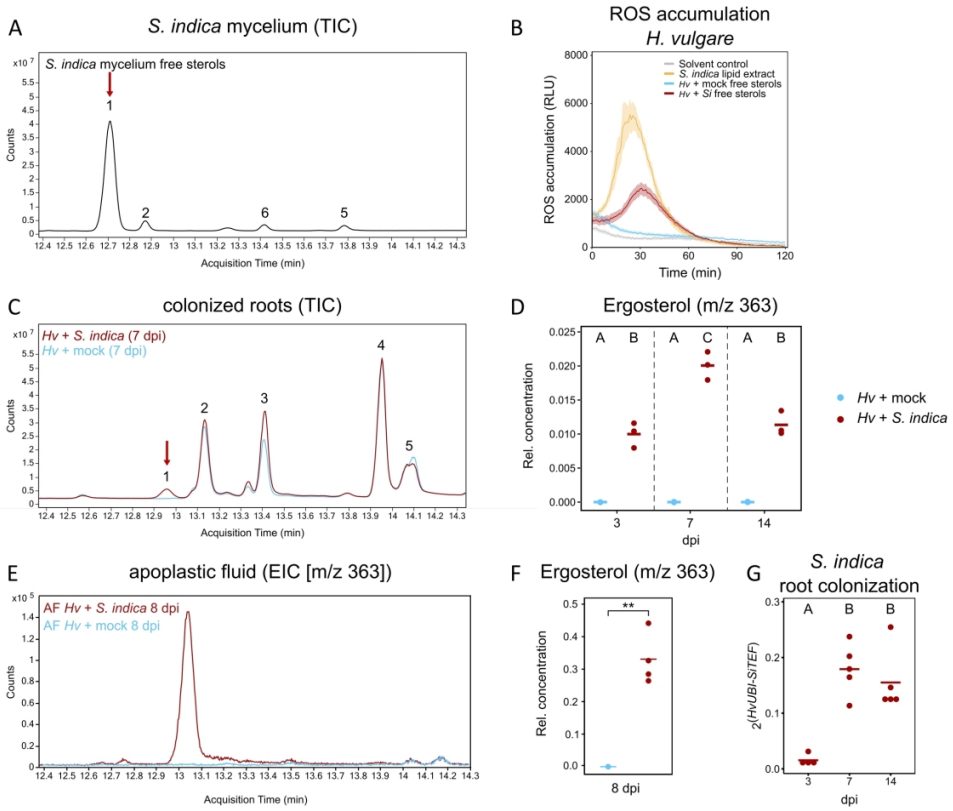

Figure 2: Ergosterol is present in the apoplast of colonized barley roots and the main immunogenic component of *Serendipita indica* lipid extract.

A, C) GC-TOF-MS total ion chromatograms (TICs) of the free sterol fraction from *S. indica* lipids isolated from mycelium (A) or whole root samples of mock-treated or *S. indica*-colonized barley roots (C). Major peaks in A) and C) are labeled in the following order: 1= Ergosterol, 2 = Ergosta-7,22-dien-3ol, 3 = Stigmasterol, 4 = β-Sitosterol, 5 = Stigmastanol (ISTD), 6 = Ergost-8(14)-en-3-ol. B) ROS accumulation in roots from seven days old barley plants, treated with *S. indica* lipid extract or sterol fractions isolated from mock-treated or *S. indica*-colonized barley roots at 7 dpi or solvent control as negative control. Values represent means ± SEM from eight wells, each containing three root pieces. *S. indica* total lipid extract and fractions were used in 1:160 (v/v) dilution. All treatments contained a final amount of 1:40 (v/v) methanol. D) Quantification of ergosterol in sterol fractions of *S. indica*-colonized barley roots at 3-, 7- and 14- dpi. E) Extracted ion chromatogram (EIC) of ergosterol (m/z 363) in total lipid extract of apoplastic fluid of mock-treated or *S. indica*-colonized barley roots (8 dpi). Representative image of one replicate. Quantification of four replicates is shown in F. G) *S. indica* intraradical colonization of barley roots determined as relative expression of the fungal housekeeping gene *SiTEF* to the barley housekeeping gene *HvUBI* at 3-, 7- and 14 dpi. Data was obtained from an independent experiment performed the same way as for D. Letters indicate significant differences based on ANOVA + post hoc Tukey test ($p \leq 0.05$). Asterisks indicate significant difference based on Student's t-test ($p \leq 0.05$ *; $p \leq 0.01$ **; $p \leq 0.001$ ***, $p \leq 0.0001$ ****). Relative ergosterol concentration was calculated based on internal standard response and normalized to sample fresh weight (D) or ml apoplastic fluid (F).

195x164mm (300 x 300 DPI)

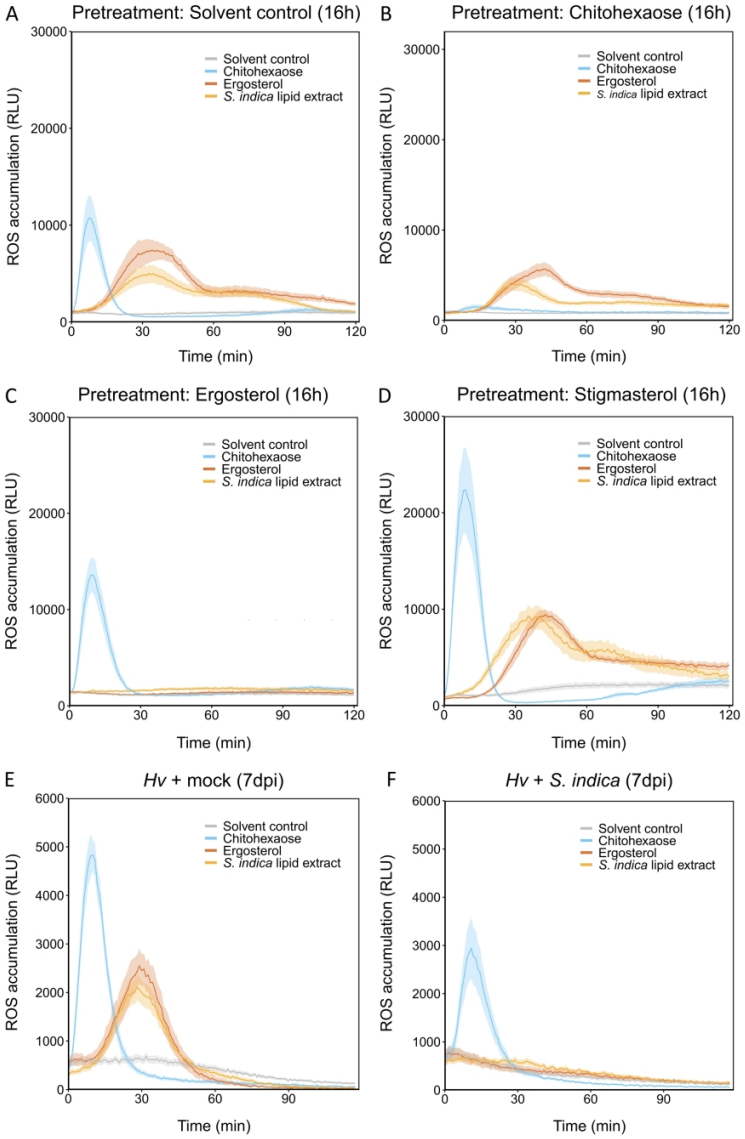

Figure 3: Ergosterol pretreatment and *Serendipita indica* colonization prevents lipid-induced ROS accumulation. A-D) ROS accumulation in roots from seven days old barley plants, treated with the indicated elicitors or solvent control after pretreatment with solvent control (A), chitohexaose (B), ergosterol (C) or stigmasterol (D). E-F) ROS accumulation in mock-treated (E) or *S. indica*-colonized barley roots (F) at 7dpi. Roots were washed thoroughly prior to assay preparations to remove extracellular fungal hyphae. Values represent means ± SEM from eight wells, each containing three root pieces. The following concentrations and dilutions were used: treatments: chitohexaose and ergosterol: 250 nM, *S. indica* lipid extract: 1:160 (v/v) dilution, pretreatments: 5 µM each. All pretreatment and treatment solutions contained a final amount of 1:40 (v/v) methanol.

195x288mm (300 x 300 DPI)

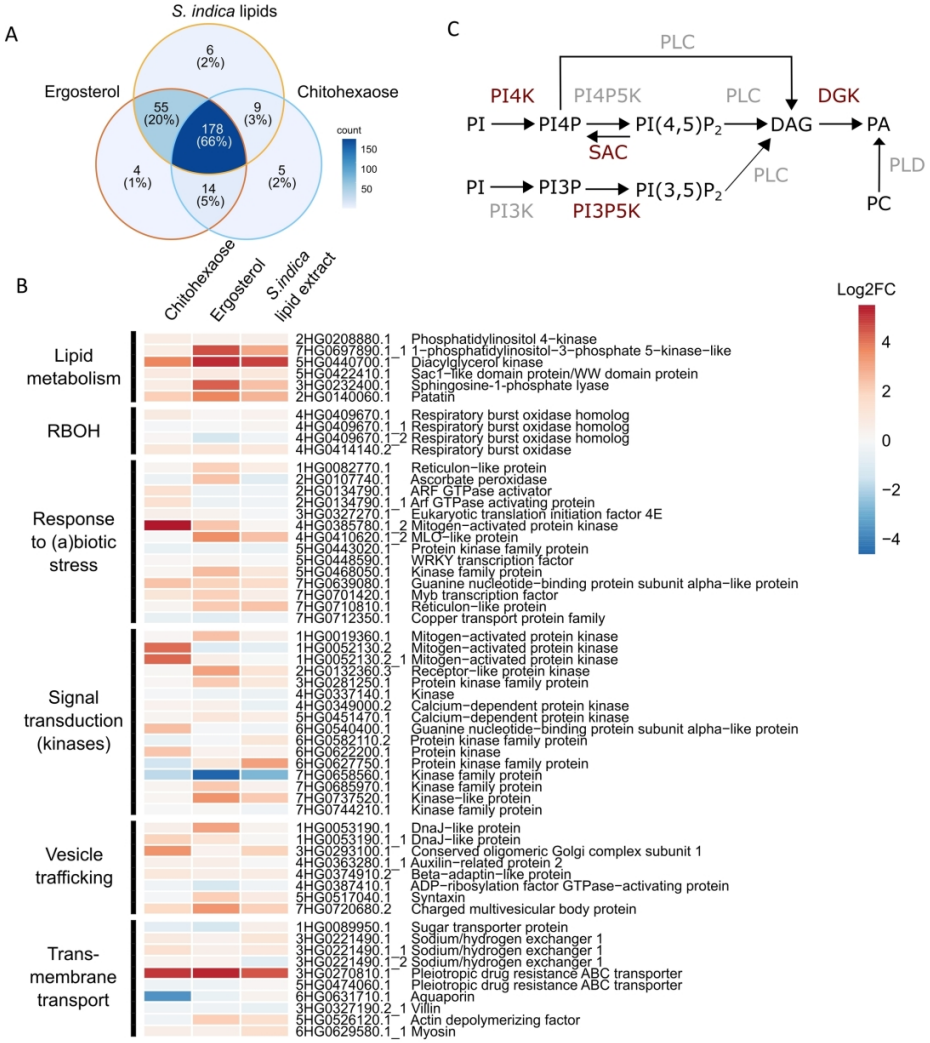

Figure 4: Changes in the phosphoproteome of barley roots upon MAMP treatment. Phosphorylated peptides were measured using LC-MS/MS in barley roots in response to chitohexaose, ergosterol or *S. indica* lipid treatment for 10 min. As negative control, solvent control was used. A) Venn diagram of phosphorylated peptides found in any of the three treatments but absent from solvent control in unimputed data. B) Heatmap showing log2 fold change (log2FC) of imputed intensities of phosphorylated peptides in response to the respective treatments compared to solvent control treatment. Peptides presented here were selected and grouped into functional categories based on GO annotations. C) Schematic depiction of the phosphatidylinositol phosphorylation pathway leading to the production of PA. Enzymes in red were found in phosphoproteome after elicitor treatment as shown in the heatmap. PI = Phosphatidylinositol; PI4P = Phosphatidylinositol-4-phosphate; $PI(4,5)P_2$ = Phosphatidylinositol-4,5-diphosphate; PI3P = Phosphatidylinositol-3-phosphate; $PI(3,5)P_2$ = Phosphatidylinositol-3,5-diphosphate; DAG = Diacylglycerol; PA = Phosphatidic acid; PI4K = Phosphatidylinositol-4 kinase; PI4P5K = Phosphatidylinositol-4-phosphate-5-lkinase; PI3K = Phosphatidylinositol-3 kinase; PI3P5K = Phosphatidylinositol-3-phosphate-5 kinase; PLC = Phospholipase C; PLD = Phospholipase D; DGK = Diacylglycerol kinase; SAC = Sac1-like domain containing protein ($PI(4,5)P_2$ phosphatase).

207x226mm (300 x 300 DPI)

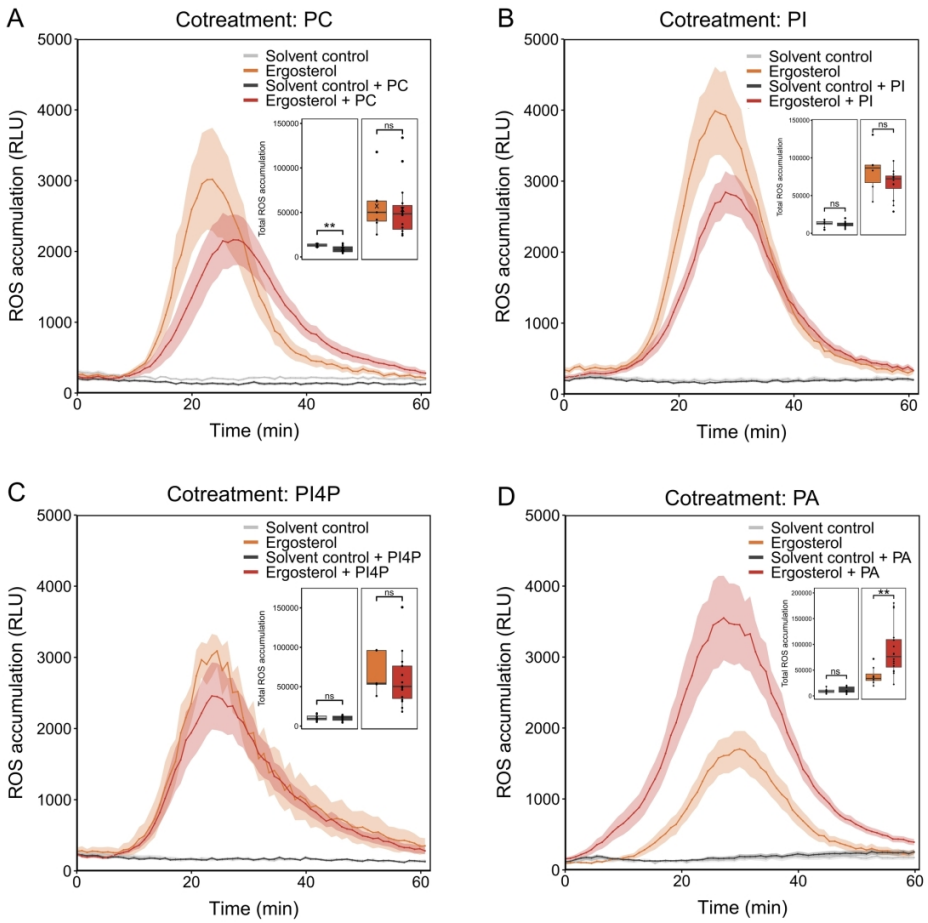

Figure 5: PA cotreatment enhances the ergosterol-induced ROS accumulation. A-D) ROS accumulation in roots of four days old barley plants, treated with the indicated elicitors or solvent control as negative control. Values represent means ± SEM from eight (without cotreatment) or sixteen (with cotreatment) wells, each containing three root pieces. Ergosterol and all phospholipids (PC, PI, PI4P, PA) were used at a final concentration of 250 nM. All treatments contained a final amount of 1:40 (v/v) methanol. Insets: total ROS accumulation depicted as boxplots from the same data. Asterisks indicate significant differences based on Student's t-test ($p \leq 0.05$ *; $p \leq 0.01$ **; $p \leq 0.001$ ***, $p \leq 0.0001$ ****).

211x206mm (300 x 300 DPI)

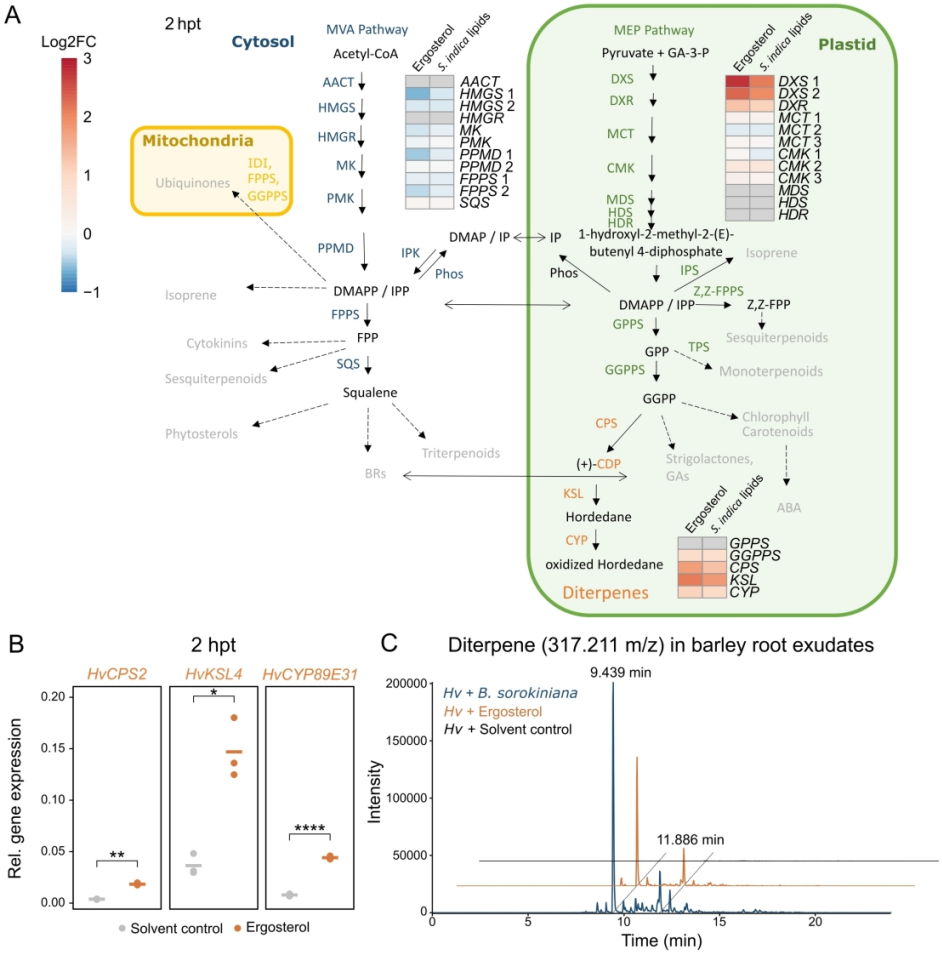

Figure 6: Fungal lipid treatment leads to induction of the MEP pathway and exudation of diterpenes in barley roots. A) Schematic representation of the plants MEP and MVA pathway (adapted from Liao *et al.*, 2016). Boxes indicate relative expression (Log2FC) of the respective barley genes upon ergosterol or *S. indica* lipid treatment relative to solvent control treatment. Expression was measured in an RNASeq analysis of barley, treated for 2 h with the respective elicitors. Ergosterol was used at a final concentration of 250 nM and *S. indica* lipid extract at a final dilution of 1:160. Grey boxes = NA. B) Confirmation of induction of diterpene biosynthesis genes *HvKSL4*, *HvCPS2* and *HvCYP89E31* in barley roots after treatment with ergosterol (250 nM) for 2 h. Gene expression was determined with qRT-PCR, relative to the housekeeping gene *HvUBI*. C) LC-MS/MS chromatogram of one of the major diterpenes found in root exudates of barley plants treated with solvent control, ergosterol (250 nM) or colonized by *B. sorokiniana* (positive control) for 6 days. The experiment was repeated with similar results. Ergosterol and solvent control treatments contained a final amount of 1:40 (v/v) methanol. Asterisks indicate significant differences based on Student's t-test ($p \leq 0.05$ *; $p \leq 0.01$ **; $p \leq 0.001$ ***, $p \leq 0.0001$ ****). DXS = 1 deoxy xylulose 5 phosphate synthase, DXR = 1 deoxy xylulose 5 phosphate reductoisomerase, KSL = kaurene synthase like, CPS = ent copalyl diphosphate synthase, CYP = cytochrome P450 oxygenase.

220x218mm (300 x 300 DPI)

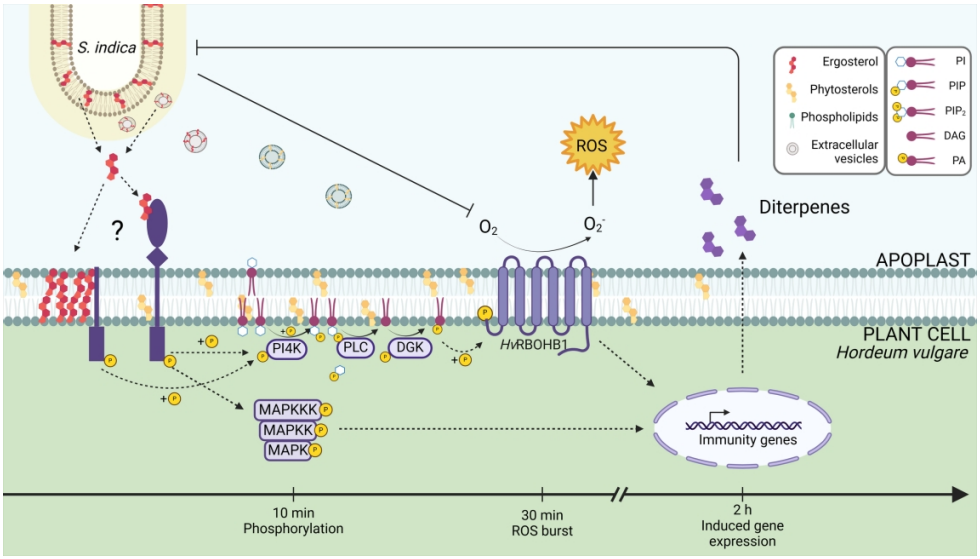

Figure 7: Proposed model of fungal lipid perception in barley roots. We propose two mechanisms for how plants perceive ergosterol. First, ergosterol could directly integrate into the plant plasma membrane, potentially activating membrane-embedded mechanosensors or specific ergosterol-binding receptors within the membrane. Second, ergosterol could bind in the apoplast to the extracellular domain of a yet unidentified membrane-bound receptor (Xu *et al.*, 2001; Klemptner *et al.*, 2014; Lindo *et al.*, 2020; Khoza *et al.*, 2019). Upon perception, ergosterol likely initiates a signaling cascade that begins with receptor phosphorylation, leading to phosphorylation of MAPKs (10-30 min) and the rapid activation of PI4K and DGK (10 min). This activation results in the production of PA, which subsequently enhances the activation and stabilization of RBOH, amplifying the ROS burst (30 min). Together, these signaling events lead to increased expression of immunity genes and diterpene biosynthesis genes (2 h), which ultimately results in the exudation of diterpenes, which were shown to inhibit growth of *S. indica*. During colonization, *S. indica* suppresses the ergosterol-mediated ROS burst. PI = Phosphatidylinositol; PIP = Phosphatidylinositolphosphate; PIP2 = Phosphatidylinositoldiphosphate; DAG = Diacylglycerol; PA = Phosphatidic acid; PI4K = Phosphatidyl-inositol-4 kinase; PLC = Phospholipase C; DGK = Diacylglycerolkinase; RBOH = Respiratory burst oxidase homolog; ROS = reactive oxygen species.

198x112mm (300 x 300 DPI)

***New Phytologist* Supporting Information**

Article title: Plant Lipids Mediate Immune Responses to Fungal Lipids in Barley
Authors: Pia Saake[1,2], Mathias Brands[1], Asmamaw Bidru Endeshaw[1], Sara Christina Stolze[4], Philipp Westhoff[2,3], Gerd Ulrich Balcke[5], Götz Hensel[2,3], Nicholas Holton[6], Cyril Zipfel[7], Alain Tissier[5], Hirofumi Nakagami[4], Alga Zuccaro[1,2]
Article acceptance date: Click here to enter a date.

The following Supporting Information is available for this article:

Fig. S1: Lipids from the beneficial root endophyte *S. indica* induce immunity in barley leaves.

Fig. S2: Ergosterol induces MAPK phosphorylation in barley roots.

Fig. S3: *S. indica* lipids are differentially perceived in different plant species.

Fig. S4: *S. indica* colonization induces modulation of the phytosterol pool in barley.

Fig. S5: BAK1/SERK3 is not involved in *S. indica* lipid perception in *S. lycopersicum* leaves.

Fig. S6: Cotreatment with PA in liposomes enhances the ergosterol-induced ROS burst in barley roots.

Fig. S7: Phospholipid cotreatment does not enhance the chitohexaose-induced ROS burst in barley roots.

Fig. S8: PA cotreatment does not enhance chitohexaose-induced ROS burst in barley roots.

Fig. S9: Diterpene exudation in response to ergosterol treatment and *B. sorokiniana* colonization.

Table S1 Phosphoproteomics data

A. Imputed data of all phosphorylated peptides
B. MNAR data of all peptides absent from the control but present in any treatment + groups based on GO terms
C. Data presented in Figure 5B (Selected groups from Table S1B, imputed data)

Table S2: RNAseq data

A. Log2FC and tpm of all genes
B. Significantly differentially expressed genes

Methods S1 Detailed description of materials and methods

Fig. S1: Lipids from the beneficial root endophyte *S. indica* induce immunity in barley leaves.

A) ROS accumulation in leaves of seven days old barley plants, treated with the indicated lipid extracts or solvent control as negative control. Values represent means ± SEM from eight wells, each containing one 3 mm leaf disc. B) Expression of *HvPR10* relative to the housekeeping gene *HvUBI* in barley leaf discs determined by qRT-PCR. Leaf discs were treated with the indicated MAMPs or solvent control for 2 or 24 h. Letters indicate significant differences based on ANOVA + post hoc Tukey test ($p \leq 0.05$). All treatments contained a final amount of 1:40 (v/v) methanol. The following concentrations / dilutions were used: *S. indica* lipid extract: 1:160 (v/v), ergosterol: 250 nM, chitohexaose: 25 µM.

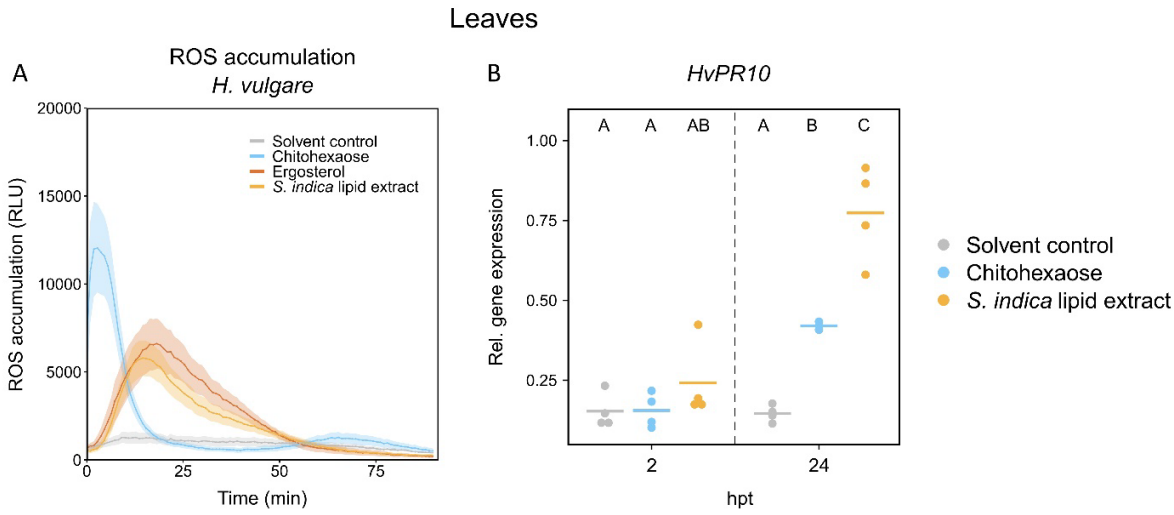

Fig. S2: Ergosterol induces MAPK phosphorylation in barley roots.

MAPK phosphorylation in roots of seven days old barley plants, treated with the indicated MAMPs or solvent control for 5-, 10-, 20- or 30-min. 1st antibody: Phospho-p44/42 MAPK (upper) or α-Actin as loading control (lower), 2nd antibody: anti-rabbit IgG. Sc = solvent control [1:160], Erg = Ergosterol [250 nM], Chit6 = chitohexaose [250 nM], *Si* = *S. indica* lipid extract [1:160], HErg = Ergosterol [25 µM]. Relative Intensity depicts the MAPK signal intensity normalized to the Actin signal intensity of the same treatment and to the solvent control for each timepoint.

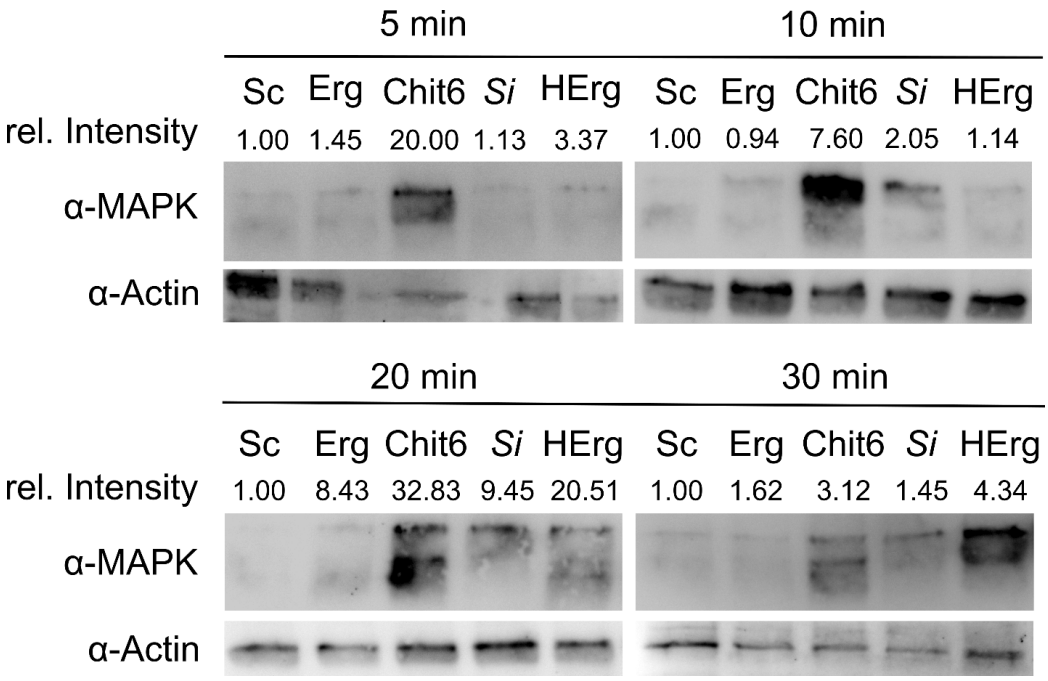

Fig. S3: *S. indica* lipids are differentially perceived in different plant species.

A-B) ROS accumulation (A) and cytosolic Ca^{2+} concentration ($[Ca^{2+}]_{cyt}$) (B) in leaves of 3-weeks old *N. benthamiana*^{AEQ} plants, treated with the indicated MAMPs or solvent control as negative control. Values represent means (normalized to maximum luminescence over all wells for Ca^{2+}) ± SEM from eight wells, each containing one 3 mm leaf disc. C) ROS accumulation in leaves of 3-weeks of *N. benthamiana* WT plants, treated with the indicated MAMPs or solvent control as negative control. Values represent means ± SEM from eight wells, each containing one 3 mm leaf disc. D-E) ROS accumulation (D) and cytosolic Ca^{2+} concentration ($[Ca^{2+}]_{cyt}$) (E) in *A. thaliana*^{AEQ} seedlings after treatment with the indicated elicitors or solvent control as negative control. Values represent means (normalized to maximum luminescence over all wells for Ca^{2+}) ± SEM from eight wells, each containing one seedling. The following concentrations and dilutions were used: *S. indica* lipid extract: 1:160 (v/v), chitohexaose: 25 µM, ergosterol: 25 µM (D), 250 nM (A, B, C, E). All treatments contained a final amount of 1:40 (v/v) methanol. Insets depict total ROS accumulation from the same experiment. Letters indicate significant differences based on ANOVA and post hoc Tukey test ($p \leq 0.05$).

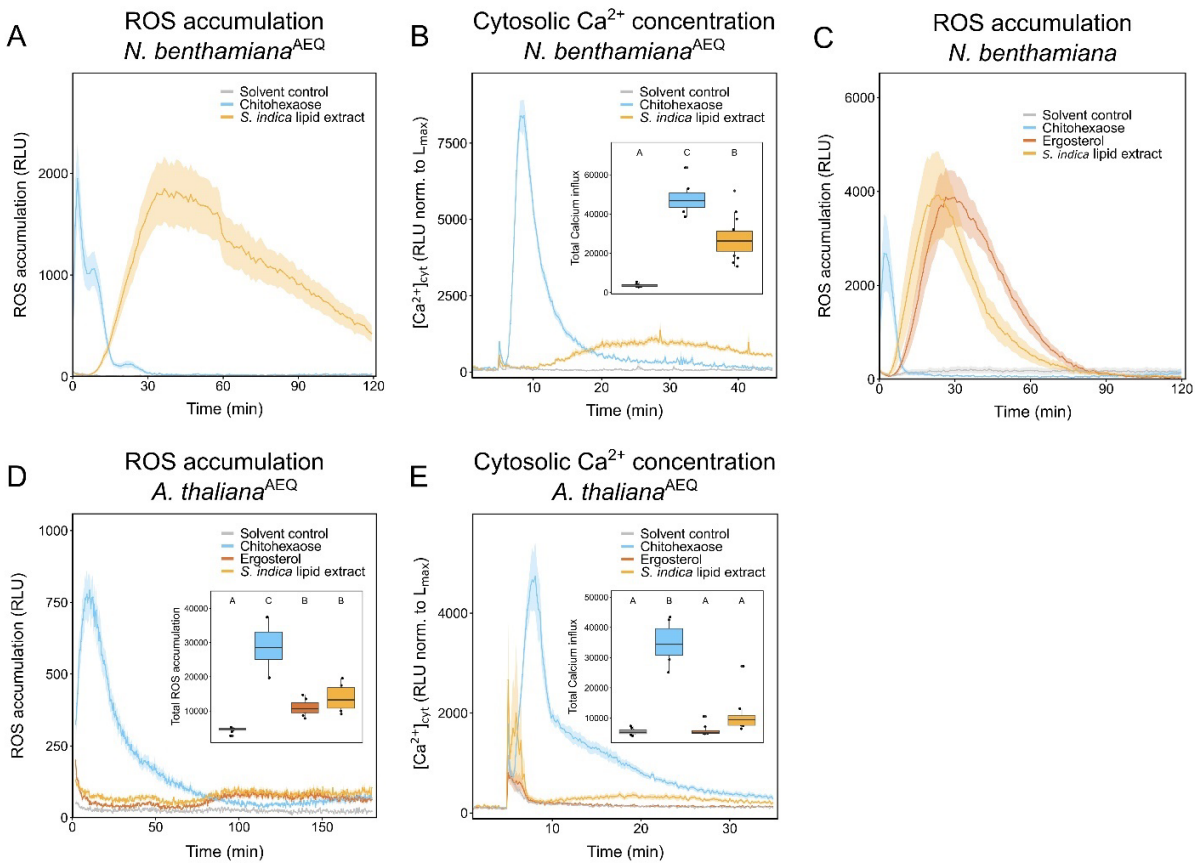

Fig. S4: *S. indica* colonization induces modulation of the phytosterol pool in barley.

Measurement of phytosterol content in mock-inoculated or *S. indica*-colonized barley roots at 3-, 7-, and 14-days post inoculation (dpi). The amounts of stigmasterol (stigmasta-5,22-dien-3β-ol) (A) and β-sitosterol (24β-ethylcholest-5-en-3β-ol) (B) were measured via GC-TOF-MS and the ratio of stigmasterol to β-sitosterol was calculated (C). Letters indicate significant differences based on ANOVA and post hoc Tukey test ($p \leq 0.05$). Relative sterol concentration was calculated based on Internal standard response and normalized to sample fresh weight.

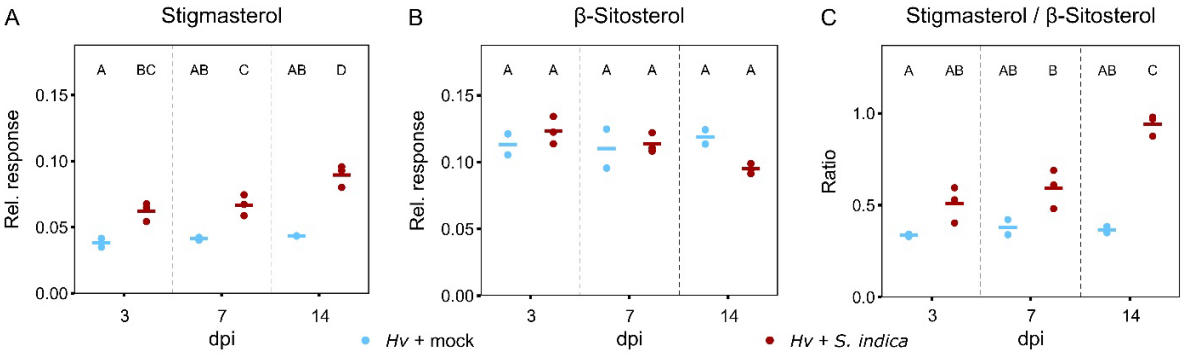

Fig. S5: BAK1/SERK3 is not involved in *S. indica* lipid perception in *S. lycopersicum* leaves.

A) ROS accumulation in *S. lycopersicum* cv Moneymaker WT and *S. lycopersicum* cv Moneymaker *serk3a serk3b* leaf discs, treated with the indicated elicitors or solvent control as negative control. Values represent means ± SEM from 12 wells, each containing one leaf disc. Two leaves were used per plant and three plants per genotype. The following concentrations/dilutions were used: ergosterol: 250 nM, flg22: 1 µM. All treatments contained 1:40 (v/v) final amount of methanol. B) Total ROS accumulation of the same experiment. Asterisks indicate significant differences based on Student's t-test ($p \leq 0.05$ *; $p \leq 0.01$ **; $p \leq 0.001$ ***, $p \leq 0.0001$ ****). C) Pictures depicting the phenotype of the mutant plants compared to WT plants (curly leaves, reduced growth). D) Sequence alignment of the coding sequence of *SERK3A* and *SERK3B* downloaded from ensembl plant (Original sequence) and amplification of the respective genes from *S. lycorpersicum* cv Moneymaker WT gDNA (first 2 rows) and *S. lycopersicum* cv Moneymaker *serk3a serk3b* mutant gDNA (last 2 rows). Mutant plants contain a 7 AA deletion for *SERK3A* and a 6 AA deletion for *SERK3B*.

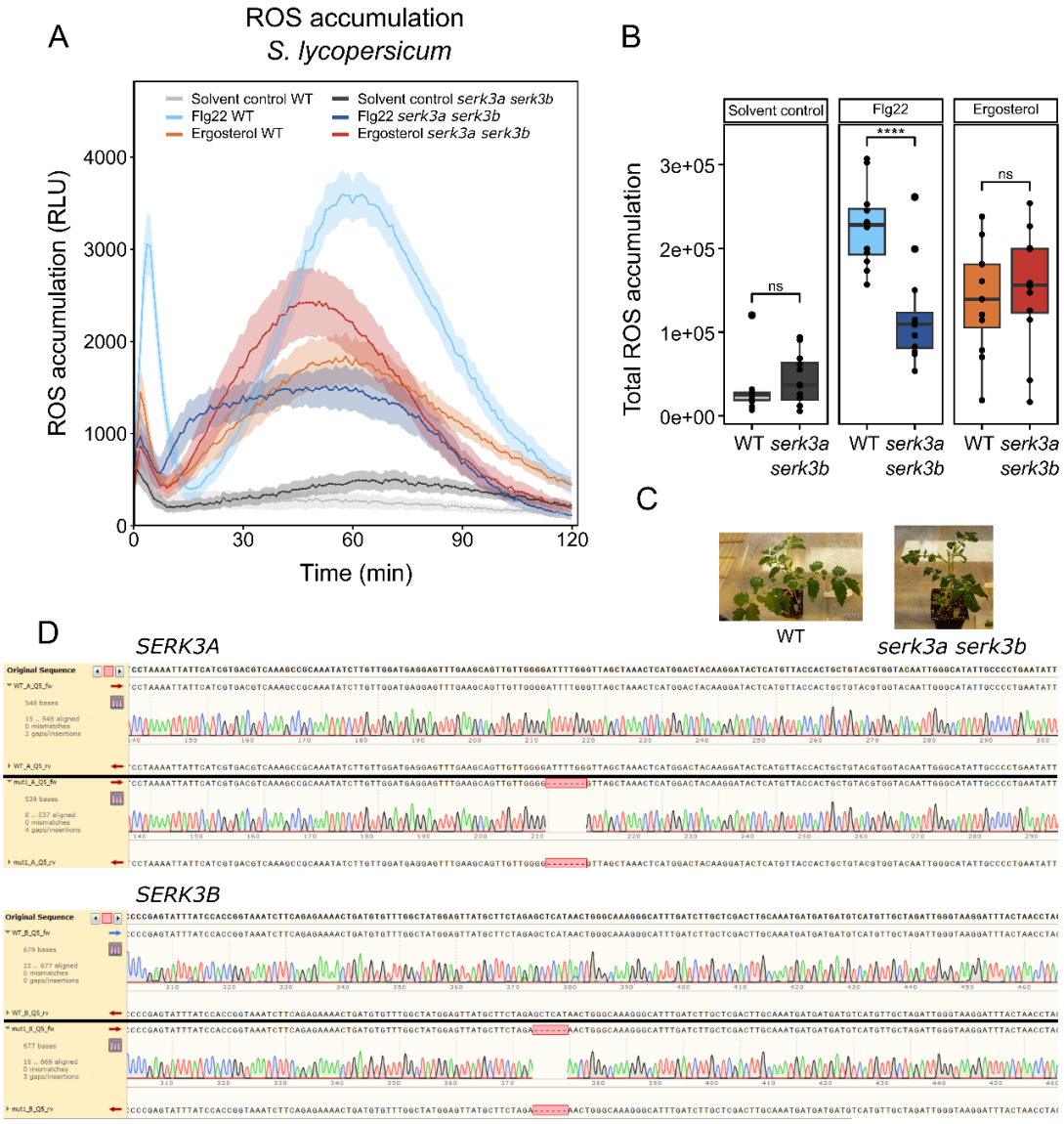
A
ROS accumulation
S. lycopersicum
Solvent control WT
Flg22 WT
Ergosterol WT
Solvent control serk3a serk3b
Flg22 serk3a serk3b
Ergosterol serk3a serk3b
ROS accumulation (RLU)
Time (min)
B
Solvent control
Flg22
Ergosterol
Total ROS accumulation
ns
****
ns
WT serk3a serk3b
C
WT
serk3a serk3b
D
SERK3A
SERK3B

Fig. S6: Cotreatment with PA liposomes enhances the ergosterol-induced ROS burst in barley roots.
ROS accumulation in roots of four days old barley plants, treated with ergosterol or ergosterol + PA liposomes. Values represent means ± SEM from wells, each containing three root pieces. The following concentrations were used: Ergosterol: 250 nM, PA: 25µM. All treatments contained a final amount of 1:40 (v/v) methanol. PA liposomes were prepared in 25 mM HEPES buffer (pH 7.5, 50 mM KCL, 1mM $MgCL_2$). Asterisks indicate significant differences based on Student's t-test ($p \leq 0.05$ *; $p \leq 0.01$ **; $p \leq 0.001$ ***, $p \leq 0.0001$ ****).

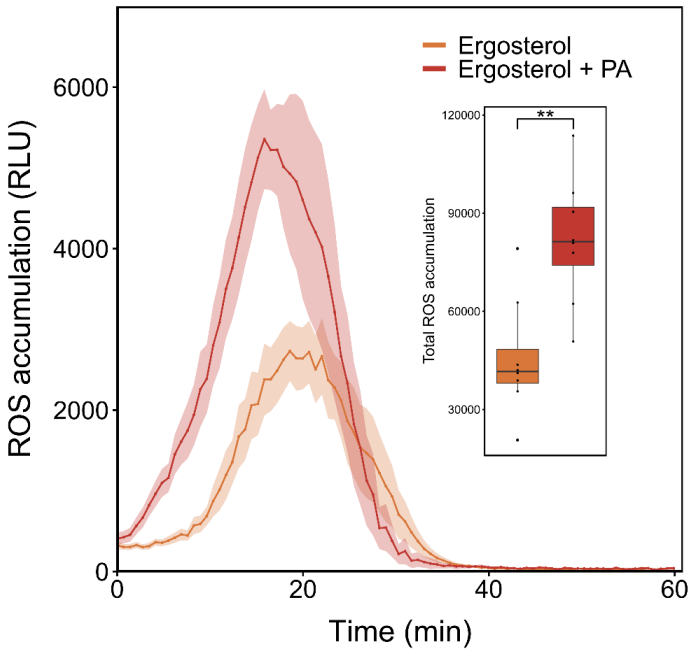

Fig. S7: Phospholipid cotreatment does not enhance the chitohexaose-induced ROS burst in barley roots.

A-D) ROS accumulation in roots of four days old barley plants, treated with the indicated elicitors or solvent control as negative control. Values represent means ± SEM from eight (without cotreatment) or sixteen (with cotreatment) wells, each containing three root pieces. The following concentrations and dilutions were used: chitohexaose: 250 nM and all phospholipids (PC, PI, PI4P, PA) were used at a final concentration of 250 nM. All treatments contained a final amount of 1:40 (v/v) methanol.

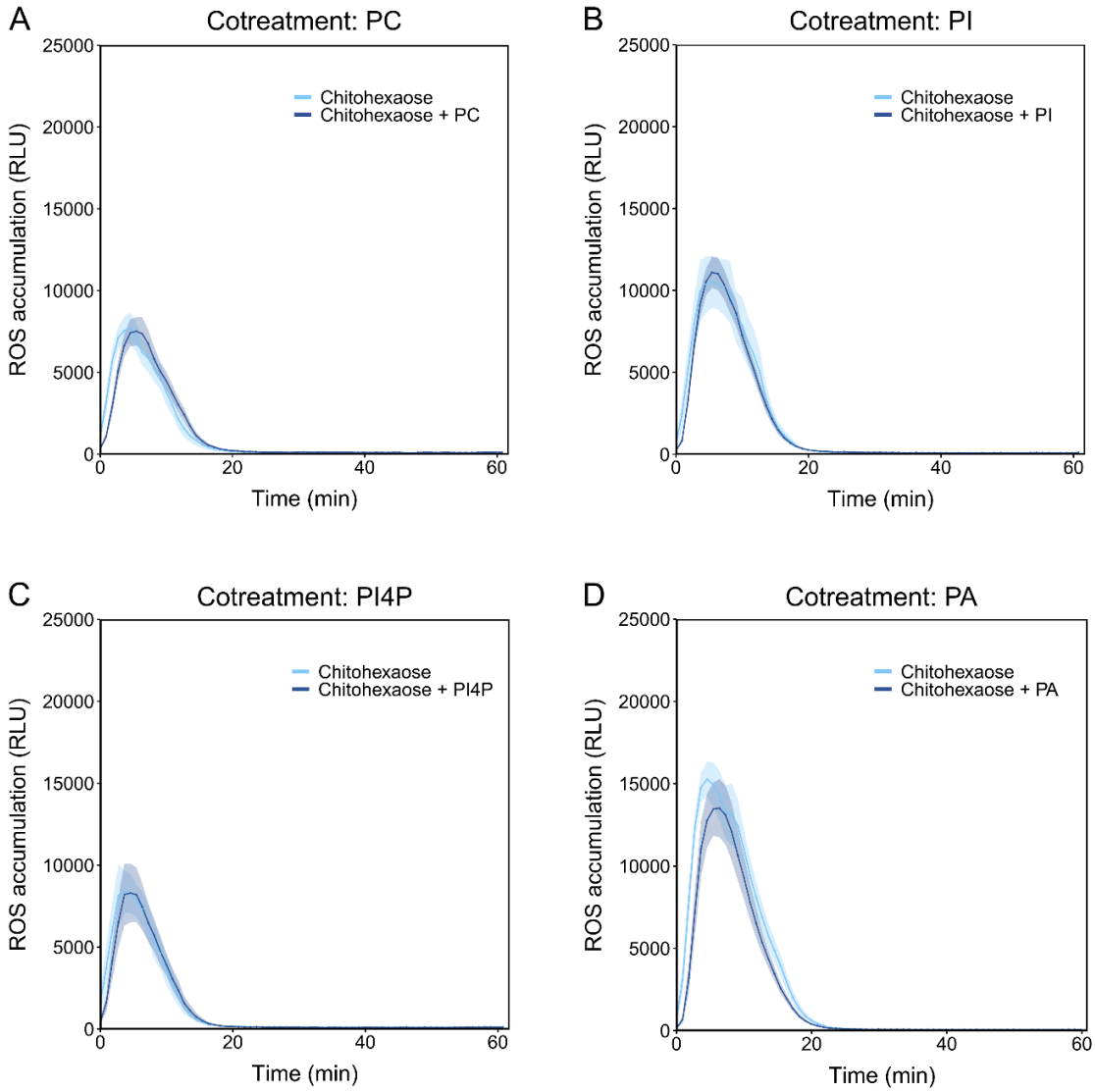

Fig. S8: PA cotreatment does not enhance chitohexaose-induced ROS burst in barley roots.

A-F) ROS accumulation in roots of four days old barley plants, treated with the indicated chitohexaose concentrations +/- 250 nM PA or solvent control as negative control. Values represent means ± SEM from eight (without cotreatment) or sixteen (with cotreatment) wells, each containing three root pieces. All treatments contained a final amount of 1:40 (v/v).

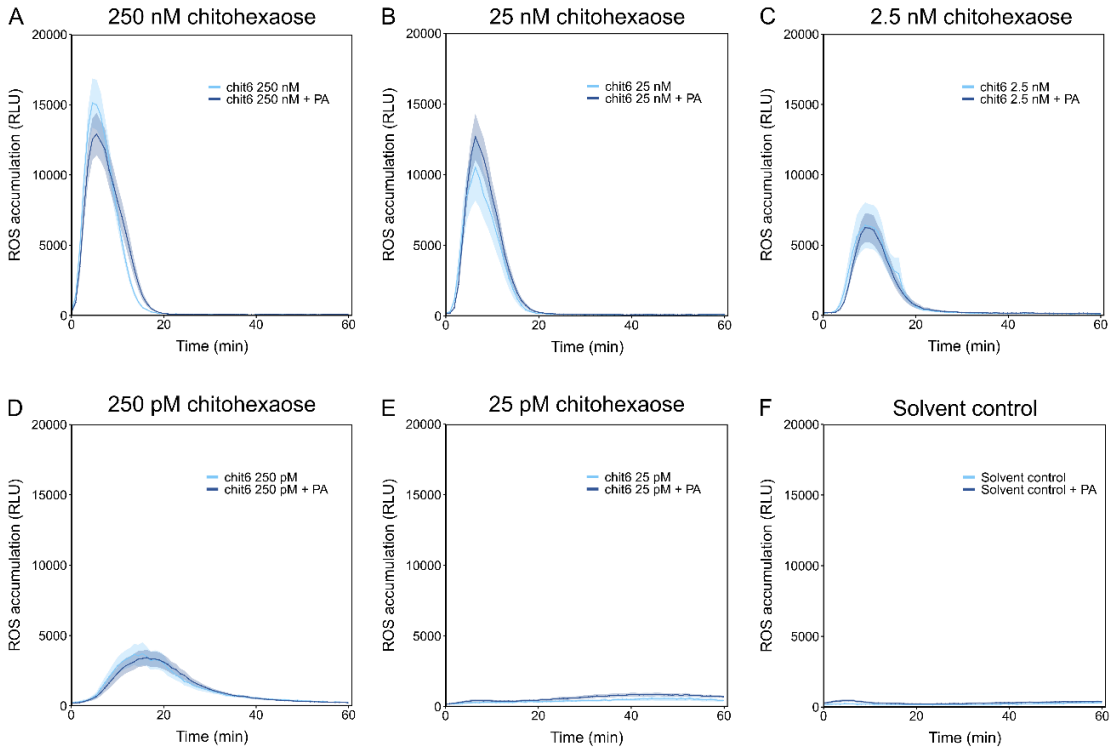

Fig. S9: Diterpene exudation in response to ergosterol treatment and *B. sorokiniana* colonization.
LC-MS/MS chromatogram of the second major diterpene found in root exudates of barley plants treated with solvent control or ergosterol or colonized by *B. sorokiniana* (positive control) for 6 days. The experiment was repeated with similar results. Ergosterol and solvent control treatments contained a final amount of 1:40 (v/v) methanol.

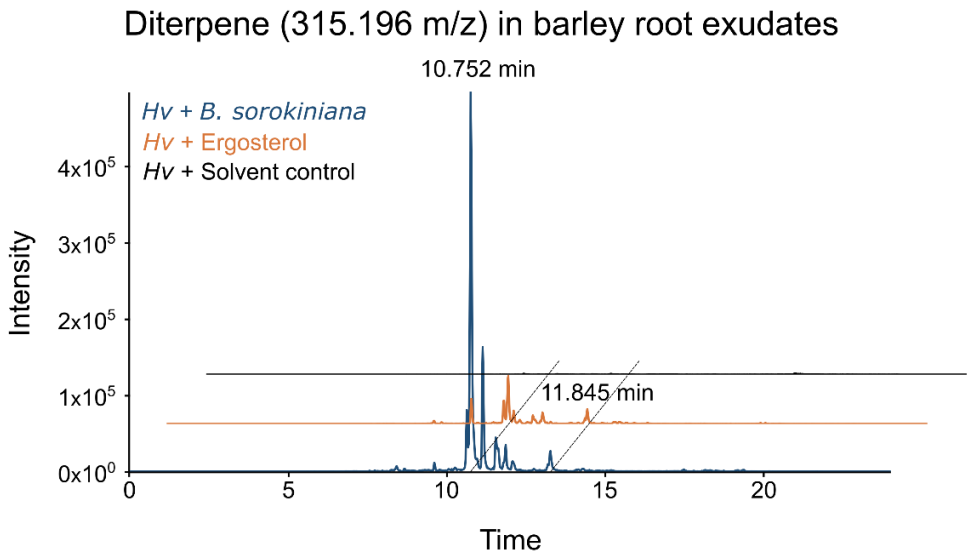

Methods S1: Detailed information on materials and methods.

Plant material and growth conditions

Seeds of *Hordeum vulgare* L. cv Golden Promise were surface sterilized with 6% sodium-hypochlorite, rotating for 1 h at 40 rpm and washed six times for 30 min with sterile milliQ-water. Seed coats were removed gently in sterile water using forceps and seeds were placed on wet filter paper (2 ml milliQ-water per 75 mm round filter paper) in a petri dish (eight seeds per filter paper). Plates were covered with aluminum foil and kept in the dark at 21 °C for three days before transfer to sterile WECK jars containing 100 ml solid 1/10 PNM (plant nutrition medium, pH 5.6) and 0.4 % (w/v) Gelrite for MAMP treatments and 1.2 % (w/v) Gelrite for fungal colonization in a growth chamber under long-day conditions (day/night cycle of 16/8 h, 22 °C/18 °C, light intensity of 108 µmol/m^2*s). For MAMP treatment, seedlings were grown for an additional four days and for fungal colonization for 3-, 7- and 14- days.

For Ca^{2+}-influx assays, barley lines expressing apoaequorin were generated. Therefore, *Aequorea victoria* aequorin was amplified from transgenic *A. thaliana* expressing cytosolic apoaequorin (Knight et al., 1991) with primers AEQ_Gib_Fw and AEQ_Gib_Rev (Supplementary Table S3) and cloned via Gibson assembly into HindIII-cut CPGE VEC00103 plasmid, which was then cut with SfiI+AhdI to allow separation of the fragments on gel and The resulting fragment with the *Sfi*I-ends (2918bp) containing the AEQ CDS under control of maize UBI promotor and NosT in between LB-RB was ligated into the SfiI-cut binary vector CPGE_VEC00006 and transformed into barley cv Golden Promise via embryo transformation (Hensel et al., 2009). Successful insertion of the transformation vector into the genome was tested by PCR (primers: Hv_AEQ_Fw, Hv_AEQ_Rev, Supplementary Table S3) on T0 plants. Positive offspring (T1) of 3:1 segregating lines were selected and further propagated to gain stable insertion lines (T2). Insertion of aequorin was verified by PCR (see above) and measuring discharge as described for the calcium assay and Plants with highest discharge levels were selected.

Solanum lycopersicum L. cv Moneymaker wildtype (WT) and *serk3a serk3b* mutant seeds were sown on soil and grown for ~2-3 weeks in the greenhouse under long-day conditions (day/night cycle of 17/7 h, 25-28 °C, ~35-40% humidity). For ROS assays, 3mm leaf discs of the two youngest, adult leaves of three weeks old tomato plants were used. *serk3a serk3b* mutant lines were generated using CRISPR/Cas9. A construct containing two sgRNAs, both of which target *Sl*SERK3A and *Sl*SERK3B was transformed (5' sgRNA AAGCAGTTGTTGGGGATTTT, 3' sgRNA ATGCTTCTAGAGCTCATAAC). Both sgRNAs target the penultimate exon within the cytoplasmic domain. Editing events were confirmed by Sanger sequencing.

Seeds of a *Nicotiana benthamiana* D. line expressing aequorin (Nb^{AEQ}) (Wanke et al., 2020) were sown on soil and grown for ~3 weeks in the greenhouse under long-day conditions (day/night cycle of 16/8 h, 22–25°C, light intensity of ~140 µmol/m^2*s, maximal humidity of 60%). For ROS and Ca^{2+}-influx assays, 3mm leaf discs of the youngest, adult leaf of 3 weeks old plants were used.

Seeds of *Arabidopsis thaliana* L. Col-0 plants expressing cytosolic apoaequorin (At^{AEQ}) were surface sterilized by incubation in 70 % EtOH for 10 min, followed by incubation in 100 % EtOH for 7 min. Subsequently, the EtOH was removed, and seeds dried under the clean bench. Dried seeds were placed on ½ MS (Murashige-Skoog-Medium, with vitamins, pH 5.7) plates containing 0.5 % sucrose and 0.4 % (w/v) Gelrite and covered with aluminum foil and stratified for 2-5 days at 4 °C. Plates were moved to the growth chamber with short day conditions (8 h light, 16 h dark, with 130 µmol/ m^2*s of light and 22 °C/18 °C) and plants grown for 7-8 days. For ROS assays, one seedling was transferred into each well of a 96 well plate and the assay was performed as described below. For Ca^{2+}-assays, seedlings were transferred to 24 well plates containing 1 ml ½ MS medium + sucrose and grown for another 4 days prior to use in the assay.

Cultivation of *S. indica* and plant colonization

Cultivation and chlamydospore isolation of *Serendipita indica* (DSM11827) was done as previously described (Sarkar et al., 2019; Wawra et al., 2016). For propagation, a stamp of 4 mm containing actively growing mycelium was removed from a 4-week-old plate with CM medium containing 1.5 % agar, transferred to a fresh plate and grown at 28 °C in darkness for 21 days prior to chlamydospore isolation for inoculation. Chlamydospores were collected in sterile milliQ water by gently scraping the surface of the mycelium on plate using a scalpel and filtered through Miracloth (Merck; 22-25 µm mesh size). Spores were pelleted by centrifugation at 3500 rpm for 7 min, washed 3x in sterile milliQ water and diluted to a final concentration of 500.000 spores/ml for inoculations. Spores were counted using the Neubauer improved counting chamber.

To grow *S. indica* mycelium in axenic culture, 100 ml liquid CM medium was inoculated with 5 ml *S. indica* chlamydospores isolated from one 28 days old plate (approximately 1 million spores per ml) and grown at 28 °C with shaking at 120 rpm in a 500 ml Erlenmeyer flask for 5 days. Mycelium was then harvested in a Miracloth filter (Merck; 22-25 µm mesh size), surface-washed twice with 50 ml 0.9% NaCl and homogenized in a blender containing ~20 ml CM medium and transferred into fresh 150 ml CM medium and grown for 2 days. Mycelium was harvested and washed again and dried on tissue paper

and snap frozen in liquid nitrogen.

For barley colonization, germinated seedlings were prepared as described above and inoculated with 3 ml of either sterile water as control or *S. indica* chlamydospores (500,000 spores/ml). Roots were harvested at 3-, 7- and 14 days post inoculation (dpi), washed thoroughly in ice-cold water to remove extraradical fungal hyphae, dried on tissue paper and frozen in liquid nitrogen. Four barley plants were used per jar and pooled per biological replicate.

ROS accumulation assay

ROS assays were performed as described previously (Chandrasekar et al., 2022). Preparation of *N. benthamiana*, tomato and *A. thaliana* material is described above. For barley, roots and shoots of seven days old seedlings were separated. The root tissue between 2 cm below the seed and 1 cm above the tip was cut into root pieces of 5 mm length and three root pieces transferred to each well of a 96-well microtiter plate (white, flat bottom) containing 200 µl of 2.5 mM MES buffer, pH 5.6. For barley shoot assays, 3 mm leaf discs were punched from one barley leaf per plant and one leaf-disc was transferred to each well of a similar 96-well microtiter plate. The plate was covered and incubated ON at 21°C for recovery. The next day, the buffer was replaced with 100 µl 2.5 mM MES buffer containing 20 µM LO-12 and 20 µg/ml HRP. After 25 min incubation in the dark, 100 µl two-fold concentrated elicitor solution or solvent control was added to each well and chemiluminescence was measured using a TECAN SPARK 10M microplate reader over all wells for 2h with an integration time of 450 msec.

Calcium influx assay

Preparation of *N. benthamiana* and *A. thaliana* material is described above. For barley, roots and shoots were prepared as described for ROS accumulation assays but plants expressing aequorin (Hv^{AEQ}) were used. Prior to ON recovery, the buffer in the wells was replaced with 100 µl 2.5 mM MES buffer containing 10 µM coelenterazine and 10 mM $CaCl_2$ per well and plates were incubated ON in the dark at 21°C. On the next day, chemiluminescence was measured using a TECAN SPARK 10M microplate plate reader. After the baseline measurement (5 min), 100 µl of two-fold concentrated elicitor solution was added manually. Photon emission was constantly measured for 30 minutes. Subsequently, 100 µl of discharge solution (3M $CaCl_2$ in 50 % EtOH) was injected into each well, followed by constant measurement for 1 minute. All steps were performed with an integration time of 450 msec. In all assays, 2 columns (16 wells) were measured per run.

MAPK phosphorylation

Barley root segments and leaf discs were prepared as described above for ROS and Ca^{2+} influx assays. Twenty-four randomly selected pieces were transferred into each well of a 24-well plate containing 1 ml 2.5 mM MES buffer. Plates were incubated ON at 21°C for recovery. On the next day, 500 µl buffer of each well were removed and replaced with two-fold concentrated elicitor solution and gently mixed. At 5-, 10-, 20- or 30-min post treatment, roots were removed from the treatment solution, gently dried on tissue paper and snap frozen in liquid nitrogen and homogenized with glass beads in the TissueLyserII (Qiagen) for 4 times 30 sec, 30 Hz in ice-cold holders. For isolation of phosphorylated proteins, 150 µl phosphoprotein extraction buffer (50 mM Tris-HCl (pH 7.5), 2 mM DTT, 5 mM EDTA, 5 mM EGTA, 10 mM NaF, 50 mM β-glycerolphosphate, 10 % glycerol, 1 tablet each of Roche Complete Mini – EDTA free and PhosStop phosphatase inhibitor per 10 ml) was added, vortexed and centrifuged for 10 min at 4 °C at 12000 rpm. The supernatant was transferred to a fresh tube and the centrifugation step was repeated two more times to ensure the extract is free of pellet debris. Protein concentration was determined using Bradford Assay following the manufacturer's instructions and 4 µg protein of each sample were separated on SDS-PAGEs and subsequently transferred to nitrocellulose membranes. Membranes were blocked for 1h with 2.5 % TBS-T BSA and incubated ON with the primary antibody (anti-p44/p42, 1:1500) in 2.5 % TBS-T BSA at 4 °C. The next day, the membranes were washed with 1xTBS-T and the secondary antibody (anti-rabbit IgG, 1:50.000) was added for 1h. After washing with 1xTBS-T and 1x TBS, blots were developed using 1ml SuperSignal™West Femto (Thermo Scientific) solution per membrane. Western Blots were imaged using the Fujifilm LAS 4000 mini camera.

Elicitor preparations

The following chemicals were used as elicitors, pre- or cotreatments. chitohexaose (Megazyme, O-CHI6), flg22 peptide (GenScript, RP19986), ergosterol pharmaceutical standard (Supelco, PHR1512), L-α-phosphatidylinositol (soy PI, Avanti, 840044), L-α-phosphatidic acid (soy PA, Avanti, 840074), L-α-phosphatidylcholine (soy PC, Avanti, 441601), L-α-phosphatidylinositol 4-monophosphate (Sigma-Aldrich, P9638), L-α-phosphatidylinositol 4,5-diphosphate (Sigma-Aldrich, P9763). Stock solutions of lipids were prepared in methanol and used to prepare elicitor solutions of appropriate concentrations in aqueous MES buffer as described below. Self-produced lipid extracts and lipid fractions were evaporated with N_2 gas and resuspended in MeOH as solvent. As control, the respective solvent was processed in the same way. All elicitor and control solutions were prepared as two-fold concentrated solutions in 2.5 mM MES buffer, pH 5.6 containing 1:20 (v/v %) MeOH. For liposomes, PA was evaporated under N_2 gas

and the lipid film hydrated with buffer (25 mM HEPES, pH=7.5, 50 mM KCL, 1 mM $MgCL_2$) at 4°C, rapidly vortexed for 30 seconds and sonicated on ice 5 times for 10 sec with each 10 sec pause prior to use in cotreatment ROS assay with ergosterol.

RNA-seq and qRT-PCR

For RNA-seq and qRT-PCR, barley roots were prepared as described for the MAPK phosphorylation assay with roots from two wells being combined per replicate and four replicates per treatment and timepoint. RNA extraction, cDNA synthesis and qRT-PCR were performed as described previously (Sarkar et al., 2019). Briefly, RNA was extracted using Trizol (Life Technologies, 15596018) and remaining DNA was removed by DNAseI (Thermo Scientific, EN0521) digestion at 37 °C for 30 min. One µg RNA was used to synthesize cDNA using the first strand cDNA kit (Thermo Scientific, K1612) according to the manufacturer's instructions. GoTaq qPCR Master Mix (Promega A60001) was used for qRT-PCR. Primers used for qRT-PCR are described in Supplementary Table S3.

RNA sequencing and data processing

For RNA sequencing, 25 µl RNA with a concentration of 100 ng/µl was used. For Illumina-compatible RNAseq libraries at first an enrichment for poly-A RNAs was performed (NEBNext® Poly(A) mRNA Magnetic Isolation Module; New England Biolabs), followed by library generation with NEBNext Ultra™II Directional RNA Library Prep Kit for Illumina (New England Biolabs). Next, sequencing-by-synthesis was done on a NextSeq 2000 device in 2 x 150 bp paired-end read mode Library construction and sequencing was performed at the Genome Centre of the Max Planck Institute for Plant Breeding, Cologne. Trimmomatic (v. 0.39) (Bolger et al., 2014) was used for quality trimming and adapter clipping and quality of the reads was assessed using fastQC. Reads were then mapped to the barley Morexv3 pseudomolecules assembly cDNA (downloaded from Ensembl plants on 18.08.2023) and quantified using kallisto (v. 0.46.1) (Bray et al., 2016), which resulted in estimated counts and transcripts per million (TPM) values. The log2 fold difference of the gene expression between conditions was calculated using R and differential expression of genes was calculated using the R package "sleuth".

Apoplastic fluid isolation of barley roots

To isolate apoplastic fluid from barley roots, barley seedlings were grown and inoculated with *S. indica* on 1/10 PNM medium as described above. Per replicate, 110 barley seedlings were used, which yielded approximately ~1 ml apoplastic fluid per replicate. For extraction of apoplastic fluid, the roots were gently removed from the jars and washed thoroughly in ice-cold water to remove external fungal

hyphae. The upper and lower 1 cm of the root were cut off and the remaining root was cut into 2 cm pieces. Root pieces of one replicate were transferred into two 50 ml falcon tubes containing approx. 35 ml of ice-cold water and covered with ice. Next, falcon tubes were submitted to five cycles of vacuum infiltration (15 min 250 mbar, 1.5 min ATM). Subsequently, roots were dried on tissue paper and transferred into a 20 ml syringe inside a 50 ml falcon tube and centrifuged for 15 min at 4 °C, 2000 rpm, lowest de- and acceleration to collect apoplastic fluid (approx. 1-2 ml per replicate) in the bottom of the falcon tube. Apoplastic fluid was stored on ice at 4 °C until further use. Roots were flash-frozen in liquid nitrogen and stored at -80 °C until further use.

Lipid extraction and fractionation by solid phase extraction

Lipid extraction was done according to the method described by Bligh and Dyer (Bligh & Dyer, 1959). To extract lipids from *S. indica* mycelium or colonized or mock-inoculated barley roots, frozen material was ground in liquid nitrogen into a very fine powder using mortar and pestle. Per sample, ~200 mg of homogenized plant or fungal tissue was transferred into a pre-cooled 2 ml Eppendorf tube and 1 ml (2 vol) chloroform:methanol:formic acid (1:1:0.1 v/v) was added to the Eppendorf tube. To isolate lipids from apoplastic fluid, ~1 ml apoplastic fluid was added to a 5 ml Eppendorf tube and 2 ml (2 vol) chloroform:methanol:formic acid (1:1:0.1 v/v) was added. The mixture was vortexed and incubated for 10 min at RT, shaking. Next, 0.5 ml (1 vol) of 300 mM ammonium acetate was added to create a phase separation and the samples were vortexed again, followed by centrifugation for 5 min at 6000 rpm. The lower organic phase was transferred to a fresh glass tube using a glass Pasteur pipette that was previously rinsed with chloroform. 0.8 ml chloroform was added again to each tube, vortexed and centrifuged for 5 min at 6000 rpm. The lower organic phase was transferred again and combined with the first extract. This step was repeated two more times. The crude lipid extract was evaporated under N_2 gas and resuspended in 4 ml MeOH for use in preparation of elicitor treatment with crude lipids.
For fractionation of crude lipids, the lipid extract was separated by two consecutive solid phase extractions (SPE). First, the crude lipid extract was dried under N_2 gas and resuspended in 1 ml chloroform and added to a Strata®SI-1 (55 µm, 70 Å, 1 ml) silica column, previously equilibrated with chloroform. Two times 1 ml chloroform was added again to the silica column and the eluate, containing neutral lipids, collected in the same tube. Then, three times 1 ml MeOH was added to the column and the fraction containing polar (phospho)lipids collected. The chloroform fraction was evaporated under N_2 gas and used for further fractionation of the neutral lipids using a hexane diethylether gradient on a second silica column as described previously (vom Dorp *et al.*, 2013). In brief, the dried lipids were

resuspended in 100 % hexane and added to the column, previously equilibrated with hexane, and a total of six fractions were collected by adding each three column volumes (1 ml) of stepwise decreasing hexane:diethylether ratios (v:v): 100:0 (hydrocarbons and squalene), 98:2 (sterol esters), 95:5 (triacylglycerol, alkyl and alkenyl acylglycerols and tocopherols; free fatty acids and fatty alcohols), 85:15 (free sterols and diacylglycerol) and finally 0:100 (diacylglycerol and monoacylglycerol). All fractions that were used in immunity assays were dried under N_2 and resuspended in 4 ml MeOH prior to usage

Phosphoproteomics

Preparation of phospho-enriched samples

Barley roots were treated as described for MAPK phosphorylation assay. Two wells were combined for each replicate per treatment and time point. Four replicates were used each. Root material was harvested 10 min post treatment. Root material was ground using mortar and pestle with liquid nitrogen into a very fine powder and 1 ml extraction buffer (8M urea, 20 µl/ml Phosphatase Inhibitor Cocktail 2 (Sigma, P5726-5ML), 20 µl/ml Phosphatase Inhibitor Cocktail 3 (Sigma, P0044-5ML), 5 mM DTT) was added and samples were incubated for 30 min with shaking, after which cell debris was removed by centrifugation. Samples were alkylated with CAA (550 mM stock, 14 mM final), the reaction was quenched with DTT (5 mM final). An equivalent of 500 µg total protein per sample was diluted to 1 M urea with 100 mM Tris-HCl pH 8.5, 1 mM $CaCl_2$ and samples were digested with 5 µg LysC (stock: 1 µg/µl Lys-C (WAKO) in 50 mM NH_4HCO_3) for 4h at RT. Next, 5 µg trypsine (stock: 1 µg/µl in 1 mM HCl,) was added and samples were diluted with 100 mM Tris-HCl pH 8.5, 1 mM $CaCl_2$, the samples were mixed and incubated ON at 37 °C. After incubation, samples were acidified with TFA to 0.5 % final concentration and samples were desalted using C18 SepPaks (1cc cartridge, 100 mg (WAT023590)). In brief, SepPaks were conditioned using methanol (1 ml), buffer B (80% acetonitrile, 0.1% TFA) (1 ml) and buffer A (0.1% TFA) (2 ml). Samples were loaded by gravity flow, washed with buffer A (1 x 1 ml, 1x 2 ml) and eluted with buffer B (2 x 400 µl). 44 µl of eluates were used for peptide measurement and total proteome and library analysis. For phosphopeptide enrichment by metal-oxide chromatography (MOC) (adapted from:(Nakagami, 2014)) the remaining samples were evaporated to a sample volume of 50 µl and diluted with sample buffer (2 ml AcN, 820 µl lactic acid (LA), 2.5 µl TFA / 80 % ACN, 0.1 % TFA, 300 mg/ml LA, final concentrations) (282 µl). MOC tips were prepared by loading a slurry of 3 mg/sample TiO_2 beads (Titansphere TiO_2 beads 10 µm (GL Science Inc, Japan, Cat. No. 5020-75010)) in 100 µl MeOH onto a C8 micro column and centrifugation for 5 min at 1500g. Tips were washed with centrifugation at 1500g for 5 min using 80 µl of solution B (80 % acetonitrile, 0.1 % TFA) and 80 µl of solution C (300 mg/ml LA in solution B). To simplify the processing, samples tips were fitted onto a 96/500 µl deep well

plate (Protein LoBind, (Eppendorf Cat. No. 0030504100). After washing MOC tips were transferred to a fresh plate, samples were loaded onto the equilibrated tips and centrifuged for 10 min at 1000g. The flow through was reloaded onto the tips and centrifugation was repeated. Tips were washed with centrifugation at 1500g for 5 min using 80 µl of solution C and 3x 80 µl of solution B. For the elution of the enriched phosphopeptides the tips were transferred to a fresh 96/500 µl deep well plate containing 100 µl/well of acidification buffer (20 % phosphoric acid). Peptides were eluted first with 50 µl elution buffer 1 (5% NH_4OH) and centrifugation for 5 min at 800g, then with 50 µl of elution buffer 2 (10% piperidine) and centrifugation for 5 min at 800g. Next, the samples were desalted using StageTips with C18 Empore disk membranes (3 M) (Rappsilber et al., 2003), dried in a vacuum evaporator, and dissolved in 10 µl 2% ACN, 0.1% TFA (A* buffer) for MS analysis.

LC-MS/MS data acquisition

Samples were analyzed using an Ultimate 3000 RSLC nano (Thermo Fisher) coupled to an Orbitrap Exploris 480 mass spectrometer equipped with a FAIMS Pro interface for Field asymmetric ion mobility separation (Thermo Fisher). Peptides were pre-concentrated on an Acclaim PepMap 100 pre-column (75 µM x 2 cm, C18, 3 µM, 100 Å, Thermo Fisher) using the loading pump and buffer A** (water, 0.1 % TFA) with a flow of 7 µl/min for 5 min. Peptides were separated on 16 cm frit-less silica emitters (New Objective, 75 µm inner diameter), packed in-house with reversed-phase ReproSil-Pur C18 AQ 1.9 µm resin (Dr. Maisch). Peptides were loaded on the column and eluted for 130 min using a segmented linear gradient of 5 % to 95 % solvent B (0 min : 5 %B; 0-5 min -> 5 %B; 5-65 min -> 20 %B; 65-90 min ->35 %B; 90-100 min -> 55 %; 100-105 min ->95 %, 105-115 min ->95 %, 115-115.1 min -> 5 %, 115.1-130 min ->5 %) (solvent A 0 % ACN, 0.1 % FA; solvent B 80 % ACN, 0.1 %FA) at a flow rate of 300 nl/min. Mass spectra were acquired in data-dependent acquisition mode with a TOP_S method using a cycle time of 2 seconds. For field asymmetric ion mobility separation (FAIMS) two compensation voltages (-45 and -65) were applied, the cycle time for the CV-45 experiment was set to 1.2 seconds and for the CV-65 experiment to 0.8 sec. MS spectra were acquired in the Orbitrap analyzer with a mass range of 320–1200 m/z at a resolution of 60,000 FWHM and a normalized AGC target of 300 %. Precursors were filtered using the MIPS option (MIPS mode = peptide), the intensity threshold was set to 5000, Precursors were selected with an isolation window of 1.6 m/z. HCD fragmentation was performed at a normalized collision energy of 30 %. MS/MS spectra were acquired with a target value of 75 % ions at a resolution of 15,000 FWHM, at an injection time of 120 ms and a fixed first mass of m/z 120. Peptides with a charge of +1, greater than 6, or with unassigned charge state were excluded from fragmentation for MS^2.

Data analysis of phosphoproteomics

Raw data were processed using MaxQuant software (version 1.6.3.4, http://www.maxquant.org/) (Cox & Mann, 2008) with label-free quantification (LFQ) and iBAQ enabled (Tyanova et al., 2016). MS/MS spectra were searched by the Andromeda search engine against a combined database containing the sequences from *H. vulgare* (Morex V3 database), and sequences of 248 common contaminant proteins and decoy sequences. Trypsin specificity was required and a maximum of two missed cleavages allowed. Minimal peptide length was set to seven amino acids. Carbamidomethylation of cysteine residues was set as fixed, phosphorylation of serine, threonine and tyrosine, oxidation of methionine and protein N-terminal acetylation as variable modifications. The match between runs option was enabled. Peptide-spectrum-matches and proteins were retained if they were below a false discovery rate of 1 % in both cases.

Statistical analysis was carried out on phospho peptide level using the intensities obtained from the "modificationSpecificPeptides" output using Perseus (version 1.6.14.0, http://www.maxquant.org/). Quantified sites were filtered for reverse hits and contaminant hits and results were filtered to retain only phospho-modified peptides. Intensities were log2 transformed and samples were grouped by condition. Next, the data was separated for a mixed imputation processing: hits were filtered for 3 valid values in one of the conditions and intensity values were normalized by subtraction of the median from each column. Then, the data was separated into two sets: one set containing mostly missing at random (MAR) hits and the other set containing mostly missing not at random (MNAR) hits by filtering the data for 1 valid hit in each group and splitting the resulting matrices (Lazar et al., 2016). The resulting matrix with at least 1 valid hit in each group is the MAR dataset, the matrix with the hits filtered out is the MNAR dataset. The missing values of each dataset were then imputed using different options of the "imputeLCMD" R package (Cosmin Lazar (2015). imputeLCMD: A collection of methods for left-censored missing data imputation. R package version 2.0. http://CRAN.R-project.org/package=imputeLCMD) integrated into Perseus: the missing values from the MAR dataset were imputed using a nearest neighbor approach (KNN, n=4), the missing values from the MNAR dataset were imputed using the MinProb option (q=0.01. tune.sigma=1). After merging of the imputed datasets two-sample Student's *t*-tests were performed using a permutation-based FDR of 5%. Alternatively, volcano plots were generated using an FDR=0.05 and an S0=1. The Perseus output was exported and further processed using Excel. For downstream analyses the imputed as well as the MNAR datasets were used.

Measurements of sterols via GC-TOF-MS

For sterol measurement via GC-TOF-MS, 5 nmol stigmastanol was added as internal standard in a chloroform:MeOH (2:1) mix prior to lipid extraction. Lipid extraction and SPE was performed as described above. Dried free sterol fractions were directly derivatized with 100 µl MSTFA for 30 min at 80 °C. Subsequently the samples were transferred to glass vials and measured in a 1:2 dilution with split ratio of 1:10. To measure crude lipid extracts of apoplastic fluid, dried lipid extracts were resuspended in 300 µl hexane and split in 2x 150 µl samples. One 150 µl sample each was evaporated under N_2 gas. Dried samples were derivatized with MSTFA for 30 min at 80°C automatically prior to measurement using a Multipurpose Autosampler (Gerstel). 1 µl of sample was injected with an automatic liner exchange system in conjunction with a cold injection system in splitless mode (ramping from 50 °C to 250 °C at 12 °C s-1) into the GC with a helium flow of 1 ml/min. Chromatography was performed using a 7890B GC system (Agilent Technologies) with a HP-5MS column with 5 % phenyl methyl siloxane film (Agilent 19091S-433, 30 m length, 0.25 mm internal diameter, 0.25 µM film). The oven temperature was held constant at 70 °C for 1 min and then ramped at 42 °C min-1 to 280 °C and in a second step with 4 °C min-1 to 320 °C which was held for 3 min resulting in a total run time of 19 minutes. Samples were ionized with an electron impact source at 70 eV and 200 °C source temperature and recorded in a mass range of m/z 60 to m/z 800 at 20 scans per second with a 7200 GC-QTOF (Agilent Technologies). Compounds were identified via MassHunter Qualitative (v b08.00, Agilent Technologies) by comparison of spectra to the NIST14 Mass Spectral Library (https://www.nist.gov/srd/nist-standard-reference-database-1a-v14). Ergosterol was verified using a pharmaceutical standard (Supelco, PHR1512) and stigmastanol was used as an internal standard. Peaks were integrated using MassHunter Quantitative (v b08.00, Agilent Technologies). For relative quantification, all metabolite peak areas were normalized to the corresponding peak area of the internal standard stigmastanol and the sample fresh weight (mycelium, roots) or volume (AF).

Diterpene measurements via LC-MS

To measure diterpenes in root exudates of barley plants, seedlings were transferred into WECK jars containing 100 ml 1/10 PNM solution and 3 ml sterile water was added to the roots. Seedlings were incubated ON in growth chamber and 5 ml treatment solution (solvent control, 250 nM Ergosterol or *Bipolaris sorokiniana* spores (5000 spores/ml, 5ml) and) were added on the next day and grown for 6 days. To harvest root exudates, plants were removed from the medium and washed gently in 25 ml water to wash off residual diterpenes attached on the outside of the roots. The medium was collected with the wash water from the roots and flash-frozen in liquid nitrogen. Diterpenes were extracted as

described previously (Liu et al., 2024). Briefly, root exudates were extracted two times with a mixture of 70 % ethylacetate and 30 % hexane (v/v) by vigorous shaking. After phase separation the organic phase was collected. 150 mg of plant matter was extracted in a modified Bligh and Dyer extraction in two rounds with 900 µl of a mixture of 67 % dichloromethane and 33 % ethanol and 150 µl of hydrochloric acid of pH 1.4. The organic phase containing diterpenoids was collected. All organic extracts were dried in nitrogen stream and stored at -80 °C until analysis.

Separation of medium polar metabolites was performed on a Nucleoshell RP18 (2.1 x 150 mm, particle size 2.1 µm, Macherey & Nagel, GmbH, Düren, Germany) using a Waters ACQUITY UPLC System, equipped with an ACQUITY Binary Solvent Manager and ACQUITY Sample Manager (20 µl sample loop, partial loop injection mode, 5 µl injection volume, Waters GmbH Eschborn, Germany). Eluents A and B were aqueous 0.3 mmol// NH_4HCOO (adjusted to pH 3.5 with formic acid) and acetonitrile, respectively. Elution was performed isocratically for 2 min at 5 % eluent B, from 2 to 19 min with linear gradient to 95 % B, from 19-21 min isocratically at 95 % B, and from 21.01 min to 24 min at 5 % B. The flow rate was set to 400 µl/min and the column temperature was maintained at 40 °C.

Mass spectrometric analysis of small molecules was performed by MS1 full scan from 65-1500 Dalton and 100 ms accumulation time (ZenoToF 7600, AB Sciex GmbH, Darmstadt, Germany) operating in negative ion mode and controlled by Sciex OS software (Sciex). The declustering potential was set to -80 V with a spread of 50 V. MS/MS-CID fragmentation was triggered by data dependent acquisition in 20 ms pockets and up to 40 candidate spectra were recorded between 65-1500 Dalton for ions were the threshold exceeded 150 cps. As for MS1 the declustering potential was set to -80 V and a spread of 50 V, while the collision energy was set to -35 V and a spread of 25 V. The source operation parameters were as the following: ion spray voltage, -4500 V; nebulizing gas, 60 psi; source temperature, 600 °C; drying gas, 70 psi; curtain gas, 35 psi CAD gas 7 psi. Instrument tuning and internal mass calibration were performed every 5 samples with the calibrant delivery system applying X500 ESI negative tuning solution (AB Sciex GmbH, Darmstadt, Germany).MS1 data for selected mz;r.t. couples were integrated using MultiQuant TF (AB Sciex GmbH, Darmstadt, Germany) within a tolerance window of 10 ppm and a smooth factor of 1.0.

References:

Bligh, E. G., & Dyer, W. J. (1959). A Rapid Method of Total Lipid Extraction and Purification. *Canadian Journal of Biochemistry and Physiology*, *37*(8).

Bolger, A. M., Lohse, M., & Usadel, B. (2014). Trimmomatic: a flexible trimmer for Illumina sequence

data. *Bioinformatics*, *30*(15), 2114–2120. https://doi.org/10.1093/BIOINFORMATICS/BTU170

Bray, N. L., Pimentel, H., Melsted, P., & Pachter, L. (2016). Near-optimal probabilistic RNA-seq quantification. *Nature Biotechnology 2016 34:5*, *34*(5), 525–527. https://doi.org/10.1038/nbt.3519

Chandrasekar, B., Wanke, A., Wawra, S., Saake, P., Charura, N., Neidert, M., Malisic, M., Thiele, M., Pauly, M., & Zuccaro, A. (2022). Fungi hijack a plant apoplastic endoglucanase to release a ROS scavenging β-glucan decasaccharide to subvert immune responses. *The Plant Cell*, *34*, 2765–2784. https://doi.org/10.1101/2021.05.10.443455

Cox, J., & Mann, M. (2008). MaxQuant enables high peptide identification rates, individualized p.p.b.-range mass accuracies and proteome-wide protein quantification. *Nature Biotechnology 2008 26:12*, *26*(12), 1367–1372. https://doi.org/10.1038/nbt.1511

Hensel, G., Kastner, C., Oleszczuk, S., Riechen, J., & Kumlehn, J. (2009). Agrobacterium-mediated gene transfer to cereal crop plants: current protocols for barley, wheat, triticale, and maize. *International Journal of Plant Genomics*, *2009*. https://doi.org/10.1155/2009/835608

Knight, M. R., Campbell, A. K., Smith, S. M., & Trewavas, A. J. (1991). Transgenic plant aequorin reports the effects of touch and cold-shock and elicitors on cytoplasmic calcium. *Nature 1991 352:6335*, *352*(6335), 524–526. https://doi.org/10.1038/352524a0

Lazar, C., Gatto, L., Ferro, M., Bruley, C., & Burger, T. (2016). Accounting for the Multiple Natures of Missing Values in Label-Free Quantitative Proteomics Data Sets to Compare Imputation Strategies. *Journal of Proteome Research*, *15*(4), 1116–1125. https://doi.org/10.1021/ACS.JPROTEOME.5B00981

Liu, Y., Esposto, D., Mahdi, L. K., Porzel, A., Stark, P., Hussain, H., Scherr-Henning, A., Isfort, S., Bathe, Ulschan., Acosta, I. F., Zuccaro, A., Balcke, G. U., & Tissier, A. (2024). Hordedane diterpenoid phytoalexins restrict Fusarium graminearum infection but enhance Bipolaris sorokiniana colonization of barley roots. *Molecular Plant*, *17*(8), 1307–1327. https://doi.org/10.1016/J.MOLP.2024.07.006

Nakagami, H. (2014). StageTip-based HAMMOC, an efficient and inexpensive phosphopeptide enrichment method for plant shotgun phosphoproteomics. *Methods in Molecular Biology (Clifton, N.J.)*, *1072*, 595–607. https://doi.org/10.1007/978-1-62703-631-3_40

Rappsilber, J., Ishihama, Y., & Mann, M. (2003). Stop And Go Extraction tips for matrix-assisted laser desorption/ionization, nanoelectrospray, and LC/MS sample pretreatment in proteomics. *Analytical Chemistry*, *75*(3), 663–670. https://doi.org/10.1021/AC026117I/ASSET/IMAGES/LARGE/AC026117IF00005.JPEG

Sarkar, D., Rovenich, H., Jeena, G., Nizam, S., Tissier, A., Balcke, G. U., Mahdi, L. K., Bonkowski, M., Langen, G., & Zuccaro, A. (2019). The inconspicuous gatekeeper: endophytic Serendipita vermifera acts

as extended plant protection barrier in the rhizo-sphere. *New Phytologist*, *224*, 886–901. https://doi.org/10.1111/nph.15904

Tyanova, S., Temu, T., & Cox, J. (2016). The MaxQuant computational platform for mass spectrometry-based shotgun proteomics. *Nature Protocols 2016 11:12*, *11*(12), 2301–2319. https://doi.org/10.1038/nprot.2016.136

Wanke, A., Rovenich, H., Schwanke, F., Velte, S., Becker, S., Hehemann, J. H., Wawra, S., & Zuccaro, A. (2020). Plant species-specific recognition of long and short β-1,3-linked glucans is mediated by different receptor systems. *Plant Journal*, *102*(6), 1142–1156. https://doi.org/10.1111/tpj.14688

Wawra, S., Fesel, P., Widmer, H., Timm, M., Seibel, J., Leson, L., Kesseler, L., Nostadt, R., Hilbert, M., Langen, G., & Zuccaro, A. (2016). The fungal-specific β-glucan-binding lectin FGB1 alters cell-wall composition and suppresses glucan-triggered immunity in plants. *Nature Communications 2016 7:1*, *7*(1), 1–11. https://doi.org/10.1038/ncomms13188

3.2 Local and systemic plant response to fungal lipids during *S. indica* colonization.

The following chapters comprise data and experiments extending the data provided in Saake *et al.* (Chapter 3.1). Information on methods, used to obtain this data can be found in the Materials and Methods section of Saake *et al.* (Chapter 3.1).

S. indica-lipids mediated ROS burst is not affected by the extracellular calcium antagonist $LaCl_3$ in *N. benthamiana*^{AEQ}.

S. indica lipids induced a distinctive ROS burst, accompanied by a minor, yet distinctive increase in cytosolic Ca^{2+} concentration ($[Ca^{2+}]_{cyt}$) with a similar peak timing in *N. benthamiana* leaves (Chapter 3.1, Figure S3 A-B). The increase in $[Ca^{2+}]_{cyt}$ is mediated by influx of Ca^{2+} from the apoplast or intracellular compartments. To investigate whether Ca^{2+}-influx from the apoplast contributes to the *S. indica* lipids-induced ROS burst, the extracellular calcium antagonist lanthanum chloride ($LaCl_3$) was added to the elicitor solutions. In the presence of $LaCl_3$, no increase in $[Ca^{2+}]_{cyt}$ was observed for all treatments (Figure 3 B), demonstrating that $LaCl_3$ effectively blocks Ca^{2+}-influx in *N. benthamiana* leaves. Moreover, $LaCl_3$ addition did not affect the *S. indica* lipid induced ROS burst, whereas the response to chitohexaose was abolished (Figure 3 A). This provided further evidence that the *S. indica* lipid-induced ROS burst might not depend on Ca^{2+}-influx in *N. benthamiana* leaves. Overall, the use of such broad-range inhibitors might affect several other plant processes, which could also affect the plant responsiveness to MAMPs. Alternatively, more specific Ca^{2+}-channel inhibitors or mutant plants, lacking specific Ca^{2+}- channels, for instance cyclic nucleotide-gated ion channels (CNGCs), glutamate receptor-like proteins (GLRs), reduced hyperosmolality-induced $[Ca^{2+}]_{cyt}$ increase channels (OSCAs), two-pore channels (TPCs) and annexins (ANNs) (G. Xu et al., 2022), could be tested. This could additionally provide more information on the Ca^{2+} source.

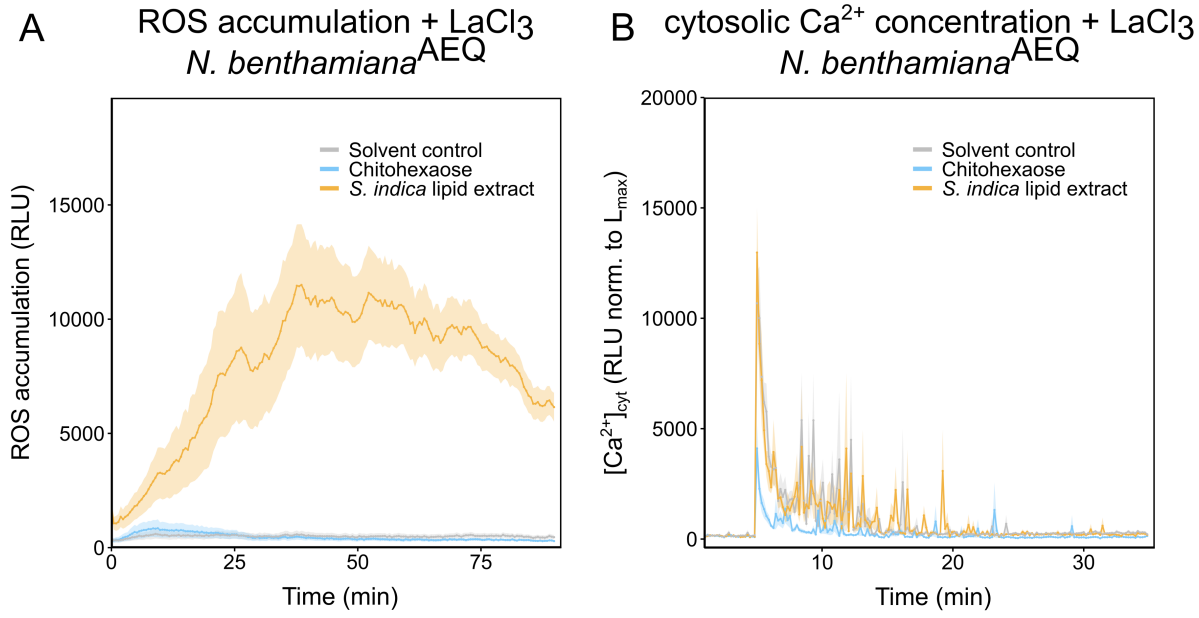

Figure 3: *S. indica*-lipids mediated ROS burst is not affected by the extracellular calcium antagonist $LaCl_3$ in *N. benthamiana*^{AEQ}. ROS accumulation (A) and cytosolic Ca^{2+} concentration ($[Ca^{2+}]_{cyt}$) (B) in leaves of 3-weeks old *N. benthamiana*^{AEQ} plants after treatment with the indicated MAMPs or solvent control as negative control. 125 μM of $LaCl_3$ was added to the treatments. Values represent means ± SEM from eight wells, each containing one 3 mm leaf disc. The following concentrations/dilutions were used: *S. indica* lipid extract: 1:160 , chitohexaose: 250 nM. All treatments contained a final amount of 1:40 (v/v) methanol. Letters indicate significant differences based on ANOVA + post hoc Tukey test ($p \leq 0.05$).

S. indica lipids induce expression of *WRKY* transcription factors.

In addition to transcriptome analysis of barley roots treated with ergosterol and *S. indica* lipids for 2 h, expression of *WRKY* transcription factors was investigated via qRT-PCR in barley roots treated with *S. indica* lipid extract for 2 h and compared to solvent control and chitohexaose treatment. Expression of *HvWRKY2* and *HvWRKY33* was induced upon both chitohexaose and *S. indica* lipid treatment, while *HvWRKY1* expression was only induced upon chitohexaose treatment. Induction of all three *WRKY* genes was higher with chitohexaose than *S. indica* lipid extract treatment (Figure 4). WRKY transcription factors are a family of transcription factors conserved in many plant species, characterized by the presence of one or two WRKY domains, approx. 60 amino acid DNA binding domains containing a conserved WRKYGQK motif in the N-terminus, and a zinc finger in the C-terminus (Rushton et al., 2010). In barley, 45 *WRKY* genes have been identified and grouped into three groups together with their *A. thaliana* orthologs (Mangelsen et al., 2008). Expression of *HvWRKY1* and *HvWRKY2*, genes from group II, was shown to be induced upon treatment with several MAMPs (Shen et al., 2007; Wanke et al., 2020). Both transcription factors were shown to be activated by MAMP perception but function as repressors of PTI during compatible powdery mildew infection of barley plants (Shen et al., 2007; D. Yu et al., 2023). *Hv*WRKY2 was suggested to suppresses the plant immune response by targeting the potential chitin receptor *Hv*CEBiP and inhibiting its expression, thus limiting PTI signaling, leading to enhanced powdery mildew infection (D. Yu et al., 2023). Similarly, *Hv*WRKY1 and *Hv*WRKY2 might negatively regulate the *S. indica*-mediated immune response in barley to enable host colonization. It would be interesting to investigate whether *Hv*WRKY2

also interacts with components involved in *S. indica* lipid perception. Upon MAMP perception and subsequent MAPK cascade activation, *At*WRKY33 is released and induces expression of plant defense components (J. L. Qiu et al., 2008; Rushton et al., 2010) *Hv*WRKY33 shows high sequence similarity to *At*WRKY33, suggesting a similar function in barley. Interestingly, both WRKY transcription factors that potentially function as negative and positive regulators of plant immunity are transcriptionally activated in response to *S. indica* lipid treatment, thus might be balancing plant immunity during *S. indica* colonization.

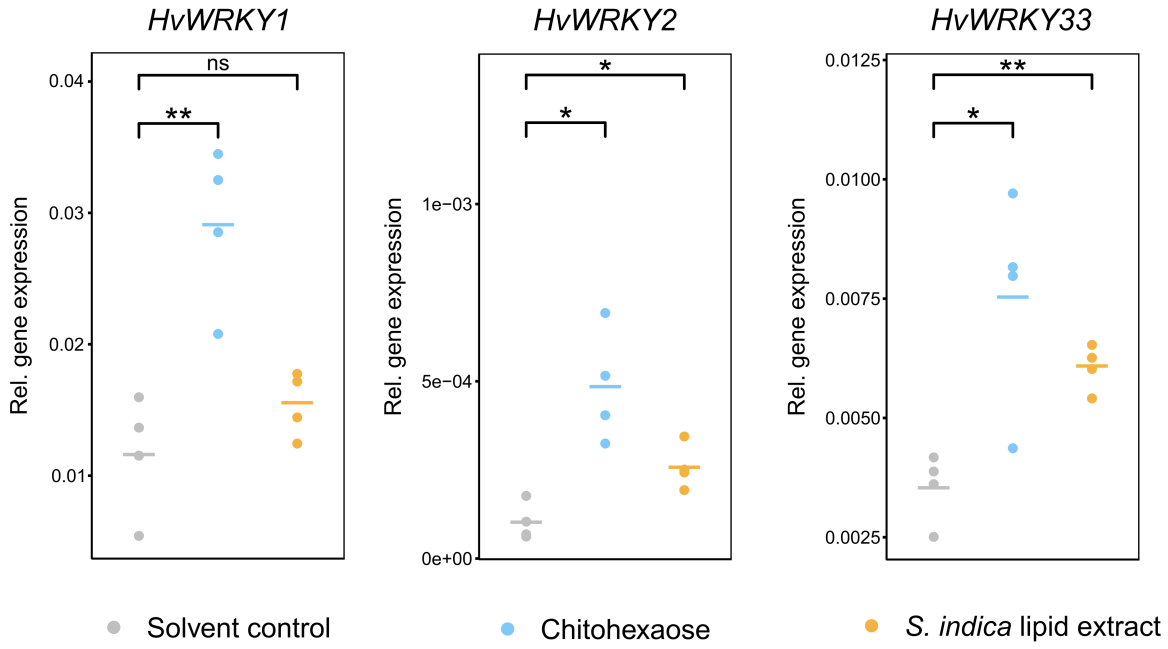

Figure 4: *S. indica* lipids induce expression of *WRKY* transcription factors at 2 hpt. Gene expression of *HvWRKY1*, *HvWRKY2* and *HvWRKY33* relative to the housekeeping gene *HvUBI* in barley roots determined by qRT-PCR. Roots were treated with the indicated MAMPs or solvent control for 2h. The following concentrations and dilutions were used: Chitohexaose: 250 nM, *S. indica* lipid extract: 1:160 (v/v) dilution. All treatment solutions contained a final amount of 1:40 (v/v) methanol. Asterisks indicate significant differences based on Student's t-test ($p \leq 0.05$ *; $p \leq 0.01$ **; $p \leq 0.001$ ***, $p \leq 0.0001$ ****).

S. indica colonization prevents lipid-mediated ROS burst locally but not systemically.

As described above, we observed that *S. indica* colonization abolished the ergosterol- and *S. indica* lipid extract-induced ROS bursts in barley roots at 7 dpi (Chapter 3.1, Figure 3). At 3- and 13 dpi, a similar response was observed. At both timepoints, all elicitors induced distinct ROS bursts in mock-treated barley roots (Figure 5 A,C). The peak heights of all ROS bursts were decreased in mock-treated roots at 13 dpi compared to 3 dpi (Figure 5 C), indicating that roots of older barley plants are generally less responsive to MAMP treatment. In *S. indica*-colonized roots, the ergosterol- and *S. indica* lipid-induced ROS bursts were completely abolished at 13 dpi (Figure 5 D), while the peak height of the chitohexaose-induced ROS burst was only slightly diminished. This resembles the observations at 7 dpi (Chapter 3.1, Figure 3 E). However, for both lipid treatments a minor ROS burst was observed in *S. indica*-colonized roots at 3 dpi (Figure 5 B). This could be due to a low amount of *S. indica* hyphae in the barley root in this

early stage of colonization or a developmental change during root colonization with *S. indica* at later stages of colonization ($\leq$ 7 dpi) being more effective in suppression of host immunity, as the apoplast becomes extensively colonized. Overall, it demonstrates that *S. indica* colonization suppresses lipid-induced ROS bursts in barley roots throughout different colonization phases, with increasing strength from 3- to 7- and 13 dpi.

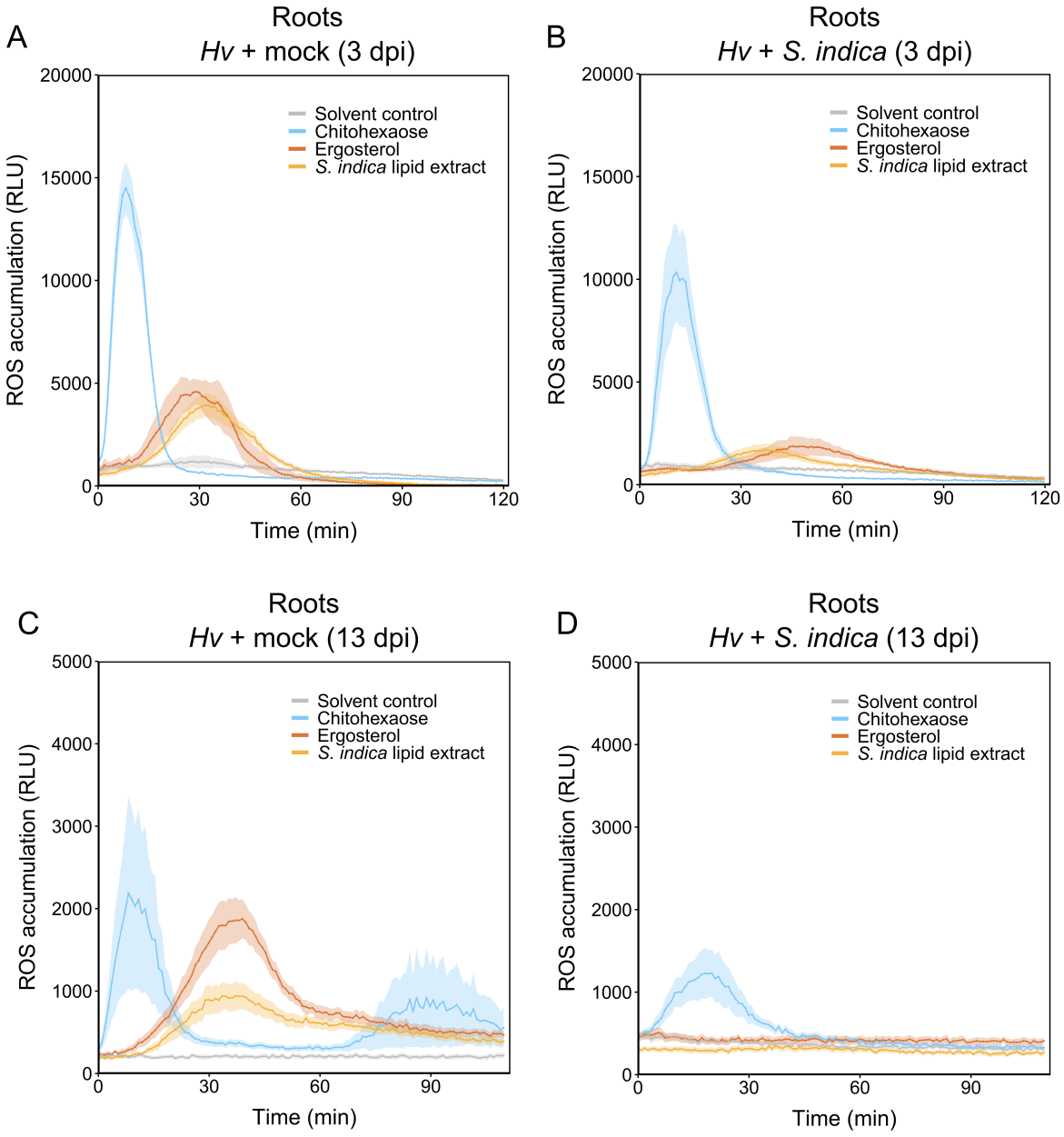

Figure 5: *S. indica* colonization prevents lipid-induced ROS burst in barley roots throughout different colonization stages. ROS accumulation in mock-treated (A, C) or *S. indica*-colonized barley roots (B, D) at 3- (A-B) and 13 dpi (C-D). Roots were washed thoroughly prior to assay preparations to remove extracellular fungal hyphae. Values represent means ± SEM from eight wells, each containing three root pieces. The following concentrations and dilutions were used: Chitohexaose and ergosterol: 250 nM, *S. indica* lipid extract: 1:160 (v/v) dilution. All treatment solutions contained a final amount of 1:40 (v/v) methanol.

To elucidate whether the suppression of lipid-mediated ROS burst occurs only locally or also systemically, ROS accumulation was investigated in leaves of *S. indica*-colonized barley seedlings. In both mock-treated and *S. indica*-colonized barley seedlings at 7 dpi, distinct ROS bursts were

observed in response to all elicitors (Figure 6) with slightly lower peak maxima in *S. indica*-colonized seedlings compared to mock-treated seedlings. This might indicate a minor systemic effect. However, a clear ROS burst was observed in leaves of *S. indica*-colonized seedlings, while the fungal lipid mediated ROS burst was completely abolished in *S. indica*-colonized roots (Chapter 3.1, Figure 3 F). Beneficial root endophytes are known to induce systemic resistance, priming their host plants for future pathogen infections. Thus, it was expected that leaves of *S. indica*-colonized barley plants are still MAMP responsive and might even show increased sensitivity. Additional immunity readouts (e.g. MAPK phosphorylation) could help clarify whether *S. indica*-colonization leads to a priming effect and ISR in barley leaves. Moreover, analysis of additional timepoints could be informative.

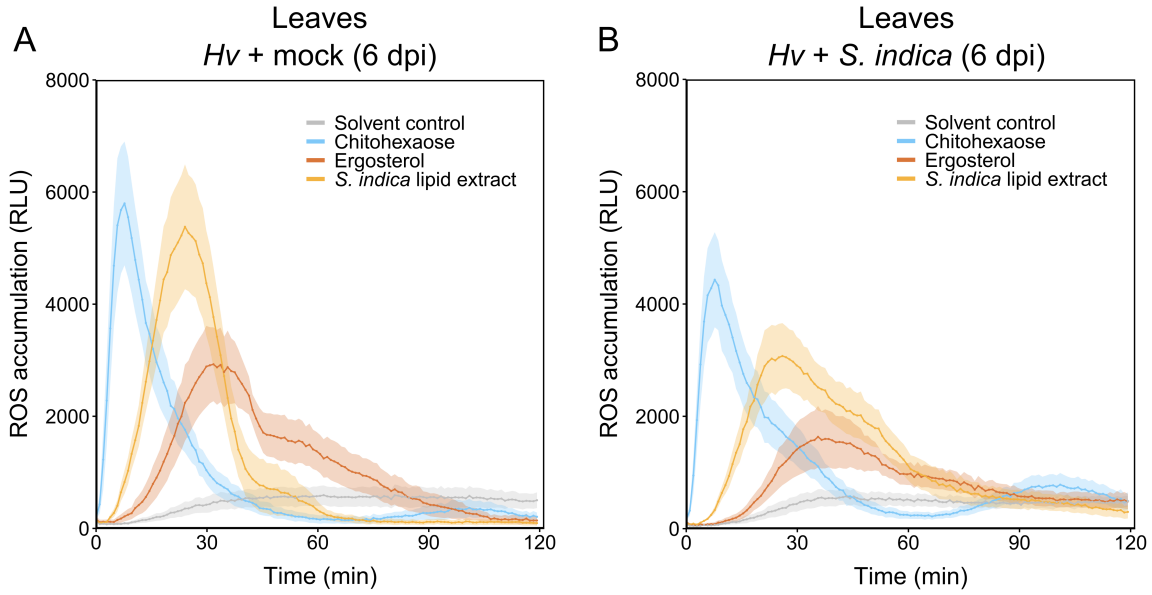

Figure 6: *S. indica* colonization does not affect lipid-induced ROS burst in barley leaves. ROS accumulation in leaves of mock-treated (A) or *S. indica*-colonized barley roots (B) at 6 dpi. Values represent means ± SEM from eight wells, each containing one 3 mm leaf disc. The following concentrations and dilutions were used: treatments: chitohexaose and ergosterol: 250 nM, *S. indica* lipid extract: 1:160 (v/v) dilution. All treatment solutions contained a final amount of 1:40 (v/v) methanol.

Barley *mlo-5* mutants are not affected in the ergosterol-mediated ROS burst.

Phosphoproteome analysis of chitohexaose-, ergosterol- and *S. indica* lipid-treated barley roots, revealed that a MLO-like protein is specifically phosphorylated in response to lipid treatment (Chapter 3.1, Figure 4 B). *Hv*MLO was initially identified due to its role in powdery mildew infection. Barley *mlo* mutant lines showed complete resistance to *Blumeria graminis* (powdery mildew) infection (Jørgensen, 1992). In the following years, the effect of *mlo* mutants in various plant species and on various microbial interactions was investigated (Jarosch et al., 1999; Acevedo-Garcia et al., 2017; Kusch & Panstruga, 2017; Hilbert et al., 2020). Acevedo-Garcia et al., 2017 provided a comprehensive overview of the *A. thaliana mlo2 mlo6 mlo12* triple mutant on interactions with microbes from different kingdoms of life (bacteria, oomycetes and fungi) and various lifestyles, proposing that a combination of lifestyle and colonization strategy or mode of plant entry determine the colonization phenotype in the *mlo2 mlo6 mlo12* triple mutant. *MLO*

mutation conferred resistance mostly against biotrophic microbes that require direct penetration to enter the plant cells (Acevedo-Garcia et al., 2017). In line with this, in *A. thaliana* and barley *mlo* mutant lines, induced formation of CWAs and subsequent prevention of penetration was observed (Acevedo-Garcia et al., 2017; Kusch et al., 2019; Hilbert et al., 2020). In barley *mlo-5* the increase of CWAs was accompanied by early and systemic iron accumulation in the epidermal layer of barley roots (Hilbert et al., 2020). Similarly, increased cell swellings and increased H_2O_2 accumulation was observed around *B. sorokiniana* penetration sites in barley leaves (J. Kumar et al., 2001). Both iron and H_2O_2 are involved in cross-linking of CWAs (Hückelhoven, 2014). Although *mlo* mutants are used in breeding and thoroughly studied on their effect on several microbial interactions, only few molecular components involved in MLO-mediated signaling were identified.

MLO genes only occur in plants and algae in small to medium-sized families. While barley contains two *MLO* genes, 15 *MLO* genes were identified in *A. thaliana* (Devoto et al., 2003; Acevedo-Garcia et al., 2014). BLAST analysis of the barley MLO-like protein (HORVU.MOREX.r3.4HG0410620.1, UniProt-ID: A0A8I6XIF7), revealed that its sequence is identical with *Hv*MLO (HORVU.MOREX.r2.4HG0342080.1, UniProt-ID: P93766) and the closely related and functionally redundant *At*MLO2, *At*MLO12 and *At*MLO6 are the closest homologs in *A. thaliana*. Using barley *mlo-5* mutant lines, we investigated whether lack of *HvMLO* affects ergosterol- and *S. indica* lipids-mediated ROS bursts. *mlo-5* mutants in the Ingrid accession (Bci *mlo-5*) and *mlo-5* mutants in the Pallas accession were used. Both mutant lines contain a mutation in the first exon of the *HvMLO* gene (Büschges et al., 1997). Golden Promise wildtype (WT) was used as reference. No difference in ergosterol or *S. indica* lipid perception was observed in the mutant lines compared to the WT control (Figure 7). This indicates that *Hv*MLO might not be involved in modulation of lipid-mediated ROS accumulation but functions in another signaling pathway. However, this finding should be confirmed with the proper control (WT) lines in the same background as used for the mutants.

MLO proteins contain seven transmembrane domains and are located in the PM with an apoplastic N-terminal domain and a cytosolic C-terminal domain (Acevedo-Garcia et al., 2014). Thus, MLO can potentially integrate both intracellular and extracellular host- or microbial signals to modulate the plant defense response. The C-terminal domain contains a calmodulin (CaM) binding domain. Ca^{2+}-dependent CaM-binding to MLO enhances MLO activity in suppression of defense responses (Kim et al., 2002). The phosphorylation site identified in our phosphoproteome analysis is located in the C-terminal domain, downstream of the CaM-binding domain. Given the previous research on MLO proteins, it is not surprising that ROS accumulation is not affected in the barley *mlo-5* mutant in response to either lipid- or chitohexaose treatment. MLO most likely regulates further downstream MAMP responses, for instance callose deposition. MLO was shown to locate to PM nanodomains beneath the penetration site and localization of MLO was accompanied by enhanced sterol localization (Bhat et al., 2005). Thus, perception of ergosterol and integration into the plant PM could target MLO to the penetration site, where it is phosphorylated and activated to reduce callose depositions and facilitate colonization. This

might explain the phosphorylation upon lipid treatment. The lack of Ca^{2+}-influx in response to ergosterol or *S. indica* lipid treatment, which would potentially enhance MLO activity, contrasts this hypothesis. It would be interesting to investigate whether fungal lipid treatment and chitohexaose treatment induce callose deposition to a different degree, potentially due to differential activation of MLO.

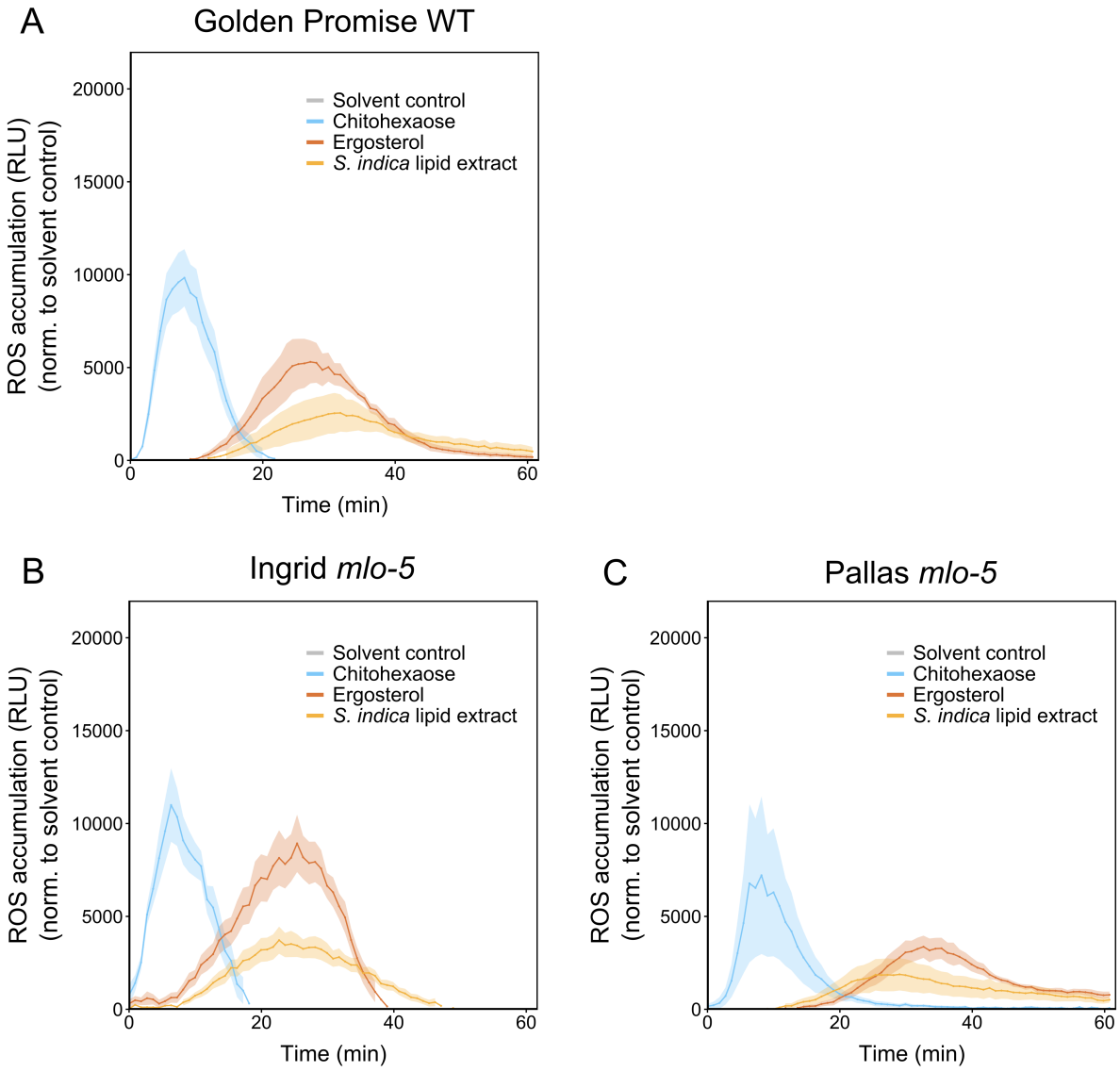

Figure 7: *mlo-5* mutants are not affected in ergosterol-mediated ROS burst. ROS accumulation in roots of seven days old barley Golden Promise WT (A), Ingrid *mlo-5* (B) or Pallas *mlo-5* (C) roots. Values were normalized to average solvent control value for each timepoint. Values represent means ± SEM from eight wells, each containing three root pieces. The following concentrations and dilutions were used: chitohexaose and ergosterol: 250 nM, *S. indica* lipid extract: 1:160 (v/v) dilution. All treatment solutions contained a final amount of 1:40 (v/v) methanol.

3.3 Lipids in *Bipolaris sorokiniana* - barley interaction

MAMP-induced ROS accumulation is abolished in *Bipolaris sorokiniana*-colonized roots.

S. indica colonization specifically suppressed the fungal-lipid mediated ROS burst in barley roots (Chapter 3.1, Figure 3 E-F). To investigate whether the suppression is specific for a symbiotic interaction or also conserved in fungi with other lifestyles, *B. sorokiniana*-colonized barley roots were investigated for their ability to perceive MAMPs. *B. sorokiniana* is a hemibiotrophic pathogen and the causal agent of spot blotch disease in several crops (J. Kumar et al., 2002). As it rapidly induces plant cell death *via* secretion of toxins, early colonization timepoints (2 dpi) were tested. Similar to *S. indica* colonization, *S. indica* lipids- and ergosterol-mediated ROS bursts were suppressed during *B. sorokiniana* colonization (Figure 8). Moreover, also the chitohexaose-induced ROS burst was abolished and the flg22-induced ROS burst was greatly diminished (Figure 8 B). At 2 dpi, slight root browning was observed in *B. sorokiniana*-colonized roots (Figure 8 B, inset), indicating an advanced immune reaction accompanied by host cell death in *B. sorokiniana*-colonized roots already at early colonization stages. Therefore,the majority of the host root cells might already be dead or insensitive to MAMP treatment due to previous, constitutive induction of immunity as a result of *B. sorokiniana* colonization. Additionally, total lipid extracts from *B. sorokiniana* mycelium induced a ROS burst in mock-treated barley roots, which was suppressed in *B. sorokiniana*-colonized roots (Figure 8). ROS burst shape and timing overlapped with the ROS bursts induced by ergosterol and *S. indica* lipids, indicating that ergosterol is also present and immunogenic in lipid extract of *B. sorokiniana* mycelium.

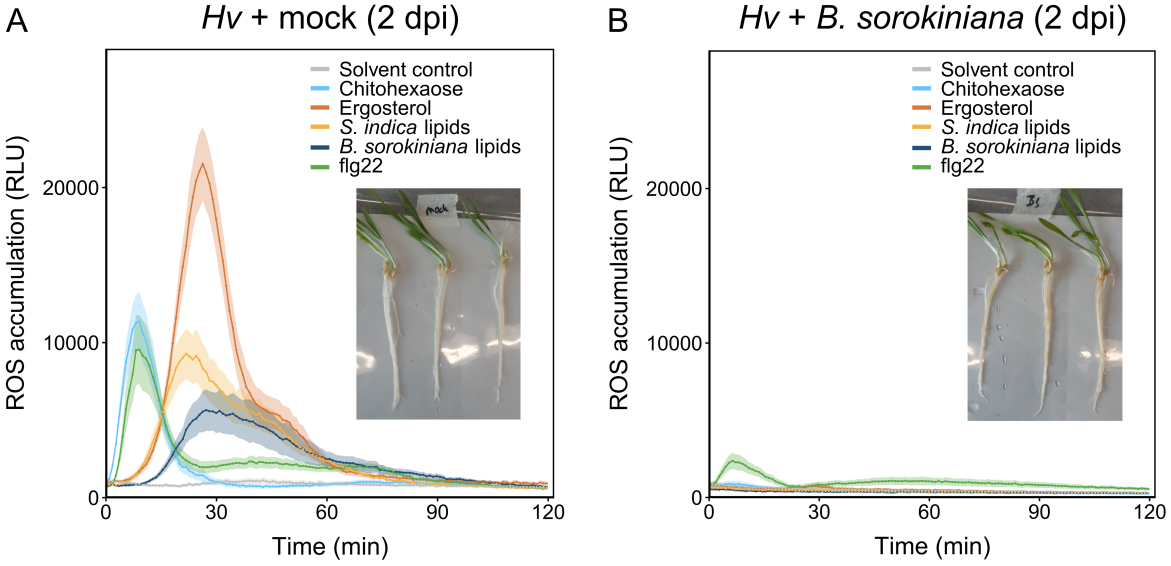

Figure 8: *B. sorokiniana* colonization prevents MAMP-induced ROS accumulation A-B) ROS accumulation in mock-treated (A) or *B. sorokiniana*-colonized barley roots (B) at 2 dpi. Roots were washed thoroughly prior to assay preparations to remove extracellular fungal hyphae. Values represent means ± SEM from eight wells, each containing three root pieces. The following concentrations and dilutions were used: treatments: chitohexaose and ergosterol: 250 nM, *S. indica* and *B. sorokiniana* lipid extract: 1:160 (v/v) dilution, flg22: 1 *mu*M. All treatment solutions contained a final amount of 1:40 (v/v) methanol.

Ergosterol levels of *B. sorokiniana*-colonized roots are lower than in *S. indica*-colonized roots.

Using GC-MS analysis, indeed ergosterol was detected in *B. sorokiniana* mycelium lipid extract. However, ergosterol levels were lower in *B. sorokiniana* mycelium than *S. indica* mycelium. While the relative concentration (normalized to internal standard and mg mycelium freshweight) of ergosterol was at 0.12 in *B. sorokiniana* mycelium, relative ergosterol concentration was approximately 3 to 4 times higher with 0.30 - 0.42 in *S. indica* mycelium. Similarly, GC-MS revealed that *B. sorokiniana*-colonized barley roots contain around 3 to 4 times less free ergosterol than *S. indica*-colonized barley roots (Figure 9A). The high ergosterol levels in *S. indica* mycelium and *S. indica*-colonized roots might have necessitated the evolution of mechanisms to suppress ergosterol perception in *S. indica*, while ergosterol perception might be less relevant during *B. sorokiniana* colonization. This could explain the specific suppression of fungal lipid perception in *S. indica*-colonized roots (Chapter 3.1, Figure 3 E-F).

In addition to their free form, sterols can be present as conjugates of a fatty acid (sterol-esters, SE), a sugar (sterol glucosides, SG) or a sugar esterified with a fatty acid (acyl sterol glycosides , ASG) (Der et al., 2024). While free sterols (FS), SG and ASGs are main components of plasma membranes, SEs accumulate in lipid droplets (LDs) or lipid bodies in the cytosol, regulating FS homeostasis, in both plants and fungi (Wewer et al., 2014; Ferrer et al., 2017). Previously, changes in FS and SE have been observed in both plant and fungi upon colonization (Kopischke et al., 2013; Wewer et al., 2014; Siebers et al., 2016). Fractionation of *S. indica* mycelium lipid extract revealed that only the FS fraction but not the SE fraction induced a ROS burst in barley roots (Chapter 3.1, Figure 1 D). Thus, conjugation of free ergosterol could be one possible mechanism to evade ergosterol-induced plant immunity. Therefore, in addition to FS, also the amount of SE in colonized barley roots was analysed using GC-MS. FS and SE of crude lipid extract were separated by solid-phase extraction and the ester bonds between sterols and fatty acids hydrolysed by alkaline hydrolysis prior to derivatisation and GC-MS measurement. Ergosterol-esters were detected in both *S. indica*- and *B. sorokiniana*-colonized barley roots at all timepoints, mimicking the pattern observed in the FS fraction (Figure 9 A-B). Similar to free ergosterol, the amount of ergosterol-esters was much higher in *S. indica*-colonized roots than *B. sorokiniana*-colonized roots and increased from 3- to 7 dpi (Figure 9 B). Overall, ergosterol ester levels were up to 80 times lower than free ergosterol levels in colonized barley roots, indicating that the majority of ergosterol is present as free ergosterol (Figure 9 C). However, the ratio of free ergosterol to ergosterol-esters was drastically reduced in *S. indica*-colonized roots compared to *S. indica* mycelium (Figure 9 C) and tendentially further decreased over time during colonization (Figure 9 C), indicating that the relative amount of ergosterol that is present as FS is reduced while the relative amount of ergosterol-esters is increased during colonization. This indicates that *S. indica* modifies its ergosterol metabolism during root colonization, leading to increased conjugation of ergosterol, even though at late stage colonization, free ergosterol is still present in colonized roots and approx. 10-fold more abundant than ergosterol-esters. For *B. sorokiniana*-colonized roots, the ratio of free ergosterol to ergosterol-esters are in the same range as found for *S. indica*-colonized roots (Figure 9 C), indicating that the low amount of free ergosterol in

B. sorokiniana-colonized roots compared to *S. indica*-colonized roots is not a result of enhanced esterification of ergosterol in *B. sorokiniana*. The amounts of sterols in the ester fraction were at the lower detection limit of the GC-MS, thus the relative concentrations detected might not accurately represent the biological situation due to technical limitations. The ratio of free ergosterol to ergosterol-esters in *S. indica* mycelium is very high, compared to the ratio of FS to SE reported in other root colonizing fungi such as *Rhizophagus irregularis* (Wewer et al., 2014). Here, only 2-3 times more FS than SE were detected in extraradical mycelium (Wewer et al., 2014). However, the lifestyle of *R. irregularis* differs greatly from *S. indica* and *R. irregularis* does not produce ergosterol. Thus, differences in FS and SE levels between the two fungi are not unexpected.

Transcriptional and functional analysis of *S. indica* genes encoding acyltransferases and SE hydrolases, responsible for SE biosynthesis and hydrolysis, respectively, could help to clarify whether SE biosynthesis is induced during barley colonization compared to axenic culture. In addition, investigation of the regulation of ergosterol biosynthesis genes during colonization and the analysis of free ergosterol and ergosterol-ester levels of mycelium of different growth stages or cultivated in different media could provide valuable insights.

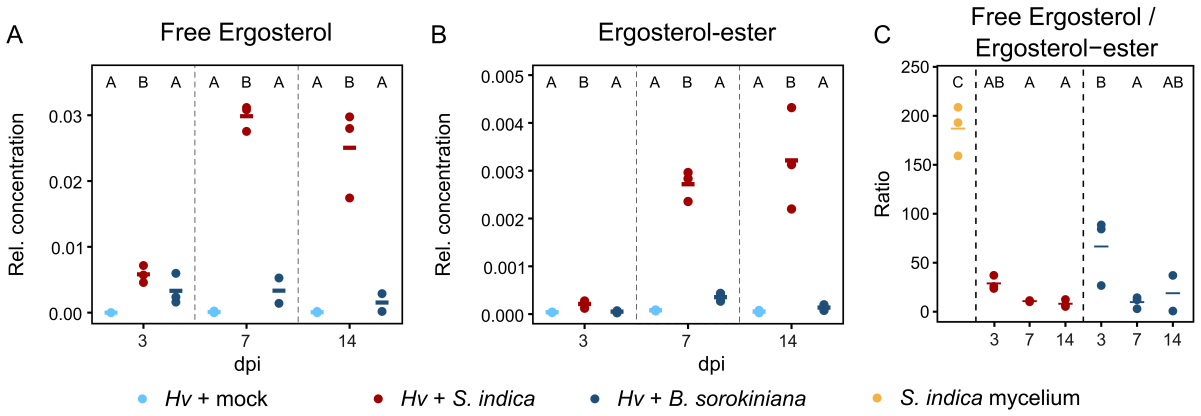

Figure 9: Ergosterol in *B. sorokiniana*- and *S. indica*-colonized barley roots. A-B) Quantification of free ergosterol (A) and ergosterol-esters (B) in free sterol fractions and sterol-ester fractions, respectively, of mock-treated, *S. indica*- or *B. sorokiniana*-colonized barley roots at 3-, 7- and 14- dpi. C) Ratio of free ergosterol to ergosterol-esters in the same samples and lipid extracts of *S. indica* mycelium as reference. Letters indicate significant differences based on ANOVA and post hoc Tukey test ($p \leq 0.05$). Statistical analysis was performed across all timepoints. Relative ergosterol concentration was calculated based on internal standard response and normalized to sample freshweight.

B. sorokiniana colonization induces modulation of the phytosterol pool in barley roots.

In *S. indica*-colonized roots, we observed an increase of the stigmasterol to β-sitosterol ratio in response to fungal colonization. In *B. sorokiniana* roots, this increase was even more pronounced (Figure 10 C). Not only an increase in stigmasterol levels, but also a decrease of β-sitosterol levels was observed upon *B. sorokiniana* colonization and over time, leading to an enhanced increase in the stigmasterol to β-sitosterol ratio in *B. sorokiniana*-colonized roots compared to *S. indica*-colonized roots across all timepoints (Figure 10 A-C). The increase in free stigmasterol in *B. sorokiniana*-colonized roots is accompanied by an increase in stigmasterol-ester levels (Figure

10 D). While the decrease in free β-sitosterol over time observed in all three treatments was enhanced in *B. sorokiniana*-colonized roots (Figure 10 B), the level of β-sitosterol-ester was not reduced in *B. sorokiniana*-colonized roots over time but in mock-treated roots (Figure 10 E). Overall, the ratio of stigmasterol- to β-sitosterol-esters increased in *B. sorokiniana*-colonized roots compared to mock-treated roots and over time (Figure 10 F), comparable to observations in FS (Figure 10 C). Increased total stigmasterol biosynthesis in *B. sorokiniana*-colonized barley roots would also provide more substrates for esterification, thus could explain the increase in stigmasterol-esters accompanying the increase in free stigmasterol. Similar to ergosterol, the relative concentrations of free phytosterols were higher than phytosterol-ester concentrations, confirming that also phytosterols are mainly present in their free form in the plant cell. Overall, the ratio of FS to SE was higher for stigmasterol than β-sitosterol (Figure 10 G-H). For both phytosterols, a decrease in FS to SE ratio was observed upon colonization with both *S. indica* and *B. sorokiniana* at 14 dpi (Figure 10 G-H).

Previously it was shown that SE biosynthesis affects resistance to pathogens in plants. *A. thaliana psat1* mutant lines, defective in SE biosynthesis, depicted an enhanced response to the non-adapted pathogens *Phytophtora infestans*, *Blumeria graminis* and the adapted pathogen *Golovinomyces cichoracearum* (Kopischke et al., 2013). This response was characterized by a macroscopic enhanced cell death phenotype and large aberrant callose depositions but not accompanied by enhanced pathogen growth (Kopischke et al., 2013). The decrease of SE in the *psat1* mutant line was also accompanied by an increase in SGs, which could contribute to the observed effect. In barley, we observed an increase in SE of both stigmasterol and β-sitosterol, leading to a reduced FS to SE ratio upon colonization of both *S. indica* and *B. sorokiniana*. This could potentially suppress an immune response and for example restrict callose deposition. Since SG levels were changed in *A. thaliana psat1* mutant lines, it would be interesting to analyse SG levels in colonized barley roots as well.

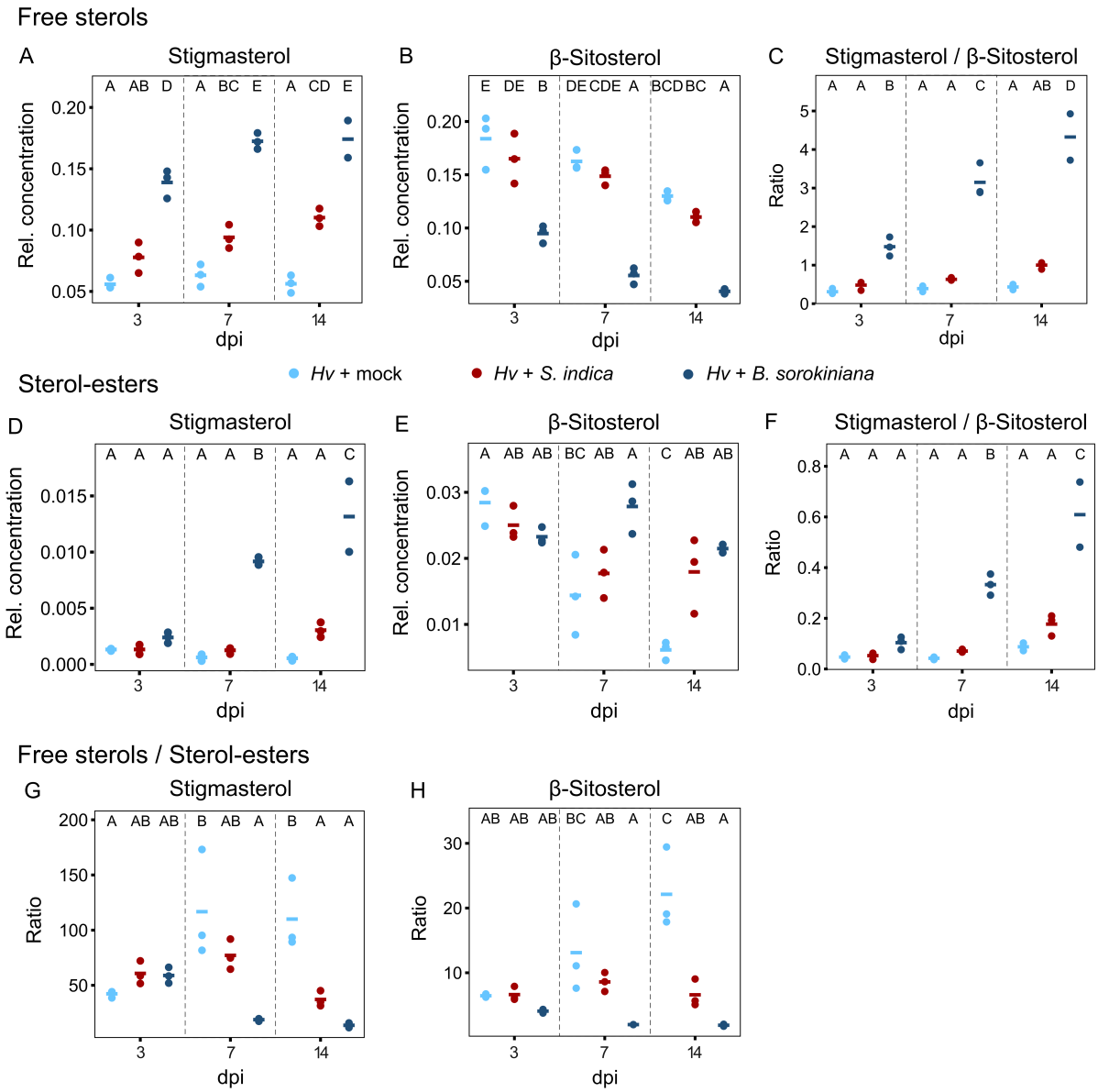

Figure 10: *B. sorokiniana* colonization induces modulation of the phytosterol pool in barley. Measurement of phytosterol content in mock-inoculated, *S. indica*- or *B. sorokiniana*-colonized barley roots at 3-, 7-, and 14-days post inoculation (dpi). The amounts of stigmasterol (stigmasta-5,22-dien-3β-ol) (A) and β-sitosterol (24β-ethylcholest-5-en-3β-ol) (B) were measured via GC-TOF-MS and the ratio of stigmasterol to β-sitosterol was calculated (C). Letters indicate significant differences based on ANOVA and post hoc Tukey test ($p \leq 0.05$). Statistical analysis was performed across all timepoints. Relative sterol concentration was calculated based on internal standard response and normalized to sample fresh weight.

In line with the enhanced increase in stigmasterol to β-sitosterol ratio in *B. sorokiniana*-colonized roots compared to *S. indica*-colonized roots, expression of the stigmasterol biosynthesis gene *HvCYP710A1*, which performs the desaturation step converting β-sitosterol to stigmasterol, was induced upon *B. sorokiniana* colonization at 6 dpi (Figure 11 A), while it was not significantly induced during *S. indica* colonization (Figure 11 B). This further indicates that *B. sorokiniana* leads to a more pronounced change in phytosterol composition, probably due to an overall enhanced immune reaction. *S. indica*, as a beneficial root endophyte suppresses activation of immunity, while *B. sorokiniana* requires host cell death for its virulence, thus seeks to induce a strong immune response leading to HR and subsequently host cell death.

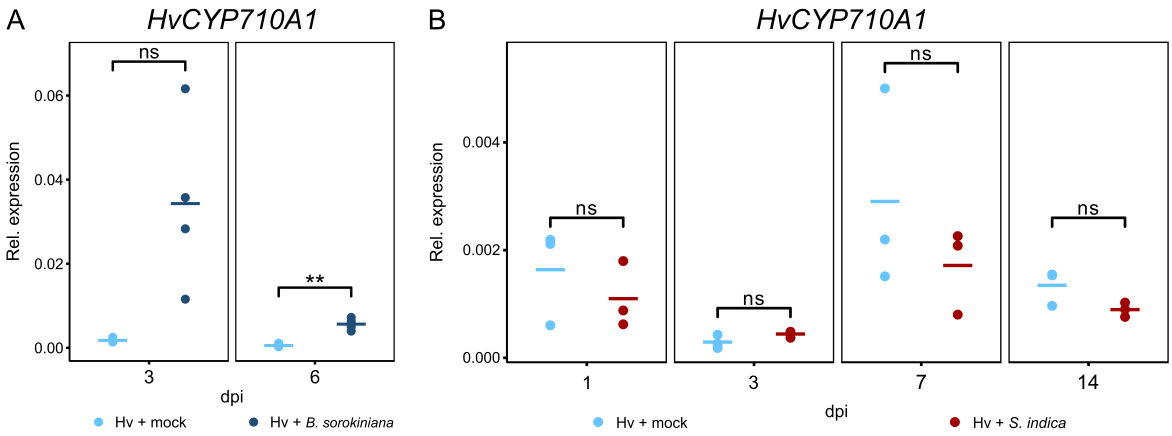

Figure 11: *B. sorokiniana* colonization induces *HvCYP710A1* expression. Expression of the stigmasterol biosynthesis gene *HvCYP710A1* relative to the housekeeping gene *HvUBI* in *B. sorokiniana*- (A) and *S. indica*- (B) colonized barley roots compared to mock-treated barley roots determined by qRT-PCR. Roots were colonized for 3- and 6 days for *B. sorokiniana* and 1-,3-,7- and 14 days for *S. indica*. Roots were washed thoroughly prior to RNA extraction. Asterisks indicate significant differences based on Student's t-test ($p \leq 0.05$ *; $p \leq 0.01$ **; $p \leq 0.001$ ***, $p \leq 0.0001$ ****).

Chapter 4

Discussion

4.1 Function of frequent branching and decoration of EPS in mutualistic plant-microbe interactions.

Bacteria are often surrounded by an EPS matrix, which serves multiple functions in modulation of plant innate immunity. On the one hand, EPS-derived carbohydrates can act as MAMPs while on the other hand they can inhibit or modulate immune responses. The ability to induce immunity or suppress immune responses depends on structure, decoration and physicochemical properties of the respective carbohydrate (Aslam et al., 2008; Silipo et al., 2010; Vanacore et al., 2022). Previous reports indicated that bacterial EPS can suppress plant immune responses due to their polyanionic nature, which allows them to bind or chelate ions like calcium and scavenge ROS (Aslam et al., 2008; Silipo et al., 2010). On the contrary, bacterial EPS, LOS (lipooligosaccharide) and LPS (lipopolysaccharides) can also induce plant immunity (Silipo et al., 2010).

In Chapter 2.1, we investigated structure and properties of the EPS produced by *Flavobacterium* sp. Root935. Using compositional and linkage analysis combined with ^{1}H-NMR, we identified a complex branched heptasaccharidic repeating unit, containing a variety of sugar moieties, including Rha, Fuc, GlcN, Fuc4N, Gal, Man and QuiN and an important and extended substitution pattern, including acetyl and lactyl groups (Chapter 2.1, Figure 2-3). Treatment of *A. thaliana* seedlings with natural EPS resulted in minor ROS accumulation, which was enhanced upon treatment with de-O-acylated EPS (EPS_{deO}), (Chapter 2.1, Figure 6). Furthermore, no increase in cytosolic calcium concentration was observed in *A. thaliana* seedlings with either natural or de-O-acylated *Flavobacterium* EPS. Thus, *Flavobacterium* EPS might sequester calcium ions and prevent calcium influx, as described previously (Aslam et al., 2008). Calcium influx and ROS accumulation are often connected in a positive feedback loop upon MAMP perception (Marcec et al., 2019; Marcec & Tanaka, 2022). Thus, the weaker ROS response to the EPS could be explained by the lack of calcium influx upon EPS perception. Lectins, a diverse group of carbohydrate binding proteins that function in both plant root symbiosis and defense (Hoff et al., 2009), displayed weak or negligible binding to the native EPS, likely due to its complex structure and decoration with multiple acetyl groups (Chapter 2.1, Figure 5). This indicates, that the structure and extensive decoration of *Flavobacterium* EPS masks it for recognition by

plant hosts and prevents binding to lectins. Whether the acetyl-decorations also contribute to the calcium chelation ability needs to be investigated. Previous studies demonstrated that LPS from *Herbaspirillum* sp. Root 189, another member of the same microbial community, isolated from *A. thaliana* roots, is shielded from perception by extensive O-acylation as well (Vanacore et al., 2022), supporting our findings. Moreover, *Rhizobia* EPS are also often O-acylated and were shown to modulate RNS, potentially by binding to symbiosis receptors (S. J. Kelly et al., 2013; Kawaharada et al., 2015; S. Kelly et al., 2023), indicating that O-acylation of EPS might act as a symbiosis signal.

Similar to bacteria, also fungi produce an EPS matrix, which is loosely attached to the outer CW layer (Wanke et al., 2021). In Chapter 2.2, we characterized the EPS matrix of *S. indica* and showed that also fungal EPS matrices can modulate the plant immune response. The EPS matrix of *S. indica* functions as a reservoir of several fungal WSC-domain containing glucan binding proteins and hydrolytic enzymes (Chapter 2.2, Figure 2), potentially involved in host colonization. One example of a WSC-domain containing proteins is *Si*WSC3, which was shown to bind to long β-1,3-linked glucans, potentially promoting adhesion between cells (Wawra et al., 2016). Moreover, fungal lectins such as *Si*FGB1, mostly found in *S. indica* cell wall- and culture filtrate (Chandrasekar et al., 2022) were shown to bind β-glucans in the EPS matrix and potentially interfere with downstream immunity components to prevent recognition of β-glucan MAMPs (Wawra et al., 2016, 2019). Furthermore, the *S. indica* EPS matrix contains β-glucan fragments with ROS scavenging properties, which are released by the host endoglucanase *Hv*BGLUII. *Hv*BGLUII digestion of the *S. indica* EPS matrix leads to release of a decasaccharide (β-GD), consisting of seven β-1,3-linked D-glucose backbone units substituted with three terminal β-1,6-glucose units. β-GD does not induce immunity but scavenges ROS in the apoplast and thereby modulates the plant immune response, enhancing *S. indica* colonization (Chapter 2.2, Figure 4). The heptasaccharide laminariheptaose, which resembles the β-GD backbone, induces plant immunity, thus we hypothesize that the β-1,6-branches of β-GD are essential for the ROS scavenging capability. Moreover, they protect the decasaccharide from further digestion by plant hydrolytic enzymes. Antioxidant properties were described for many β-glucans and shown to be determined by several physico-chemical properties such as the degree of branching (H. Wang et al., 2013). While β-1,3-linked backbones, substituted with β-1,6-linked glucans are common in fungi and oomycetes, there is no evidence for β-1,6-linked glucans in plants. Therefore, β-1,6-linkages could be recognized as non-self in plants (Nars et al., 2013). However, Wanke et al., 2020 showed that perception of immunogenic long-chain β-glucans does not rely on β-1,6-linkages but is rather regulated by degree of polymerization (DP) (Wanke et al., 2020). Interestingly, perception of the highly substituted long-chain β-1,3-glucan laminarin isolated from *Eisenia bicyclis* (*Eb*), is reduced compared to laminarin isolated from *Laminaria digitata* (*Ld*), which shows a less frequent branching pattern in barley (Wanke et al., 2020). This indicates, that a high branching frequency could hinder perception of β-1,3-glucans by immunity receptors.

It was shown that branched and unbranched β-1,3-glucans are often arranged in triple helices.

A high frequency of side chains leads to formation of a more condensed triple helix and the formation of a one-dimensional cavity in the middle. Further, the unbranched glucan curdlan, is water-insoluble, while the presence of β-1,6-side chains makes glucans such as shizophyllan water-soluble (Okobira et al., 2008). Triple helix formation requires a DP of more than 200, thus only applies for very long-chain β-glucans. *Ld* Laminarin, which usually has a DP of around 25 is mostly found in its monomeric, water soluble and disordered form rather than in triplex structures (Manabe & Yamaguchi, 2021). However, the short β-glucan laminarihexaose was shown to form pseudo-quadruplex structures mimicking β-glucan triple helices to bind proteins. Further, β-glucan binding affinity to lectin-domains is affected by β-1,6-branching (Pluvinage et al., 2017). In combination with the results from bacterial EPS, this indicates that frequent branches and decorations might be a common mechanism to prevent receptor binding and subsequent immunity activation. Interestingly, *Hv*BGLUII also released a similar decasaccharide from *B. sorokiniana* EPS matrix and the β-GD released from *B. sorokiniana* EPS matrix showed the same ROS suppressing activity (Chapter 2.2, Figure 6), indicating both pathogenic and beneficial microbes use similar mechanisms to evade host immunity and facilitate colonization.

Chapter 2.3 summarizes the recent study by S. Kelly et al., 2023, in which the *Lotus japonicus* LysM receptor kinase *Lj*EPR3a was identified (S. Kelly et al., 2023). *Lj*EPR3a is a close relative of the known EPS receptor *Lj*EPR3 (Kawaharada et al., 2015) and highly expressed during arbuscular mycorrhiza symbiosis. Recently, the structure of the EPR3 ectodomain was resolved and EPR3 thus identified as a representative of a unique class of plant LysM-RLKs (Wong et al., 2020). Microscale thermophoresis (MST) binding assays revealed that both *Lj*EPR3 and *Lj*EPR3a bind β-1,3/1,6-linked glucans with similar affinity (S. Kelly et al., 2023). EPR3a was able to bind both *Eb* and *Ld* laminarin. However, binding affinity to *Eb* laminarin was much higher than to *Ld* laminarin, indicating that *Lj*EPR3a preferably binds highly branched β-1,3-glucans. In line with this, *Lj*EPR3a showed the highest binding affinity to *S. indica* β-GD, which is also highly branched. Moreover, *Lj*EPR3 and *Lj*EPR3a bound EPS from different *Rhizobia* and affinity of *Lj*EPR3a to *M. loti* EPS was comparable to *S. indica* β-GD. Similar to *S. indica* EPS, *Rhizobia* EPS comprise also β-1,6-branched glucans (S. J. Kelly et al., 2013; Kawaharada et al., 2015; S. Kelly et al., 2023). Altogether, this suggests multiple roles for β-1,6-branching frequency of β-1,3-backbones. Frequent β-glucan branching prevents perception of β-glucans as MAMPs and mediates modulation of downstream immune responses such as ROS scavenging. Moreover, frequently branched β-glucans are perceived by symbiosis receptors such as *Lj*EPR3a, potentially activating symbiosis signaling pathways. *Lj*EPR3a was shown to modulate AMS. Thus, isolation and characterization of *Rhizophagus irregularis* EPS would be beneficial to evaluate whether AM fungi harbour similar structures like the *S. indica* β-GD. Transcriptomic analysis of β-GD or *Eb* laminarin treated *L. japonicus* plants would be a valuable next step to identify genes and pathways differentially regulated upon ligand binding of *Lj*EPR3 and *Lj*EPR3a and compare these to the known symbiosis signaling pathways induced by AMS or RNS. Additionally, crystallization of the receptors could reveal ligand binding pockets and preferential substrate structures to verify that branching is essential for binding.

4.2 Plant- and microbial lipids modulate plant immunity.

Upon plant colonization, microbial lipids can be perceived as MAMPs and activate host immunity (Figure 2, pink box). In relation to other MAMP classes, only few lipid MAMPs have been identified so far. Examples are the sterol lipid ergosterol, the main sterol of fungal membranes, medium chain 3-OH fatty acids, released from bacterial LPS, and a 9-methyl-sphingoid base (9-me-Spd), released from the oomycete ceramide *Pi*-Cer-D as well as eicosapentaenoic acid (EPA), derived from *Pi*-DAG (Figure 2). While 3-OH fatty acids and 9-me-Spd were shown to be perceived by lectin-RLKs in *A. thaliana*, no receptor was identified for *Pi*-DAG or ergosterol so far. In Chapter 3.1, we investigate the perception of lipids isolated from the beneficial root endophytic fungus *Serendipita indica* in the crop barley. We demonstrate that *S. indica* lipids induce a canonical PTI response in barley roots and identify ergosterol as the main immunogenic component of *S. indica* lipid extract. Although, chitohexaose, ergosterol- and *S. indica* lipids activate similar PTI mechanisms, timing and intensity of the responses vary, indicating that the fungal lipid-induced immune response in barley roots is distinct from the chitohexaose-induced response. Ergosterol- and *S. indica* lipids-mediated ROS burst might not depend on Ca^{2+}-influx in barley roots and desensitization experiments revealed that the fungal lipids are perceived by distinct receptors compared to chitohexaose (Chapter 3.1, Figure 1, 3). The hydrophobic nature of lipids might allow novel perception mechanisms distinct from membrane bound, apoplastic receptors. In an aqueous space as the apoplast, lipids are likely to associate to hydrophobic compartments and potentially integrate into the plant PM (X. Xu et al., 2001; Klemptner et al., 2014). For a long time, it was not clear if and in which form lipids exist in the apoplastic space. Here, we provide evidence that ergosterol is present in apoplastic fluid of *S. indica*-colonized barley roots (Chapter 3.1, Figure 2). Different fungi were shown to release ergosterol-containing extracellular vesicles (Rodrigues et al., 2007; Vargas et al., 2015), thus we propose a similar mechanisms for *S. indica* during host colonization. We provide evidence for the activation of plant lipid signaling pathways in response to ergosterol treatment. Specifically proteins involved in PIP signaling were phospho-regulated and expression of diterpene biosynthesis genes induced, leading to exudation of hordedanes, diterpenes with antimicrobial properties (Y. Liu et al., 2024). Thereby, we demonstrate that fungal lipid perception activates plant lipid signaling, modulating host immunity.

Plant membrane lipids are integral for early PTI responses. They control protein distribution in membranes, modulate endo- and exocytosis, interact with the cytoskeleton and regulate membrane trafficking (Xing et al., 2021). Anionic phospholipids, which include phosphatidic acid (PA) and phosphatidylinositol phosphates (PIPs) only represent a small percentage of all membrane lipids, but their production can be massively increased upon stresses, characterizing them as important lipid signals (Noack & Jaillais, 2020). Due to their negative charge, anionic phospholipids modulate the physico-chemical properties of membranes such as surface charges or curvature and protein assembly (Noack & Jaillais, 2020). PIPs and PA function as landmarks for different membranes inside the plant cell and were shown to accumulate in specific zones of the plant PM during microbial interactions. For instance, upon powdery mildew infection of *A. thaliana*, PI4P was depleted, while PI(4,5)P_2 was recruited to haustorial membranes, acting

as a susceptibility factor (Qin et al., 2020). Similarly, PI4P, PI(4,5)P_2 and PA accumulated in discrete regions of the periarbuscular membrane during AMS (Ivanov & Harrison, 2019). During infection by *Blumeria graminis*, *A. thaliana* phospholipase D (PLD) was shown to re-localize from the PM to papillae,leading to PA accumulation, which initiates ROS and JA signaling at the pathogen entry site (Xing et al., 2019).

In both plants and animals, accumulation of PIPs and PA was shown to target proteins to anionic lipid-enriched membrane regions, forming membrane nanodomains (Gronnier et al., 2017; Barnett & Kagan, 2020; Jaillais & Ott, 2020; Abe et al., 2024), local accumulations of molecules, lipids and proteins in the membrane plane on a nanometer scale (Jaillais et al., 2024). In plants, one of the major protein groups, that assemble into nanodomains are remorins (REMs), which are targeted to PI4P-enriched membrane regions (Gronnier et al., 2017). Plant receptor kinases, such as *At*FLS2 and the growth receptor BRASSINOSTEROID INSENSITIVE 1 (*At*BRI1), were shown to associate in receptor clusters in the PM which co-localize to REM membrane nanodomains (L. Wang et al., 2015; Bücherl et al., 2017). Whether this co-localization is mediated by recruitment of RLKs *via* PIPs or REMs is not known. Besides anionic phospholipids, also sphingolipids and sterols can assemble in and recruit proteins to membrane nanodomains (Gronnier et al., 2017; Grosjean et al., 2018; Ukawa et al., 2022; Der et al., 2024). For instance, localization of *At*RBOHD was disrupted in PMs of *A. thaliana fah1cfah2* mutant lines, displaying reduced 2-hydroxy sphingolipid levels and subsequently affected in sterol composition (Ukawa et al., 2022).REMs associate to nanodomains in a β-sitosterol dependent manner (Bhat et al., 2005) and flg22-binding to *At*FLS2 was shown to enhance co-localization with *At*Flotilin1 (Flot1), a marker for sterol-rich membrane nanodomains (M. Yu et al., 2017). Sterol deficient *A. thaliana steroid methyltransferase 1 (smt1)* mutants were defective in proper flg22 immune response (Cui et al., 2018). Similar to PIPs, an enrichment of phytosterols was observed in barley root epidermal cells at the penetration site of powdery mildew (Bhat et al., 2005). In fungi, sterol-enriched nanodomains were shown to regulate polar growth (Bühler et al., 2015) and during the *Magnaporthe oryzae*-rice interaction, ergosterol nanodomains are proposed to act as effector translocation platforms in the fungal membrane and activate clathrin mediated endocytosis (CME) (Guo et al., 2023; Oliveira-Garcia et al., 2023). This indicates that formation of lipid nanodomains is a conserved mechanism in both plants and microbes at the interaction interface, controlling immunity signaling and effector translocation, respectively. Thus lipid biosynthesis and localization needs to be tightly regulated.

Phosphoproteomic analysis of barley roots revealed rapid phospho-regulation of several proteins involved in PIP signaling, namely a PI4K, PI3P5K, DGK and SacI-like domain containing protein, upon ergosterol and *S. indica* lipid treatment (Chapter 3.1, Figure 4). Together, PI4K, PI3P5K, DGK and the SacI-like domain containing protein can modulate PI4P, PI(4,5)P_2, DAG and PA levels in host cells. In addition, we observed an increase of the stigmasterol to β-sitosterol ratio in *S. indica*-colonized roots (Chapter 3.1, Figure S4). Altogether, this suggests that proteins involved in ergosterol perception and signaling might associate in membrane nanodomains at the fungal penetration site, induced by modulation of PIP and phytosterol levels. These

nanodomains might not only facilitate MAMP perception but also modulate the host immune response. Fungal lipid treatment induced phosphoregulation of *Hv*MLO, which was shown to be targeted to nanodomains (Bhat et al., 2005) and thus might also associate to nanodomains upon ergosterol perception. *Hv*MLO was shown to reduce callose depositions (Kusch et al., 2019; Hilbert et al., 2020), thereby potentially mediating fungal entry into the host cell. Similarly, *Hv*GBP1 restricts callose depositions, acting as a compatibility factor during *S. indica* colonization (Wanke et al., 2023). Additionally, PRR complexes, perceiving other MAMPs could be recruited to allow trans-phosphorylation of co-RLKs of different PRRs to prime the plant for detection of additional MAMPs as described for *At*BAK1 and *At*CERK1 (Gong et al., 2019). At the same time, a change in PIP levels might activate endocytosis of PRR complexes to avoid constant activation of immunity signaling, as indicated by desensitization experiments in barley roots (Chapter 3.1, Figure 3). Additionally, integration of ergosterol into the plant PM could trigger phospholipid production, to retain lipid homeostasis in the membrane. Finally, activation of DGK indicates production of PA upon ergosterol perception, which enhances the ergosterol-induced ROS burst (Chapter 3.1, Figure 5), potentially *via* inhibition of RBOH degradation as described in *A. thaliana* (Kong et al., 2024; Qi et al., 2024). This suggests that membrane lipid remodelling affects several components involved in plant immunity signaling. Further investigations are needed to clarify the role of plant membrane lipids in ergosterol perception and *S. indica* colonization.

4.2.1 Oxysterol binding proteins mediate lipid transport and perception in plant-fungal interactions.

Despite being present in the apoplast during root colonization and likely being able to integrate into the plant PM, it is unclear how ergosterol is transported.Oxysterol binding proteins (OSBPs) and OSBP-related proteins (ORPs) are a family of evolutionary conserved lipid transfer proteins (LTPs) that share a C-terminal OSBP-related domain (ORD), which can bind sterols or phospholipids (Chen et al., 2022). Additionally, ORPs might contain a pleckstrin homology (PH) domain, or ankyrin repeat domain, allowing PIP and protein binding, respectively (Chen et al., 2022). OSBPs and ORPs were shown to mediate non-vesicular lipid transport and act as lipid sensors or transporters at membrane contact sites (MCSs) in mammals, yeast and filamentous fungi (Stefan et al., 2011; S. Qiu & Zeng, 2019; Nakatsu & Kawasaki, 2021). While PI4P is abundant in the PM, it is degraded in the endoplasmic reticulum (ER) by Sac1, producing a PI4P gradient. Along this gradient, ORPs can transport PI4P from the PM to the ER, while simultaneously allowing a counter-transport of sterols from the ER to the PM (Nakatsu & Kawasaki, 2021). Thereby, ORPs present a way to transport sterols, synthesized at the ER to the PM. Structural analysis of the yeast oxysterol-binding protein homologue 4 (Osh4 or Kes1) revealed a barrel like structure with a hydrophilic outside and a hydrophobic tunnel in the center, which is closed with a lid and resembles other lipid transport proteins (Im et al., 2005). Osh proteins of filamentous fungi such as *Aspergillus nidulans* and *Candida albicans* were shown to control filamentous growth and conidiospore formation potentially by controlling PI4P and sterol localization (Bühler et al., 2015; Ghugtyal et al., 2015). ORPs of the filamentous plant pathogenic fungus *Magnaporthe oryzae* are also involved in hyphal growth

and conidiation of the fungus and important for its virulence (Chen et al., 2022). This indicates that defined sterol and PI4P distribution in the plasma membrane is essential for fungal proliferation and virulence. Ergosterol is the most abundant sterol of many fungal membranes and several mammalian ORPs and yeast Osh proteins were demonstrated to bind ergosterol or dehydroxyergosterol (DHE) (S. Qiu & Zeng, 2019; Nakatsu & Kawasaki, 2021), thus fungal ORPs or Osh proteins likely transport ergosterol.

In *A. thaliana*, twelve OSBP homologs were identified, which showed similar structure and function as the yeast Osh proteins (Saravanan et al., 2009), thus plant ORPs potentially also function in non-vesicular lipid trafficking and regulate sterol and PIP distribution inside the cell. In addition, plant and fungal ORPs might function as danger signals. Infiltration of *A. thaliana* leaves with ORPs isolated from *A. thaliana* (*At*ORP4C) or *M. oryzae* (*Mo*ORP3) induced an immune response and enhanced disease resistance against *Pseudmonas syringae* DC 3000 (Chen et al., 2022). Moreover, all six *M. oryzae* ORPs induced ROS accumulation in *N. benthamiana* leaves, leading to different levels of cell death (Chen et al., 2022). ORPs are thought to be cytoplasmic proteins and do not carry predicted signal peptides. However, Chen et al., 2022 detected *Mo*ORP3 in culture filtrate of *M. oryzae* liquid cultures and apoplastic fluid of barley leaves, infected with *M. oryzae*, indicating secretion via unconventional secretion pathways potentially mediated by their lipid transporter function or secretion in EVs.
In some aspects, the immune response induced by *Mo*ORPs in *N. benthamiana* and *A. thaliana* resembles our observations on ergosterol and *S. indica* lipid perception (Chapter 3.1). In both studies, the immune response is independent of the co-receptor kinase BAK1 and no clear ROS burst could be observed in *A. thaliana*, while the response in *N. benthamiana* was more clear. For both ORPs and ergosterol, the immune response was weaker and occurred later compared to the model MAMPs flg22 (Chen et al., 2022) or chitohexaose (Chapter 3.1, Figure 1). Thus, the question arises whether ergosterol might be bound to the *Mo*ORPs, isolated from *M. oryzae* and responsible for the observed immune response or fungal ORPs might mediate ergosterol perception. On the other hand, the typical ORP funnel structure could make ergosterol inaccessible for perception by plant proteins, shielding it from plant perception. In turn, plants might have evolved receptors to perceive ORPs instead. A similar mechanism was observed for the *M. oryzae* GH17 exoglucanase (Ebg1). *M. oryzae* secretes *Mo*Ebg1 to degrade β-glucan MAMPs released from the fungal cell wall and EPS matrix and prevent immunity activation. However, *Mo*Ebg1 itself induces host immunity. Thus *M. oryzae* secretes elongation factor 1 alpha (*Mo*EF1α) which sequesters *Mo*Ebg1 (H. Liu et al., 2023). Further, fungal ORPs could mediate ergosterol perception by the plant host, by transferring ergosterol from fungal EVs to the host PM. Thus, it would be interesting to co-treat barley roots with ergosterol and *S. indica* ORPs to investigate whether the immune response is enhanced. Currently, our experimental system to examine ergosterol perception in barley roots is devoid of fungal proteins, hence ergosterol perception does not fully rely on fungal ORPs. However, the observed response to ergosterol is weaker than for instance to chitohexaose, thus could potentially be enhanced by ORP co-treatment. Upregulation of *ORP* gene expression was observed in potato and barley upon pathogen infection (Avrova et al., 2004; Hein et al., 2004), indicating a role for plant ORPs

in plant immunity, potentially as sterol receptors. Although *At*ORP3 did not bind ergosterol (Saravanan et al., 2009), it cannot be excluded that other plant ORPs can bind ergosterol. Assessment of barley *ORP* expression and protein levels in response to ergosterol treatment and *S. indica* colonization is needed to evaluate the role of host ORPs in ergosterol perception and during *S. indica* colonization. Additionally, a search for ORP homologs in *S. indica* and their regulation in the available phosphoproteomics and transcriptomics data from Saake *et al.* (Chapter 3.1) will help clarify their contribution to fungal lipid perception. Moreover, plant ORPs could potentially mediate the changes in phytosterol composition in *S. indica*-colonized barley roots (Chapter 3.1, Figure S4). The observed phosphorylation of barley PI4K (Chapter 3.1, Figure 4) could lead to enhanced PI4P production, which might result in an enhanced PI4P gradient from the PM to the ER to allow increased transport of sterols to the PM by ORPs. Moreover, changes in PI4P levels could recruit plant ORPs to the PM, potentially facilitating ergosterol perception.

4.2.2 Differential effect of colonization by pathogenic and beneficial fungi on phytosterol composition and fungal lipid perception.

In Chapter 3.3, we compare the suppression of ergosterol perception and the changes in phytosterol composition in barley roots upon *S. indica* colonization to colonization with the pathogen *B. sorokiniana*. We observed an enhanced increase in the stigmasterol to β-sitosterol ratio in barley roots upon *B. sorokiniana* colonization, which was also present but less pronounced upon *S. indica* colonization (Chapter 3.3, Figure 9). This is in line with the observation that colonization by beneficial microbes induces only mild plant immune responses while the immune response to pathogens is much stronger (Zamioudis & Pieterse, 2012). Moreover, these results indicate that an increase in the stigmasterol to β-sitosterol ratio is a conserved immune response upon colonization of fungi of different lifestyles. In addition, we investigated the ratio of FS to SEs in colonized barley roots. We observed an increase in SE of both stigmasterol and β-sitosterol, leading to a reduced FS to SE ratio upon colonization of both *S. indica* and *B. sorokiniana* (Chapter 3.3, Figure 10 G-H). Callose deposition was shown to be enhanced in the *A. thaliana psat1* mutant, defective in SE formation (Kopischke et al., 2013). Thus, the increase in SE could potentially suppress an immune response and for example callose deposition to facilitate fungal accommodation.

Moreover, as we observed that *S. indica* colonization suppresses the ergosterol-induced ROS burst, presence of high amounts of ergosterol in *S. indica* mycelium and *S. indica*-colonized barley roots might have necessitated evolution of immunity suppression pathways in *S. indica*, which are not required in *B. sorokiniana*. In addition to ergosterol, flg22 and chitooctase perception in *A. thliana* and laminarin perception in barley were also shown to be suppressed during *S. indica* colonization (Jacobs et al., 2011; Wawra et al., 2016), which indicates that the ability to suppress the ergosterol-induced ROS burst is part of a general mechanism to suppress immunity by for instance suppressing the synthesis of apoplastic ROS. Characterization of *S. indica* effectors is constantly advancing and will greatly contribute to understanding the molecular mechanisms whereby *S. indica* suppresses the host immune response to establish a stable interaction.

4.2.3 Recent advances in lipid visualization and quantification methods.

In recent years, research on plant lipids and their role in plant immunity gained a lot of interest, leading to the establishment of new concepts unifying protein and lipid research to explain PTI signaling in more depth. Recent advances in life-imaging techniques and the development of lipid biosensors have paved the way to visualize lipid dynamics *in vivo* on a cellular level in steady-state conditions but also under abiotic or biotic stresses (Xing et al., 2021). Photoactivated localization microscopy (PALM), stochastic optical reconstruction microscopy (STORM) and variable angle-total internal reflection fluorescence microscopy (VA-TIRFM) provide localization information on single molecules, labelled with a fluorescent dye or -protein, on a nanometer scale (Xing et al., 2021; L. Wang et al., 2024). These single molecule techniques allow not only visualization of fluorescently labelled lipid molecules but also membrane proteins (L. Wang et al., 2024). While proteins can be easily fused to fluorescent dyes or -proteins such as green fluorescent protein (GFP), only few fluorescent lipid markers are known. The transgenic *A. thaliana* PIP-lines expressing one or multiple protein lipid binding domains (LBDs), were shown to specifically bind PIPs, fused to different fluorescent proteins including CITRINE, CHERRY and CyPET (Simon et al., 2014). Due to the use of multiple fluorescent proteins, PIP-lines can be easily combined with compartment markers and crosses of single marker lines allow co-labelling of multiple PIPs at a time. Similarly, known PA binding domains were used to develop PA biosensors such as the Spo20p-based PA biosensor (Potocký et al., 2014) and PAleon, a PM-anchored Förster resonance energy transfer (FRET)-based PA specific biosensor using the first 250 N-terminal amino acids of *A. thaliana* RBOHD (W. Li et al., 2019). Recently, a modified RBOHD-based PA biosensor, using only the first 160 N-terminal amino acids fused to GFP, was shown to function as a dynamic and mobile fluorescent PA sensor (T. Li et al., 2023). Fusion of peptide tags to the N- or C-terminal of the sensor target the sensor to membranes inside a cell to visualize PA in distinct subcellular compartments (T. Li et al., 2023). This allows monitoring of dynamic PA responses to environmental stimuli in plant cells, expanding our understanding of synthesis, transport and metabolism of PA and associated processes. To visualize sterol localization in plant- or fungal cells, often proteins associated with sterol-enriched membrane nanodomains such as flotillin or remorins are used (Guo et al., 2023; Oliveira-Garcia et al., 2023). Furthermore, the fluorescent antibiotic filipin or fluorescently labelled sterol analogues are used as sterol markers (Leeuwen et al., 2008; Sezgin et al., 2016). However, filipin does not allow live imaging due to toxicity and sterol analogues often carry bulky chemical groups which might alter their behaviour. Fluorescent probes such as domain 4 (D4) of the bacterial toxin perfringolysin O or the improved allele D4H are promising alternatives (Mizuno et al., 2011; Maekawa et al., 2016; Marek et al., 2020). Sterol biosensors often bind the sterol backbone and thus do not distinguish between different sterols, making their use in bipartite systems difficult. Moreover, most lipid biosensors are established in *A. thaliana*, while transfer to other plant hosts such as barley might be challenging. Lipid quantification methods such as radioactive isotope labelling and lipidomics, can provide important information about lipid abundance but cannot distinguish between lipids originating from plants or microbes when they are present in

both organisms. Although chromatography techniques to detect lipids have greatly advanced in the past decades, still many challenges remain. For instance, most liquid chromatography-mass spectrometry (LC-MS) methods are information dependent and cannot detect unknown lipids, isomers are very difficult to separate and the matrix effect affects ionization of co-eluted analytes (Y. Liu et al., 2024). Changes in total abundance might be only minor and differences in low-abundance lipids difficult to detect with these bulk methods. Therefore, establishment of lipid biosensors in other plant hosts is essential to deepen our understanding of lipid localization during plant-microbe interactions. Moreover, depletion of specific phospholipids is a useful tool to decipher their importance in certain responses. Since steady-state depletion might trigger indirect effects, inducible and tunable systems such as iDePP (inducible depletion of PI(4,5)P_2 in plants) are essential (Doumane et al., 2021).

In this study, we postulate that PIP signaling is activated and potentially involved in facilitating and enhancing ergosterol perception in barley roots. Thus, investigation of PIP levels using bulk lipid quantification methods and PIP localization using biosensors is required to monitor the changes upon ergosterol treatment. Additionally, it would be interesting to develop *S. indica* strains expressing sterol marker probes such as D4H to decipher whether ergosterol integrates into the host membrane during colonization. Moreover, PIP signaling is highly intertwined with membrane trafficking processes. Often, chemical inhibitors of endo- and exocytosis are used to investigate the contribution of these processes to signaling events. However, broad-range inhibition of membrane trafficking can lead to various off-target effects, making the results difficult to interpret. Especially monitoring ROS accumulation, which can be triggered by various stresses is difficult to combine with strong inhibitors. Furthermore, vesicle trafficking is coupled to cytoskeleton remodelling but many factors regulating these processes during plant-microbe interactions remain still unknown. The contribution of the complex cell wall-PM-cytoskeleton continuum to host immune responses during plant microbe interactions needs further investigation.

4.3 Beneficial microbes as promising alternatives to chemical fertilizers and pesticides.

With the constantly growing world population, potentially reaching 10 billion people by 2050 and an overall increase in prosperity, the global food demand increases. At the same time, arable land decreases and crop plants are exposed to increasing abiotic and biotic stresses due to climate change. The Intergovernmental Panel on Climate Change (IPCC) proposes an increase in temperature of around of 2.2 °C to 3.5 °C and sea level rise of 2 to 3 m by 2100 (Calvin et al., 2023). With that, extreme weather phenomena such as droughts, flooding and heavy winds increase. This increase of abiotic stress also renders crop plants more vulnerable to pathogen infection (Lahlali et al., 2024). Moreover, rising temperatures are projected to increase the abundance and broaden the range of many soil-borne pathogens (Delgado-Baquerizo et al., 2020; Singh et al., 2023). Increased global interactions allow spread of pathogens to new areas and new hosts, further increasing the pathogen thread for crop plants and potentially leading

to pandemic outbreaks (Ristaino et al., 2021; Lahlali et al., 2024). Furthermore, monocultures and high-density crops as well as the excessive use of pesticides promote rapid emergence of new pathogenic strains, capable of overcoming disease-resistant crop plants (Singh et al., 2023). Together, this leads to reduced crop yields, increasing the gap between global food demand and supply. However, agriculture is not only affected by climate change, but also highly contributes to climate change. The IPCC special report on climate change and land use estimates that 14-28 % of the global greenhouse gas (GHG) emissions are attributable to crop and livestock production and land use (Shukla et al., 2019). Thus, developing strategies to increase crop yields in a more sustainable way is crucial to reduce agricultural contributions to GHG emissions and climate change while meeting the increasing food demand.

While the extensive use of synthetic pesticides in the past led to environmental concerns and pesticide resistance, cultural control measures such as crop rotation and intercropping together with the cultivation of resistant varieties can promote sustainable agriculture (Lahlali et al., 2024). In the past years, fundamental research has led to the emergence of improved traditional breeding approaches and novel plant breeding techniques to develop pathogen resistant crop varieties (Langner et al., 2018). Modern technologies rely on precise DNA manipulation by programmable nucleases including zinc-finger nucleases, TAL (transcription-activator-like) effector nucleases (TALENs) and CRISPR (clutered regularly interspaced palindromic repeat) RNA-guided Cas (CRISPR-associated protein) endonucleases, which target specific DNA sequences and avoid integration of random mutations as observed in classic breeding approaches (Langner et al., 2018). However, politic regulations regarding genetic modified organisms and the lack of public acceptance impede exploitation of the full potential of these techniques in Europe. Therefore, alternative solutions to enhance stress resilience of crop plants are needed. For instance, the use of beneficial microbes or secondary metabolites, produced by beneficial microbes, as biofertilizers and biocontrol agents is a promising alternative to chemical solutions (Daniel et al., 2022). Beneficial microbes can directly or indirectly impact pathogen virulence on host plants. They can either directly antagonize pathogens in the rhizosphere or protect the plant indirectly by enhancing its nutrient and water uptake and thus reducing abiotic stress factors (dos Santos Lopes et al., 2021; Mikiciuk et al., 2024). Further, beneficial microbes were shown to activate the plant immune system, triggering ISR allowing an enhanced and faster response to pathogens (Pieterse et al., 2014). Thus, it is essential to understand the interaction of beneficial microbes with their host plants and the mechanisms employed to facilitate stable accommodations on a molecular level. Moreover, characterization of the plant immune response to MAMPs might lead to discovery of novel targets for plant breeding approaches. Since in nature, the plant microbiome consists of a variety of microbes, it is difficult to decipher molecular mechanisms in these complex systems. Therefore, single-association studies are important to understand and engineer beneficial plant microbe associations. The work presented in this thesis expands our knowledge on the role of lipids and polysaccharides in plant immunity during beneficial plant-microbe interactions on a molecular level. This newly acquired knowledge can be implemented to develop novel strategies to enhance plant resistance to abiotic and biotic stresses and apply more sustainable agricultural procedures.

References

Abe, M., Yanagawa, M., Hiroshima, M., Kobayashi, T., & Sako, Y. (2024). Bilateral regulation of egfr activity and local pi(4,5)p2 dynamics in mammalian cells observed with superresolution microscopy. *eLife*, *13*. https://doi.org/10.7554/eLife.101652

Acevedo-Garcia, J., Kusch, S., & Panstruga, R. (2014). Magical mystery tour: Mlo proteins in plant immunity and beyond. *New Phytologist*, *204*, 273–281. https://doi.org/10.1111/NPH.12889

Acevedo-Garcia, J., Gruner, K., Reinstädler, A., Kemen, A., Kemen, E., Cao, L., Takken, F. L., Reitz, M. U., Schäfer, P., O'Connell, R. J., Kusch, S., Kuhn, H., & Panstruga, R. (2017). The powdery mildew-resistant arabidopsis mlo2 mlo6 mlo12 triple mutant displays altered infection phenotypes with diverse types of phytopathogens. *Scientific reports*, *7*. https://doi.org/10.1038/S41598-017-07188-7

Aerts, N., Mendes, M. P., & Wees, S. C. V. (2021). Multiple levels of crosstalk in hormone networks regulating plant defense. *The Plant Journal*, *105*, 489–504. https://doi.org/10.1111/TPJ.15124

Albrecht, C., Boutrot, F., Segonzac, C., Schwessinger, B., Gimenez-Ibanez, S., Chinchilla, D., Rathjen, J. P., Vries, S. C. D., & Zipfel, C. (2012). Brassinosteroids inhibit pathogen-associated molecular pattern-triggered immune signaling independent of the receptor kinase bak1. *Proceedings of the National Academy of Sciences of the United States of America*, *109*, 303–308. https://doi.org/10.1073/PNAS.1109921108/SUPPL_FILE/PNAS.201109921SI.PDF

Albrecht, T., & Argueso, C. T. (2016). Should i fight or should i grow now? the role of cytokinins in plant growth and immunity and in the growth–defence trade-off. *Annals of Botany*, *119*, 725. https://doi.org/10.1093/AOB/MCW211

Albus, U., Baier, R., Holst, O., Pühler, A., & Niehaus, K. (2001). Suppression of an elicitor-induced oxidative burst reaction in medicago sativa cell cultures by sinorhizobium meliloti lipopolysaccharides. *The New phytologist*, *151*, 597–606. https://doi.org/10.1046/J.0028-646X.2001.00214.X

Anthony, M. A., Bender, S. F., & van der Heijden, M. G. (2023). Enumerating soil biodiversity. *Proceedings of the National Academy of Sciences of the United States of America*, *120*. https://doi.org/10.1073/pnas.2304663120

Aslam, S. N., Newman, M. A., Erbs, G., Morrissey, K. L., Chinchilla, D., Boller, T., Jensen, T. T., Castro, C. D., Ierano, T., Molinaro, A., Jackson, R. W., Knight, M. R., & Cooper, R. M. (2008). Bacterial polysaccharides suppress induced innate immunity by calcium

chelation. *Current biology : CB*, *18*, 1078–1083. https://doi.org/10.1016/J.CUB.2008.06.061

Avrova, A. O., Taleb, N., Rokka, V. M., Heilbronn, J., Campbell, E., Hein, I., Gilroy, E. M., Cardle, L., Bradshaw, J. E., Stewart, H. E., Fakim, Y. J., Loake, G., & Birch, P. R. (2004). Potato oxysterol binding protein and cathepsin b are rapidly up-regulated in independent defence pathways that distinguish r gene-mediated and field resistances to phytophthora infestans. *Molecular plant pathology*, *5*, 45–56. https://doi.org/10.1111/J.1364-3703.2004.00205.X

Bai, B., Liu, W., Qiu, X., Zhang, J., Zhang, J., & Bai, Y. (2022). The root microbiome: Community assembly and its contributions to plant fitness. *Journal of Integrative Plant Biology*, *64*, 230–243. https://doi.org/10.1111/jipb.13226

Bai, Y., Müller, D. B., Srinivas, G., Garrido-Oter, R., Potthoff, E., Rott, M., Dombrowski, N., Münch, P. C., Spaepen, S., Remus-Emsermann, M., Hüttel, B., McHardy, A. C., Vorholt, J. A., & Schulze-Lefert, P. (2015). Functional overlap of the arabidopsis leaf and root microbiota. *Nature*, *528*, 364–369. https://doi.org/10.1038/nature16192

Bakker, M. G., Schlatter, D. C., Otto-Hanson, L., & Kinkel, L. L. (2014). Diffuse symbioses: Roles of plant-plant, plant-microbe and microbe-microbe interactions in structuring the soil microbiome. *Molecular Ecology*, *23*, 1571–1583. https://doi.org/10.1111/mec.12571

Barnett, K. C., & Kagan, J. C. (2020). Lipids that directly regulate innate immune signal transduction. *Innate Immunity*, *26*, 4–14. https://doi.org/10.1177/1753425919852695

Bhat, R. A., Miklis, M., Schmelzer, E., Schulze-Lefert, P., & Panstruga, R. (2005). Recruitment and interaction dynamics of plant penetration resistance components in a plasma membrane microdomain. *PNAS*, *102*, 3135–3140. https://doi.org/10.1073/PNAS.0500012102/SUPPL_FILE/00012FIG7.JPG

Blaum, B. S., Mazzotta, S., Nöldeke, E. R., Halter, T., Madlung, J., Kemmerling, B., & Stehle, T. (2014). Structure of the pseudokinase domain of bir2, a regulator of bak1-mediated immune signaling in arabidopsis. *Journal of structural biology*, *186*, 112–121. https://doi.org/10.1016/J.JSB.2014.02.005

Boutrot, F., & Zipfel, C. (2017). Function, discovery, and exploitation of plant pattern recognition receptors for broad-spectrum disease resistance. *Annual Review of Phytopathology Downloaded from www.annualreviews.org. University of Koln*, *33*, 59. https://doi.org/10.1146/annurev-phyto-080614

Boutrot, F., Segonzac, C., Chang, K. N., Qiao, H., Ecker, J. R., Zipfel, C., & Rathjen, J. P. (2010). Direct transcriptional control of the arabidopsis immune receptor fls2 by the ethylene-dependent transcription factors ein3 and eil1. *Proceedings of the National Academy of Sciences of the United States of America*, *107*, 14502–14507. https://doi.org/10.1073/PNAS.1003347107

Brown, H. E., Esher, S. K., & Alspaugh, J. (2020). Chitin: A "hidden figure" in the fungal cell wall. In J.-P. Latgé (Ed.). Springer. http://www.springer.com/series/82

Bücherl, C. A., Jarsch, I. K., Schudoma, C., Segonzac, C., Mbengue, M., Robatzek, S., MacLean, D., Ott, T., & Zipfel, C. (2017). Plant immune and growth receptors share common

signalling components but localise to distinct plasma membrane nanodomains. *eLife*. https://doi.org/10.7554/eLife.25114.001

Bühler, N., Hagiwara, D., & Takeshita, N. (2015). Functional analysis of sterol transporter orthologues in the filamentous fungus aspergillus nidulans. *Eukaryotic Cell*, *14*, 908–921. https://doi.org/10.1128/EC.00027-15

Bulgarelli, D., Schlaeppi, K., Spaepen, S., Themaat, E. V. L. V., & Schulze-Lefert, P. (2013). Structure and functions of the bacterial microbiota of plants. *Annual Review of Plant Biology*, *64*, 807–838. https://doi.org/10.1146/ANNUREV-ARPLANT-050312-120106/CITE/REFWORKS

Büschges, R., Hollricher, K., Panstruga, R., Simons, G., Wolter, M., Frijters, A., Daelen, R. V., der Lee, T. V., Diergaarde, P., Groenendijk, J., Töpsch, S., Vos, P., Salamini, F., & Schulze-Lefert, P. (1997). The barley mlo gene: A novel control element of plant pathogen resistance. *Cell*, *88*, 695–705. https://doi.org/10.1016/S0092-8674(00)81912-1

Calvin, K., Dasgupta, D., Krinner, G., Mukherji, A., Thorne, P. W., Trisos, C., Romero, J., Aldunce, P., Barrett, K., Blanco, G., Cheung, W. W., Connors, S., Denton, F., Diongue-Niang, A., Dodman, D., Garschagen, M., Geden, O., Hayward, B., Jones, C., ... Ha, M. (2023, July). *Ipcc, 2023: Climate change 2023: Synthesis report.* (P. Arias, M. Bustamante, I. Elgizouli, G. Flato, M. Howden, C. Méndez-Vallejo, J. J. Pereira, R. Pichs-Madruga, S. K. Rose, Y. Saheb, R. S. Rodríguez, D. Ürge-Vorsatz, C. Xiao, N. Yassaa, J. Romero, J. Kim, E. F. Haites, Y. Jung, R. Stavins, ... C. Péan, Eds.). https://doi.org/10.59327/IPCC/AR6-9789291691647

Cao, Y., Liang, Y., Tanaka, K., Nguyen, C. T., Jedrzejczak, R. P., Joachimiak, A., & Stacey, G. (2014). The kinase lyk5 is a major chitin receptor in arabidopsis and forms a chitin-induced complex with related kinase cerk1. *eLife*, *3*. https://doi.org/10.7554/eLife.03766

Carlson, H., Nilsson, P., Jansson, H.-B., & Odham, G. (1991). Characterization and determination of prehelminthosporol, a toxin from the plant pathogenic fungus bipolaris sorokiniana, using liquid chromatography/mass spectrometry. *Journal of Microbiological Methods*, *13*, 259–269.

Castells, E., & Casacuberta, J. M. (2007). Signalling through kinase-defective domains: The prevalence of atypical receptor-like kinases in plants. *Journal of Experimental Botany*, *58*, 3503–3511. https://doi.org/10.1093/JXB/ERM226

Caunt, C. J., & Keyse, S. M. (2013). Dual-specificity map kinase phosphatases (mkps): Shaping the outcome of map kinase signalling. *The FEBS journal*, *280*, 489–504. https://doi.org/10.1111/J.1742-4658.2012.08716.X

Chacón, M. V. A., Dingenen, J. V., & Goormachtig, S. (2023). Characterization of arbuscular mycorrhizal effector proteins. *International Journal of Molecular Sciences*, *24*, 9125. https://doi.org/10.3390/IJMS24119125

Chacón, M. V. A., Luelmo, S. H., Devlieghere, V., Robichez, L., Leroy, T., Stuer, N., Keyser, A. D., Ceulemans, E., Goossens, A., Goormachtig, S., & Dingenen, J. V. (2024). Exploring the potential role of four rhizophagus irregularis nuclear effectors: Opportunities and technical limitations. *Frontiers in Plant Science*, *15*, 1384496. https://doi.org/10.3389/FPLS.2024.1384496/BIBTEX

Chandrasekar, B., Wanke, A., Wawra, S., Saake, P., Mahdi, L., Charura, N., Neidert, M., Poschmann, G., Malisic, M., Thiele, M., Stühler, K., Dama, M., Pauly, M., & Zuccaro, A. (2022). Fungi hijack a ubiquitous plant apoplastic endoglucanase to release a ros scavenging β-glucan decasaccharide to subvert immune responses. *The Plant Cell*. https://doi.org/10.1093/plcell/koac114

Chang, M., Chen, H., Liu, F., & Fu, Z. Q. (2022). Pti and eti: Convergent pathways with diverse elicitors. *Trends in Plant Science*, *27*, 113–115. https://doi.org/10.1016/j.tplants.2021.11.013

Chen, M. M., Yang, S. R., Wang, J., Fang, Y. L., Peng, Y. L., & Fan, J. (2022). Fungal oxysterol-binding protein-related proteins promote pathogen virulence and activate plant immunity. *Journal of Experimental Botany*, *73*, 2125–2141. https://doi.org/10.1093/jxb/erab530

Chinchilla, D., Bauer, Z., Regenass, M., Boller, T., & Felix, G. (2006). The arabidopsis receptor kinase fls2 binds flg22 and determines the specificity of flagellin perception. *Plant Cell*, *18*, 465–476. https://doi.org/10.1105/tpc.105.036574

Choi, J., Tanaka, K., Cao, Y., Qi, Y., Qiu, J., Liang, Y., Lee, S. Y., & Stacey, G. (2014). Identification of a plant receptor forextracellular atp. *science*, *343*, 290–293. https://doi.org/10.1126/science.343.6168.290

Claus, L. A. N., Savatin, D. V., & Russinova, E. (2018). The crossroads of receptor-mediated signaling and endocytosis in plants. *Journal of Integrative Plant Biology*, *60*, 827–840. https://doi.org/10.1111/jipb.12672

Conrath, U., Beckers, G. J., Flors, V., García-Agustín, P., Jakab, G., Mauch, F., Newman, M. A., Pieterse, C. M., Poinssot, B., Pozo, M. J., Pugin, A., Schaffrath, U., Ton, J., Wendehenne, D., Zimmerli, L., & Mauch-Mani, B. (2006). Priming: Getting ready for battle. *Molecular plant-microbe interactions : MPMI*, *19*, 1062–1071. https://doi.org/10.1094/MPMI-19-1062

Couto, D., & Zipfel, C. (2016). Regulation of pattern recognition receptor signalling in plants. *Nature Reviews Immunology*, *16*, 537–552. https://doi.org/10.1038/nri.2016.77

Couto, D., Niebergall, R., Liang, X., Bücherl, C. A., Sklenar, J., Macho, A. P., Ntoukakis, V., Derbyshire, P., Altenbach, D., Maclean, D., Robatzek, S., Uhrig, J., Menke, F., Zhou, J. M., & Zipfel, C. (2016). The arabidopsis protein phosphatase pp2c38 negatively regulates the central immune kinase bik1. *PLOS Pathogens*, *12*, e1005811. https://doi.org/10.1371/JOURNAL.PPAT.1005811

Cui, Y., Li, X., Yu, M., Li, R., Fan, L., Zhu, Y., & Lin, J. (2018). Sterols regulate endocytic pathways during flg22-induced defense responses in arabidopsis. *Development (Cambridge)*, *145*. https://doi.org/10.1242/dev.165688

Daniel, A. I., Fadaka, A. O., Gokul, A., Bakare, O. O., Aina, O., Fisher, S., Burt, A. F., Mavumengwana, V., Keyster, M., & Klein, A. (2022). Biofertilizer: The future of food security and food safety. *Microorganisms*, *10*. https://doi.org/10.3390/microorganisms10061220

DeFalco, T. A., & Zipfel, C. (2021). Molecular mechanisms of early plant pattern-triggered immune signaling [all LRR RK-type PRRs use SERK family coreceptors]. *Molecular Cell*, *81*, 3449–3467. https://doi.org/10.1016/j.molcel.2021.07.029

Delgado-Baquerizo, M., Guerra, C. A., Cano-Díaz, C., Egidi, E., Wang, J. T., Eisenhauer, N., Singh, B. K., & Maestre, F. T. (2020). The proportion of soil-borne pathogens increases with warming at the global scale. *Nature Climate Change*, *10*, 550–554. https://doi.org/10.1038/s41558-020-0759-3

Der, C., Courty, P. E., Recorbet, G., Wipf, D., Simon-Plas, F., & Gerbeau-Pissot, P. (2024). Sterols, pleiotropic players in plant–microbe interactions. *Trends in Plant Science*, *29*, 524–534. https://doi.org/10.1016/j.tplants.2024.03.002

Deshmukh, S., Hückelhoven, R., Schäfer, P., Imani, J., Sharma, M., Weiss, M., Waller, F., & Kogel, K. H. (2006). The root endophytic fungus pirifomospora indica requires host cell for proliferation during mutualistic symbiosis with barley. *Proceedings of the National Academy of Sciences of the United States of America*, *103*, 18450–18457. https://doi.org/10.1073/pnas.0605697103

Devoto, A., Hartmann, H. A., Piffanelli, P., Elliott, C., Simmons, C., Taramino, G., Goh, C. S., Cohen, F. E., Emerson, B. C., Schulze-Lefert, P., & Panstruga, R. (2003). Molecular phylogeny and evolution of the plant-specific seven-transmembrane mlo family. *Journal of Molecular Evolution*, *56*, 77–88. https://doi.org/10.1007/s00239-002-2382-5

Diao, Z., Yang, R., Wang, Y., Cui, J., Li, J., Wu, Q., Zhang, Y., Yu, X., Gong, B., Huang, Y., Yu, G., Yao, H., Guo, J., Zhang, H., Shen, J., Gust, A. A., & Cai, Y. (2024). Functional screening of the arabidopsis 2c protein phosphatases family identifies pp2c15 as a negative regulator of plant immunity by targeting bri1-associated receptor kinase 1. *Molecular Plant Pathology*, *25*, e13447. https://doi.org/10.1111/MPP.13447

dos Santos Lopes, M. J., Dias-Filho, M. B., & Gurgel, E. S. C. (2021). Successful plant growth-promoting microbes: Inoculation methods and abiotic factors. *Frontiers in Sustainable Food Systems*, *5*. https://doi.org/10.3389/fsufs.2021.606454

Doumane, M., Lebecq, A., Colin, L., Fangain, A., Stevens, F. D., Bareille, J., Hamant, O., Belkhadir, Y., Munnik, T., Jaillais, Y., & Caillaud, M. C. (2021). Inducible depletion of pi(4,5)p2 by the synthetic idepp system in arabidopsis. *Nature Plants*, *7*, 587–597. https://doi.org/10.1038/s41477-021-00907-z

Dunken, N., Widmer, H., Balcke, G. U., Straube, H., Langen, G., Charura, N. M., Saake, P., Quattro, C. D., Schön, J., Rövenich, H., Wawra, S., Khan, M., Djamei, A., Zurbriggen, M. D., Tissier, A., Witte, C.-P., & Zuccaro, A. (2024). A nucleoside signal generated by a fungal endophyte regulates host cell death and promotes root colonization. *Cell Host & Microbe*, *32*, 2161–2177.e7. https://doi.org/10.1016/j.chom.2024.10.020

Duran, P., Thiergart, T., Garrido-Oter, R., Agler, M., Kemen, E., Schulze-Lefert, P., & Hacquard, S. (2018). Microbial interkingdom interactions in roots promote arabidopsis survival. *Cell*, *175*, 973–983.e14. https://doi.org/10.1016/j.cell.2018.10.020

Eichfeld, R., Mahdi, L. K., Quattro, C. D., Armbruster, L., Endeshaw, A. B., Miyauchi, S., Hellmann, M. J., Cord-Landwehr, S., Peterson, D., Singan, V., Lail, K., Savage, E., Ng, V., Grigoriev, I. V., Langen, G., Moerschbacher, B. M., & Zuccaro, A. (2024). Transcriptomics reveal a mechanism of niche defense: Two beneficial root endophytes deploy an antimicrobial gh18-cbm5 chitinase to protect their hosts. *New Phytologist*, *244*, 980–996. https://doi.org/10.1111/NPH.20080

Ekanayake, G., Smith, J. M., Jones, K. B., Stiers, H. M., Robinson, S. J., LaMontagne, E. D., Kostos, P. H., Cornish, P. V., Bednarek, S. Y., & Heese, A. (2021). Dynamin-related protein drp1a functions with drp2b in plant growth, flg22-immune responses, and endocytosis. *Plant Physiology*, *185*, 1986–2002. https://doi.org/10.1093/plphys/kiab024

Ent, S. V. D., Hulten, M. V., Pozo, M. J., Czechowski, T., Udvardi, M. K., Pieterse, C. M., & Ton, J. (2009). Priming of plant innate immunity by rhizobacteria and beta-aminobutyric acid: Differences and similarities in regulation. *The New phytologist*, *183*, 419–431. https://doi.org/10.1111/J.1469-8137.2009.02851.X

Feng, F., Sun, J., Radhakrishnan, G. V., Lee, T., Bozsóki, Z., Fort, S., Gavrin, A., Gysel, K., Thygesen, M. B., Andersen, K. R., Radutoiu, S., Stougaard, J., & Oldroyd, G. E. (2019). A combination of chitooligosaccharide and lipochitooligosaccharide recognition promotes arbuscular mycorrhizal associations in medicago truncatula. *Nature Communications*, *10*, 1–12. https://doi.org/10.1038/s41467-019-12999-5

Ferrer, A., Altabella, T., Arró, M., & Boronat, A. (2017). Emerging roles for conjugated sterols in plants. *Progress in Lipid Research*, *67*, 27–37. https://doi.org/10.1016/J.PLIPRES.2017.06.002

Gao, M., Wang, X., Wang, D., Xu, F., Ding, X., Zhang, Z., Bi, D., Cheng, Y. T., Chen, S., Li, X., & Zhang, Y. (2009). Regulation of cell death and innate immunity by two receptor-like kinases in arabidopsis. *Cell Host & Microbe*, *6*, 34–44. https://doi.org/10.1016/J.CHOM.2009.05.019

Ghugtyal, V., Garcia-Rodas, R., Seminara, A., Schaub, S., Bassilana, M., & Arkowitz, R. A. (2015). Phosphatidylinositol-4-phosphate-dependent membrane traffic is critical for fungal filamentous growth. *Proceedings of the National Academy of Sciences of the United States of America*, *112*, 8644–8649. https://doi.org/10.1073/pnas.1504259112

Gibelin-Viala, C., Amblard, E., Puech-Pages, V., Bonhomme, M., Garcia, M., Bascaules-Bedin, A., Fliegmann, J., Wen, J., Mysore, K. S., le Signor, C., Jacquet, C., & Gough, C. (2019). The medicago truncatula lysm receptor-like kinase lyk9 plays a dual role in immunity and the arbuscular mycorrhizal symbiosis. *New Phytologist*, *223*, 1516–1529. https://doi.org/10.1111/nph.15891

Giovannetti, M., Binci, F., Navazio, L., & Genre, A. (2024). Nonbinary fungal signals and calcium-mediated transduction in plant immunity and symbiosis. *New Phytologist*, *241*, 1393–1400. https://doi.org/10.1111/nph.19433

Gómez-Gómez, L., Bauer, Z., & Boller, T. (2001). Both the extracellular leucine-rich repeat domain and the kinase activity of fls2 are required for flagellin binding and signaling in arabidopsis. *The Plant Cell*, *13*, 1155–1163. www.plantcell.org

Gong, B. Q., Guo, J., Zhang, N., Yao, X., Wang, H. B., & Li, J. F. (2019). Cross-microbial protection via priming a conserved immune co-receptor through juxtamembrane phosphorylation in plants. *Cell Host and Microbe*, *26*, 810–822.e7. https://doi.org/10.1016/j.chom.2019.10.010

Gronnier, J., Crowet, J. M., Habenstein, B., Nasir, M. N., Bayle, V., Hosy, E., Platre, M. P., Gouguet, P., Raffaele, S., Martinez, D., Grelard, A., Loquet, A., Simon-Plas, F., Gerbeau-Pissot, P., Der, C., Bayer, E. M., Jaillais, Y., Deleu, M., Germain, V., ... Mongrand, S.

(2017). Structural basis for plant plasma membrane protein dynamics and organization into functional nanodomains. *eLife*, *6*. https://doi.org/10.7554/eLife.26404

Grosjean, K., Der, C., Robert, F., Thomas, D., Mongrand, S., Simon-Plas, F., & Gerbeau-Pissot, P. (2018). Interactions between lipids and proteins are critical for organization of plasma membrane-ordered domains in tobacco by-2 cells. *Journal of Experimental Botany*, *69*, 3545–3557. https://doi.org/10.1093/JXB/ERY152

Guo, Z., Liu, X., Wang, N., Mo, P., Shen, J., Liu, M., Zhang, H., Wang, P., & Zhang, Z. (2023). Membrane component ergosterol builds a platform for promoting effector secretion and virulence in magnaporthe oryzae. *New Phytologist*, *237*, 930–943. https://doi.org/10.1111/nph.18575

Halter, T., Imkampe, J., Mazzotta, S., Wierzba, M., Postel, S., Bücherl, C., Kiefer, C., Stahl, M., Chinchilla, D., Wang, X., Nürnberger, T., Zipfel, C., Clouse, S., Borst, J. W., Boeren, S., Vries, S. C. D., Tax, F., & Kemmerling, B. (2014). The leucine-rich repeat receptor kinase bir2 is a negative regulator of bak1 in plant immunity. *Current biology*, *24*, 134–143. https://doi.org/10.1016/J.CUB.2013.11.047

Han, X., & Kahmann, R. (2019). Manipulation of phytohormone pathways by effectors of filamentous plant pathogens. *Frontiers in Plant Science*, *10*, 464951. https://doi.org/10.3389/FPLS.2019.00822/BIBTEX

Harris, J. M., Balint-Kurti, P., Bede, J. C., Day, B., Gold, S., Goss, E. M., Grenville-Briggs, L. J., Jones, K. M., Wang, A., Wang, Y., Mitra, R. M., Sohn, K. H., & Alvarez, M. E. (2020). What are the top 10 unanswered questions in molecular plant-microbe interactions? *Molecular Plant-Microbe Interactions*, *33*, 1354–1365. https://doi.org/10.1094/MPMI-08-20-0229-CR/ASSET/IMAGES/LARGE/MPMI-08-20-0229-CRF3-1605056467136.JPEG

Hayafune, M., Berisio, R., Marchetti, R., Silipo, A., Kayama, M., Desaki, Y., Arima, S., Squeglia, F., Ruggiero, A., Tokuyasu, K., Molinaro, A., Kaku, H., & Shibuya, N. (2014). Chitin-induced activation of immune signaling by the rice receptor cebip relies on a unique sandwich-type dimerization. *Proceedings of the National Academy of Sciences of the United States of America*, *111*. https://doi.org/10.1073/pnas.1312099111

Heese, A., Hann, D. R., Gimenez-Ibanez, S., Jones, A. M. E., He, K., Li, J., Schroeder, J. I., Peck, S. C., & Rathjen, J. P. (2007). The receptor-like kinase serk3/bak1 is a central regulator of innate immunity in plants. *Proceedings of the National Academy of Sciences of the United States of America*, *104*, 12217–12222. www.pnas.org/cgi/content/full/

Hein, I., Campbell, E. I., Woodhead, M., Hedley, P. E., Young, V., Morris, W. L., Ramsay, L., Stockhaus, J., Lyon, G. D., Newton, A. C., & Birch, P. R. (2004). Characterisation of early transcriptional changes involving multiple signalling pathways in the mla13 barley interaction with powdery mildew (blumeria graminis f. sp. hordei). *Planta*, *218*, 803–813. https://doi.org/10.1007/S00425-003-1159-4

Hilbert, M., Novero, M., Rovenich, H., Mari, S., Grimm, C., Bonfante, P., & Zuccaro, A. (2020). Mlo differentially regulates barley root colonization by beneficial endophytic and mycorrhizal fungi. *Frontiers in Plant Science*, *10*, 490627. https://doi.org/10.3389/FPLS.2019.01678/BIBTEX

Hoff, P. L. D., Brill, L. M., & Hirsch, A. M. (2009). Plant lectins: The ties that bind in root symbiosis and plant defense. *Molecular Genetics and Genomics*, *282*, 1. https://doi.org/10.1007/S00438-009-0460-8

Hückelhoven, R. (2014). The effective papilla hypothesis. *New Phytologist*, *204*, 438–440. https://doi.org/10.1111/NPH.13026

Im, Y. J., Raychaudhuri, S., Prinz, W. A., & Hurley, J. H. (2005). Structural mechanism for sterol sensing and transport by osbp-related proteins. *Nature*, *437*, 154–158. https://doi.org/10.1038/nature03923

Ivanov, S., & Harrison, M. J. (2019). Accumulation of phosphoinositides in distinct regions of the periarbuscular membrane. *New Phytologist*, *221*, 2213–2227. https://doi.org/10.1111/nph.15553

Jacobs, S., Zechmann, B., Molitor, A., Trujillo, M., Petutschnig, E., Lipka, V., Kogel, K.-H., & Schäfer, P. (2011). Broad-spectrum suppression of innate immunity is required for colonization of arabidopsis roots by the fungus piriformospora indica. *Plant Physiology*, *156*, 726–740. https://doi.org/10.1104/pp.111.176446

Jahani, M., Aggarwal, R., Gupta, S., Sharma, S., & Dureja, P. (2014). Purification and characterization of a novel toxin from bipolaris sorokiniana, causing spot blotch of wheat and analysis of variability in the pathogen. *Cereal Research Communications*, *42*, 252–261. https://doi.org/10.1556/CRC.2013.0053

Jaillais, Y., & Ott, T. (2020). The nanoscale organization of the plasma membrane and its importance in signaling: A proteolipid perspective. *Plant Physiology*, *182*, 1682–1696. https://doi.org/10.1104/PP.19.01349

Jaillais, Y., Bayer, E., Bergmann, D. C., Botella, M. A., Boutté, Y., Bozkurt, T. O., Caillaud, M. C., Germain, V., Grossmann, G., Heilmann, I., Hemsley, P. A., Kirchhelle, C., Martinière, A., Miao, Y., Mongrand, S., Müller, S., Noack, L. C., Oda, Y., Ott, T., ... Gronnier, J. (2024). Guidelines for naming and studying plasma membrane domains in plants. *Nature Plants*, *10*, 1172–1183. https://doi.org/10.1038/s41477-024-01742-8

Jarosch, B., Kogel, K.-H., & Schaffrath, U. (1999). The ambivalence of the barley mlo locus: Mutations conferring resistance against powdery mildew (blumeria graminis f. sp. hordei) enhance susceptibility to the rice blast fungus magnaporthe grisea. *MPMI*, *12*, 508–514.

Javed, T., & Gao, S. J. (2023). Wrky transcription factors in plant defense. *Trends in Genetics*, *39*, 787–801. https://doi.org/10.1016/J.TIG.2023.07.001

Jia, M., Gong, X., Fan, M., Liu, H., Zhou, H., Gu, S., Liu, Y., & Dong, J. (2023). Identification and analysis of the secretome of plant pathogenic fungi reveals lifestyle adaptation. *Frontiers in Microbiology*, *14*, 1171618. https://doi.org/10.3389/FMICB.2023.1171618/BIBTEX

Jones, J. D. G., & Dangl, J. L. (2006). The plant immune system. *nature*.

Jørgensen, I. H. (1992). Discovery, characterization and exploitation of mlo powdery mildew resistance in barley. *Euphytica*, *63*, 141–152. https://doi.org/10.1007/BF00023919/METRICS

Jung, E. J., Choi, S. Y., Lee, S. M., Song, J. Y., Lee, H. J., Kim, E., Lee, P. A., Choi, K., Kim, J. F., & Lee, S. W. (2021). Flavobacterium dauae sp. nov., isolated from rhizosphere soil

of a tomato plant. *International journal of systematic and evolutionary microbiology*, *71*. https://doi.org/10.1099/IJSEM.0.005033

Jung, S. C., Martinez-Medina, A., Lopez-Raez, J. A., & Pozo, M. J. (2012). Mycorrhiza-induced resistance and priming of plant defenses. *Journal of Chemical Ecology 2012 38:6*, *38*, 651–664. https://doi.org/10.1007/S10886-012-0134-6

Kadota, Y., Sklenar, J., Derbyshire, P., Stransfeld, L., Asai, S., Ntoukakis, V., Jones, J. D., Shirasu, K., Menke, F., Jones, A., & Zipfel, C. (2014). Direct regulation of the nadph oxidase rbohd by the prr-associated kinase bik1 during plant immunity. *Molecular Cell*, *54*, 43–55. https://doi.org/https://doi.org/10.1016/j.molcel.2014.02.021

Kato, H., Nemoto, K., Shimizu, M., Abe, A., Asai, S., Ishihama, N., Matsuoka, S., Daimon, T., Ojika, M., Kawakita, K., Onai, K., Shirasu, K., Yoshida, M., Ishiura, M., Takemoto, D., Takano, Y., & Terauchi, R. (2022). Recognition of pathogen-derived sphingolipids in arabidopsis. *Science*, *376*, 857–860. https://doi.org/10.1126/science.abn0650

Kawaharada, Y., Kelly, S., Nielsen, M. W., Hjuler, C. T., Gysel, K., Muszyński, A., Carlson, R. W., Thygesen, M. B., Sandal, N., Asmussen, M. H., Vinther, M., Andersen, S. U., Krusell, L., Thirup, S., Jensen, K. J., Ronson, C. W., Blaise, M., Radutoiu, S., & Stougaard, J. (2015). Receptor-mediated exopolysaccharide perception controls bacterial infection. *Nature*, *523*, 308–312. https://doi.org/10.1038/NATURE14611

Kawaharada, Y., Nielsen, M. W., Kelly, S., James, E. K., Andersen, K. R., Rasmussen, S. R., Füchtbauer, W., Madsen, L. H., Heckmann, A. B., Radutoiu, S., & Stougaard, J. (2017). Differential regulation of the epr3 receptor coordinates membrane-restricted rhizobial colonization of root nodule primordia. *Nature communications*, *8*. https://doi.org/10.1038/NCOMMS14534

Kelly, S., Hansen, S. B., Rübsam, H., Saake, P., Pedersen, E. B., Gysel, K., Madland, E., Wu, S., Wawra, S., Reid, D., Sullivan, J. T., Blahovska, Z., Vinther, M., Muszynski, A., Azadi, P., Thygesen, M. B., Aachmann, F. L., Ronson, C. W., Zuccaro, A., ... Stougaard, J. (2023). A glycan receptor kinase facilitates intracellular accommodation of arbuscular mycorrhiza and symbiotic rhizobia in the legume lotus japonicus. *PLOS Biology*, *21*. https://doi.org/10.1371/JOURNAL.PBIO.3002127

Kelly, S. J., Muszyński, A., Kawaharada, Y., Hubber, A. M., Sullivan, J. T., Sandal, N., Carlson, R. W., Stougaard, J., & Ronson, C. W. (2013). Conditional requirement for exopolysaccharide in the mesorhizobium-lotus symbiosis. *Molecular Plant-Microbe Interactions*, *26*, 319–329. https://doi.org/10.1094/MPMI-09-12-0227-R

Khaled, S. B., Postma, J., & Robatzek, S. (2015). A moving view: Subcellular trafficking processes in pattern recognition receptor-triggered plant immunity. *Annual review of phytopathology*, *53*, 379–402. https://doi.org/10.1146/ANNUREV-PHYTO-080614-120347

Kim, M. C., Panstruga, R., Elliott, C., Möller, J., Devoto, A., Yoon, H. W., Park, H. C., Cho, M. J., & Schulze-Lefert, P. (2002). Calmodulin interacts with mlo protein to regulate defence against mildew in barley. *Nature*, *416*, 447–451. https://doi.org/10.1038/416447a

Klemptner, R. L., Sherwood, J. S., Tugizimana, F., Dubery, I. A., & Piater, L. A. (2014). Ergosterol, an orphan fungal microbe-associated molecular pattern (mamp). *Molecular Plant Pathology*, *15*, 747–761. https://doi.org/10.1111/mpp.12127

Kolton, M., Erlacher, A., Berg, G., & Cytryn, E. (2016). The flavobacterium genus in the plant holobiont: Ecological, physiological, and applicative insights . In S. Castro-Sowinski (Ed.). Springer. http://www.springer.com/series/14379

Kong, L., Ma, X., Zhang, C., Kim, S.-I., Li, B., Xie, Y., Yeo, I.-C., Thapa, H., Chen, S., Devarenne, T. P., Munnik, T., He, P., & Shan, L. (2024). Dual phosphorylation of dgk5-mediated pa burst regulates ros in plant immunity. *Cell*, *187*, 609–623.e21. https://doi.org/10.1016/j.cell.2023.12.030

Kopischke, M., Westphal, L., Schneeberger, K., Clark, R., Ossowski, S., Wewer, V., Fuchs, R., Landtag, J., Hause, G., Dörmann, P., Lipka, V., Weigel, D., Schulze-Lefert, P., Scheel, D., & Rosahl, S. (2013). Impaired sterol ester synthesis alters the response of arabidopsis thaliana to phytophthora infestans. *The Plant Journal*, *73*, 456–468. https://doi.org/10.1111/TPJ.12046

Kouzai, Y., Nakajima, K., Hayafune, M., Ozawa, K., Kaku, H., Shibuya, N., Minami, E., & Nishizawa, Y. (2014). Cebip is the major chitin oligomer-binding protein in rice and plays a main role in the perception of chitin oligomers. *Plant Molecular Biology*, *84*, 519–528. https://doi.org/10.1007/s11103-013-0149-6

Krönauer, C., & Radutoiu, S. (2021). Understanding nod factor signalling paves the way for targeted engineering in legumes and non-legumes. *Current Opinion in Plant Biology*, *62*, 102026. https://doi.org/10.1016/J.PBI.2021.102026

Kumar, J., Hückelhoven, R., Beckhove, U., Nagarajan, S., & Kogel, K.-H. (2001). Genetics and resistance a compromised mlo pathway affects the response of barley to the necrotrophic fungus bipolaris sorokiniana (teleomorph: Cochliobolus sativus) and its toxins. *Phytopathology*, *91*, 127.

Kumar, J., Schäfer, P., Hückelhoven, R., Langen, G., Baltruschat, H., Stein, E., Nagarajan, S., & Kogel, K. H. (2002). Bipolaris sorokiniana, a cereal pathogen of global concern: Cytological and molecular approaches towards better control‡. *Molecular Plant Pathology*, *3*, 185–195. https://doi.org/10.1046/J.1364-3703.2002.00120.X

Kumar, V., Sarma, M. V., Saharan, K., Srivastava, R., Kumar, L., Sahai, V., Bisaria, V. S., & Sharma, A. K. (2012). Effect of formulated root endophytic fungus piriformospora indica and plant growth promoting rhizobacteria fluorescent pseudomonads r62 and r81 on vigna mungo. *World journal of microbiology & biotechnology*, *28*, 595–603. https://doi.org/10.1007/S11274-011-0852-X

Kusch, S., & Panstruga, R. (2017). Mlo-based resistance: An apparently universal "weapon" to defeat powdery mildew disease. *Molecular Plant-Microbe Interactions*, *30*, 179–189. https://doi.org/10.1094/MPMI-12-16-0255-CR/ASSET/IMAGES/LARGE/MPMI-12-16-0255-CR_T1-1491248712271.JPEG

Kusch, S., Thiery, S., Reinstädler, A., Gruner, K., Zienkiewicz, K., Feussner, I., & Panstruga, R. (2019). Arabidopsis mlo3 mutant plants exhibit spontaneous callose deposition and signs of early leaf senescence. *Plant molecular biology*, *101*, 21–40. https://doi.org/10.1007/S11103-019-00877-Z

Kwak, M. J., Kong, H. G., Choi, K., Kwon, S. K., Song, J. Y., Lee, J., Lee, P. A., Choi, S. Y., Seo, M., Lee, H. J., Jung, E. J., Park, H., Roy, N., Kim, H., Lee, M. M., Rubin, E. M.,

Lee, S. W., & Kim, J. F. (2018). Rhizosphere microbiome structure alters to enable wilt resistance in tomato. *Nature Biotechnology*, *36*, 1100–1116. https://doi.org/10.1038/nbt.4232

Lahlali, R., Taoussi, M., Laasli, S. E., Gachara, G., Ezzouggari, R., Belabess, Z., Aberkani, K., Assouguem, A., Meddich, A., Jarroudi, M. E., & Barka, E. A. (2024). Effects of climate change on plant pathogens and host-pathogen interactions. *Crop and Environment*, *3*, 159–170. https://doi.org/10.1016/j.crope.2024.05.003

Lahrmann, U., Ding, Y., Banhara, A., Rath, M., Hajirezaei, M. R., Döhlemann, S., Wirén, N. V., Parniske, M., & Zuccaro, A. (2013). Host-related metabolic cues affect colonization strategies of a root endophyte. *Proceedings of the National Academy of Sciences of the United States of America*, *110*, 13965–13970. https://doi.org/10.1073/pnas.1301653110

Lahrmann, U., Strehmel, N., Langen, G., Frerigmann, H., Leson, L., Ding, Y., Scheel, D., Herklotz, S., Hilbert, M., & Zuccaro, A. (2015). Mutualistic root endophytism is not associated with the reduction of saprotrophic traits and requires a noncompromised plant innate immunity. *New Phytologist*, *207*, 841–857. https://doi.org/10.1111/nph.13411

Lal, N. K., Nagalakshmi, U., Hurlburt, N. K., Flores, R., Bak, A., Sone, P., Ma, X., Song, G., Walley, J., Shan, L., He, P., Casteel, C., Fisher, A. J., & Dinesh-Kumar, S. P. (2018). The receptor-like cytoplasmic kinase bik1 localizes to the nucleus and regulates defense hormone expression during plant innate immunity. *Cell Host & Microbe*, *23*, 485–497.e5. https://doi.org/https://doi.org/10.1016/j.chom.2018.03.010

Langner, T., Kamoun, S., & Belhaj, K. (2018). Crispr crops: Plant genome editing toward disease resistance. *annual reviews*, *56*, 43. https://doi.org/10.1146/annurev-phyto-080417

Leeuwen, M. R. V., Smant, W., de Boer, W., & Dijksterhuis, J. (2008). Filipin is a reliable in situ marker of ergosterol in the plasma membrane of germinating conidia (spores) of penicillium discolor and stains intensively at the site of germ tube formation. *Journal of Microbiological Methods*, *74*, 64–73. https://doi.org/10.1016/j.mimet.2008.04.001

Li, L., Li, M., Yu, L., Zhou, Z., Liang, X., Liu, Z., Cai, G., Gao, L., Zhang, X., Wang, Y., Chen, S., & Zhou, J.-M. (2014). The fls2-associated kinase bik1 directly phosphorylates the nadph oxidase rbohd to control plant immunity. *Cell Host & Microbe*, *15*, 329–338. https://doi.org/https://doi.org/10.1016/j.chom.2014.02.009

Li, T., Xiao, X., Liu, Q., Li, W., Li, L., Zhang, W., Munnik, T., Wang, X., & Zhang, Q. (2023). Dynamic responses of pa to environmental stimuli imaged by a genetically encoded mobilizable fluorescent sensor. *Plant Communications*, *4*. https://doi.org/10.1016/j.xplc.2022.100500

Li, W., Song, T., Wallrad, L., Kudla, J., Wang, X., & Zhang, W. (2019). Tissue-specific accumulation of ph-sensing phosphatidic acid determines plant stress tolerance. *Nature Plants*, *5*, 1012–1021. https://doi.org/10.1038/s41477-019-0497-6

Liang, Y., Cao, Y., Tanaka, K., Thibivilliers, S., Wan, J., Choi, J., Kang, C. H., Qiu, J., & Stacey, G. (2013). Nonlegumes respond to rhizobial nod factors by suppressing the innate immune response. *Science (New York, N.Y.)*, *341*, 1384–1387. https://doi.org/10.1126/SCIENCE.1242736

Limpens, E., Zeijl, A. V., & Geurts, R. (2015). Lipochitooligosaccharides modulate plant host immunity to enable endosymbioses. *Annual review of phytopathology*, *53*, 311–334. https://doi.org/10.1146/ANNUREV-PHYTO-080614-120149

Liu, H., Lu, X., Li, M., Lun, Z., Yan, X., Yin, C., Yuan, G., Wang, X., Liu, N., Liu, D., Wu, M., Luo, Z., Zhang, Y., Bhadauria, V., Yang, J., Talbot, N. J., & Peng, Y.-L. (2023). Plant immunity suppression by an exo-β-1,3-glucanase and an elongation factor 1α of the rice blast fungus. *nature communications*. https://doi.org/10.1038/s41467-023-41175-z

Liu, L., Kloepper, J. W., & Tuzun, S. (1995). Induction of systemic resistance in cucumber against fusarium wilt by plant growth-promoting rhizobacteria. *Phytopathology*, *85*, 695–698. https://doi.org/10.1094/PHYTO-85-695

Liu, Y., Esposto, D., Mahdi, L. K., Porzel, A., Stark, P., Hussain, H., Scherr-Henning, A., Isfort, S., Bathe, U., Acosta, I. F., Zuccaro, A., Balcke, G. U., & Tissier, A. (2024). Hordedane diterpenoid phytoalexins restrict fusarium graminearum infection but enhance bipolaris sorokiniana colonization of barley roots. *Molecular Plant*, *17*, 1307–1327. https://doi.org/10.1016/J.MOLP.2024.07.006

Lopez-Gomez, M., Sandal, N., Stougaard, J., & Boller, T. (2012). Interplay of flg22-induced defence responses and nodulation in lotus japonicus. *Journal of Experimental Botany*, *63*, 393–401. https://doi.org/10.1093/JXB/ERR291

Lu, D., Wu, S., Gao, X., Zhang, Y., Shan, L., & He, P. (2010). A receptor-like cytoplasmic kinase, bik1, associates with a flagellin receptor complex to initiate plant innate immunity. *Proceedings of the National Academy of Sciences of the United States of America*, *107*, 496–501. https://doi.org/10.1073/pnas.0909705107

Lu, D., Lin, W., Gao, X., Wu, S., Cheng, C., Avila, J., Heese, A., Devarenne, T. P., He, P., & Shan, L. (2011). Direct ubiquitination of pattern recognition receptor fls2 attenuates plant innate immunity. *Science (New York, N.Y.)*, *332*, 1439–1442. https://doi.org/10.1126/SCIENCE.1204903

Lundberg, D. S., Lebeis, S. L., Paredes, S. H., Yourstone, S., Gehring, J., Malfatti, S., Tremblay, J., Engelbrektson, A., Kunin, V., Rio, T. G. D., Edgar, R. C., Eickhorst, T., Ley, R. E., Hugenholtz, P., Tringe, S. G., & Dangl, J. L. (2012). Defining the core arabidopsis thaliana root microbiome. *Nature*, *488*, 86–90. https://doi.org/10.1038/nature11237

Maekawa, M., Yang, Y., & Fairn, G. D. (2016). Perfringolysin o theta toxin as a tool to monitor the distribution and inhomogeneity of cholesterol in cellular membranes. *Toxins*, *8*. https://doi.org/10.3390/toxins8030067

Mahdi, L. K., Miyauchi, S., Uhlmann, C., Garrido-Oter, R., Langen, G., Wawra, S., Niu, Y., Guan, R., Robertson-Albertyn, S., Bulgarelli, D., Parker, J. E., & Zuccaro, A. (2022). The fungal root endophyte serendipita vermifera displays inter-kingdom synergistic beneficial effects with the microbiota in arabidopsis thaliana and barley. *ISME*, *16*, 876–889. https://doi.org/10.1038/s41396-021-01138-y

Malviya, D., Singh, U. B., Dehury, B., Singh, P., Kumar, M., Singh, S., Chaurasia, A., Yadav, M. K., Shankar, R., Roy, M., Rai, J. P., Mukherjee, A. K., Solanki, I. S., Kumar, A., Kumar, S., & Singh, H. V. (2022). Novel insights into understanding the molecular dialogues between bipolaroxin and the gα and gβ subunits of the wheat heterotrimeric

g-protein during host–pathogen interaction. *Antioxidants*, *11*. https://doi.org/10.3390/antiox11091754

Manabe, N., & Yamaguchi, Y. (2021). 3d structural insights into β-glucans and their binding proteins. *International Journal of Molecular Sciences*, *22*, 1–13. https://doi.org/10.3390/ijms22041578

Mangelsen, E., Kilian, J., Berendzen, K. W., Kolukisaoglu, Ü. H., Harter, K., Jansson, C., & Wanke, D. (2008). Phylogenetic and comparative gene expression analysis of barley (hordeum vulgare) wrky transcription factor family reveals putatively retained functions between monocots and dicots. *BMC Genomics*, *9*, 1–17. https://doi.org/10.1186/1471-2164-9-194/FIGURES/5

Mao, G., Meng, X., Liu, Y., Zheng, Z., Chen, Z., & Zhang, S. (2011). Phosphorylation of a wrky transcription factor by two pathogen-responsive mapks drives phytoalexin biosynthesis in arabidopsis. *The Plant cell*, *23*, 1639–1653. https://doi.org/10.1105/TPC.111.084996

Marcec, M. J., & Tanaka, K. (2022). Crosstalk between calcium and ros signaling during flg22-triggered immune response in arabidopsis leaves. *Plants*, *11*. https://doi.org/10.3390/plants11010014

Marcec, M. J., Gilroy, S., Poovaiah, B. W., & Tanaka, K. (2019). Mutual interplay of ca2+ and ros signaling in plant immune response. *Plant Science*, *283*, 343–354. https://doi.org/10.1016/J.PLANTSCI.2019.03.004

Marek, M., Vincenzetti, V., & Martin, S. G. (2020). Sterol biosensor reveals lam-family ltc1-dependent sterol flow to endosomes upon arp2/3 inhibition. *Journal of Cell Biology*, *219*. https://doi.org/10.1083/JCB.202001147

Martin, F., Aerts, A., Ahrén, D., Brun, A., Danchin, E. G., Duchaussoy, F., Gibon, J., Kohler, A., Lindquist, E., Pereda, V., Salamov, A., Shapiro, H. J., Wuyts, J., Blaudez, D., Buée, M., Brokstein, P., Canbäck, B., Cohen, D., Courty, P. E., ... Grigoriev, I. V. (2008). The genome of laccaria bicolor provides insights into mycorrhizal symbiosis. *Nature*, *452*, 88–92. https://doi.org/10.1038/nature06556

Martin, F., Kohler, A., Murat, C., Balestrini, R., Coutinho, P. M., Jaillon, O., Montanini, B., Morin, E., Noel, B., Percudani, R., Porcel, B., Rubini, A., Amicucci, A., Amselem, J., Anthouard, V., Arcioni, S., Artiguenave, F., Aury, J. M., Ballario, P., ... Wincker, P. (2010). Périgord black truffle genome uncovers evolutionary origins and mechanisms of symbiosis. *Nature*, *464*, 1033–1038. https://doi.org/10.1038/nature08867

Mesny, F., Bauer, M., Zhu, J., & Thomma, B. P. (2024). Meddling with the microbiota: Fungal tricks to infect plant hosts. *Current Opinion in Plant Biology*, *82*, 102622. https://doi.org/10.1016/J.PBI.2024.102622

Mikiciuk, G., Miller, T., Kisiel, A., Cembrowska-Lech, D., Mikiciuk, M., Łobodzińska, A., & Bokszczanin, K. (2024). Harnessing beneficial microbes for drought tolerance: A review of ecological and agricultural innovations. *Agriculture (Switzerland)*, *14*. https://doi.org/10.3390/agriculture14122228

Mizuno, H., Abe, M., Dedecker, P., Makino, A., Rocha, S., Ohno-Iwashita, Y., Hofkens, J., Kobayashi, T., & Miyawaki, A. (2011). Fluorescent probes for superresolution imaging

of lipid domains on the plasma membrane. *Chemical Science*, *2*, 1548–1553. https://doi.org/10.1039/c1sc00169h

Monaghan, J., Matschi, S., Shorinola, O., Rovenich, H., Matei, A., Segonzac, C., Malinovsky, F. G., Rathjen, J. P., MacLean, D., Romeis, T., & Zipfel, C. (2014). The calcium-dependent protein kinase cpk28 buffers plant immunity and regulates bik1 turnover. *Cell Host & Microbe*, *16*, 605–615. https://doi.org/https://doi.org/10.1016/j.chom.2014.10.007

Nakatsu, F., & Kawasaki, A. (2021, June). Functions of oxysterol-binding proteins at membrane contact sites and their control by phosphoinositide metabolism. https://doi.org/10.3389/fcell.2021.664788

Nars, A., Lafitte, C., Chabaud, M., Drouillard, S., Mélida, H., Danoun, S., Costaouëc, T. L., Rey, T., Benedetti, J., Bulone, V., Barker, D. G., Bono, J. J., Dumas, B., Jacquet, C., Heux, L., Fliegmann, J., & Bottin, A. (2013). Aphanomyces euteiches cell wall fractions containing novel glucan-chitosaccharides induce defense genes and nuclear calcium oscillations in the plant host medicago truncatula. *PLOS ONE*, *8*, e75039. https://doi.org/10.1371/JOURNAL.PONE.0075039

Ngou, B. P. M., Ahn, H. K., Ding, P., & Jones, J. D. (2021). Mutual potentiation of plant immunity by cell-surface and intracellular receptors. *Nature*, *592*, 110–115. https://doi.org/10.1038/s41586-021-03315-7

Ngou, B. P. M., Ding, P., & Jones, J. D. (2022). Thirty years of resistance: Zig-zag through the plant immune system. *Plant Cell*, *34*, 1447–1478. https://doi.org/10.1093/plcell/koac041

Nguyen, Q. M., Iswanto, A. B. B., Son, G. H., & Kim, S. H. (2021). Recent advances in effector-triggered immunity in plants: New pieces in the puzzle create a different paradigm. *International Journal of Molecular Sciences*, *22*. https://doi.org/10.3390/ijms22094709

Nishad, R., Ahmed, T., Rahman, V. J., & Kareem, A. (2020). Modulation of plant defense system in response to microbial interactions. *Frontiers in Microbiology*, *11*. https://doi.org/10.3389/fmicb.2020.01298

Nizam, S., Qiang, X., Wawra, S., Nostadt, R., Getzke, F., Schwanke, F., Dreyer, I., Langen, G., & Zuccaro, A. (2019). Serendipita indica e5nt modulates extracellular nucleotide levels in the plant apoplast and affects fungal colonization. *EMBO reports*, *20*. https://doi.org/10.15252/embr.201847430

Noack, L. C., & Jaillais, Y. (2020). Functions of anionic lipids in plants. *Annual Review of Plant Biology*. https://doi.org/10.1146/annurev-arplant-081519

Okobira, T., Miyoshi, K., Uezu, K., Sakurai, K., & Shinkai, S. (2008). Molecular dynamics studies of side chain effect on the β-1,3-d-glucan triple helix in aqueous solution. *Biomacromolecules*, *9*, 783–788. https://doi.org/10.1021/bm700511d

Oliveira-Garcia, E., Tamang, T. M., Park, J., Dalby, M., Martin-Urdiroz, M., Herrero, C. R., Vu, A. H., Park, S., Talbot, N. J., & Valent, B. (2023). Clathrin-mediated endocytosis facilitates the internalization of magnaporthe oryzae effectors into rice cells. *Plant Cell*, *35*, 2527–2551. https://doi.org/10.1093/plcell/koad094

Park, C. J., Peng, Y., Chen, X., Dardick, C., Ruan, D. L., Bart, R., Canlas, P. E., & Ronald, P. C. (2008). Rice xb15, a protein phosphatase 2c, negatively regulates cell death and

xa21-mediated innate immunity. *PLoS biology*, *6*, 1910–1926. https://doi.org/10.1371/JOURNAL.PBIO.0060231

Pham, A. Q., Cho, S. H., Nguyen, C. T., & Stacey, G. (2020). Arabidopsis lectin receptor kinase p2k2 is a second plant receptor for extracellular atp and contributes to innate immunity. *Plant Physiology*, *183*, 1364–1375. https://doi.org/10.1104/pp.19.01265

Pieterse, C. M., Does, D. V. D., Zamioudis, C., Leon-Reyes, A., & Wees, S. C. V. (2012). Hormonal modulation of plant immunity. *Annual review of cell and developmental biology*, *28*, 489–521. https://doi.org/10.1146/ANNUREV-CELLBIO-092910-154055

Pieterse, C. M., Zamioudis, C., Berendsen, R. L., Weller, D. M., Wees, S. C. V., & Bakker, P. A. (2014). Induced systemic resistance by beneficial microbes. *Annual Review of Phytopathology*, *52*, 347–375. https://doi.org/10.1146/annurev-phyto-082712-102340

Plett, J. M., & Plett, K. L. (2022). Leveraging genomics to understand the broader role of fungal small secreted proteins in niche colonization and nutrition. *ISME Communications*, *2*. https://doi.org/10.1038/s43705-022-00139-y

Pluvinage, B., Fillo, A., Massel, P., & Boraston, A. B. (2017). Structural analysis of a family 81 glycoside hydrolase implicates its recognition of β-1,3-glucan quaternary structure. *Structure*, *25*, 1348–1359.e3. https://doi.org/10.1016/j.str.2017.06.019

Potocký, M., Pleskot, R., Pejchar, P., Vitale, N., Kost, B., & Žárský, V. (2014). Live-cell imaging of phosphatidic acid dynamics in pollen tubes visualized by spo20p-derived biosensor. *New Phytologist*, *203*, 483–494. https://doi.org/10.1111/nph.12814

Presti, L. L., Lanver, D., Schweizer, G., Tanaka, S., Liang, L., Tollot, M., Zuccaro, A., Reissmann, S., & Kahmann, R. (2015). Fungal effectors and plant susceptibility. *Annual Review of Plant Biology*, *66*, 513–545. https://doi.org/10.1146/ANNUREV-ARPLANT-043014-114623

Pruitt, R. N., Gust, A. A., & Nürnberger, T. (2021). Plant immunity unified. *Nature Plants*, *7*, 382–383. https://doi.org/10.1038/s41477-021-00903-3

Qader, M. M., Kumar, N. S., Jayasinghe, L., Araya, H., & Fujimoto, Y. (2017). Bioactive sesquiterpenes from an endophytic fungus bipolaris sorokiniana isolated from a popular medicinal plant costus speciosus. *Mycology*, *8*, 17–20. https://doi.org/10.1080/21501203.2016.1269844

Qi, F., Li, J., Ai, Y., Shangguan, K., Li, P., Lin, F., & Liang, Y. (2024). Dgk5β-derived phosphatidic acid regulates ros production in plant immunity by stabilizing nadph oxidase. *Cell Host and Microbe*, 1–16. https://doi.org/10.1016/j.chom.2024.01.011

Qin, L., Zhou, Z., Li, Q., Zhai, C., Liu, L., Quilichini, T. D., Gao, P., Kessler, S. A., Jaillais, Y., Datla, R., Peng, G., Xiang, D., & Wei, Y. (2020). Specific recruitment of phosphoinositide species to the plant-pathogen interfacial membrane underlies arabidopsis susceptibility to fungal infection. *Plant Cell*, *32*, 1665–1688. https://doi.org/10.1105/tpc.19.00970

Qiu, J. L., Fiil, B. K., Petersen, K., Nielsen, H. B., Botanga, C. J., Thorgrimsen, S., Palma, K., Suarez-Rodriguez, M. C., Sandbech-Clausen, S., Lichota, J., Brodersen, P., Grasser, K. D., Mattsson, O., Glazebrook, J., Mundy, J., & Petersen, M. (2008). Arabidopsis map kinase 4 regulates gene expression through transcription factor release in the nucleus.

EMBO Journal, *27*, 2214–2221. https://doi.org/10.1038/EMBOJ.2008.147/SUPPL_FILE/EMBJ2008147-SUP-0001.PDF

Qiu, S., & Zeng, B. (2019, June). Advances in understanding of the oxysterol-binding protein homologous in yeast and filamentous fungi. https://doi.org/10.1007/s10123-019-00056-6

Ramachandran, P., J., B. J., Maupin-Furlow, J. A., & Uthandi, S. (2021). Bacterial effectors mimicking ubiquitin-proteasome pathway tweak plant immunity. *Microbiological Research*, *250*, 126810. https://doi.org/10.1016/J.MICRES.2021.126810

Ristaino, J. B., Anderson, P. K., Bebber, D. P., Brauman, K. A., Cunniffe, N. J., Fedoroff, N. V., Finegold, C., Garrett, K. A., Gilligan, C. A., Jones, C. M., Martin, M. D., Macdonald, G. K., Neenan, P., Records, A., Schmale, D. G., Tateosian, L., & Wei, Q. (2021). The persistent threat of emerging plant disease pandemics to global food security. *PNAS*, *118*. https://doi.org/10.1073/pnas.2022239118/-/DCSupplemental

Robatzek, S., Chinchilla, D., & Boller, T. (2006). Ligand-induced endocytosis of the pattern recognition receptor fls2 in arabidopsis. *Genes and Development*, *20*, 537–542. https://doi.org/10.1101/gad.366506

Rodrigues, M. L., Nimrichter, L., Oliveira, D. L., Frases, S., Miranda, K., Zaragoza, O., Alvarez, M., Nakouzi, A., Feldmesser, M., & Casadevall, A. (2007). Vesicular polysaccharide export in cryptococcus neoformans is a eukaryotic solution to the problem of fungal trans-cell wall transport. *Eukaryotic Cell*, *6*, 48–59. https://doi.org/10.1128/EC.00318-06

Rushton, P. J., Somssich, I. E., Ringler, P., & Shen, Q. J. (2010). Wrky transcription factors. *Trends in Plant Science*, *15*, 247–258. https://doi.org/10.1016/J.TPLANTS.2010.02.006

Saravanan, R. S., Slabaugh, E., Singh, V. R., Lapidus, L. J., Haas, T., & Brandizzi, F. (2009). The targeting of the oxysterol-binding protein orp3a to the endoplasmic reticulum relies on the plant vap33 homolog pva12. *Plant Journal*, *58*, 817–830. https://doi.org/10.1111/j.1365-313X.2009.03815.x

Sarkar, D., Rovenich, H., Jeena, G., Nizam, S., Tissier, A., Balcke, G. U., Mahdi, L. K., Bonkowski, M., Langen, G., & Zuccaro, A. (2019). The inconspicuous gatekeeper: Endophytic serendipita vermifera acts as extended plant protection barrier in the rhizo-sphere. *New Phytologist*, *224*, 886–901. https://doi.org/10.1111/nph.15904

Scheidle, H., Groß, A., & Niehaus, K. (2005). The lipid a substructure of the sinorhizobium meliloti lipopolysaccharides is sufficient to suppress the oxidative burst in host plants. *The New phytologist*, *165*, 559–566. https://doi.org/10.1111/J.1469-8137.2004.01214.X

Schlaeppi, K., & Bulgarelli, D. (2015). The plant microbiome at work. *Molecular Plant-Microbe Interactions*, *28*, 212–217. https://doi.org/10.1094/MPMI-10-14-0334-FI

Segonzac, C., Macho, A. P., Sanmartín, M., Ntoukakis, V., Sánchez-Serrano, J. J., & Zipfel, C. (2014). Negative control of bak1 by protein phosphatase 2a during plant innate immunity. *The EMBO journal*, *33*, 2069–2079. https://doi.org/10.15252/EMBJ.201488698

Seo, H., Kim, J. H., Lee, S. M., & Lee, S. W. (2024). The plant-associated flavobacterium: A hidden helper for improving plant health. *Plant Pathology Journal*, *40*, 251–260. https://doi.org/10.5423/PPJ.RW.01.2024.0019

Sezgin, E., Can, F. B., Schneider, F., Clausen, M. P., Galiani, S., Stanly, T. A., Waithe, D., Colaco, A., Honigmann, A., Wüstner, D., Platt, F., & Eggeling, C. (2016). A comparative

study on fluorescent cholesterol analogs as versatile cellular reporters. *Journal of Lipid Research*, *57*, 299–309. https://doi.org/10.1194/jlr.M065326

Shaw, A. S., Kornev, A. P., Hu, J., Ahuja, L. G., & Taylor, S. S. (2014). Kinases and pseudokinases: Lessons from raf. *Molecular and Cellular Biology*, *34*, 1538. https://doi.org/10.1128/MCB.00057-14

Shen, Q.-H., Saijo, Y., Mauch, S., Biskup, C., Bieri, S., Keller, B., Seki, H., Ülker, B., Somssich, I. E., & Schulze-Lefert, P. (2007). Nuclear activity of mla immune receptors links isolate-specific and basal disease-resistance responses. *23 FEBRUARY*, *315*. www.sciencemag.org

Shukla, P., Skea, J., Slade, R., van Diemen, R., Haughey, E., Malley, J., Pathak, M., Pereira, J. P., & (eds.) (2019). Technical summary. *IPCC Special Report on Climate Change and Land*, 37–74. https://doi.org/10.1017/9781009157988.002

Siebers, M., Brands, M., Wewer, V., Duan, Y., Hölzl, G., & Dörmann, P. (2016). Lipids in plant–microbe interactions. *Biochimica et Biophysica Acta - Molecular and Cell Biology of Lipids*, *1861*, 1379–1395. https://doi.org/10.1016/j.bbalip.2016.02.021

Silipo, A., Erbs, G., Shinya, T., Dow, J. M. M., Parrilli, M., Lanzetta, R., Shibuya, N., Newman, M. A., & Molinaro, A. (2010). Glyco-conjugates as elicitors or suppressors of plant innate immunity. *Glycobiology*, *20*, 406–419. https://doi.org/10.1093/GLYCOB/CWP201

Simon, M. L. A., Platre, M. P., Assil, S., Wijk, R. V., Chen, W. Y., Chory, J., Dreux, M., Munnik, T., & Jaillais, Y. (2014). A multi-colour/multi-affinity marker set to visualize phosphoinositide dynamics in arabidopsis. *Plant Journal*, *77*, 322–337. https://doi.org/10.1111/tpj.12358

Singh, B. K., Delgado-Baquerizo, M., Egidi, E., Guirado, E., Leach, J. E., Liu, H., & Trivedi, P. (2023). Climate change impacts on plant pathogens, food security and paths forward. *Nature Reviews Microbiology*, *21*, 640–656. https://doi.org/10.1038/s41579-023-00900-7

Smith, J. M., Salamango, D. J., Leslie, M. E., Collins, C. A., & Heese, A. (2014). Sensitivity to flg22 is modulated by ligand-induced degradation and de novo synthesis of the endogenous flagellin-receptor flagellin-sensing2. *Plant Physiology*, *164*, 440–454. https://doi.org/10.1104/pp.113.229179

Stefan, C. J., Manford, A. G., Baird, D., Yamada-Hanff, J., Mao, Y., & Emr, S. D. (2011). Osh proteins regulate phosphoinositide metabolism at er-plasma membrane contact sites. *Cell*, *144*, 389–401. https://doi.org/10.1016/j.cell.2010.12.034

Sun, C., Shao, Y., Vahabi, K., Lu, J., Bhattacharya, S., Dong, S., Yeh, K.-W., Sherameti, I., Lou, B., Baldwin, I. T., & Oelmüller, R. (2014). The beneficial fungus piriformospora indica protects arabidopsis from verticillium dahliae infection by downregulation plant defense responses. *BMC Plant Biology*. http://www.biomedcentral.com/1471-2229/14/268

Sun, Y., Li, L., Macho, A. P., Han, Z., Hu, Z., Zipfel, C., Zhou, J.-M., & Chai, J. (2013). Structural basis for flg22-induced activation of the arabidopsis fls2-bak1 immune complex. *Science*, *342*, 624–628. https://doi.org/10.1126/science.1243768

Tanaka, S., Han, X., & Kahmann, R. (2015). Microbial effectors target multiple steps in the salicylic acid production and signaling pathway. *Frontiers in Plant Science*, *6*, 1–10. https://doi.org/10.3389/FPLS.2015.00349/BIBTEX

Thoms, D., Liang, Y., & Haney, C. H. (2021). Maintaining symbiotic homeostasis: How do plants engage with beneficial microorganisms while at the same time restricting pathogens? *Molecular Plant-Microbe Interactions*, *34*, 462–469. https://doi.org/10.1094/MPMI-11-20-0318-FI/ASSET/IMAGES/LARGE/MPMI-11-20-0318-FIF2-1623661352128.JPEG

Thor, K., Jiang, S., Michard, E., George, J., Scherzer, S., Huang, S., Dindas, J., Derbyshire, P., Leitão, N., DeFalco, T. A., Köster, P., Hunter, K., Kimura, S., Gronnier, J., Stransfeld, L., Kadota, Y., Bücherl, C. A., Charpentier, M., Wrzaczek, M., ... Zipfel, C. (2020). The calcium-permeable channel osca1.3 regulates plant stomatal immunity. *Nature*, *585*, 569–573. https://doi.org/10.1038/s41586-020-2702-1

Tian, H., Wu, Z., Chen, S., Ao, K., Huang, W., Yaghmaiean, H., Sun, T., Xu, F., Zhang, Y., Wang, S., Li, X., & Zhang, Y. (2021). Activation of tir signalling boosts pattern-triggered immunity. *Nature*, *598*, 500–503. https://doi.org/10.1038/s41586-021-03987-1

Tian, W., Hou, C., Ren, Z., Wang, C., Zhao, F., Dahlbeck, D., Hu, S., Zhang, L., Niu, Q., Li, L., Staskawicz, B. J., & Luan, S. (2019). A calmodulin-gated calcium channel links pathogen patterns to plant immunity. *Nature*, *572*, 131–135. https://doi.org/10.1038/s41586-019-1413-y

Tiemblo-Martín, M., Pistorio, V., Saake, P., Mahdi, L., Campanero-Rhodes, M. A., Girolamo, R. D., Carluccio, C. D., Marchetti, R., Molinaro, A., Solís, D., Zuccaro, A., & Silipo, A. (2024). Structure and properties of the exopolysaccharide isolated from flavobacterium sp. root935. *Carbohydrate Polymers*, *343*, 122433. https://doi.org/10.1016/J.CARBPOL.2024.122433

Todd, J. N. A., Carreón-Anguiano, K. G., Islas-Flores, I., & Canto-Canché, B. (2022). Microbial effectors: Key determinants in plant health and disease. *Microorganisms*, *10*, 1980. https://doi.org/10.3390/MICROORGANISMS10101980

Trujillo, M., Ichimura, K., Casais, C., & Shirasu, K. (2008). Negative regulation of pamp-triggered immunity by an e3 ubiquitin ligase triplet in arabidopsis. *Current biology*, *18*, 1396–1401. https://doi.org/10.1016/J.CUB.2008.07.085

Ukawa, T., Banno, F., Ishikawa, T., Kasahara, K., Nishina, Y., Inoue, R., Tsujii, K., Yamaguchi, M., Takahashi, T., Fukao, Y., Kawai-Yamada, M., & Nagano, M. (2022). Sphingolipids with 2-hydroxy fatty acids aid in plasma membrane nanodomain organization and oxidative burst. *Plant Physiology*, *189*, 839. https://doi.org/10.1093/PLPHYS/KIAC134

van Boerdonk, S., Saake, P., Wanke, A., Neumann, U., & Zuccaro, A. (2024). β-glucan-binding proteins are key modulators of immunity and symbiosis in mutualistic plant–microbe interactions. *Current Opinion in Plant Biology*, *81*, 102610. https://doi.org/10.1016/J.PBI.2024.102610

Vanacore, A., Vitiello, G., Wanke, A., Cavasso, D., Clifton, L. A., Mahdi, L., Campanero-Rhodes, M. A., Solís, D., Wuhrer, M., Nicolardi, S., Molinaro, A., Marchetti, R., Zuccaro, A., Paduano, L., & Silipo, A. (2022). Lipopolysaccharide o-antigen molecular and supramolecular modifications of plant root microbiota are pivotal for host recognition. *Carbohydrate Polymers*, *277*, 118839. https://doi.org/10.1016/J.CARBPOL.2021.118839

Vargas, G., Rocha, J. D., Oliveira, D. L., Albuquerque, P. C., Frases, S., Santos, S. S., Nosanchuk, J. D., Gomes, A. M. O., Medeiros, L. C., Miranda, K., Sobreira, T. J., Nakayasu, E. S.,

Arigi, E. A., Casadevall, A., Guimaraes, A. J., Rodrigues, M. L., Freire-de-Lima, C. G., Almeida, I. C., & Nimrichter, L. (2015). Compositional and immunobiological analyses of extracellular vesicles released by candida albicans. *Cellular Microbiology*, *17*, 389–407. https://doi.org/10.1111/CMI.12374/SUPPINFO

Waller, F., Achatz, B., Baltruschat, H., zsef Fodor, J., Becker, K., Fischer, M., Heier, T., ckelhoven, R. H., Neumann, C., von Wettstein, D., Franken, P., & Kogel, K.-H. (2005). The endophytic fungus piriformospora indica reprograms barley to salt-stress tolerance, disease resistance, and higher yield. *PNAS*. www.pnas.orgcgidoi10.1073pnas.0504423102

Wang, H., Liu, Y. M., Qi, Z. M., Wang, S. Y., Liu, S. X., Li, X., Wang, H. J., & Xia, X. C. (2013). An overview on natural polysaccharides with antioxidant properties. *Current Medicinal Chemistry*, *20*, 2899–2913.

Wang, L., Li, H., Lv, X., Chen, T., Li, R., Xue, Y., Jiang, J., Jin, B., Baluška, F., Šamaj, J., Wang, X., & Lin, J. (2015). Spatiotemporal dynamics of the bri1 receptor and its regulation by membrane microdomains in living arabidopsis cells. *Molecular Plant*, *8*, 1334–1349. https://doi.org/10.1016/j.molp.2015.04.005

Wang, L., Xue, Y., Xing, J., Song, K., & Lin, J. (2024). Exploring the spatiotemporal organization of membrane proteins in living plant cells. *Annual Review of Plant Biology*, *12*, 16. https://doi.org/10.1146/annurev-arplant-042817

Wanke, A., Rovenich, H., Schwanke, F., Velte, S., Becker, S., Hehemann, J. H., Wawra, S., & Zuccaro, A. (2020). Plant species-specific recognition of long and short β-1,3-linked glucans is mediated by different receptor systems. *Plant Journal*, *102*, 1142–1156. https://doi.org/10.1111/tpj.14688

Wanke, A., Malisic, M., Wawra, S., & Zuccaro, A. (2021). Unraveling the sugar code: The role of microbial extracellular glycans in plant-microbe interactions. *Journal of Experimental Botany*, *72*, 15–35. https://doi.org/10.1093/jxb/eraa414

Wanke, A., van Boerdonk, S., Mahdi, L. K., Wawra, S., Neidert, M., Chandrasekar, B., Saake, P., Saur, I. M., Derbyshire, P., Holton, N., Menke, F. L., Brands, M., Pauly, M., Acosta, I. F., Zipfel, C., & Zuccaro, A. (2023). A gh81-type β-glucan-binding protein enhances colonization by mutualistic fungi in barley. *Current Biology*, *33*, 5071–5084.e7. https://doi.org/10.1016/J.CUB.2023.10.048

Wawra, S., Fesel, P., Widmer, H., Timm, M., Seibel, J., Leson, L., Kesseler, L., Nostadt, R., Hilbert, M., Langen, G., & Zuccaro, A. (2016). The fungal-specific β-glucan-binding lectin fgb1 alters cell-wall composition and suppresses glucan-triggered immunity in plants. *Nature Communications*, *7*, 1–11. https://doi.org/10.1038/ncomms13188

Wawra, S., Fesel, P., Widmer, H., Neumann, U., Lahrmann, U., Becker, S., Hehemann, J. H., Langen, G., & Zuccaro, A. (2019). Fgb1 and wsc3 are in planta-induced β-glucan-binding fungal lectins with different functions. *New Phytologist*, *222*, 1493–1506. https://doi.org/10.1111/nph.15711

Wei, G., JosephW., K., & Tuzun, S. (1991). Induction of systemic resistance of cucumber to colletotrichum orbiculare by select strains of plant growth-promoting rhizobacteria. *Phytopathology*, *81*, 1508–1512.

Weiß, M., Waller, F., Zuccaro, A., & Selosse, M.-A. (2016). Sebacinales-one thousand and one interactions with land plants. *New Phytologist*. https://doi.org/10.1111/nph.13977

Wewer, V., Brands, M., & Dörmann, P. (2014). Fatty acid synthesis and lipid metabolism in the obligate biotrophic fungus rhizophagus irregularis during mycorrhization of lotus japonicus. *The Plant Journal*, *79*, 398–412. https://doi.org/10.1111/TPJ.12566

Whitman, W. B., & Trust, B. M. (2015). *Bergey's manual of systematics of archaea and bacteria*. Wiley. https://doi.org/10.1002/9781118960608

Wippel, K., Tao, K., Niu, Y., Zgadzaj, R., Kiel, N., Guan, R., Dahms, E., Zhang, P., Jensen, D. B., Logemann, E., Radutoiu, S., Schulze-Lefert, P., & Garrido-Oter, R. (2021). Host preference and invasiveness of commensal bacteria in the lotus and arabidopsis root microbiota. *Nature Microbiology*, *6*, 1150–1162. https://doi.org/10.1038/s41564-021-00941-9

Wong, J. E., Gysel, K., Birkefeldt, T. G., Vinther, M., Muszyński, A., Azadi, P., Laursen, N. S., Sullivan, J. T., Ronson, C. W., Stougaard, J., & Andersen, K. R. (2020). Structural signatures in epr3 define a unique class of plant carbohydrate receptors. *Nature Communications*, *11*. https://doi.org/10.1038/s41467-020-17568-9

Xing, J., Li, X., Wang, X., Lv, X., Wang, L., Zhang, L., Zhu, Y., Shen, Q., Baluska, F., Samaj, J., & Lin, J. (2019). Secretion of phospholipase dδ functions as a regulatory mechanism in plant innate immunity. *The Plant Cell*, *31*, 3015–3032. https://doi.org/10.1105/tpc.19.00534

Xing, J., Zhang, L., Duan, Z., & Lin, J. (2021). Coordination of phospholipid-based signaling and membrane trafficking in plant immunity. *Trends in Plant Science*, *26*, 407–420. https://doi.org/10.1016/j.tplants.2020.11.010

Xu, G., Moeder, W., Yoshioka, K., & Shan, L. (2022). A tale of many families: Calcium channels in plant immunity. *The Plant Cell*, *34*, 1551. https://doi.org/10.1093/PLCELL/KOAC033

Xu, X., Bittman, R., Duportail, G., Heissler, D., Vilcheze, C., & London, E. (2001). Effect of the structure of natural sterols and sphingolipids on the formation of ordered sphingolipid/sterol domains (rafts). *Journal of Biological Chemistry*, *276*, 33540–33546. https://doi.org/10.1074/JBC.M104776200

Yi, S. Y., Shirasu, K., Moon, J. S., Lee, S. G., & Kwon, S. Y. (2014). The activated sa and ja signaling pathways have an influence on flg22-triggered oxidative burst and callose deposition. *PLOS ONE*, *9*, e88951. https://doi.org/10.1371/JOURNAL.PONE.0088951

Yu, D., Fan, R., Zhang, L., Xue, P., Liao, L., Hu, M., Cheng, Y., Li, J., Qi, T., Jing, S., Wang, Q., Bhatt, A., & Shen, Q. H. (2023). Hvwrky2 acts as an immunity suppressor and targets hvcebip to regulate powdery mildew resistance in barley. *The Crop Journal*, *11*, 99–107. https://doi.org/10.1016/J.CJ.2022.05.010

Yu, H., Bai, F., Ji, C., Fan, Z., Luo, J., Ouyang, B., Deng, X., Xiao, S., Bisseling, T., Limpens, E., & Pan, Z. (2023). Plant lysin motif extracellular proteins are required for arbuscular mycorrhizal symbiosis. *Proceedings of the National Academy of Sciences of the United States of America*, *120*. https://doi.org/10.1073/pnas.2301884120

Yu, M., Liu, H., Dong, Z., Xiao, J., Su, B., Fan, L., Komis, G., Šamaj, J., Lin, J., & Li, R. (2017). The dynamics and endocytosis of flot1 protein in response to flg22 in arabidopsis. *Journal of Plant Physiology*, *215*, 73–84. https://doi.org/10.1016/j.jplph.2017.05.010

Yuan, M., Ngou, B. P. M., Ding, P., & Xin, X. F. (2021). Pti-eti crosstalk: An integrative view of plant immunity. *Current Opinion in Plant Biology*, *62*, 102030. https://doi.org/10.1016/J.PBI.2021.102030

Zamioudis, C., & Pieterse, C. M. J. (2012). Modulation of host immunity by beneficial microbes. *MPMI*, *25*, 139–150. https://doi.org/10.1094/MPMI

Zeqiraj, E., & van Aalten, D. M. (2010). Pseudokinases-remnants of evolution or key allosteric regulators? *Current Opinion in Structural Biology*, *20*, 772–781. https://doi.org/10.1016/J.SBI.2010.10.001

Zhang, J., Sun, J., Chiu, C. H., Landry, D., Li, K., Wen, J., Mysore, K. S., Fort, S., Lefebvre, B., Oldroyd, G. E., & Feng, F. (2024). A receptor required for chitin perception facilitates arbuscular mycorrhizal associations and distinguishes root symbiosis from immunity. *Current biology*, *34*, 1705–1717.e6. https://doi.org/10.1016/J.CUB.2024.03.015

Zipfel, C., & Oldroyd, G. E. (2017). Plant signalling in symbiosis and immunity. *Nature*, *543*, 328–336. https://doi.org/10.1038/nature22009

Acknowledgements

First of all, I want to thank Prof Dr. Alga Zuccaro for the opportunity to do my PhD in her group on the exciting topic of beneficial plant-microbe interactions but also for the great guidance and support throughout the last four years, helping me to advance as a scientist and also personally.

I want to thank Prof. Dr. Oliver Ebenhöh and Prof. Dr. Gabriel Schaaf for the valuable discussions and great feedback and support throughout my PhD as members of my thesis advisory committee.

I want to thank Prof. Dr. Bart Thomma and Prof. Dr. Jan Riemer for being part of my thesis defense committee.

I want to thank all my collaborators who supported the work performed in the context of this thesis, especially Dr. Philipp Westhoff (and his great team of TAs), Dr. Hirofumi Nakagami, Dr. Sara Stolze, Dr. Götz Hensel, Dr. Gerd Balcke, Prof. Dr. Cyril Zipfel and Prof. Dr. Alba Silipo.

I want to thank CEPLAS for giving me the chance to do my PhD in such a thriving and supporting scientific network. I am very thankful that I got the chance to be part of this great initiative and meet many great scientists, collaborators and friends. A big thank you goes to the CEPLAS Office, especially Nadine, for helping me with any questions and administrative tasks making my life much easier. A very big thank you also to my whole CEPLAS Graduate School cohort and especially Laura and Daniel.

A big thank you also to the neighbouring working groups, AG Bucher, AG Thomma, AG Höcker, AG Kopriva, AG Döhlemann for the collaborative and supportive work environment.

A big thank you goes to all current and former Bambinis for a really great working environment and all the helpful scientific discussions and collaborations, but most importantly for making work fun. Thanks for all the nights at Stiefel, singing Karaoke, ice skating, trips to the swimming pool, hiking trips, Karneval parties...

A special thank you to Alan Wanke for the great support during my first year even when you were already in Cambridge. For teaching me how to do ROS and Calcium assays and introducing me to β-glucans. It was a lot of fun to work with you!

Many thanks also go to Asmamaw for supporting me with my experiments so many times.

A very big thank you also to Patricia, Sarah and Sena for being not only colleagues but very good friends and always being there for me!

A big thank you also to Ruben for always helping me and being the best Karaoke partner.

A very big, if not the biggest, thank you goes to Mathias Brands, for showing me that lipids are cool and supporting me at every step of my PhD! Thank you for answering all my stupid questions and all the way too long discussions how we can do an experiment the best way ;) Thanks for being a great Lipid Team partner and a good friend!

I want to thank the best Boulder-Crew for all the fun evenings we spent and will spend together!

A very big thank you goes to my family, especially my parents, who always support me at every step of the way.

Finally, I want to thank Martin for getting through all ups and downs in the last four years with me and always having my back. Thank you so much for your love and support.

Erklärung zur Dissertation

gemäß der Promotionsordnung vom 12. März 2020

Hiermit versichere ich an Eides statt, dass ich die vorliegende Dissertation selbstständig und ohne die Benutzung anderer als der angegebenen Hilfsmittel und Literatur angefertigt habe. Alle Stellen, die wörtlich oder sinngemäß aus veröffentlichten und nicht veröffentlichten Werken dem Wortlaut oder dem Sinn nach entnommen wurden, sind als solche kenntlich gemacht. Ich versichere an Eides statt, dass diese Dissertation noch keiner anderen Fakultät oder Universität zur Prüfung vorgelegen hat; dass sie - abgesehen von unten angegebenen Teilpublikationen und eingebundenen Artikeln und Manuskripten - noch nicht veröffentlicht worden ist sowie, dass ich eine Veröffentlichung der Dissertation vor Abschluss der Promotion nicht ohne Genehmigung des Promotionsausschusses vornehmen werde. Die Bestimmungen dieser Ordnung sind mir bekannt. Darüber hinaus erkläre ich hiermit, dass ich die Ordnung zur Sicherung guter wissenschaftlicher Praxis und zum Umgang mit wissenschaftlichem Fehlverhalten der Universität zu Köln gelesen und sie bei der Durchführung der Dissertation zugrundeliegenden Arbeiten und der schriftlich verfassten Dissertation beachtet habe und verpflichte mich hiermit, die dort genannten Vorgaben bei allen wissenschaftlichen Tätigkeiten zu beachten und umzusetzen. Ich versichere, dass die eingereichte elektronische Fassung der eingereichten Druckfassung vollständig entspricht.

Teilpublikationen: siehe Publications (Seite iv)

Köln, January 13, 2025	Pia Saake
City & Date	Pia Saake

Appendix

Table S1: Detailed information and references for MAMP/DAMP-PRR pairs depicted in Figure 2

MAMP	origin (organism)	biomolecule class	PRR	PRR Type	co-receptor kinase	RLCK	References
flagellin / flg22	bacteria	protein	*At*FLS2 *Nb*FLS2 *Os*FLS2 *Vv*FLS2	LRR	*At*BAK1	*At*BIK1, *At*PBL1, *At*BSK1m, *At*PBL39, *At*PBL40, *At*PBL13, *At*RLCK-VII-5, *At*RLCK-VII-7, *At*PBL19	*At*: (Gómez-Gómez & Boller, 2000; Robatzek *et al.*, 2006; Boller & Felix, 2009) *Nb*:(Hann & Rathjen, 2007) *Os*:(Takai *et al.*, 2008) *Vv*: (Trdá *et al.*, 2014)
EF-Tu (elf18)	bacteria	protein	*At*EFR	LRR	*At*BAK1	*At*BIK1, *At*PBL1, *At*BSK1m, *At*PBL39, *At*PBL40, *At*PBL13, *At*RLCK-VII-5, *At*RLCK-VII-7, *At*PBL19	(Kunze *et al.*, 2004; Zipfel *et al.*, 2006)
Xanthine/ uracil permease (xup25)	bacteria	protein	*At*XPS1	LRR			(Mott *et al.*, 2016)
IF1	bacteria	protein	*At*RLP32 (RLP), *At*SOBIR1	LRR	*At*BAK1		(Fan *et al.*, 2022)
eMax	bacteria	protein	*At*RLP1/ ReMAX (RLP); *At*SOBIR1	LRR			(Jehle *et al.*, 2013)
Flagellin (flgII-28	bacteria	protein	*Sl*FLS3	LRR			(Hind *et al.*, 2016)
csp22	bacteria	protein	*Sl*CORE, *Nb*CSPR, *Nb*CORE	LRR	*Nb*BAK1		(Saur *et al.*, 2016; Wang *et al.*, 2016; Wei *et al.*, 2018; Dodds *et al.*, 2023)
RaxX	bacteria	protein	*Os*XA21	LRR	*Os*SERK2	*Os*RLCK107, *Os*RLCK57, *Os*RLCK118, *Os*RLCK176, *Os*RLCK102	(Pruitt *et al.*, 2015; Ercoli *et al.*, 2022)
nlp20	oomycete / bacteria	protein	*At*RLP23 (RLP) + *At* SOBIR1	LRR	*At*BAK1	*At*PBL31	(Albert *et al.*, 2015)

nlp20	oomycete	protein	*At*SBP1 *At*SBP2 + *At* SOBIR1	G-Lectin			(Bao *et al.*, 2023)
Elicitins (INF1)	oomycete	protein	SmELR, *Nb*EIR1, *Nb*REL (RLP), *Nb*SOBIR1	LRR	*Nb*BAK1	*Nb*BSK1	(Du *et al.*, 2015; Chen *et al.*, 2023; Zhang *et al.*, 2023)
elicitin PpEli2	oomycete	protein	*Nb*REli (RLP), *Nb*SOBIR1		*Nb*BAK1		(Yang *et al.*, 2023)
XEG1	oomycete	protein	*Nb*REXG1 (RLP), *Nb*SOBIR1,	LRR	*Nb*BAK1		(Ma *et al.*, 2015; Sun *et al.*, 2022)
***Pc*EXLX1**	oomycete	protein	*Nb*ERK1	G-lectin			(Pi *et al.*, 2022)
CBM1/CBEL	oomycete	protein					(Raaymakers & Van Den Ackerveken, 2016)
OPEL	oomycete	protein					(Raaymakers & Van Den Ackerveken, 2016)
Pep-13	oomycete	protein					(Raaymakers & Van Den Ackerveken, 2016)
VmE02	fungus	protein	*Nb*RE02/ *Nb*CSPR (RLP), *Nb*SOBIR1	LRR	*Nb*BAK1		(Nie *et al.*, 2021)
EndoPG	fungi	protein	*At*RLP42/ *At*RBPG1 + *At*SOBIR1	LRR	*At*SERK		(Zhang *et al.*, 2014)
SCFE1	fungi	extract	*At*RLP30 + *At*SOBIR1	LRR	*At*BAK1		(Zhang *et al.*, 2013)
Ave1	fungi	protein	*Sl*Ve1 (RLP) + *Sl*SOBIR1	LRR	*Sl*BAK1		(De Jonge *et al.*, 2012; Fradin *et al.*, 2014)
EIX	fungi	protein	*Sl*Eix2/ *Sl*Eix1, *Nb*EIX2 (RLP)	LRR			Sl: (Ron & Avni, 2004) Nb: (Yin *et al.*, 2021)
Avr1/Six4	fungi	protein	*Sl*I + *Sl*SOBIR1	LRR	*Sl*BAK1		(Catanzariti *et al.*, 2017)

Avr2/Gr-VAP1	fungi	protein	*Sl*Cf-2b + *Sl*SOBIR1	LRR	*Sl*BAK1		(Dixon *et al.*, 1996; Rooney *et al.*, 2005)
Avr4	fungi	protein	*Sl*Cf-4b + *Sl*SOBIR1	LRR	*Sl*BAK1		(Thomas *et al.*, 1997)
Avr5	fungi	protein	*Sl*Cf-5 + *Sl*SOBIR1	LRR	*Sl*BAK1		(Dixon *et al.*, 1998)
Avr9	fungi	protein	*Sl*Cf-9 + *Sl*SOBIR1	LRR	*Sl*BAK1		(Jones *et al.*, 1994)
AvrLm1 and AvrLm2	fungi	protein	*Bn*LepR3/ *Bn*RLM2, *Nb*LEPR3 + *Bn*SOBIR1, *Nb* SOBIR1	LRR	*BNb*AK1 *Nb*BAK1		(Larkan *et al.*, 2013, 2015; Ma & Borhan, 2015)
AvrLm5-9 / AvrLm4, AvrLm4-7	fungi	protein	*Bn*Rlm9/ *Bn*Rlm4/ *Bn*Rlm7	WAK			(Larkan *et al.*, 2020; Haddadi *et al.*, 2022)
Avr3/Six1	fungi	protein	*Sl*I-3	G-Lectin			(Catanzariti *et al.*, 2015)
AvrStb6	fungi	protein	*Ta*Stb6	WAK, noEGF			(Saintenac *et al.*, 2018)
SnTox1	fungi	protein	Snn1/ *Ta*WAK,	WAK/ EGF			(Shi *et al.*, 2016)
SCOOP	fungi, plants	protein	*At*MIK2, *Bn*MIK2	LRR	*At*BAK1, *BNb*AK1		(Wu *et al.*, 2024)
AtPep1, OsPep3	plant	protein	*At*PEPR1, *At*PEPR2; *Os*PEPR1/2	LRR	*At*BAK1	*At*BIK1, *At*PBL1, *At*BSK5, *At*PBL19	(Yamaguchi *et al.*, 2006, 2012) *Os*: (Shinya *et al.*, 2018; Shen *et al.*, 2022)
AtPIP1	plant	protein	*At*RLK7	LRR	*At*BAK1		(Hou *et al.*, 2014)
AtRALF23	plant	protein	*At*LLG1	GPI-AP	*At*FER	*At*PBL14/*At*RIPK	(Haruta *et al.*, 2014; Stegmann *et al.*, 2017)
AtCTNIPs	plant	protein	*At*H*SL*3	LRR	*At*BAK1		(Rhodes *et al.*, 2022)
Systemin	plant	protein	*Sp*SR160, *Sl*SYR1/2	LRR	*Sl*PORK1 ?		(Scheer & Ryan, 2002; Wang *et al.*, 2018)
AMPs, PtRISP1	plant	protein	PtRALR + PtSOBIR1	LRR			(Lintz *et al.*, 2024)
Peptidoglycan	bacteria	poly-saccharide	*At*LYM1b and *At*LYM3b	LysM	*At*CERK1		(Willmann *et al.*, 2011)

Peptidoglycans/chitin	bacteria	poly-saccharide	*OSl*YP4 and *OSl*YP6	LysM-RP	*Os*CERK 1	*Os*RLCK176, *Os*RLCK107, *Os*RLCK57, *Os*RLCK118	(Liu *et al.*, 2012)
Chitin	fungi	poly-saccharide	*At*LYK4 and *At*LYK5	LysM	*At*CERK1	*At*PBL27, *At*RLCK-VII-5, *At*RLCK-VII-7, *At*PBL19	(Miya *et al.*, 2007; Wan *et al.*, 2008; Iizasa *et al.*, 2010; Petutschnig *et al.*, 2010; Cao *et al.*, 2014)
chitin	fungi	poly-saccharide	MmLYP1, GbLyp1, *At*LYM2, *Mt*LYM2	LysM	MmLYK2 (homolog of CERK1)		(Fliegmann *et al.*, 2011; Faulkner *et al.*, 2013)
Chitin	fungi	poly-saccharide	*Os*CEBiP, *Hv*CEBiP?	LysM RP	*Os*CERK 1	*Os*RLCK185, *Os*RLCK176, *Os*BSR1, *Os*RLCK107, *Os*RLCK57, *Os*RLCK118, *Os*BSK1-2	(Kaku *et al.*, 2006; Shimizu *et al.*, 2010; Tanaka *et al.*, 2010; Hayafune *et al.*, 2014)
lam6, short, linear ß-1,3 glucans	fungi	poly-saccharide		LysM	*At*CERK1		(Mélida *et al.*, 2018)
MLGs	plant	poly-saccharide	*Os*CERK1, *OSl*ecRK1	LysM	*Os*CEBIP		(Dai *et al.*, 2023)
MLGs, CEL3, XYL4?	plant	poly-saccharide	*At*IGP1; *At*LYK4/5, *At*CERK1 (for MLG)	LRR-malectin	*At*IGP3, *At*IGP4		(Rebaque *et al.*, 2021; Martín-Dacal *et al.*, 2023; Fernández-Calvo *et al.*, 2024)
Oligogalacturonides	plant /fungi	poly-saccharide	*At*WAK1 and *At*WAK2	WAK/ EGF			(Brutus *et al.*, 2010)
chitin	fungi	poly-saccharide	*Ps*LYR4	LysM	*Ps*LYK9 (CERK1)		(Leppyanen *et al.*, 2021)
chitin	fungi	poly-saccharide	*Lj*LYR4	LysM	*Lj*LYS6(CERK1)		(Bozsoki *et al.*, 2017)
chitin	fungi	poly-saccharide	*Vv*LYK5-1	LysM	*Vv*LYK1-1, LYK1-2		(Brulé *et al.*, 2019; Roudaire *et al.*, 2023)
chitooligosaccharid	fungi	poly-saccharide	*Mt*LYR4	LysM	*Mt*CERK1 (LYK9)		(Bozsoki *et al.*, 2017; Feng *et al.*, 2019)

es (CO4-CO8)							
Ergosterol	fungi	lipid	?	?			
3-OH-FA	bacteria	lipid	*At*LORE	G-Lectin		*At*PBL34	(Ranf *et al.*, 2015; Kutschera *et al.*, 2019)
Pi-Cer-D, 9-me-Spd	oomycete	lipid	*At*RDA2	Lectin			(Kato *et al.*, 2022)
Pi-DAG/EPA, 5,8,11,14-TEFA	oomycete	lipid					(Monjil *et al.*, 2024)
NAD+	plant	nucleotide	*At*LecRKI-8	Lectin			(Wang *et al.*, 2017)
eATP	plant	nucleotide	*At*P2K1/*At*LecRK-I.9/ *At*DORN1; *At*P2K2/*At*LecRK-I.5	L-Lectin			(Choi *et al.*, 2014; Pham *et al.*, 2020)
short ß-1,6-branched ß-1,3-glucans	fungi	poly-saccharide	*Lj*EPR3a	LysM			(Kelly *et al.*, 2023)
Extracellular polysaccharides (EPS)	bacteria	poly-saccharide	*Lj*EPR3, *Lj*EPR3a	LysM			(Kawaharada *et al.*, 2015; Kelly *et al.*, 2023)
Lipochito-oligosaccharides (Nod factor)	bacteria	poly-saccharide	*Lj*NFR1 and *Lj*NFR5; *Mt*LyK3 and *Mt*NFP; *Ps*SYM10 and *Ps*SYM37	LysM	*Lj*SymRK, *Mt*DMI2	LjNiCK4	(Krönauer & Radutoiu, 2021)
chitooligosaccharides (CO4-CO8)	fungi	poly-saccharide	*Mt*LYR4, *Mt*LYK8	LysM	*Mt*CERK1 (LYK9), *Mt*DMI2		(Gibelin-Viala *et al.*, 2019; Feng *et al.*, 2019; Zhang *et al.*, 2024)

References:

Albert I, Böhm H, Albert M, Feiler CE, Imkampe J, Wallmeroth N, Brancato C, Raaymakers TM, Oome S, Zhang H, *et al.* 2015. An RLP23–SOBIR1–BAK1 complex mediates NLP-triggered immunity. *Nature Plants 2015 1:10* **1**: 1–9.

Bao Y, Li Y, Chang Q, Chen R, Wang W, Zhang Q, Chen S, Xu G, Wang X, Cui F, *et al.* 2023. A pair of G-type lectin receptor-like kinases modulates nlp20-mediated immune responses by coupling to the RLP23 receptor complex. *Journal of Integrative Plant Biology* **65**: 1312–1327.

Boller T, Felix G. 2009. A renaissance of elicitors: Perception of microbe-associated molecular patterns and danger signals by pattern-recognition receptors. *Annual Review of Plant Biology* **60**: 379–407.

Bozsoki Z, Cheng J, Feng F, Gysel K, Vinther M, Andersen KR, Oldroyd G, Blaise M, Radutoiu S, Stougaard J. 2017. Receptor-mediated chitin perception in legume roots is functionally separable from Nod factor perception. *Proceedings of the National Academy of Sciences of the United States of America* **114**: E8118–E8127.

Brulé D, Villano C, Davies LJ, Trdá L, Claverie J, Héloir MC, Chiltz A, Adrian M, Darblade B, Tornero P, *et al.* 2019. The grapevine (Vitis vinifera) LysM receptor kinases VvLYK1-1 and VvLYK1-2 mediate chitooligosaccharide-triggered immunity. *Plant biotechnology journal* **17**: 812–825.

Brutus A, Sicilia F, Macone A, Cervone F, De Lorenzo G. 2010. A domain swap approach reveals a role of the plant wall-associated kinase 1 (WAK1) as a receptor of oligogalacturonides. *Proceedings of the National Academy of Sciences of the United States of America* **107**: 9452–9457.

Cao Y, Liang Y, Tanaka K, Nguyen CT, Jedrzejczak RP, Joachimiak A, Stacey G. 2014. The kinase LYK5 is a major chitin receptor in Arabidopsis and forms a chitin-induced complex with related kinase CERK1. *eLife* **3**.

Catanzariti AM, Do HTT, Bru P, de Sain M, Thatcher LF, Rep M, Jones DA. 2017. The tomato I gene for Fusarium wilt resistance encodes an atypical leucine-rich repeat receptor-like protein whose function is nevertheless dependent on SOBIR1 and SERK3/BAK1. *The Plant journal : for cell and molecular biology* **89**: 1195–1209.

Catanzariti AM, Lim GTT, Jones DA. 2015. The tomato I-3 gene: a novel gene for resistance to Fusarium wilt disease. *New Phytologist* **207**: 106–118.

Chen Z, Liu F, Zeng M, Wang L, Liu H, Sun Y, Wang L, Zhang Z, Chen Z, Xu Y, *et al.* 2023. Convergent evolution of immune receptors underpins distinct elicitin recognition in closely related Solanaceous plants. *The Plant Cell* **35**: 1186–1201.

Choi J, Tanaka K, Cao Y, Qi Y, Qiu J, Liang Y, Lee SY, Stacey G. **2014**. Identification of a Plant Receptor forExtracellular ATP. *science* **343**.

Dai YS, Liu D, Guo W, Liu ZX, Zhang X, Shi LL, Zhou DM, Wang LN, Kang K, Wang FZ, *et al.* 2023. Poaceae-specific β-1,3;1,4-d-glucans link jasmonate signalling to OsLecRK1-mediated defence response during rice-brown planthopper interactions. *Plant Biotechnology Journal* **21**: 1286–1300.

Dixon MS, Hatzixanthis K, Jones DA, Harrison K, Jones JDG. **1998**. The Tomato Cf-5 Disease Resistance Gene and Six Homologs Show Pronounced Allelic Variation in Leucine-Rich Repeat Copy Number. *The Plant Cell* **10**: 1915–1925.

Dixon MS, Jones DA, Keddie JS, Thomas CM, Harrison K, Jones JDG. **1996**. The Tomato Cf-2 Disease Resistance Locus Comprises Two Functional Genes Encoding Leucine-Rich Repeat Proteins. *Cell* **84**: 451–459.

Dodds I, Chen C, Buscaill P, van der Hoorn RAL. **2023**. Depletion of the NbCORE receptor drastically improves agroinfiltration productivity in older Nicotiana benthamiana plants. *Plant Biotechnology Journal* **21**: 1103–1105.

Du J, Verzaux E, Chaparro-Garcia A, Bijsterbosch G, Keizer LCP, Zhou J, Liebrand TWH, Xie C, Govers F, Robatzek S, *et al.* 2015. Elicitin recognition confers enhanced resistance to Phytophthora infestans in potato. *Nature Plants 2015 1:4* **1**: 1–5.

Ercoli MF, Luu DD, Rim EY, Shigenaga A, de Araujo AT, Chern M, Jain R, Ruan R, Joe A, Stewart V, *et al.* 2022. Plant immunity: Rice XA21-mediated resistance to bacterial infection. *Proceedings of the National Academy of Sciences of the United States of America* **119**: e2121568119.

Fan L, Fröhlich K, Melzer E, Pruitt RN, Albert I, Zhang L, Joe A, Hua C, Song Y, Albert M, *et al.* 2022. Genotyping-by-sequencing-based identification of Arabidopsis pattern recognition receptor RLP32 recognizing proteobacterial translation initiation factor IF1. *Nature Communications 2022 13:1* **13**: 1–13.

Faulkner C, Petutschnig E, Benitez-Alfonso Y, Beck M, Robatzek S, Lipka V, Maule AJ. **2013**. LYM2-dependent chitin perception limits molecular flux via plasmodesmata. *Proceedings of the National Academy of Sciences of the United States of America* **110**: 9166–9170.

Feng F, Sun J, Radhakrishnan G V., Lee T, Bozsóki Z, Fort S, Gavrin A, Gysel K, Thygesen MB, Andersen KR, *et al.* 2019. A combination of chitooligosaccharide and lipochitooligosaccharide recognition promotes arbuscular mycorrhizal associations in Medicago truncatula. *Nature Communications 2019 10:1* **10**: 1–12.

Fernández-Calvo P, López G, Martín-Dacal M, Aitouguinane M, Carrasco-López C, González-Bodí S, Bacete L, Mélida H, Sánchez-Vallet A, Molina A. **2024**. Leucine rich repeat-malectin receptor kinases IGP1/CORK1, IGP3 and IGP4 are required for arabidopsis immune responses triggered by β-1,4-D-Xylo-oligosaccharides from plant cell walls. *The Cell Surface* **11**.

Fliegmann J, Uhlenbroich S, Shinya T, Martinez Y, Lefebvre B, Shibuya N, Bono JJ. **2011**. Biochemical and phylogenetic analysis of CEBiP-like LysM domain-containing extracellular proteins in higher plants. *Plant Physiology and Biochemistry* **49**: 709–720.

Fradin EF, Zhang Z, Rovenich H, Song Y, Liebrand TWH, Masini L, Van Den Berg GCM, Joosten MHAJ, Thomma BPHJ. **2014**. Functional Analysis of the Tomato Immune Receptor Ve1 through Domain Swaps with Its Non-Functional Homolog Ve2. *PLoS ONE* **9**: e88208.

Gibelin-Viala C, Amblard E, Puech-Pages V, Bonhomme M, Garcia M, Bascaules-Bedin A, Fliegmann J, Wen J, Mysore KS, le Signor C, *et al*. 2019. The Medicago truncatula LysM receptor-like kinase LYK9 plays a dual role in immunity and the arbuscular mycorrhizal symbiosis. *New Phytologist* **223**: 1516–1529.

Gómez-Gómez L, Boller T. **2000**. FLS2: An LRR Receptor–like Kinase Involved in the Perception of the Bacterial Elicitor Flagellin in Arabidopsis. *Molecular Cell* **5**: 1003–1011.

Haddadi P, Larkan NJ, Van deWouw A, Zhang Y, Xiang Neik T, Beynon E, Bayer P, Edwards D, Batley J, Borhan MH. **2022**. Brassica napus genes Rlm4 and Rlm7, conferring resistance to Leptosphaeria maculans, are alleles of the Rlm9 wall-associated kinase-like resistance locus. *Plant Biotechnology Journal* **20**: 1229–1231.

Hann DR, Rathjen JP. **2007**. Early events in the pathogenicity of Pseudomonas syringae on Nicotiana benthamiana. *The Plant Journal* **49**: 607–618.

Haruta M, Sabat G, Stecker K, Minkoff BB, Sussman MR. **2014**. A peptide hormone and its receptor protein kinase regulate plant cell expansion. *Science (New York, N.Y.)* **343**: 408–411.

Hayafune M, Berisio R, Marchetti R, Silipo A, Kayama M, Desaki Y, Arima S, Squeglia F, Ruggiero A, Tokuyasu K, *et al*. 2014. Chitin-induced activation of immune signaling by the rice receptor CEBiP relies on a unique sandwich-type dimerization. *Proceedings of the National Academy of Sciences of the United States of America* **111**: E404–E413.

Hind SR, Strickler SR, Boyle PC, Dunham DM, Bao Z, O'Doherty IM, Baccile JA, Hoki JS, Viox EG, Clarke CR, *et al*. 2016. Tomato receptor FLAGELLIN-SENSING 3 binds flgII-28 and activates the plant immune system. *Nature plants* **2**.

Hou S, Wang X, Chen D, Yang X, Wang M, Turrà D, Di Pietro A, Zhang W. **2014**. The Secreted Peptide PIP1 Amplifies Immunity through Receptor-Like Kinase 7. *PLOS Pathogens* **10**: e1004331.

Iizasa E, Mitsutomi M, Nagano Y. **2010**. Direct Binding of a Plant LysM Receptor-like Kinase, LysM RLK1/CERK1, to Chitin in Vitro. *Journal of Biological Chemistry* **285**: 2996–3004.

Jehle AK, Lipschis M, Albert M, Fallahzadeh-Mamaghani V, Fürst U, Mueller K, Felix G. 2013. The Receptor-Like Protein ReMAX of Arabidopsis Detects the Microbe-Associated Molecular Pattern eMax from Xanthomonas. *The Plant Cell* **25**: 2330–2340.

Jones DA, Thomas CM, Hammond-Kosack KE, Balint-Kurti PJ, Jones JDG. 1994. Isolation of the tomato Cf-9 gene for resistance to Cladosporium fulvum by transposon tagging. *Science* **266**: 789–793.

De Jonge R, Van Esse HP, Maruthachalam K, Bolton MD, Santhanam P, Saber MK, Zhang Z, Usami T, Lievens B, Subbarao K V., *et al.* 2012. Tomato immune receptor Ve1 recognizes effector of multiple fungal pathogens uncovered by genome and RNA sequencing. *Proceedings of the National Academy of Sciences of the United States of America* **109**: 5110–5115.

Kaku H, Nishizawa Y, Ishii-Minami N, Akimoto-Tomiyama C, Dohmae N, Takio K, Minami E, Shibuya N. 2006. Plant cells recognize chitin fragments for defense signaling through a plasma membrane receptor. *Proceedings of the National Academy of Sciences of the United States of America* **103**: 11086–11091.

Kato H, Nemoto K, Shimizu M, Abe A, Asai S, Ishihama N, Matsuoka S, Daimon T, Ojika M, Kawakita K, *et al.* 2022. Recognition of pathogen-derived sphingolipids in Arabidopsis. *Science* **376**: 857–860.

Kawaharada Y, Kelly S, Nielsen MW, Hjuler CT, Gysel K, Muszyński A, Carlson RW, Thygesen MB, Sandal N, Asmussen MH, *et al.* 2015. Receptor-mediated exopolysaccharide perception controls bacterial infection. *Nature* **523**: 308–312.

Kelly S, Hansen SB, Rübsam H, Saake P, Pedersen EB, Gysel K, Madland E, Wu S, Wawra S, Reid D, *et al.* 2023. A glycan receptor kinase facilitates intracellular accommodation of arbuscular mycorrhiza and symbiotic rhizobia in the legume Lotus japonicus. *PLOS Biology* **21**: e3002127.

Krönauer C, Radutoiu S. 2021. Understanding Nod factor signalling paves the way for targeted engineering in legumes and non-legumes. *Current Opinion in Plant Biology* **62**: 102026.

Kunze G, Zipfel C, Robatzek S, Niehaus K, Boller T, Felix G. 2004. The N Terminus of Bacterial Elongation Factor Tu Elicits Innate Immunity in Arabidopsis Plants. *The Plant Cell* **16**: 3496–3507.

Kutschera A, Dawid C, Gisch N, Schmid C, Raasch L, Gerster T, Schäffer M, Smakowska-Luzan E, Belkhadir Y, Corina Vlot A, *et al.* 2019. Bacterial medium-chain 3-hydroxy fatty acid metabolites trigger immunity in Arabidopsis plants. *Science* **364**: 178–181.

Larkan NJ, Lydiate DJ, Parkin IAP, Nelson MN, Epp DJ, Cowling WA, Rimmer SR, Borhan MH. 2013. The Brassica napus blackleg resistance gene LepR3 encodes a receptor-like protein triggered by the Leptosphaeria maculans effector AVRLM1. *New Phytologist* **197**: 595–605.

Larkan NJ, Ma L, Borhan MH. **2015**. The Brassica napus receptor-like protein RLM2 is encoded by a second allele of the LepR3/Rlm2 blackleg resistance locus. *Plant Biotechnology Journal* **13**: 983–992.

Larkan NJ, Ma L, Haddadi P, Buchwaldt M, Parkin IAP, Djavaheri M, Borhan MH. **2020**. The Brassica napus wall-associated kinase-like (WAKL) gene Rlm9 provides race-specific blackleg resistance. *The Plant Journal* **104**: 892–900.

Leppyanen I V., Pavlova OA, Vashurina MA, Bovin AD, Dolgikh A V., Shtark OY, Sendersky I V., Dolgikh V V., Tikhonovich IA, Dolgikh EA. **2021**. LysM Receptor-Like Kinase LYK9 of Pisum Sativum L. May Regulate Plant Responses to Chitooligosaccharides Differing in Structure. *International journal of molecular sciences* **22**: 1–16.

Lintz J, Goto Y, Bender KW, Bchini R, Dubrulle G, Cawston E, Zipfel C, Duplessis S, Petre B. **2024**. Genetically clustered antifungal phytocytokines and receptor protein family members cooperate to trigger plant immune signaling. *Journal of Experimental Botany*.

Liu B, Li JF, Ao Y, Qu J, Li Z, Su J, Zhang Y, Liu J, Feng D, Qi K, *et al.* 2012. Lysin Motif–Containing Proteins LYP4 and LYP6 Play Dual Roles in Peptidoglycan and Chitin Perception in Rice Innate Immunity. *The Plant Cell* **24**: 3406–3419.

Ma L, Borhan MH. **2015**. The receptor-like kinase SOBIR1 interacts with brassica napus LepR3 and is required for leptosphaeria maculans AvrLm1-triggered immunity. *Frontiers in Plant Science* **6**: 167792.

Ma Z, Song T, Zhu L, Ye W, Wang Y, Shao Y, Dong S, Zhang Z, Dou D, Zheng X, *et al.* 2015. A Phytophthora sojae Glycoside Hydrolase 12 Protein Is a Major Virulence Factor during Soybean Infection and Is Recognized as a PAMP. *The Plant cell* **27**: 2057–2072.

Martín-Dacal M, Fernández-Calvo P, Jiménez-Sandoval P, López G, Garrido-Arandía M, Rebaque D, del Hierro I, Berlanga DJ, Torres MÁ, Kumar V, *et al.* 2023. Arabidopsis immune responses triggered by cellulose- and mixed-linked glucan-derived oligosaccharides require a group of leucine-rich repeat malectin receptor kinases. *Plant Journal* **113**: 833–850.

Mélida H, Sopeña-Torres S, Bacete L, Garrido-Arandia M, Jordá L, López G, Muñoz-Barrios A, Pacios LF, Molina A. **2018**. Non-branched β-1,3-glucan oligosaccharides trigger immune responses in Arabidopsis. *The Plant Journal* **93**: 34–49.

Miya A, Albert P, Shinya T, Desaki Y, Ichimura K, Shirasu K, Narusaka Y, Kawakami N, Kaku H, Shibuya N. **2007**. CERK1, a LysM receptor kinase, is essential for chitin elicitor signaling in Arabidopsis. *Proceedings of the National Academy of Sciences of the United States of America* **104**: 19613–19618.

Monjil MS, Kato H, Ota S, Matsuda K, Suzuki N, Tenhiro S, Tatsumi A, Pring S, Miura A, Camagna M, *et al.* 2024. Two structurally different oomycete lipophilic MAMPs induce distinctive plant immune responses. *bioRxiv*.

Mott GA, Thakur S, Smakowska E, Wang PW, Belkhadir Y, Desveaux D, Guttman DS. **2016**. Genomic screens identify a new phytobacterial microbe-associated molecular pattern and the cognate Arabidopsis receptor-like kinase that mediates its immune elicitation.

Nie J, Zhou W, Liu J, Tan N, Zhou JM, Huang L. **2021**. A receptor-like protein from Nicotiana benthamiana mediates VmE02 PAMP-triggered immunity. *The New phytologist* **229**: 2260–2272.

Petutschnig EK, Jones AME, Serazetdinova L, Lipka U, Lipka V. **2010**. The Lysin Motif Receptor-like Kinase (LysM-RLK) CERK1 Is a Major Chitin-binding Protein in Arabidopsis thaliana and Subject to Chitin-induced Phosphorylation. *Journal of Biological Chemistry* **285**: 28902–28911.

Pham AQ, Cho SH, Nguyen CT, Stacey G. **2020**. Arabidopsis lectin receptor kinase P2K2 is a second plant receptor for extracellular atp and contributes to innate immunity. *Plant Physiology* **183**: 1364–1375.

Pi L, Yin Z, Duan W, Wang N, Zhang Y, Wang J, Dou D. **2022**. A G-type lectin receptor-like kinase regulates the perception of oomycete apoplastic expansin-like proteins. *Journal of Integrative Plant Biology* **64**: 183–201.

Pruitt RN, Schwessinger B, Joe A, Thomas N, Liu F, Albert M, Robinson MR, Chan LJG, Luu DD, Chen H, *et al.* 2015. The rice immune receptor XA21 recognizes a tyrosine-sulfated protein from a Gram-negative bacterium. *Science Advances* **1**.

Raaymakers TM, Van Den Ackerveken G. **2016**. Extracellular recognition of oomycetes during biotrophic infection of plants. *Frontiers in Plant Science* **7**.

Ranf S, Gisch N, Schäffer M, Illig T, Westphal L, Knirel YA, Sánchez-Carballo PM, Zähringer U, Hückelhoven R, Lee J, *et al.* 2015. A lectin S-domain receptor kinase mediates lipopolysaccharide sensing in Arabidopsis thaliana. *Nature Immunology* **16**: 426–433.

Rebaque D, del Hierro I, opez GL, Bacete L, Vilaplana F, Dallabernardina P, Pfrengle F, ıa Jord L, anchez-Vallet AS, erez RP, *et al.* 2021. Cell wall-derived mixed-linked b-1,3/1,4-glucans trigger immune responses and disease resistance in plants. *The Plant Journal*.

Rhodes J, Roman AO, Bjornson M, Brandt B, Derbyshire P, Wyler M, Schmid MW, Menke FLH, Santiago J, Zipfel C. **2022**. Perception of a conserved family of plant signalling peptides by the receptor kinase HSL3. *eLife* **11**.

Robatzek S, Chinchilla D, Boller T. **2006**. Ligand-induced endocytosis of the pattern recognition receptor FLS2 in Arabidopsis. *Genes & Development* **20**: 537–542.

Rooney HCE, Van't Klooster JW, Van Der Hoorn RAL, Joosten MHAJ, Jones JDG, De Wit PJGM. **2005**. Plant science: Cladosporium Avr2 inhibits tomato Rcr3 protease required for Cf-2-dependent disease resistance. *Science* **308**: 1783–1786.

Roudaire T, Marzari T, Landry D, Löffelhardt B, Gust AA, Jermakow A, Dry I, Winckler P, Héloir MC, Poinssot B. 2023. The grapevine LysM receptor-like kinase VvLYK5-1 recognizes chitin oligomers through its association with VvLYK1-1. *Frontiers in Plant Science* **14**.

Saintenac C, Lee WS, Cambon F, Rudd JJ, King RC, Marande W, Powers SJ, Bergès H, Phillips AL, Uauy C, *et al.* 2018. Wheat receptor-kinase-like protein Stb6 controls gene-for-gene resistance to fungal pathogen Zymoseptoria tritici. *Nature Genetics 2018 50:3* **50**: 368–374.

Saur IML, Kadota Y, Sklenar J, Holton NJ, Smakowska E, Belkhadir Y, Zipfel C, Rathjen JP. 2016. NbCSPR underlies age-dependent immune responses to bacterial cold shock protein in Nicotiana benthamiana. *Proceedings of the National Academy of Sciences of the United States of America* **113**: 3389–3394.

Scheer JM, Ryan CA. 2002. The systemin receptor SR160 from Lycopersicon peruvianum is a member of the LRR receptor kinase family. *Proceedings of the National Academy of Sciences of the United States of America* **99**: 9585–9590.

Shen W, Zhang X, Liu J, Tao K, Li C, Xiao S, Zhang W, Li JF. 2022. Plant elicitor peptide signalling confers rice resistance to piercing-sucking insect herbivores and pathogens. *Plant Biotechnology Journal* **20**: 991–1005.

Shi G, Zhang Z, Friesen TL, Raats D, Fahima T, Brueggeman RS, Lu S, Trick HN, Liu Z, Chao W, *et al.* 2016. The hijacking of a receptor kinase-driven pathway by a wheat fungal pathogen leads to disease. *Science Advances* **2**.

Shimizu T, Nakano T, Takamizawa D, Desaki Y, Ishii-Minami N, Nishizawa Y, Minami E, Okada K, Yamane H, Kaku H, *et al.* 2010. Two LysM receptor molecules, CEBiP and OsCERK1, cooperatively regulate chitin elicitor signaling in rice. *The Plant Journal* **64**: 204–214.

Shinya T, Yasuda S, Hyodo K, Tani R, Hojo Y, Fujiwara Y, Hiruma K, Ishizaki T, Fujita Y, Saijo Y, *et al.* 2018. Integration of danger peptide signals with herbivore-associated molecular pattern signaling amplifies anti-herbivore defense responses in rice. *The Plant Journal* **94**: 626–637.

Stegmann M, Monaghan J, Smakowska-Luzan E, Rovenich H, Lehner A, Holton N, Belkhadir Y, Zipfel C. 2017. The receptor kinase FER is a RALF-regulated scaffold controlling plant immune signaling. *Science (New York, N.Y.)* **355**: 287–289.

Sun Y, Wang Y, Zhang X, Chen Z, Xia Y, Wang L, Sun Y, Zhang M, Xiao Y, Han Z, *et al.* 2022. Plant receptor-like protein activation by a microbial glycoside hydrolase. *Nature 2022 610:7931* **610**: 335–342.

Takai R, Isogai A, Takayama S, Che FS. 2008. Analysis of Flagellin Perception Mediated by flg22 Receptor OsFLS2 in Rice. *https://doi.org/10.1094/MPMI-21-12-1635* **21**: 1635–1642.

Tanaka S, Ichikawa A, Yamada K, Tsuji G, Nishiuchi T, Mori M, Koga H, Nishizawa Y, O'Connell R, Kubo Y. 2010. HvCEBiP, a gene homologous to rice chitin receptor CEBiP, contributes to basal resistance of barley to Magnaporthe oryzae. *BMC plant biology* **10**.

Thomas CM, Jones DA, Parniske M, Harrison K, Balint-Kurti P, Hatzixanthis K, Jones JD. **1997**. Characterization of the tomato Cf-4 gene for resistance to Cladosporium fulvum identifies sequences that determine recognitional specificity in Cf-4 and Cf-9. *The Plant Cell* **9**: 2209–2224.

Trdá L, Fernandez O, Boutrot F, Héloir MC, Kelloniemi J, Daire X, Adrian M, Clément C, Zipfel C, Dorey S, *et al.* 2014. The grapevine flagellin receptor VvFLS2 differentially recognizes flagellin-derived epitopes from the endophytic growth-promoting bacterium Burkholderia phytofirmans and plant pathogenic bacteria. *New Phytologist* **201**: 1371–1384.

Wan J, Zhang XC, Neece D, Ramonell KM, Clough S, Kim SY, Stacey MG, Stacey G. **2008**. A LysM Receptor-Like Kinase Plays a Critical Role in Chitin Signaling and Fungal Resistance in Arabidopsis. *The Plant Cell* **20**: 471–481.

Wang L, Albert M, Einig E, Fürst U, Krust D, Felix G. **2016**. The pattern-recognition receptor CORE of Solanaceae detects bacterial cold-shock protein. *Nature Plants 2016 2:12* **2**: 1–9.

Wang L, Einig E, Almeida-Trapp M, Albert M, Fliegmann J, Mithöfer A, Kalbacher H, Felix G. **2018**. The systemin receptor SYR1 enhances resistance of tomato against herbivorous insects. *Nature Plants 2018 4:3* **4**: 152–156.

Wang C, Zhou M, Zhang X, Yao J, Zhang Y, Mou Z. **2017**. A lectin receptor kinase as a potential sensor for extracellular nicotinamide adenine dinucleotide in arabidopsis thaliana. *eLife* **6**.

Wei Y, Caceres-Moreno C, Jimenez-Gongora T, Wang K, Sang Y, Lozano-Duran R, Macho AP. **2018**. The Ralstonia solanacearum csp22 peptide, but not flagellin-derived peptides, is perceived by plants from the Solanaceae family. *Plant biotechnology journal* **16**: 1349–1362.

Willmann R, Lajunen HM, Erbs G, Newman MA, Kolb D, Tsuda K, Katagiri F, Fliegmann J, Bono JJ, Cullimore J V., *et al.* 2011. Arabidopsis lysin-motif proteins LYM1 LYM3 CERK1 mediate bacterial peptidoglycan sensing and immunity to bacterial infection. *Proceedings of the National Academy of Sciences of the United States of America* **108**: 19824–19829.

Wu H, Wan L, Liu Z, Jian Y, Zhang C, Mao X, Wang Z, Wang Q, Hu Y, Xiong L, *et al.* 2024. Mechanistic study of SCOOPs recognition by MIK2–BAK1 complex reveals the role of N-glycans in plant ligand–receptor–coreceptor complex formation. *Nature Plants 2024 10:12* **10**: 1984–1998.

Yamaguchi Y, Huffaker A, Bryan AC, Tax FE, Ryan CA. **2012**. PEPR2 Is a Second Receptor for the Pep1 and Pep2 Peptides and Contributes to Defense Responses in Arabidopsis. *The Plant Cell* **22**: 508–522.

Yamaguchi Y, Pearce G, Ryan CA. **2006**. The cell surface leucine-rich repeat receptor for AtPep1, an endogenous peptide elicitor in Arabidopsis, is functional in transgenic tobacco cells. *Proceedings of the National Academy of Sciences of the United States of America* **103**: 10104–10109.

Yang K, Wang Y, Li J, Du Y, Zhai Y, Liang D, Shen D, Ji R, Ren X, Peng H, *et al.* 2023. The Pythium periplocum elicitin PpEli2 confers broad-spectrum disease resistance by triggering a novel receptor-dependent immune pathway in plants. *Horticulture Research* **10**.

Yin Z, Wang N, Pi L, Li L, Duan W, Wang X, Dou D. 2021. Nicotiana benthamiana LRR-RLP NbEIX2 mediates the perception of an EIX-like protein from Verticillium dahliae. *Journal of integrative plant biology* **63**: 949–960.

Zhang W, Fraiture M, Kolb D, Löffelhardt B, Desaki Y, Boutrot FFG, Tör M, Zipfel C, Gust AA, Brunner F. 2013. Arabidopsis RECEPTOR-LIKE PROTEIN30 and Receptor-Like Kinase SUPPRESSOR OF BIR1-1/EVERSHED Mediate Innate Immunity to Necrotrophic Fungi. *The Plant Cell* **25**: 4227–4241.

Zhang L, Kars I, Essenstam B, Liebrand TWH, Wagemakers L, Elberse J, Tagkalaki P, Tjoitang D, van den Ackerveken G, van Kan JAL. 2014. Fungal Endopolygalacturonases Are Recognized as Microbe-Associated Molecular Patterns by the Arabidopsis Receptor-Like Protein RESPONSIVENESS TO BOTRYTIS POLYGALACTURONASES1. *Plant Physiology* **164**: 352–364.

Zhang J, Sun J, Chiu CH, Landry D, Li K, Wen J, Mysore KS, Fort S, Lefebvre B, Oldroyd GED, *et al.* 2024. A receptor required for chitin perception facilitates arbuscular mycorrhizal associations and distinguishes root symbiosis from immunity. *Current biology : CB* **34**: 1705-1717.e6.

Zhang Y, Yin Z, Pi L, Wang N, Wang J, Peng H, Dou D. 2023. A Nicotiana benthamiana receptor-like kinase regulates Phytophthora resistance by coupling with BAK1 to enhance elicitin-triggered immunity. *Journal of Integrative Plant Biology* **65**: 1553–1565.

Zipfel C, Kunze G, Chinchilla D, Caniard A, Jones JDG, Boller T, Felix G. 2006. Perception of the Bacterial PAMP EF-Tu by the Receptor EFR Restricts Agrobacterium-Mediated Transformation. *Cell* **125**: 749–760.